

ALMA MATER STUDIORUM – Università di Bologna

FACOLTÀ DI CHIMICA INDUSTRIALE
DIPARTIMENTO DI CHIMICA INDUSTRIALE E DEI MATERIALI

TESI DI DOTTORATO DI RICERCA

**Study of the reaction mechanism in the
alkylation of activated aromatic
substrates with heterogeneous
acid and basic catalysts**

Presentata da:
dott. Sauro Passeri

Relatore:
prof. Fabrizio Cavani
Co-relatore:
dott. Nicola Ballarini

Coordinatore:
chiar.mo prof. Luigi Angiolini

DOTTORATO DI RICERCA IN CHIMICA INDUSTRIALE

SETTORE CHIM/04

XXI CICLO

Esame Finale anno 2009

Contents

Chapter 1 - General Introduction

1.1.	The alkylation of phenols.....	9
1.2.	The role of methanol in the gas-phase methylation of phenol	13
1.3.	The Mechanism of the methylation of phenol in the gas phase	16
1.4.	References	21

Chapter 2 - Experimental

2.1.	Catalysts preparation.....	29
2.2.	Catalytic tests	32
2.2.1.	Products analysis	33
2.2.2.	Yields, conversion and selectivity.....	33
2.3.	Catalyst characterization.....	34
2.3.1.	X-ray diffraction.....	34
2.3.2.	Specific surface area.....	34
2.3.3.	Thermal analysis	34
2.3.4.	Raman spectroscopy.....	35
2.3.5.	FT-IR tests	35
2.3.6.	Coke analysis.....	35
2.4.	UV-Vis tests	36
2.5.	Computational details.....	36
2.6.	References	37

Chapter 3 - Methylation with basic catalysts, the role of the formaldehyde

3.1.	Introduction	39
3.2.	Experimental.....	40
3.3.	Results	42
3.3.1.	The alkylation of phenol with formaldehyde	42
3.3.2.	The alkylation of phenol with methylformate.....	48
3.3.3.	The alkylation of phenol with methyl iodide.....	51
3.3.4.	IR spectra recorded after adsorption and co-adsorption of reactants, with the MgO catalyst	52
3.4.	Discussion.....	56
3.4.1.	Formaldehyde as the alkylating agent: a comparison with methanol	56
3.4.2.	Formaldehyde as the alkylating agent in the basic-catalyzed reaction between phenol and methanol	60
3.4.3.	Methylformate as the alkylating agent: a comparison with methanol	62
3.5.	Conclusions	64
3.6.	References.....	66

Chapter 4 - The interaction between the reactants and the surface

4.1.	Introduction	69
4.2.	Experimental.....	70
4.3.	Results	71
4.3.1.	Catalytic phenol methylation	71
4.3.2.	Sorption of phenol, <i>o</i> -cresol, salicylic alcohol, and salicylic aldehyde on MgO.....	73
4.3.3.	IR Spectra of methanol under reaction conditions	92
4.3.4.	IR Spectra during reaction of methanol and phenol.....	95

4.4.	Discussion	96
4.4.1.	The interaction of reactants and products with MgO	96
4.4.2.	The reaction between adsorbed reactants	97
4.5.	Conclusions.....	101
4.6.	Acknowledgments.....	102
4.7.	References	103

Chapter 5 - The reaction pathway of the phenol methylation

5.1.	Introduction	107
5.2.	Experimental.....	107
5.3.	Results and discussions	109
5.3.1.	Catalytic tests	109
5.3.2.	Theoretical approach.....	110
5.3.3.	The evolution of the reaction.....	115
5.4.	Conclusions.....	120
5.5.	References	122

Chapter 6 - Nanoparticulate CoFe_2O_4 spinel catalysts: the effect of morphology on catalytic performances

Part 1	123	
6.1.	Introduction	123
6.2.	Experimental.....	125
6.2.1.	Catalyst characterization.....	125
6.2.2.	Methylation of Phenol.....	125
6.3.	Results.....	126
6.4.	Bulk and surface characterization of calcined samples.....	126
6.4.1.	The reactivity in the gas-phase methylation of phenol.....	133
6.4.2.	The characterization of used catalysts.....	137
6.4.3.	The catalytic behaviour in function of chemical-physical features	139

6.5.	Conclusions	144
Part 2	145
6.6.	Introduction	145
6.7.	Experimental.....	146
6.8.	Results and discussions.....	146
6.8.1.	Samples characterization	146
6.8.2.	Reduction step	147
6.8.3.	Oxidation step.....	151
6.9.	Conclusions	153
6.10.	Acknowledgments	153
6.11.	References.....	153

Chapter 7 - Imogolite, a nanostructured acid catalyst

7.1.	Introduction	157
7.2.	Experimental.....	161
7.2.1.	Methods	161
7.2.2.	Catalytic tests.....	162
7.3.	Results and discussion	162
7.3.1.	Textural characterization	162
7.3.2.	FT-IR spectroscopic characterization of bare samples.....	164
7.3.3.	FT-IR spectroscopic characterization of acidic species: adsorption of CO and NH ₃	166
7.3.4.	FT-IR spectroscopic characterization of hydroxyls accessibility to reactants of catalytic tests: adsorption of phenol and methanol at room temperature.....	171
7.3.5.	Catalytic results of gas-phase phenol methylation with methanol	173
7.3.6.	The reactivity of PR-IM	174
7.3.7.	The reactivity of IM-300 and L-IM	176
7.3.8.	The reactivity of reference materials: alumina and silica	178

7.3.9.	The comparison of catalytic materials.....	180
7.4.	Conclusions.....	182
7.5.	Acknowledgments.....	183
7.6.	References	183

Chapter 8 - Methylation of phenol over high-silica beta zeolites

8.1.	Introduction.....	187
8.2.	Experimental.....	188
8.2.1.	Catalysts characterization.....	188
8.2.2.	Catalytic tests	189
8.3.	Results and discussion	189
8.3.1.	Catalysts characterisation	189
8.3.1.1.	Crystal phase, surface area, crystal size and Si/Al ratio	189
8.3.1.2.	Acidity characterization by means of pyridine adsorption	192
8.3.2.	Catalyst activity and deactivation rate	193
8.3.2.1.	Performance of beta-2 and beta-3 catalysts in phenol methylation 195	
8.3.3.	Transformation of methanol into poly-alkylated benzenes.....	200
8.3.3.1.	Coke composition	204
8.4.	Conclusions.....	206
8.5.	Acknowledgments.....	207
8.6.	References	207

Chapter 9 Coke deposition over zeolites during phenol methylation

9.1.	Introduction.....	211
9.2.	Experimental.....	212
9.3.	Results and discussions	213
9.3.1.	The influence of the SiO ₂ /Al ₂ O ₃ ratio in the coke formation	213

Chapter 1

9.3.2.	The role of phenol on coke formation.....	216
9.4.	Conclusions	220
9.5.	Acknowledgments	220
9.6.	References.....	220

Chapter 1

General Introduction

1.1. The alkylation of phenols

The methylation of phenols is a very important industrial reaction. Methylphenols are important chemicals and intermediates and they can be used in a wide range of applications as chemicals or intermediates for pharmaceutical, agrochemical and polymer industries.

For example:

- pure **o-cresol** (ortho-methylphenol) is processed, especially in Japan, to epoxy-o-cresol novolak resins. o-cresol is also used to modify phenol-formaldehyde resins. Moreover it is also important as precursor of various dyes and pharmaceutical intermediates. The alkylation of *o*-cresol with propene gives carvacrol (3-isopropyl-6-methylphenol), which is used as an antiseptic and in fragrances. In addition, small amounts of *o*-cresol are alkylated with isobutene and used as starting materials in the production of various antioxidants, for the production of components for thermal recording materials, and for pharmaceuticals[1].
- **p-cresol** (para-methylphenol) is an important intermediate in the formation of antioxidant and preservatives for plastics, motor oil and foods [2].

- **2,6-xylenol** (2,6-dimethylphenol) is used primarily to produce poly(phenylene oxide) (PPO) resins, which are distinguished by high impact resistance, thermal stability, fire resistance, and dimensional stability. Oxidation of 2,6-xylenol gives 2,6-xylenol dimer, a speciality monomer to produce epoxy resins for encapsulating advanced semiconductors [1].
- **Anisole** can be used as an octane booster for gasoline [3] and as an intermediate in the field of flavours and fragrances.

Olefins, alcohols and alkyl halides can be used as alkylating agents but preferred alkylating agents are methanol and dimethylcarbonate, while more conventional reactants, such as methylchloride and dimethylsulphate, although still employed industrially, are nowadays less attractive due to environmental concerns [4].

Industrially the phenol methylation is carried out by means of three types of processes:

- *Liquid-phase alkylation;*
- *Fixed-bed liquid-phase processes;*
- *Vapor-phase alkylation.*

The reaction when carried out in the liquid phase give numerous products and their separation is difficult. In opposite vapour phase alkylation is simplest and more selective.

Depending on the catalysts and on the reaction conditions the process can be chemoselective to C-methylated (ring methylated) or O-methylated (ether) phenols and regioselective to ortho-methylated or para-methylated phenols.

With catalysts possessing basic characteristics and using methanol as alkylating agent the ortho-C-methylation reaction is preferred. Industrially these catalysts are used for the production of o-cresol and 2,6-xylenol. Catalysts are made of either (i) supported and unsupported alkali and alkaline-earth metal oxides, or (ii)

transition or post-transition mixed metal oxides or (iii) mixed oxides containing both alkaline-earth metals and transition metal ions [4 and references therein].

The basicity of catalysts is essentially related to the properties of the O^{2-} anion, and hence to the covalent character of the Me-O bond in the oxide. Strongest ones are alkali and alkaline-earth metal oxides, which however may deactivate by interaction with acid molecules, included carbon dioxide and water, therefore from the industrial point of view, preferred catalysts are those based on either supported V/Fe mixed oxides [5], or Mn oxide-based systems [6], or doped MgO [7].

These catalysts may also possess Lewis-type acid characteristics towards the aromatic ring; this interaction further enhances the selectivity to the products of ortho-C-methylation, with negligible formation of the product of O-methylation and of that of para-C-methylation [8-11]. Therefore, general characteristics of catalysts possessing basic features are: (i) the very high regio-selectivity in C-methylation, where the ortho/para-C-methylation ratio, though being in all cases largely higher than 2, is nevertheless affected by catalyst characteristics, and (ii) a O/C-selectivity ratio which is a function of the basic strength of catalysts, but which in general is low, and becomes close to zero for catalysts having bi-functional properties.

Amongst catalysts having Brønsted-type acid characteristics, the most studied are (i) metal phosphates (e.g., $AlPO_4$, RE phosphates, BPO_4) [12-24], (ii) γ - Al_2O_3 , either as such or doped with alkali or alkaline earth metal ions, to confer basic-type characteristics [25-32], and (iii) zeolites, also in this case sometimes exchanged with other metals, typically alkali or alkaline earth ions [2,3,33-42]. Catalysts having Brønsted-type acid characteristics are usually very active, and high conversions of the aromatic substrate can be reached at relatively mild temperature (300-350°C). The main characteristics of these materials is the preferred formation of the product of O-methylation (or etherification), especially for less acid catalysts. It is in general accepted that C-alkylation requires stronger acid sites than those

responsible for O-alkylation [16,40,43-45], and indeed less acid zeolites are more selective to anisole than to cresols [3,46,47]. Anisole itself may then act as a methylating agent; this may occur at higher reaction temperature, and contribute to the formation of cresols, which become the prevailing products for higher reactant conversion (and temperature), together with polymethylated phenols and polymethylated anisoles. The direct formation of cresols may instead occur with more acid catalysts, in competition with the O-methylation reaction [48]. Therefore, the acid strength is a key parameter, together with the control of reaction parameters (especially temperature), to obtain high selectivity to the ether at relatively high reactant conversion. Surprisingly, amongst cresols, the ortho-isomer is the preferred one, against classical rules which govern the electrophilic substitution in aromatics. A slight enhancement of the para/ortho-C-alkylated selectivity ratio can be obtained through exploitation of the shape-selectivity effects in zeolites, but nevertheless this ratio remains lower than the expected one.

The very high regio-selectivity in basic-catalyzed phenol methylation, if compared to acid-catalyzed alkylation, is explained through the widely accepted model proposed by Tanabe [48,49]. The model describes the vertical adsorption of the phenate anion over the oxide surface, due to the repulsion between highly nucleophilic O^{2-} anions and the aromatic ring. This makes the para position less available for attack by adsorbed methanol, while the ortho positions, closer to the surface, are readily available. All models later described in literature refer to the Tanabe's one, and therefore are mainly centred on the mode of adsorption of phenol. Methanol is assumed to adsorb on surface, develop the methoxy species or simply be activated by interaction with the acid-base pairs, but in most cases no specific role is attributed to this reactant in regard to the reaction pathway or mechanism. However, a wide literature exists which demonstrates that methanol undergoes different transformations, depending on the catalyst surface properties [50-52]. Also, it has to be mentioned that several contradictions exist in literature, concerning the role of the acid and basic sites and of their number and strength on the selectivity to the different products obtained in phenol and phenol derivatives

methylation. Once again, the reason for this may be related to the fact that in most cases, the reactivity is discussed in reference to the activation of the aromatic reactant, while little attention is given to the transformations which may occur on the alkylating agent, and on how these transformations may affect the catalytic performance. Indeed, the concept of acidity and of basicity towards the reactants is very different if related either to the phenol, or to methanol; while most oxides have a basic behaviour towards phenol, this is probably not the case if we consider the behaviour as regards methanol. For this reason, a classification of catalysts into acid or basic ones in the alkylation of phenol derivatives should rather take into consideration the transformations occurring upon the alkylating agent.

1.2. The role of methanol in the gas-phase methylation of phenol

One major problem of the industrial process of phenol methylation is the low yield with respect to methanol, due to its decomposition; consequently, a large excess of methanol is usually fed in order to reach an acceptable per-pass conversion of phenol. Various solutions have been proposed to minimize this side reaction (see, for example, [53]), amongst which the co-feeding of water seems to be the most effective [5,54]. This aspect, however, is often forgotten in scientific literature, and only few papers take into consideration the methanol decomposition [55-59] and the transformations that occur on the alkylating alcohol. On the other hand, a wide literature demonstrates that methanol undergoes different transformations on metal oxides, depending on the catalyst surface properties [50-52].

Basic dehydrogenating catalytic systems. In the 60's infrared studies have demonstrated that the chemisorption of methanol on alumina leads to the formation of methoxide in the 35-170 °C range; its transformation at higher temperatures into formate-like surface compound [60,61] is accompanied by evolution of H₂, with the possible intermediate formation of formaldehyde [62].

Several reviews have examined the nature of the species that develop by interaction between methanol and redox-type solid oxides [58,59]. The interaction

with cations having Lewis-type acid properties yields an undissociated $\text{CH}_3\text{OH}_{\text{ads}}$, bonded species [63]. Dissociated methoxy species are preferentially formed over basic (ionic) oxides (Bi_2O_3 , Fe_2O_3 , NiO , ZnO , ZrO_2). The covalent and Lewis-type acid oxides (WO_3 , SiO_2 , V_2O_5 , Nb_2O_5 , MoO_3) and the amphoteric ones (CeO_2 , TiO_2) produce both undissociated and dissociated terminal methoxy. Bridging methoxy, the intermediate for the formate species, can also form, e.g., on ZnO [64].

The interaction of methanol with non-reducible metal oxides has been the object of several investigations as well. MgO is known to catalyze the dehydrogenation of methanol to formaldehyde [65]. Methanol gives rise to physisorption, chemisorption or heterolytic dissociation [66] *via* acid-base mechanism, with formation of the CH_3O^- species [67]. The development of the adsorbed formate species occurs through a Cannizzaro-type reaction with intermolecular disproportionation; a nucleophilic attack of the O^{2-} surface species to the carbonyl (with development of the formate), is accompanied by a hydride transfer to a second molecule of adsorbed formaldehyde, which is converted to a methoxy species [68, 69]. The formate may finally decompose to CO and H_2 , without any supply of O^{2-} from the solid. The disproportionation mechanism may also occur on metal oxides such as ZnO , through intermediate dioxymethylene species; finally, carbonate and bicarbonate species develop, with evolution of CO_2 . Alternatively, the adsorbed methoxy and formate species may yield methylformate; however, the latter also forms by the direct dimerization of adsorbed formaldehyde (Tischenko reaction).

An overview of the interactions that formaldehyde may develop with metal oxides has been reported in the review of Barteau [52, and references therein]. Over redox-type oxides (ZnO , CuO , etc.), formaldehyde gives rise to adsorbed formates, with incorporation of the O^{2-} species. The nucleophilic attack on the carbonyl moiety occurs with the concomitant abstraction of an H^+ by a second O^{2-} species. A nucleophilic attack of surface O^{2-} at the carbonyl produces a

dioxymethylene complex, further evolved to the formate species. The desorption of HCOOH, or its decomposition, leads to the reduction of the metal ion.

Formic acid on alumina may decompose either through a dehydrative route to $\text{H}_2\text{O} + \text{CO}$, or through a dehydrogenative route to $\text{H}_2 + \text{CO}_2$ [69-71], *via* intermediate surface formate species [72]. The formation of methylformate from methanol may occur through different mechanisms, depending on the nature of the oxide (either easily reducible or non reducible), the conditions (temperature, pressure, presence of H_2O), and the surface concentration of formaldehyde, the latter being primarily a function of the dehydrogenative properties of the oxide. Methylformate decomposes to yield either $\text{CH}_4 + \text{CO}_2$ or $\text{CH}_3\text{OH} + \text{CO}$, or gives back formaldehyde through a reverse Tischenko reaction [73]. In the presence of water, methylformate decomposes to formic acid and methanol.

In conclusion, several examples exist in literature showing that methanol undergoes several transformations on metal oxides, depending on redox properties of the cation and on the “basicity” of the oxygen anion.

Acid catalytic systems. Over zeolites, the adsorption of methanol can generate framework-bonded methoxonium CH_3OH_2^+ and methoxy species that can co-exist at low temperature, but when the temperature is increased the equilibrium is shifted towards the methoxy species [74]; the latter acts as an electrophilic alkylating agent on alkylaromatics [75,76]. In the Methanol-To-Olefins process, the first step is the dehydration of methanol to dimethylether. Two mechanisms have been proposed: (a) an indirect pathway, in which the adsorbed methanol first reacts with methoxy species and then converts into dimethylether in the presence of another methanol molecule [77]; (b) a direct pathway, in which two methanol molecules react on an acid site with formation of dimethylether and H_2O in one step [78]. Surface methoxy species $\text{SiO}(\text{CH}_3)\text{Al}$ play a role in the formation of dimethylether [79]. The conversion of the equilibrium mixture of methanol and dimethylether (and water as well) is dominated by a “hydrocarbon pool” route [80,81], in which methanol is directly added onto reactive organic compounds to form aliphatic and aromatic hydrocarbons. The

methoxy species also plays a role in the kinetic “induction period”, leading to the reactive hydrocarbon pool. Alternative “direct” mechanisms have been proposed, in which a carbenium ion CH_3^+ reacts with dimethylether to generate either a carbonium ion $\text{CH}_3\text{-CH}_3^+\text{-OCH}_3$, or a oxonium ylide species. Other mechanisms include a carbene species $:\text{CH}_2$, as the reaction intermediate (see the review [82], for an analysis of the several mechanisms proposed in literature). The surface-stabilized ylide or the carbene species [83] are responsible for the methylation of aliphatic compounds and the formation of hydrocarbons, both aliphatics and aromatics (polymethylbenzenes) [84]. At $T > 420$ °C, relevant amounts of methane and formaldehyde were found, whose formation was attributed to a reaction between methanol and methoxy groups [85].

In the case of the H-BEA zeolite, the main products in methanol transformation at high temperature were light aliphatics, both saturated and unsaturated, hexamethylbenzene and pentamethylbenzene, while ZSM-5 gave mostly dimethyl and trimethylbenzenes. These compounds were further converted to naphthalene derivatives that were finally responsible for the formation of coke precursors and the deactivation of the zeolite.

It is worth mentioning that hexamethylbenzene also formed by reaction between phenol and methanol over $\gamma\text{-Al}_2\text{O}_3$ at $T > 400$ °C, while in benzene and toluene methylation the same compounds were not formed. Lower temperatures led to the formation of anisole and cresols. Therefore, the phenolic group was proposed to play an important role in the formation of hexamethylbenzene through oxygen-containing intermediates [4].

1.3. The Mechanism of the methylation of phenol in the gas phase

A pioneer in the study on the mechanism of alkylation of hydroxyarenes was Klemm [62,86-91], who was the first to point out the importance of the geometry adsorption on the regioselectivity of phenol and 1-naphthol methylation. In 1-naphthol methylation catalyzed by alumina [86] the products found were naphthyl ethers, methylated naphthols (especially at T lower than 350°C, amongst

which the most important one was 2-methyl-1-naphthol, followed by 4-methyl-1-naphthol; the yield to these compounds fell to zero at high T), and methylated naphthalenes (the prevailing products at T > 350°C, were dimethyl, trimethyl and tetramethylnaphthalene), and small amounts of 1-oxo-2-methyl-1,2-dihydronaphthalene and 1-oxo-2,2-dimethyl-1,2-dihydronaphthalene at low temperature. The necessary presence of the arenolic group for effective ring methylation was established, which also oriented the regio-selectivity. Methyl-naphthols and oxo compounds were considered as intermediate products in the formation of methylated naphthalenes. Specifically [86], the elimination of the O atom occurred by hydrogen transfer from methanol (or by a product of methanol transformation), with intermediate formation of carbinols, followed by dehydration and skeletal rearrangements to yield the final alkyl-naphthalenes. Therefore, the reductive step is found to be fundamental to shift from products of methylation formed at low temperature, and methylated aromatics formed at high temperature [62]. The mechanism of reduction mediated by alcohols in alumina-catalyzed reactions of hydroxyarenes was studied in depth for different alkylations [62,88]. Besides the usual electronic effects which address the ring methylation, additional entropy effects were hypothesized to be relevant, including effects of orientation of the substrate with respect to the catalyst surface. An adsorption of naphthol or of the anion in a vertical configuration, and a confinement of the methylating agent in a surface layer, were proposed to favour substitution at the C-2 position, while a flatwise configuration may favour the substitution at the other positions in the ring. Alternatively, the intervention of a cyclic transition state involving one molecule of a flatwise adsorbed naphthol, one molecule of methanol and an acidic site on the catalyst surface, was proposed. Cyclic intermediates were also proposed to be involved in other reactions, such as the Claisen reaction, for the ortho alkylation of Na phenoxide with an alkylhalide, and the Tiffeneau rearrangement of a benzylmagnesium halide with formaldehyde, leading to the ortho-hydroxymethylated compound [92]. The absence of the product of O-methylation (1-methoxynaphthalene) was attributed to the reversibility of the O-

methylation reaction, and to the shielding effect by the catalyst surface of the O atom. Moreover, 1-methoxynaphthalene was found to easily demethylate to yield 1-naphthol, or, at a lower extent, to rearrange into 2-methyl-1-naphthol.

The same authors [93] also demonstrated, by means of IR spectroscopy, that the chemisorption of phenol on alumina in the 300 to 450°C temperature range leads to the development of an aluminum phenoxide surface species, and obtained some evidences that the phenol molecule is oriented with the ring almost coplanar with the surface but tilted upward such that the para position is farther from the surface than the ortho position.

Tanabe [48,49,94] demonstrated that in solids having acid characteristics, an interaction also develops between the aromatic ring of the phenolate anion and the catalyst surface, while the same did not occur in the case of catalysts having basic characteristics, such as MgO. As a consequence of this, in the former case, the plane of the benzene ring is close to the surface, and any position can be methylated, while in the latter case only the ortho position is close to the surface, and can be methylated. Therefore, the model attributes to a geometric factor the high regioselectivity typical of the basic catalysis. This model has been invoked by the vast majority of papers dealing with the reaction of phenol or diphenols methylation with catalysts having basic characteristics, to justify the high regioselectivity to the product of ortho-C-methylation.

An alternative explanation has been provided by Grabowska et al [95,96], to justify the high ortho-C-methylation selectivity in the basic-catalyzed reaction between 1-naphthol and methanol, for the production of 2-methyl-1-naphthol, intermediate for the synthesis of vitamin K3 with the Vikasib technology. The authors hypothesized that the coordinative properties of Fe^{3+} might favour the adsorption of both naphthol (after abstraction of the proton) and methanol over the same site; as a consequence of this, the ortho position is in close proximity of methanol. Also in this case, the model is essentially adsorptive/geometric.

Gopinath et al [9] also identified by means of IR study the development of formaldehyde, dioxymethylene, formate species by feeding methanol over

Cu/Co/Fe/O catalysts, with decomposition at above 300°C, but due to the competition of phenol for adsorption on the same sites responsible for methanol oxidation, the latter did not apparently occur in the contemporaneous presence of the two compounds. Therefore, the authors proposed a mechanism in methanol is adsorbed on protons released by phenol, and the protonated methanol interacts with the ortho position of phenol. The same authors obtained spectroscopical evidences about the perpendicular orientation of phenol and phenolate [97,98], and attributed to this the high selectivity to the product of ortho methylation.

However, while in the alkylation of alkylbenzenes (e.g., toluene) with methanol it is possible to obtain high selectivity to the para-C-alkylated compound, even in the case of the acid-catalyzed alkylation of activated arenes, such as phenol and diphenols, and aniline as well, with olefins or with alcohols, the product of para-electrophilic substitution is obtained with lower selectivity than the expected one, even with zeolites catalysts [99]. On amorphous acid catalysts, the selectivity to o-cresol can even approach 100% [18,38,100].

The thermodynamic equilibrium ratio between para and ortho-cresol at 380°C is close to 0.43 (the statistical kinetic ratio is instead 0.5), but experimental ratios are usually lower than these values, and only in a few cases values higher than 0.7 have been reported [2,101] thanks to the exploitation of shape-selectivity effects, and to the enhancement of diffusional effects in larger crystalites. The low selectivity to p-cresol in phenol methylation has been attributed to different reasons [102] and specifically:

The heteroatom alkylation is an intermediate step in C alkylation [99] by the olefin or by the alcohol. In 10MR zeolites, the bimolecular formation of cresol isomers by reaction between phenol and methanol is suppressed in favour of the intramolecular rearrangement of anisole to o-cresol; this does not occur with 12MR zeolites, and hence a higher para-selectivity is obtained in this case [44].

A concerted cycloaddition of the olefin on the protonated arylamine occurs [104]. In general, an interaction between the alkylating agent and the O atom of phenol, which favours the alkylation at the ortho position [34,35,38]

Beltrame et al [38] formulated the hypothesis of a reaction between adsorbed anisole, which acts as the alkylating agent, and gas-phase phenol, in which the interaction between the two O atoms puts the methyl group of anisole closer to the ortho position of phenol.

It is relevant the observation that even in homogeneous acid electrophilic substitution on phenols, usually ortho/para ratios higher than the statistic value 2/1 are found [99]. This implies that adsorptive/geometric effects are not the main reason for the regioselectivity observed. So, the overall mechanism for the acid-catalyzed methylation of phenol [99] includes direct C alkylation at the ortho and para positions (in confined environments the direct para-C-alkylation can be preferred), and O-alkylation to yield anisole, the ratio C/O-alkylation being a function of the catalyst acid strength. The consecutive intramolecular rearrangement of anisole to o-cresol makes the final ortho/para-C-alkylation ratio to become very high, especially in less acid catalysts (i.e., on amorphous materials).

It is worth mentioning that indications exist in literature that in the methylation of toluene, the initial regioselectivity (thus, without taking into consideration consecutive reactions of isomerization occurring on primary products of alkylation is a function of the strength of the acid sites [104]. Other authors, correlated the regio-selectivity to the properties of the electrophilic species; Wendlandt and Bremer [105] assumed that the reaction was orbitally controlled, and that the catalyst modified the hardness/softness characteristics of the electrophile; softer electrophiles prefer substitution in para [106]. Corma et al. [76,107,108] calculated that the softness of the zeolitic proton and of the carbenium ion formed by protonation of the alkylating agent were considerably affected by the Si/Al ratio in the zeolite. This also agrees with the view of the zeolite as a polar solvent for reactants, in which a variation of the Si/Al ratio affects the softness of the acid site, and the solvation effect on the reactants, depending on their polarity [109]

1.4. References

- [1] H. Fiege, Cresols and Xylenols, Ullmann's Encyclopedia of Industrial Chemistry, 7th Ed., Wiley-VCH
- [2] G. Moon, W. Böhringer, C.T. O'Connor, Catal. Today, 97 (2004) 291
- [3] M. Renaud, P.D. Chantal, S. Kaliaguine, Can. J. Chem. Eng. 64 (1986) 787
- [4] N. Ballarini, F. Cavani, L. Maselli, A. Montaletti, S. Passeri, D. Scagliarini, C. Flego, C. Perego, J. Catal. 251 (2007) 423
- [5] US Patent 3,855,318 (1974), assigned to Asahi Chem.
- [6] JP 58208244, assigned to Mitsui Toatsu
- [7] US Patent 3,446,856 (1964), assigned to General Electric.
- [8] T. Kotanigawa, K. Shimokawa, Bull. Chem. Soc. Japan, 47 (1974) 950 and 1535.
- [9] T. Mathew, M. Vijayaraj, S. Pai, B.B. Tope, S.G. Hegde, B.S. Rao, C.S. Gopinath, J. Catal., 227 (2004) 175.
- [10] F. Cavani, L. Dal Pozzo, C. Felloni, L. Maselli, D. Scagliarini, C. Flego, C. Perego, in "Catalysis of Organic Reactions", J.R. Sowa Jr., Ed., Taylor & Francis, Boca Raton, p. 347 (2005).
- [11] F. Cavani, L. Maselli, D. Scagliarini, C. Flego, C. Perego, Stud. Surf. Sci. Catal., 155, 167 (2005).
- [12] G. Sarala Devi, D. Giridhar, B.M. Reddy, J. Molec. Catal., 181 (2002) 173.
- [13] B.M. Reddy, G. Sarala Devi, P.M. Sreekanth, Res. Chem. Int., 28(6) (2002) 595.

Chapter 1

- [14] F.M. Bautista, J.M. Campelo, A. Garcia, D. Luna, J.M. Marinas, A. Romero, J.A. Navio, M. Macias, *Appl. Catal., A*, 99 (1993) 161.
- [15] V. Durgakumari, S. Narayanan, L. Guzzi, *Catal. Lett.*, 5 (1990) 377.
- [16] R. Pierantozzi, A.F. Nordquist, *Appl. Catal.*, 21 (1986) 263.
- [17] F. Nozaki, I. Kimura, *Bull. Chem. Soc. Japan*, 50(3) (1977) 614.
- [18] J.M. Campelo, A. Garcia, D. Luna, J.M. Marinas, M.S. Moreno, *Stud. Surf. Sci. Catal.*, 41 (1988) 249.
- [19] L. Calzolari, F. Cavani, T. Monti, *C.R. Acad. Sci. Paris, Série IIc, Chimie*, 3 (2000) 533.
- [20] F. Cavani, T. Monti, in “Catalysis of Organic Reactions”, M.E. Ford (Ed.), Marcel Dekker, New York (2000), p. 123.
- [21] F. Cavani, T. Monti, D. Paoli, *Stud. Surf. Sci. Catal.*, 130 (2000) 2633.
- [22] F. Cavani, T. Monti, P. Panseri, B. Castelli, V. Messori, WO Patent 74,485 (2001), assigned to Borregaard Italia.
- [23] L. Gilbert, M. Janin, A.M. Le Govic, P. Pommier and A. Aubry, in “The Roots of Organic Development”, J.R. Desmurs and S. Ratton (Eds.), Elsevier, Amsterdam (1996), p. 48.
- [24] Y. Shiomi, Y. Nakamura, T. Manabe, S. Furusaki, M. Matsuda and M. Saito, US Patent 5,248,835 (1993), assigned to UBE Ind.
- [25] E. Santacesaria, D. Grasso, D. Gelosa, S. Carrà, *Appl. Catal.*, 64 (1990) 83 and 101.

- [26] R. Tleimat-Manzalji, D. Bianchi, G.M. Pajonk, *Appl. Catal. A*, 101 (1993) 339.
- [27] Y. Fu, T. Baba, Y. Ono, *Appl. Catal. A*, 166 (1998) 419 and 425.
- [28] Y. Fu, T. Baba, Y. Ono, *Appl. Catal. A*, 178 (1998) 219.
- [29] L. Kiwi-Minsker, S. Porchet, R. Doepper, A. Renken, *Stud. Surf. Sci. Catal.* 108 (1997) 149.
- [30] S. Porchet, L. Kiwi-Minsker, R. Doepper, A. Renken, *Chem. Eng. Sci.*, 51(11) (1996) 2933.
- [31] L. Kiwi-Minsker, S. Porchet, P. Moeckli, R. Doepper, A. Renken, *Stud. Surf. Sci. Catal.* 101 (1996) 171.
- [32] M.C. Samolada, E. Grigoriadou, Z. Kiparissides, I.A. Vasalos, *J. Catal.*, 152 (1995) 52.
- [33] S.C. Lee, S.W. Lee, K.S. Kim, T.J. Lee, D.H. Kim, J.Chang Kim, *Catal. Today*, 44 (1998) 253.
- [34] M. Marczewski, G. Perot, M. Guisnet, *Stud. Surf. Sci. Catal.*, 41 (1988) 273.
- [35] M. Marczewski, J.-P. Bodibo, G. Perot, M. Guisnet, *J. Molec. Catal.*, 50 (1989) 211.
- [36] L. Garcia, G. Giannetto, M.R. Goldwasser, M. Guisnet, P. Magnoux, *Catal. Lett.*, 37 (1996) 121.
- [37] S. Balsama, P. Beltrame, P.L. Beltrame, P. Carniti, L. Forni, G. Zuretti, *Appl. Catal.*, 13 (1984) 161.

- [38] P. Beltrame, P.L. Beltrame, P. Carniti, A. Castelli, L. Forni, *Appl. Catal.*, 29 (1987) 327.
- [39] R.F. Parton, J.M. Jacobs, H. van Ooteghem, P.A. Jacobs, *Stud. Surf. Sci. Catal.*, 46 (1989) 211.
- [40] S. Namba, T. Yashima, Y. Itaba, N. Hara, *Stud. Surf. Sci. Catal.*, 5 (1980) 105.
- [41] Z.-H. Fu, Y. Ono, *Catal. Lett.*, 21 (1993) 43.
- [42] M.D. Romero, G. Ovejero, A. Rodriguez, J.M. Gomez, I. Agueda, *Ind. Eng. Chem. Res.*, 43 (2004) 8194.
- [43] J.B. Moffat, *Catal. Rev. Sci. Eng.*, 18 (1978) 199.
- [44] Jacobs et al, *Stud. Surf. Sci. Catal.*, 41 (1989) 228.
- [45] A. Corma, H. Garcia, J. Primo, *J. Chem. Res. (S)* (1988) 40.
- [46] P.D. Chantal, S. Kaliaguine, J.L. Grandmaison, *Stud. Surf. Sci. Catal.*, 19 (1984) 93.
- [47] L.B. Young, N.J. Skillman, US Patent 4,371,714 (1983), assigned to Mobil Oil Co.
- [48] K. Tanabe, T. Nishizaki, *Proceed. 6th ICC*, G.C. Bond et al. (Eds), The Chemical Society, London (1977), p. 863.
- [49] K. Tanabe, *Stud. Surf. Sci. Catal.*, 20 (1985) 1.
- [50] M. Barteau, *Chem. Rev.*, 96 (1996) 1413
- [51] G. Busca, *Catal. Today*, 27 (1996) 457.
- [52] J.C. Lavalley, *Catal. Today*, 27 (1996) 377.

- [53] US Patent 4,933,509 (1989), assigned to General Electric.
- [54] US Patent 4,041,085 (1975), assigned to General Electric.
- [55] V. Durgakumari, S. Narayanan, J. Molec. Catal. 65 (1991) 385
- [56] S. Sato, K. Koizumi, F. Nozaki, J. Catal. 178 (1998) 264.
- [57] K.-T. Li, I. Wang, K.-R. Chang, Ind. Eng. Chem. Res. 32 (1993) 1007
- [58] J. Kaspi, G.A. Olah, J. Org. Chem. 43(16) (1978) 3142
- [59] P.D. Chantal, S. Kaliaguine, J.L. Grandmaison, Appl. Catal. 18 (1985) 133
- [60] R.C. Greenler, J. Chem. Phys. 37 (1962) 2094
- [61] R.O. Kagel, J. Phys. Chem. 71 (1967) 844
- [62] J. Shabtai, L.H. Klemm, D.R. Taylor, J. Org. Chem. 35 (1970) 1075
- [63] L.J. Burcham, L.E. Briand, I.E. Wachs, Langmuir 17 (2001) 6164 and 6175
- [64] N.D. Lazo, D.K. Murray, M.L. Kieke, J.H. Haw, J. Am. Chem. Soc. 114 (1992) 8552
- [65] P. Mars, J.J. Scholten, P. Zwietering, Adv. Catal. 14 (1963) 35
- [66] C. Di Valentin, A. Del Vitto, G. Pacchioni, S. Abbet, A.S. Wörz, K. Judai, U. Heiz, J. Phys. Chem. B 106 (2002) 11961
- [67] M. Ziolk, J. Kujawa, O. Saur, J.C. Lavalley, J. Phys. Chem. 97 (1992) 9761
- [68] X.D. Peng, M.A. Barteau, Langmuir 5 (1989) 1051.
- [69] G. Patermarakis, Appl. Catal. A 252 (2003) 231.

Chapter 1

- [70] T. Yumura, T. Amenomori, Y. Kagawa, K. Yoshizawa, *J. Phys. Chem. A* 106 (2002) 621.
- [71] K.S. Kim, M.A. Barteau, *Langmuir* 4 (1988) 945.
- [72] D.E. Fein, I.E. Wachs, *J. Catal.* 210 (2002) 241.
- [73] J.S. Francisco, *J. Am. Chem. Soc.* 125 (2003) 10475.
- [74] J. Rakoczy, T. Romotowski, *Zeolites* 13 (1993) 256.
- [75] G. Mirth, J. Lercher, *J. Catal.* 132 (1991) 244.
- [76] A. Corma, G. Sastre, P.M. Viruela, *J. Mol. Catal. A* 100 (1995) 75.
- [77] T.R. Forester, R.F. Howe, *J. Am. Chem. Soc.* 109 (1987) 5076.
- [78] J. Bandiera, C. Naccache, *Appl. Catal.* 69 (1991) 139.
- [79] W. Wang, M. Seiler, M. Hunger, *J. Phys. Chem. B* 105 (2001) 12553.
- [80] I.M. Dahl, S. Kolboe, *J. Catal.* 149 (1994) 458.
- [81] B. Arstad, S. Kolboe, *J. Am. Chem. Soc.* 123 (2001) 8137.
- [82] J.F. Haw, W. Song, D.M. Marcus, J.B. Nicholas, *Acc. Chem. Res.* 26 (2003) 317.
- [83] P.E. Sinclair, C.R.A. Catlow, *J. Phys. Chem. B* 101 (1997) 295.
- [84] W. Wang, A. Buchholz, M. Seiler, M. Hunger, *J. Am. Chem. Soc.* 125 (2003) 15260.
- [85] O. Dewaele, V.L. Geers, G.F. Froment, G.B. Marin, *Chem. Eng. Sci.* 54 (1999) 4385

- [86] J. Shabtai, L.H. Klemm, D.R. Taylor, *J. Org. Chem.*, 33 (1968) 1489
- [87] L.H. Klemm, C.E. Klopfenstein, J. Shabtai, *J. Org. Chem.*, 35 (1970) 1069
- [88] L.H. Klemm, D.R. Taylor, *J. Org. Chem.*, 35 (1970) 3216
- [89] L.H. Klemm, R. Zell, J.S. Shabtai, *J. Org. Chem.*, 39 (1974) 698
- [90] L.H. Klemm, D.R. Taylor, *J. Org. Chem.*, 45 (1980) 4320
- [91] L.H. Klemm, D.R. Taylor, *J. Org. Chem.*, 45 (1980) 4326
- [92] C.C. Price, *Org. Reactions*, 3 (1946) 1
- [93] D.R. Taylor, K.H. Ludlum, *J. Phys. Chem.*, 76(20) (1972) 2882
- [94] H. Hattori, K. Shimazu, N. Yoshii, K. Tanabe, *Bull. Chem. Soc. Japan*, 49 (1976) 969
- [95] H. Grabowska, W. Mista, L. Syper, J. Wrzyszczyk and M. Zawadzki, *J. Catal.*, 160 (1996) 134
- [96] H. Grabowska, W. Kaczmarczyk, J. Wrzyszczyk, *Appl. Catal.*, 47 (1989) 351
- [97] R. Sokoll, H. Hobert, *J. Catal.*, 125 (1990) 285
- [98] S. Sciré, C. Crisafulli, R. Maggiore, S. Minico, S. Galvagno, *Appl. Surf. Sci.*, 93 (1996) 309
- [99] R.F. Parton, J.M. Jacobs, D.R. Huybrechts and P.A. Jacobs, *Stud. Surf. Sci. Catal.*, 46 (1989) 163
- [100] J.M. Campelo, A. Garcia, D. Luna, J.M. Marinas, M.S. Moreno, *Bull. Soc. Chim. France*, 2 (1988) 283

Chapter 1

- [101] R.F. Parton, J.M. Jacobs, H. van Ooteghem, P.A. Jacobs, *Stud. Surf. Sci. Catal.*, 46 (1989) 211;
- [102] P. Espeel, R. Parton, H. Toufar, J. Martens, W. Hölderich, P. Jacobs, in “Catalysis and Zeolites. Fundamentals and Applications”, J. Weitkamp and L. Puppe (Eds.), Springer, Berlin, 1999, Ch. 6, p.377; J.B. Moffat, *Catal. Rev. Sci. Eng.*, 18 (1978) 199
- [103] W.F. Burgoyne, D.D. Dixon, J.P. Casey, *Chemtech*, (1989) 690.
- [104] T. Yashima, H. Ahamad, K. Yamazaki, M. Katsuka, N. Hara, *J. Catal.*, 17 (1970) 151
- [105] K.P. Wendlandt, H. Bremer, *Proceed. 8th Int. Congress on catalysis*, Berlin, 1984, Verlag Chemie, vol. 4, p. 507
- [106] W. Langenaeker, K. Demel, P. Geerlings, *J. Molec. Struct. (Theochem)*, 234 (1991) 329
- [107] A. Corma, G. Sastre, R. Viruela, C. Zicovich, *J. Catal.*, 136 (1992) 521
- [108] A. Corma, F. Lopic, P. Viruela, C. Zicovich-Wilson, *J. Am. Chem. Soc.*, 116 (1994) 134
- [109] L. Gilbert, C. Mercier, *Stud. Surf. Sci. Catal.*, 78 (1993) 51]

Chapter 2

Experimental

2.1. Catalysts preparation

Mg/Fe/O and Mg/O catalysts were prepared by precipitation from an aqueous solution containing the corresponding metal nitrates. For instance, to obtain 15 g of MgO, 96.15 g of $\text{Mg}(\text{NO}_3)_2 \cdot 6\text{H}_2\text{O}$ (Carlo Erba Reagenti, 99% purity) were dissolved in 375 ml of distilled water. The solution was dropwise added to another solution containing 39.75 g of Na_2CO_3 (Carlo Erba Reagenti) dissolved in 375 ml of distilled water. While adding the first solution to the second one, the pH was continuously adjusted, in order to keep it close to 10.0. Under these conditions the precipitation of $\text{Mg}(\text{OH})_2$ occurred. The so obtained slurry was left under stirring for 40 min; then the precipitate was separated from the liquid by filtration, and washed with 6 liters of distilled water at 40 °C. The solid was then dried at 110 °C overnight, and calcined at 450 °C for 8h in air. The preparation of Mg/Fe mixed oxide was carried out with the same procedure, using $\text{Fe}(\text{NO}_3)_3 \cdot 9\text{H}_2\text{O}$ (Carlo Erba Reagenti) and $\text{Mg}(\text{NO}_3)_2 \cdot 6\text{H}_2\text{O}$ as starting material and the corresponding amount of the two salts to obtain the desired atomic ratio between components.

H-MOR 40E sample having a Si/Al atomic ratio of 20 and with a specific surface area 400 m²/g was supplied by Süd-Chemie AG.

CoFe₂O₄ catalyst was prepared by co-precipitation. A 50ml solution of 0.5 M $\text{Fe}(\text{NO}_3)_3 \cdot 9\text{H}_2\text{O}$ 1M (Carlo Erba Reagenti) and $\text{Co}(\text{NO}_3)_2 \cdot 6\text{H}_2\text{O}$ (Carlo Erba Reagenti)

was added dropwise to an aqueous solution of 250ml NaOH (0.8 M) at 40°C under vigorous stirring for 3h while maintaining pH 11 by controlled of NaOH. A precipitate was observed on addition of the Fe³⁺ and Co²⁺ solution to NaOH with the colour of the solution changing from brown to dark-brown indicative of spinel formation. The solid was isolated by vacuum filtration and washed with 1.5 l of demineralized water to remove the Na⁺ and NO₃⁻ then dried in air at 120°C overnight. Final materials were obtained by calcination at different temperatures. Calcination temperature allows better control over the growth of the oxides and overall particle size than changing other synthetic parameters like pH, concentration or temperature of heat-treatment.

Imogolite was synthesised according to Farmer *et al.* [1]: at 20°C TEOS (Tetraethoxysilane) and Al(s-butoxide)₃ were added to a 75 mM aqueous solution of HClO₄ in the molar ratios Si: Al: HClO₄ = 1,x : 2 : 1. A slight excess of TEOS was used, in order to prevent preferential formation of aluminum hydroxide during hydrolysis. The solution was stirred for 18 h, diluted to 20 mM in Al, autoclaved at 100°C for 4 days, dialyzed for 4 days against de-ionized water and then dried at 50°C. Reaction conditions are rather strict, and unsuccessful syntheses lead to amorphous PR-IM. m² g⁻¹.

γ-Al₂O₃ catalyst was prepared by precipitation from an aqueous solution containing the corresponding nitrate. For instance, to obtain 10 g of γ-Al₂O₃, 73.56 g of Al(NO₃)₃·9H₂O (Carlo Erba Reagenti, 99% purity) were dissolved in 196 ml of distilled water. The solution was drop-wise added to another solution containing 20.78 g of Na₂CO₃ (Carlo Erba Reagenti) dissolved in 196 ml of distilled water. While adding the first solution to the second one, the pH was continuously adjusted, in order to keep it close to 10.0. The so obtained slurry was left under stirring for 40 min; then the precipitate was separated from the liquid by filtration, and washed with 5 l of distilled water at 40°C. The solid was then dried at 110 °C overnight and calcined at 450 °C for 8 h in air. The final surface area of the calcined sample was 110 m² g⁻¹.

SiO₂ was Grace Silica Catalyst Support (GRACE Catalyst and Carriers), with a surface area of 291 m² g⁻¹.

Beta zeolite. Three main samples of Beta zeolite, named beta-1, beta-2 e beta-3, were prepared by hydrothermal synthesis [2,3]. Tetraethyl-orthosilicate (TEOS, 98% pure, Aldrich), tetraethylammonium hydroxide (TEAOH, 40% aqueous solution, Fluka), sodium aluminate (56% Al₂O₃, 37% Na₂O, Carlo Erba) and NaOH (97% pure, Aldrich) were used as reagents. The silico-aluminate precursor gel was obtained by vigorously stirring the mixture of reagents at room temperature for several hours. After the complete hydrolysis of the organo-silicon compound, stirring was further continued for at least 24 h with final gentle warming, to remove the ethanol released.

The synthesis of the zeolite was then carried out at 135°C (beta-1) or 150°C (beta-2, beta-3) in PTFE-lined stainless steel autoclaves, tumbling at 20 r.p.m. After 24 h for beta-1, 48 h for beta-2 and 94 h for beta-3 the autoclaves were rapidly cooled and the solid was recovered from the milky suspension by centrifugation at 40,000 *g*. The solid was then repeatedly washed with distilled water till neutrality of the washing liquid, dried at 120°C overnight and calcined in nitrogen and air flow up to 550°C, to remove the TEAOH trapped in the channels of the zeolite crystals. The as-prepared samples were then ion-exchanged three times for three hours at 80°C with fresh 0.1 M ammonium nitrate (Janssen, “pro analysis”) solution. After the final exchange, the solid was separated by centrifugation, repeatedly washed with distilled water and calcined in air at 550°C, to obtain the final protonated zeolite by decomposition of the ammonium ion.

A fourth sample (beta-silicalite, with Si/Al ratio >500) was also prepared for characterisation comparison purposes only. This required the preparation of the special templating agent 4,4'-trimethylene-bis(N-benzyl,N-methyl-piperidinium)-dihydroxide, the usually employed TEAOH failing in leading to the desired BEA structure for very high Si/Al ratios [4].

Beta-10 was a sample kindly supplied by Polimeri Europa srl and it has been used for comparative characterisation purposes only.

The template solution was prepared as follows: 77 g of 4,4'-trimethylene-bis-(1-methyl-piperidine) (Aldrich, 98+% pure) were dissolved in 103 g of ethanol (Fluka, anhydrous). To this solution 110 g of benzyl bromide (Fluka, 98% pure) were added dropwise under vigorous stirring. The solid dibromide precipitate so formed was repeatedly washed with anhydrous ethanol and dried under flowing nitrogen. The dihydroxide was then obtained from the dibromide by electro-dialysis, by employing an electrolytic cell equipped with an anionic membrane separating the cathodic 0.46 M bromide solution from the anodic 25 wt% aqueous ammonia solution. The final 0.79 M solution of the templating agent was finally obtained by low-temperature removal of excess water.

The synthesis of beta-silicalite was then carried out as previously described, in the absence of sodium aluminate and by substituting the 4,4'-trimethylene-bis(N-benzyl,N-methyl-piperidinium)-dihydroxide for TEAOH.

H-ZSM-5 samples, named respectively CBV-2314; CBV-5524G and CBV-8014, were supplied by Zeolyst. The samples, with a specific surface area of 425 m²/g were characterized by a different SiO₂/Al₂O₃ molar ratio.

	CBV-2314	CBV-5524G	CBV-8014
SiO ₂ /Al ₂ O ₃ molar ratio	23	50	80

Samples, in ammonium salt form, were calcined at the temperature of 450°C before carrying the tests.

2.2. Catalytic tests

Catalytic test were carried out in a down stream tubular stainless steel or glass reactor. Liquid reagent solutions were fed using a syringe pump, vaporised and carried by a nitrogen flow. The reactor temperature was maintained at the desired temperature by an electric furnace (MFT122525/301 Carbolite) surrounding the reactor that governed by a temperature controller connected to a thermocouple placed within the catalyst bed.

In a typical reaction, the powder was pelleted and sieved to an average particle size of 30-60 mesh then loaded into the reactor tube to form a catalyst bed. The reactor was purged with flowing N₂ then heated to the reaction temperature after which the liquid organic feed was introduced.

Catalyst particles were prepared by pressing the calcined powder to obtain pellets that were then broken into smaller granules.

Condensable down stream were collected in a bubbler containing HPLC-grade acetone. Gases (CO, CO₂, H₂, CH₄) were analyzed by sampling the gaseous stream with a syringe at the reactor outlet before bubbling into acetone.

2.2.1. Products analysis

Products condensed in acetone were analyzed by gas chromatography, using a GC 6000 Carlo Erba instrument equipped with a FID and a HP-5 column. The GC oven temperature was programmed from 50°C to 250°C, with a heating rate of 10°C/min.

Gases were analysed by injecting the sample into a GC 4300 Carlo Erba gas chromatograph, equipped with a TCD and a Carbosieve SII column. The GC oven temperature was programmed from 55 to 220°C, with a heating rate of 10°C/min. The same GC was also equipped with a CP-Poraplot Q column (FID detector) for the separation of methanol, dimethylether, formaldehyde, methylformate and formic acid; in this case, the GC over was programmed from 50°C to 250°C, with a heating rate of 10°C/min.

2.2.2. Yields, conversion and selectivity

Molar yields were calculated as follows (\dot{n} is the molar flow).

Yield of phenolic products = $\frac{\dot{n}_{product}^{out}}{\dot{n}_{phenol}^{in}}$, where “product” stands for *o*-cresol, *p*-

cresol, 2,6-xylene, anisole and polyalkylated phenols.

Yield of light products, from formaldehyde: $\frac{\dot{n}_{product}^{out}}{\dot{n}_{formaldehyde}^{in}}$, where “product”

stands for CH₃OH, CO, CO₂ and CH₄.

Yield of H₂, from formaldehyde: $\frac{\dot{n}_{H_2}^{out}}{\dot{n}_{formaldehyde}^{in}}$

Conversions are expressed as follows:

Conversion of phenol or formaldehyde: $\frac{\dot{n}_{phenol\ or\ formaldehyde}^{in} - \dot{n}_{phenol\ or\ formaldehyde}^{out}}{\dot{n}_{phenol\ or\ formaldehyde}^{in}}$

Selectivity to a compound is expressed as the ratio between the corresponding yield and the reactant conversion.

2.3. Catalyst characterization

2.3.1. X-ray diffraction

Powder X-ray diffraction (XRD) experiments of the catalysts were performed with Ni-filtered CuK α radiation ($\lambda = 1.54178 \text{ \AA}$) on a Philips X'Pert vertical diffractometer equipped with a pulse height analyser and a secondary curved graphite-crystal monochromator.

2.3.2. Specific surface area

Surface area was measured by means of the BET single-point method (N₂ adsorption at the temperature of liquid N₂), using a Sorptly 1750 Fisons Instrument.

2.3.3. Thermal analysis

Temperature programmed reduction (TPR) was performed on a Stanton Redcroft STA-780 series thermal analyser.

TPR measurements were also performed in a Thermoquest TPR-1100 instrument, using a gas composition of 5% H₂ in He, and total flow of 20 mL min⁻¹. In

this case, the consumption of hydrogen during the sample reduction was measured by means of a TCD detector.

2.3.4. Raman spectroscopy

Laser Raman spectra were recorded at room temperature using a Renishaw 1000 spectrometer equipped with a Leica DMLM microscope. Samples were excited with a Argon laser beam (514 nm).

2.3.5. FT-IR tests

The IR measurements under static conditions were carried out using a Perkin Elmer 1750 FT-IR Spectrometer equipped with a DLaTGS detector. For recording spectra, 25 scans were co-added at a resolution of 2 cm^{-1} . Tests were carried out pressing the samples in a self supported wafer and activating it at high temperature under vacuum.

The in situ IR spectra were recorded using a Bruker IFS 88 FT-IR spectrometer equipped with an in situ flow cell. Either methanol, or methanol and phenol (molar ratio 10/1) were vaporized in a He stream (20 mol% of organics in the He stream), and fed to the cell. The same procedure of catalyst vacuum cleaning was adopted as for FT-IR measurements done under static conditions. Spectra are reported after subtraction of MgO.

2.3.6. Coke analysis

Samples of aged catalyst, recovered after a few hours on-stream at 390°C , were analysed according to a well-known technique [5], to collect information on the amount and nature of the fouling carbonaceous material (coke). A weighed portion of aged catalyst was disaggregated in HF (40% aqueous solution) to dissolve the zeolite and to collect the remaining carbonaceous solid particles by filtration and drying. The carbonaceous solid particles were repeatedly leached with small portions of fresh CH_2Cl_2 and then dried and weighed. The leaching CH_2Cl_2 solutions were combined and most of the solvent removed *in vacuo* at room temperature. The concentrated

solution of the soluble coke was then analysed by gas chromatography-quadrupolar mass spectrometry (GC-QMS) by an Agilent HP 5973N GC-MS instrument.

2.4. UV-Vis tests

Olympus BX41 upright research microscope equipped with a 10X objective was used for the UV/Vis measurements. The in-situ setup was equipped with a 50/50 double viewport tube, that accommodates a CCG video camera (ColorView IIIu, Soft ImagingSystem GmbH) and a optical fibre mount. A 200- μm -core fibre connected the microscope to a CCD UV/Vis spectrometer (AvaSpec-2048TEC, Avantes).

In situ UV/Vis experiments feeding methanol were performed in a in-situ cell, LINKAM FTIR 600, equipped with a temperature controller (LINKAM TMS 93).

In-situ UV/Vis experiments feeding a phenol/methanol solution, with a molar ratio 1:10 and pure methanol were carried out in a horizontal tubular quartz reactor heated with heating wires.

2.5. Computational details

The computational study was carried out on a model MgO cluster. The cluster geometry was taken from ref. [6], where the Mg-O distance is 2.10850 Å. Density functional theory (DFT) calculation were performed using the B3LYP hybrid density functional and 6-31G(d,p) or 6-31G(d) basis set was used. The geometry of all adsorbed molecules was fully optimized, but the substrate cluster was not relaxed in the optimization process in agreement with an experimental study that demonstrated a poor relaxation in this oxide [7]. In order to improve the visual comparison between experimental and calculated IR spectra, wavenumbers have been scaled by a factor of 0.9613 [8]. The adsorption energies were computed as the difference between the energy of MgO/molecule system and the sum of the energies of separated fragments, $E_{\text{ads}} = E_{(\text{MgO-MOL})} - E_{\text{MgO}} - E_{\text{MOL}}$. Correction for the zero point contribution and, when needed, basis set superimposition error (BSSE), by the counterpoise method, were applied. All calculations were carried out using Gaussian 03 program package [9].

Optimized structures are visualized using GaussView program [8]. Calculations have been carried out on IBM SP5/512 supercomputer at CINECA.

2.6. References

- [1] V.C. Farmer, M.J. Adams, A.R. Fraser, F. Palmieri, *Clay Miner.* 18 (1983) 459.
- [2] J. Pérez-Pariente et al., *Appl. Catal.*, 31 (1987) 35
- [3] M.A. Cambor, J. Pérez-Pariente, *Zeolites*, 11 (1991) 202
- [4] U.S. Patent 5,453,511, Sept. 26,1995
- [5] P. Magnoux, P. Roger, C. Canaff, V. Fouché, N.S. Gnep, M. Guisnet, *Stud. Surf. Sci. Catal.*, 34 (1987) 317
- [6] S. Sasaki, K. Fujino, Y. Takeuchi, *Proceed. Japan Acad.* 55 (1979) 43.
- [7] E.A. Colbourn, J. Kendrick, C. Mackrodt, *Surf. Sci.* 126 (1983) 350.
- [8] M.W. Wong, *Chem. Phys. Lett.* 256 (1996) 391.
- [9] Gaussian 03, Revision C.02, M. J. Frisch, G. W. Trucks, H. B. Schlegel, G. E. Scuseria, M. A. Robb, J. R. Cheeseman, J. A. Montgomery, Jr., T. Vreven, K. N. Kudin, J. C. Burant, J. M. Millam, S. S. Iyengar, J. Tomasi, V. Barone, B. Mennucci, M. Cossi, G. Scalmani, N. Rega, G. A. Petersson, H. Nakatsuji, M. Hada, M. Ehara, K. Toyota, R. Fukuda, J. Hasegawa, M. Ishida, T. Nakajima, Y. Honda, O. Kitao, H. Nakai, M. Klene, X. Li, J. E. Knox, H. P. Hratchian, J. B. Cross, V. Bakken, C. Adamo, J. Jaramillo, R. Gomperts, R. E. Stratmann, O. Yazyev, A. J. Austin, R. Cammi, C. Pomelli, J. W. Ochterski, P. Y. Ayala, K. Morokuma, G. A. Voth, P. Salvador, J. J. Dannenberg, V. G. Zakrzewski, S. Dapprich, A. D. Daniels, M. C. Strain, O. Farkas, D. K. Malick, A. D. Rabuck, K. Raghavachari, J. B. Foresman, J. V. Ortiz, Q. Cui, A. G. Baboul, S. Clifford, J. Cioslowski, B. B. Stefanov, G. Liu, A. Liashenko, P. Piskorz, I. Komaromi, R. L.

Chapter 2

Martin, D. J. Fox, T. Keith, M. A. Al-Laham, C. Y. Peng, A. Nanayakkara, M. Challacombe, P. M. W. Gill, B. Johnson, W. Chen, M. W. Wong, C. Gonzalez, and J. A. Pople, Gaussian, Inc., Wallingford CT, 2004.

- [10] GaussView, Version 3.09, Roy Dennington II, Todd Keith, John Millam, Ken Eppinnett, W. Lee Hovell and Ray Gilliland, Semichem, Inc., Shawnee Mission, KS, 2003.

Chapter 3

Methylation with basic catalysts, the role of the formaldehyde

3.1. Introduction

The characteristics of catalysts with basic features when used for phenol methylation are: (i) very high regioselectivity in *C*-methylation, since the ortho/para-methylation ratio is always much higher than 2, and (ii) high chemoselectivity, since the *O/C*-methylation ratio, a function of the basic strength of the catalysts, in general is very low. The very high regioselectivity is explained through the widely accepted model proposed by Tanabe [1,2]. That model describes the adsorption of the phenolate anion orthogonal to the oxide surface, due to the repulsion between the highly nucleophilic O²⁻ anions and the aromatic ring. This makes the para position less accessible by adsorbed methanol, while ortho positions, closer to the surface, are readily accessible. All models described in literature later refer to the Tanabe model and, therefore, are mainly focused on the mode of phenol adsorption. Methanol is assumed to adsorb on the surface, develop a methoxy species or be activated by interaction with the acid-base pairs [3,4]. In most cases, however, no hypothesis is reported about the role of the reactions of methanol with regard to the mechanism of phenol methylation.

In [5], we reported that the transformation of methanol is the factor that mainly determines the performance in phenol methylation when catalysed by either

basic or acidic catalysts. Specifically, catalysts that activate methanol through an acid-type mechanism led to the formation of anisole, which further reacted yielding cresols via an intramolecular rearrangement. At high temperature, the formation of polymethylated compounds was preferred. On the other hand, catalysts with basic features dehydrogenated methanol to formaldehyde, which in turn formed other intermediates (formate and methylformate) and then decomposed to yield CO, CO₂, H₂ and CH₄. Evidence was given that, with these catalysts, dehydrogenation of methanol is essential in order to obtain alkylation of phenol; in this case, the main product was *o*-cresol [5].

In the present chapter, we report about the study of the reaction of phenol with compounds formed by methanol dehydrogenation, i.e., formaldehyde and methylformate, in order to highlight their role as possible methylating agents in the reaction of methanol with phenol. Catalysts investigated were: (a) MgO, which is the main component in alkaline earth metal oxide-based catalysts used in the General Electric process for the synthesis of *o*-cresol and 2,6-xyleneol [6]; (b) Magnesium-iron mixed oxide (sample Mg/Fe/O); Fe oxide is claimed to be the main component in the optimal catalyst for the selective ring methylation of phenol and 1-naphthol [7,8], while Mg/Fe/O catalyses the liquid-phase and the gas-phase methylation of both *m*-cresol [9] and phenol [10,11]; and (c) a commercial H-mordenite.

3.2. Experimental

Three catalysts were investigated; (i) MgO, (ii) Magnesium-iron mixed oxide (sample Mg/Fe/O) and (iii) a commercial H-mordenite (see Chapter 2.1).

Catalytic tests were carried out by vaporization of an aqueous phenol/formaldehyde solution, containing 20.6 wt % formaldehyde, 0.4 wt % methanol and 17.5 wt % phenol (supplied by Sigma Aldrich, 99+% purity), remainder water, in a N₂ stream (N₂ gas flow 20 Nml/min). The aqueous formalin solution was prepared containing the minimal amount of methanol; the latter is usually added in commercial formalin solutions to limit formaldehyde

polymerization. The reactor feed composition was the following (molar fractions): nitrogen 89.3%, formaldehyde 1.7% (considering all the formaldehyde oligomers as being in the monomeric form), methanol 0.03%, phenol 0.46% and water 8.5%. Overall gas residence time was 2.7 s, $GHSV_{\text{phenol}}$ 6.2 h⁻¹. Total pressure was 1 bar. The gas/vapor stream was fed into a stainless steel reactor, containing 1 cm³ of catalyst shaped either in 30-60 mesh particles (catalyst weight: MgO 0.85 g, Mg/Fe/O 0.95 g), or in 1/16" extrudates (H-mordenite 0.64 g). Tests with the H-mordenite were carried out in a glass reactor, in order to minimize the dehydrogenation due to the reactor wall.

Additional tests were carried out by vaporization of a phenol/methylformate (molar ratio 1/1) solution in a N₂ stream (N₂ gas flow 20 Nml/min). Feed composition was the following: N₂ 90.5%, methylformate (supplied by Carlo Erba Reagenti, 97% purity) 4.7% and phenol 4.7%. Overall gas residence time was 2.7 s.

Finally, tests were carried out feeding a phenol/methyliodide solution (molar ratio 1/10). Feed composition was the following: N₂ 89.0%, methyliodide (supplied by Sigma Aldrich) 10.0% and phenol 1.0%. Overall gas residence time was 2.7 s.

Blank reactivity tests made at 390°C with the empty steel reactor and with the phenol/formaldehyde mixture gave phenol conversion 2% (with formation of *o*-cresol and 2,6-xylenol) and overall yield of light compounds, from formaldehyde decomposition, of 10-15% at 390°C. This indicates that the reactor wall gives a small but non-negligible contribution to the reactivity. Indeed, it was also found that the catalytic effect of the wall is greater when a steel reactor is used in which the protective passive coating has been removed due to the prolonged exposure to an H₂-containing atmosphere. In this case, the blank test at 390°C led to a phenol conversion of 7% and to a relevant decomposition of formaldehyde. Finally, when the same tests were done with a glass reactor, the conversion of phenol was 1%, and the decomposition of formaldehyde was 5%.

For recording IR spectra, 25 scans were co-added at a resolution of 2 cm^{-1} . MgO sample were pressed into thin self-supported wafer and activated in situ into the IR cell at 450°C under vacuum (10^{-5} mbar) for 2 h, until disappearance of the adsorbed water. The adsorption procedure involved contact of the vacuum-cleaned sample wafer with vapors of either the single reactants, i.e., formaldehyde (obtained by heating in vacuum of paraformaldehyde, supplied by Sigma Aldrich) and phenol, or both reactants in different order of adsorption, at room temperature, followed by evacuation at increasing temperatures, i.e., 100, 200, 300, 350, 400 and 450°C . Moreover, IR spectra of *o*-cresol (supplied by Fluka, >99,5 purity) and salicylaldehyde (supplied by Aldrich, 98% purity) adsorbed on MgO were also collected for comparison. The infrared spectra reported are difference absorbance spectra of the MgO sample with and without the adsorbed molecules.

3.3. Results

3.3.1. The alkylation of phenol with formaldehyde

Figures 1-2 show the results of tests carried out with catalysts MgO and Mg/Fe/O, respectively. The conversion of phenol and the molar selectivity to the phenolic products are plotted as a function of the reaction temperature. The yields of CH_3OH , CH_4 , CO , CO_2 and H_2 , obtained by the transformation of formaldehyde, are also reported.

Figure 1 shows that with MgO the principal product of the reaction between formaldehyde and phenol was *o*-cresol, with minor formation of *p*-cresol and of xylenols, mainly the 2,6-dimethyl isomer. The selectivity to *o*-cresol was very high at low temperature, and slightly decreased when the reaction temperature was increased.

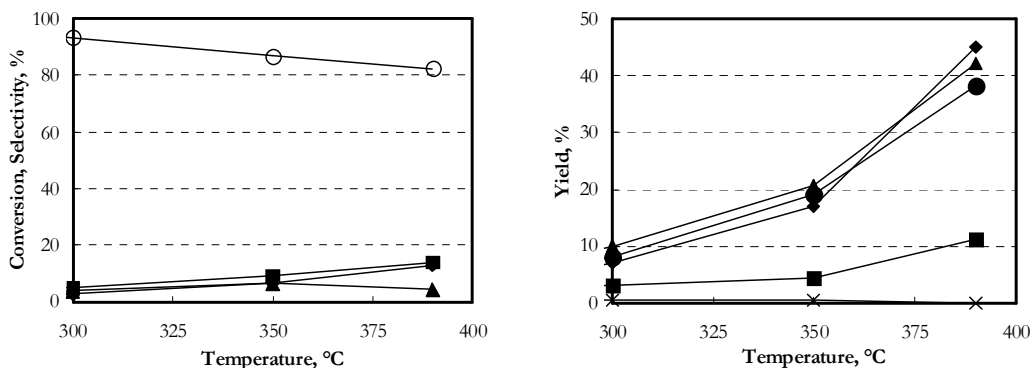


Figure 1. Left: Conversion of phenol (■), molar selectivity to *o*-cresol (○), *p*-cresol (▲) and xylenols (◆) as a function of temperature. Right: Molar yield of CH₃OH (●), CO (■), CO₂ (▲), CH₄ (×) and H₂ (◆) as a function of temperature. Catalyst: MgO.

The main C-containing products of formaldehyde transformation were CO₂ and methanol; the two compounds formed with similar yields. The yields of CH₄ and methylformate were lower than 0.5%; the yield of formic acid was nil. These results indicate that due to the presence of a large amount of water in the feed (in the formalin solution), formaldehyde gave formic acid and methanol through the Cannizzaro reaction :



Then, formic acid completely decomposed to CO₂ + H₂, for an overall stoichiometry (reported for mass balance purpose only):



In fact, the experimental yield of H₂ was similar to that of CO₂. Minor amounts of CO formed either by dehydrogenation of formaldehyde or by decomposition of HCOOH to CO + H₂O; the latter is more likely, because the former reaction would have led to an overall yield of H₂ higher than that of CO₂. For the same reason, it can be inferred that also the dehydrogenation of methanol to formaldehyde did not occur extensively.

The overall yield of light C-containing compounds derived from formaldehyde at 390°C was 92%, because the remaining fraction of formaldehyde

was consumed in phenol alkylation; in fact, under these conditions the conversion of formaldehyde was total.

It is worth noting that when tests of phenol methylation were carried out with MgO and feeding a methanol/phenol mixture (molar ratio 10/1) [5], the overall conversion of methanol was less than 10% at 390°C; the conversion of methanol did not increase when water was added to the feed. Therefore, the lower reactivity of methanol, as compared to formaldehyde, explains why the methanol generated by formaldehyde transformation (Figure 1, right) was not extensively converted to light decomposition compounds.

The formation of methylformate was negligible; this indicates that due to the large excess of water, the reaction between methanol and formic acid to yield the ester was unfavoured, and that the Tischenko dimerization of formaldehyde to yield the ester was kinetically unfavoured with respect to the Cannizzaro disproportionation. Indeed, methylformate might have quickly decomposed to methanol + CO; in this case, however, the yield of CO should have been equimolar to that one of methanol.

Figure 2 shows the catalytic performance of Mg/Fe/O.

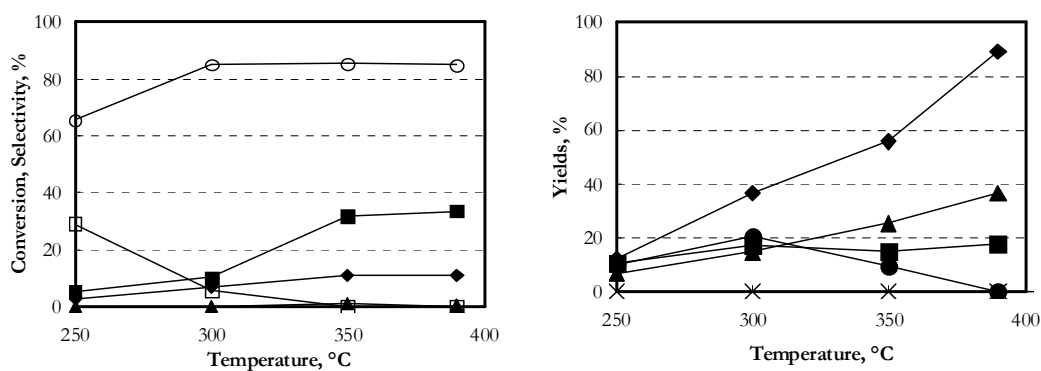


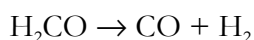
Figure 2. Left: Conversion of phenol (■), molar selectivity to *o*-cresol (○), *p*-cresol (▲), xylenols (◆) and salicylaldehyde (□) as a function of temperature. Right: Molar yield of CH₃OH (●), CO (■), CO₂ (▲), CH₄ (×) and H₂ (◆) as a function of temperature. Reaction conditions as in Figure 1. Catalyst: Mg/Fe/O.

This catalyst was more active than MgO, as it was in the reaction between phenol and methanol [5]. The phenolic products were *o*-cresol and 2,6-xylenol and

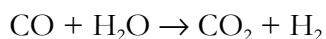
with no formation of anisole. The selectivity to *p*-cresol was very low, while this compound was obtained with selectivity higher than 2-3% with MgO; the same difference between the two catalysts was observed in the reaction between phenol and methanol [5]. Below 350°C, also salicylaldehyde (2-hydroxybenzaldehyde) formed; its selectivity was close to 30% at 250°C, and then decreased down to zero at 350°C, with a corresponding increase in the selectivity to *o*-cresol. This is the main difference with respect to tests carried out with methanol [5]; in the latter case, in fact, salicylaldehyde was not obtained. In the case of MgO, salicylaldehyde did not form even in the reaction between phenol and formaldehyde (Figure 1); this can be due to the fact that this catalyst was less active than Mg/Fe/O, and gave non-negligible conversion of phenol only at above 300°C; under these conditions, salicylaldehyde is likely rapidly transformed to *o*-cresol.

For what concerns the side reactions occurring on formaldehyde, main differences with respect to MgO were the following: (i) an higher yield of CO, that at low temperature formed in an amount comparable to CO₂; (ii) a much higher yield of H₂, that at 390°C approached the theoretical limit value of 100%, and (iii) a lower yield of methanol, that showed a maximum at 300°C, and became nil at 390°C. The decrease of the yield of methanol was accompanied by an increase of yields of CO₂ and H₂. Also with this catalyst, the yields of formic acid and methylformate were negligible.

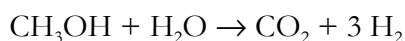
The formation of CO is explained by considering the contribution of formaldehyde dehydrogenation



However, the relevant yield of H₂ can be explained only by considering a role of H₂O in the WGS reaction, catalysed by the Fe cation:



Another contribution to H₂ formation may derive from methanol reforming :



Clearly, an important contribution of these reactions might cause the yield of H_2 to become higher than the 100%. In fact, the yield of H_2 is referred to the formaldehyde fed; therefore, an additional H_2 formation deriving from a co-reactant (water in this case) may make it become higher than the theoretical limit for the stoichiometry of formaldehyde dehydrogenation.

The overall conversion of formaldehyde was lower than that obtained with MgO: 70% at 390°C, considering also the fraction of formaldehyde reacted with phenol. Mg/Fe/O was much more active than MgO in methanol dehydrogenation to formaldehyde in the absence of phenol, but the two catalysts had similar activity when also phenol was present in the stream [5]. This was interpreted by assuming a competition between methanol and phenol for adsorption over the Fe^{3+} ions that led to an inhibition of methanol dehydrogenation. In the present case, the lower conversion of formaldehyde observed with Mg/Fe/O may be either attributed to an inhibition effect due to the presence of phenol, or to a lower activity of this catalyst in the Cannizzaro reaction.

With both MgO and Mg/Fe/O catalysts, no deactivation phenomena were observed, when reaction temperatures not higher than 390°C were used.

Figure 3 reports the catalytic performance of the H-mordenite in phenol methylation with formaldehyde.

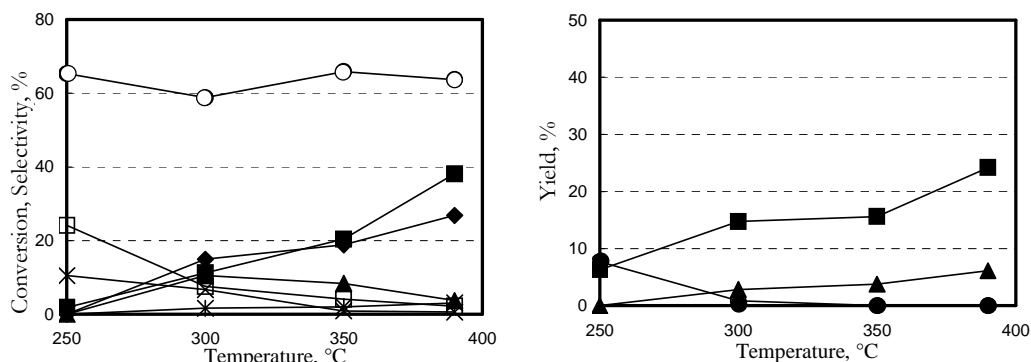


Figure 3. Conversion of phenol (■), molar selectivity to anisole (×), *o*-cresol (○), *p*-cresol (▲), xylenols (◆), salicylaldehyde (□) and polyalkylated phenols (*) as a function of temperature. Right: Molar yield of CH_3OH (●), CO (■) and CO_2 (▲) as a function of temperature. Reaction conditions as in Figure 1. Catalyst: H-mordenite.

The results were different from those obtained with methanol [5]; in the latter case, in fact, the main reaction product at low temperature was anisole, while over 300°C the products were *o*-cresol, *p*-cresol and polyalkylated phenols. With formaldehyde, instead, the nature and amount of products were similar to those obtained with MgO and Mg/Fe/O. At low temperature, the prevailing products were *o*-cresol and salicylaldehyde, whereas anisole formed with selectivity of 10%. At high temperature, the prevailing products were *o*-cresol and 2,6-xylenol, with lesser amounts of *p*-cresol and of polyalkylated phenols.

For what concerns the formation of light compounds (Figure 3, right), the prevailing compounds were CO and methanol that formed in equimolar amount at 250°C; there was no formation of methane and hydrogen. This result suggests that formaldehyde yields methylformate by dimerization, which is then further decomposed to yield the two light compounds. The formation of formic acid, further decomposed to CO and water, cannot be excluded. For temperatures higher than 250°C, the yield of methanol decreased while that of CO increased; in fact, methanol reacted to yield anisole, alkylphenols and alkylaromatics [5].

Two aspects are worth mentioning; polyalkylbenzenes (mainly pentamethylbenzene and hexamethylbenzene), which were obtained in large amounts from methanol [5], formed with an overall yield lower than 1% from formaldehyde. Furthermore, no short-term deactivation phenomena were observed, while they were evident from methanol. In the latter case, it was suggested that the deactivation was due to the formation of alkylaromatics, precursors of coke formation. This indicates that with formaldehyde the formation of coke precursors is hindered; this effect can be due either to the low amount of methanol generated, or to the presence of water, which inhibits the formation of dimethylether.

Tests were carried out with variation of the residence time in order to obtain information on the reaction scheme. Very low residence times (e.g., smaller than 0.1 s) and a low temperature (250°C) were used in order to isolate the intermediates, which were supposed to be extremely reactive. Figure 4 plots the

selectivity to the products as a function of phenol conversion, for tests carried out with the Mg/Fe/O catalyst.

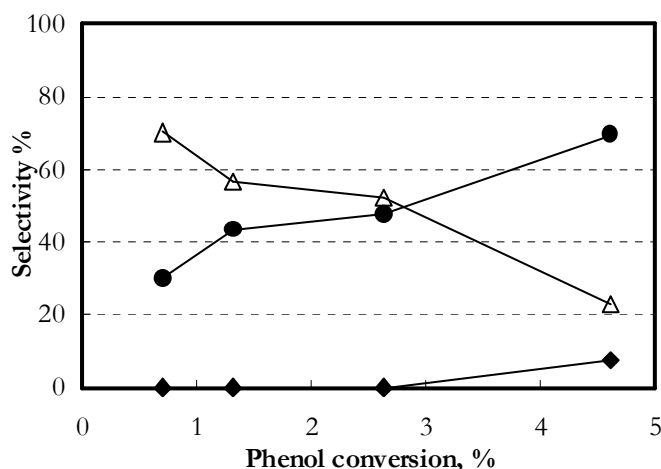


Figure 4. Molar selectivity to salicylaldehyde (Δ), *o*-cresol (\bullet) and xylenols (\blacklozenge) as a function of phenol conversion. Temperature 250°C; residence time was varied. Other conditions as in Figure 1. Catalyst: Mg/Fe/O.

Salicylaldehyde was clearly a primary product, since its selectivity, if extrapolated to nil conversion, was higher than zero; however, it rapidly declined when the conversion was increased. The decrease of selectivity to the aldehyde led to an increase of that to *o*-cresol; this evidently support the hypothesis that the latter compound forms by consecutive transformation of salicylaldehyde. The further reaction of *o*-cresol gave the formation of 2,6-xylenol, the selectivity of which however was lower than 10% under these experimental conditions.

3.3.2. The alkylation of phenol with methylformate

The results of catalytic tests performed by feeding phenol and methylformate are reported in Figures 5-7. The figures show the conversion of phenol and the molar selectivity to the phenolic products, i.e., *o*-cresol, 2,6-xylenol and anisole.

With MgO (Figure 5), the prevailing product was anisole, while this compound was obtained with selectivity lower than 10% in tests carried out with either methanol [5] or formaldehyde (Figure 1).

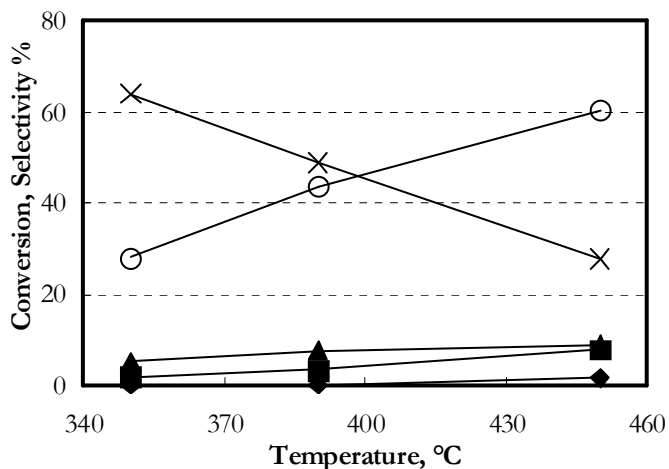


Figure 5. Conversion of phenol (■), molar selectivity to anisole (x), *o*-cresol (o), *p*-cresol (▲) and 2,6-xylene (◆) as a function of temperature. Feed composition: N₂ 90.5%, methylformate 4.7% and phenol 4.7%. Overall gas residence time 2.7 s; total pressure 1 bar. Catalyst: MgO.

With Mg/Fe/O (Figure 6) the formation of anisole was low, as it was in tests carried out with either methanol [5] or formaldehyde (Figure 2); the main phenolic products were *o*-cresol and 2,6-xylene.

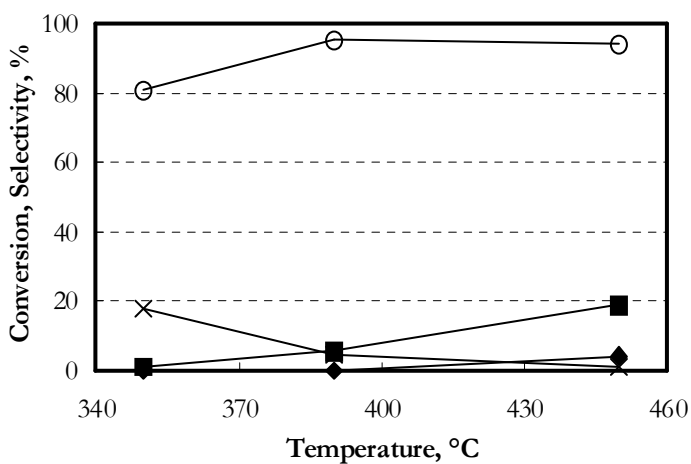


Figure 6. Conversion of phenol (■), molar selectivity to anisole (x), *o*-cresol (o) and 2,6-xylene (◆) as a function of temperature. Reaction conditions as in Figure 5. Catalyst: Mg/Fe/O.

With both catalysts the conversion of phenol was low; in fact, most methylformate decomposed, and only a minor fraction of it reacted with phenol.

Figure 7 shows the catalytic performance obtained with the H-mordenite catalyst.

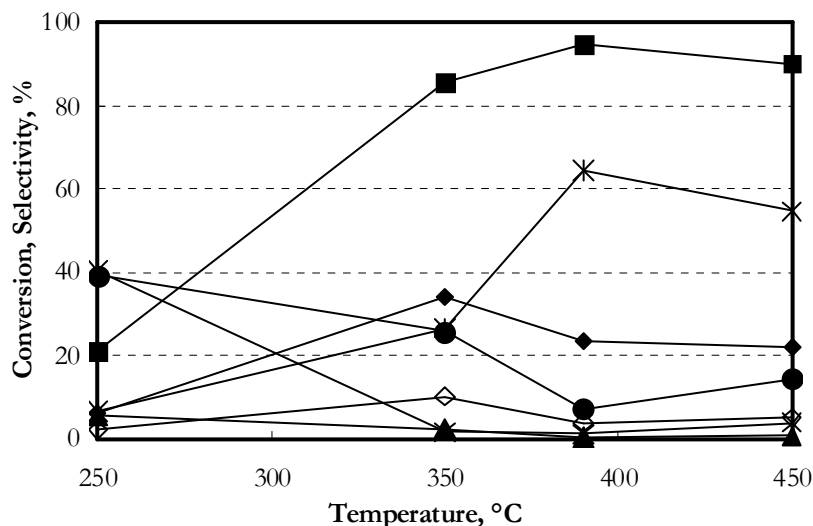


Figure 7. Conversion of phenol (■), molar selectivity to *o*-cresol (●), 2,6-xylene (◆), *p*-cresol (▲), anisole (×), 2,4-xylene (◇) and polyalkylated phenols (*) as a function of temperature. Reaction conditions as in Figure 5. Catalyst: H-mordenite.

At low temperature, the products of reaction with phenol were anisole and cresols (mainly *o*-cresol); the same distribution of products was obtained starting from methanol [5], whereas that obtained from formaldehyde (Figure 3) was different. An increase of the reaction temperature led to the formation of xylenols.

For what concerns the formation of light compounds (results not reported in Figures), with MgO methylformate decomposed to CO (yield 21% at 390°C) and methanol; the yield of methane was nil. The amount of H₂ generated was relatively low (at 390°C, yield was < 1%), suggesting that the fraction of methanol dehydrogenated to formaldehyde was low. With the Mg/Fe/O catalyst, the yields of CO and CO₂ at 390°C were similar (19% and 14%, respectively), the yield of methane was 3% and that of H₂, 8%. With the H-mordenite, methylformate mainly

decomposed to CH_3OH and CO (yield 30% at 390°C); the yield of CH_4 and CO_2 was 3%.

3.3.3. The alkylation of phenol with methyl iodide

In order to demonstrate the role of the methylating agent, tests were carried out feeding methyl iodide and phenol over the $\text{Mg}/\text{Fe}/\text{O}$ catalyst. Results are reported in Figure 8.

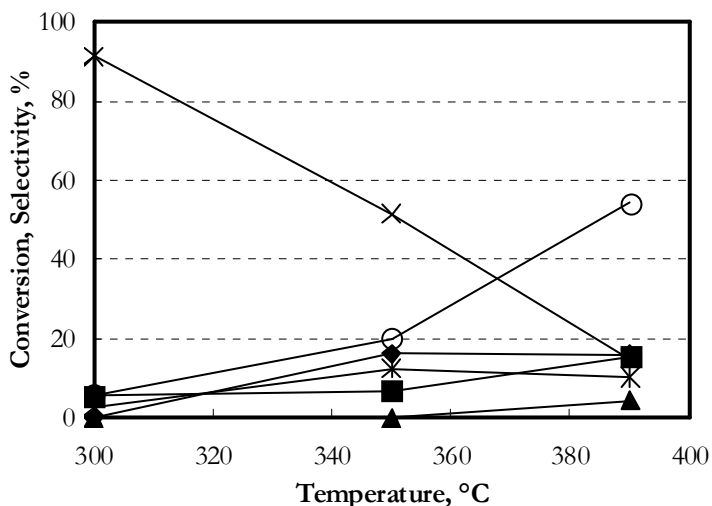


Figure 8. Conversion of phenol (■), molar selectivity to anisole (×), *o*-cresol (○), 2,6-xylenol (◆), *p*-cresol (▲) and polyalkylated phenols (*) as a function of temperature. Feed composition: N_2 89.0%, methyl iodide 10.0% and phenol 1.0%. Overall gas residence time 2.7 s; total pressure 1 bar. Catalyst: $\text{Mg}/\text{Fe}/\text{O}$.

The conversion of phenol was low, due to the fact that the activation of methyl iodide was not efficient because of the absence of acidic sites. The nature and relative amount of the products obtained in phenol methylation were the same as those obtained in tests made by feeding methanol and phenol with the H-mordenite [5]. The main product at low temperature was anisole; an increase of the reaction temperature led to the formation of cresols (the ortho isomer being the prevailing one) and polyalkylated phenols.

Therefore, when the formation of the aldehyde is not possible, the methylating species that are generated with the basic catalyst yields the same

phenolic products that are obtained with methanol and with acid catalysts. These tests demonstrate that the nature of the products obtained in phenol methylation is a function of the type of methylating species generated.

3.3.4. IR spectra recorded after adsorption and co-adsorption of reactants, with the MgO catalyst

Figure 9 plots the IR spectrum of MgO, and spectra of the sample recorded after sorption of vapours of formalin, phenol, salicylaldehyde and *o*-cresol, at room temperature. The spectra of MgO show the presence of carbonates (1200-1700 cm^{-1} region) and -OH group (3753 cm^{-1}), also after the pre-treatment at 450°C.

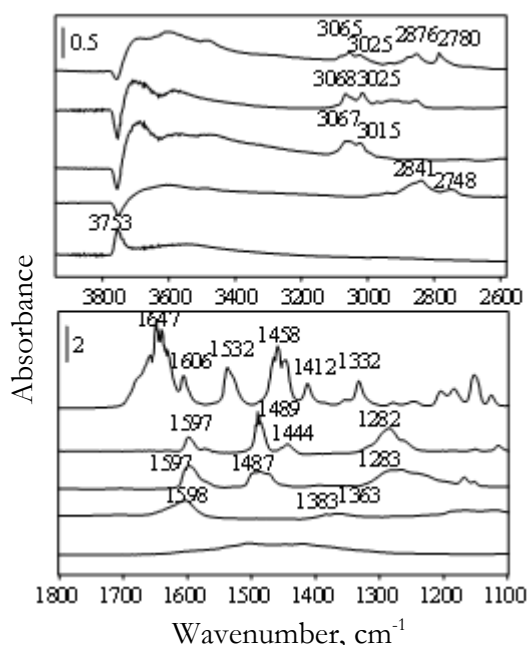


Figure 9. FT-IR spectra recorded after adsorption at room temperature and evacuation on MgO, from bottom to top: formaldehyde, phenol, *o*-cresol and salicylaldehyde.

The spectrum recorded after adsorption of phenol is similar to that one reported in the literature [12,13]. In the spectral zone between 3010 and 3070 cm^{-1} are the stretching vibrations of C-H in the aromatic ring. Bands at 1602 cm^{-1} and 1495 cm^{-1} are attributed to C-C ring vibrations, and bands at 1170 and 1074 cm^{-1} to C-H bending. The band at 1285 cm^{-1} is related to C-O stretching for the phenolate

species, evidence for the dissociation of the hydroxy group. For what concerns the spectrum of salicylaldehyde, bands in the spectral zone between 3000 and 3090 cm^{-1} can be attributed to the stretching of the C-H of the aromatic ring. Bands at 2876 and 2780 cm^{-1} are related to the stretching of the C-H in the aldehydic moiety; the latter one derives from the Fermi resonance. The band at 1647 cm^{-1} is characteristic of the aldehydic C-O stretching. Bands at 1606 and 1532 cm^{-1} are related to the aromatic ring stretching vibrations; in the zone between 1409 and 1466 cm^{-1} are the bands due to the C-H bending, the former one being attributable to the aldehydic C-H. The band at 1332 cm^{-1} is due to the stretching of C-O, whereas the band at 1155 cm^{-1} corresponds to the stretching of C-CHO. Additional bands in the spectrum of *o*-cresol, if compared with the corresponding spectrum of phenol, are attributed to the -C-H vibrations of the methyl group (between 2800 and 3000 cm^{-1}), and to the bending of -CH₃ at 1444 cm^{-1} . In the region between 3400 and 3800 cm^{-1} the bands are attributed to the interaction between the adsorbed molecules and the -OH groups of MgO.

Figure 10 shows the spectra recorded after adsorption of formaldehyde at different temperatures.

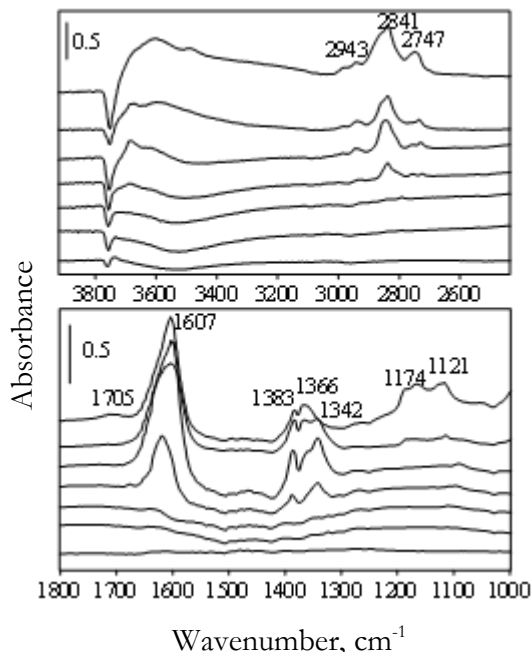


Figure 10. FT-IR spectra recorded after adsorption of formaldehyde at room temperature on MgO and evacuation, and after heating under vacuum at increasing temperatures. From top to bottom at: Room temperature, 100°C, 200°C, 300°C, 350°C, 400°C and 450°C.

At low temperature the typical frequencies of formaldehyde, 2841, 2748 cm^{-1} (ν CH), and 1383, 1363 cm^{-1} (δ CH) are present; however, these peaks disappear for temperatures higher than 300°C, evidence for a complete desorption or decomposition of formaldehyde. The peak at 1338 cm^{-1} in the spectra recorded at 100 and 200°C is due to the formate species. The main result of this experiment is that formaldehyde is weakly bound to the surface sites of MgO, and does not remain adsorbed at those temperatures at which the reaction between phenol and formaldehyde takes place. This suggests the hypothesis that the latter reaction may also occur via a Rideal-type mechanism, involving adsorbed phenolate and gas-phase formaldehyde.

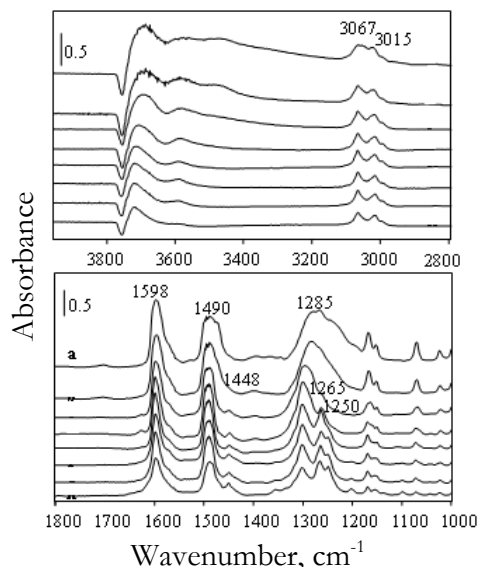


Figure 11. FT-IR spectra recorded after adsorption at room temperature on MgO of phenol and then of formaldehyde and evacuation, and after heating under vacuum at increasing temperatures. From top to bottom at room temperature, phenol and then formaldehyde, room temperature, 100°C, 200°C, 300°C, 350°C, 400°C, 450°C.

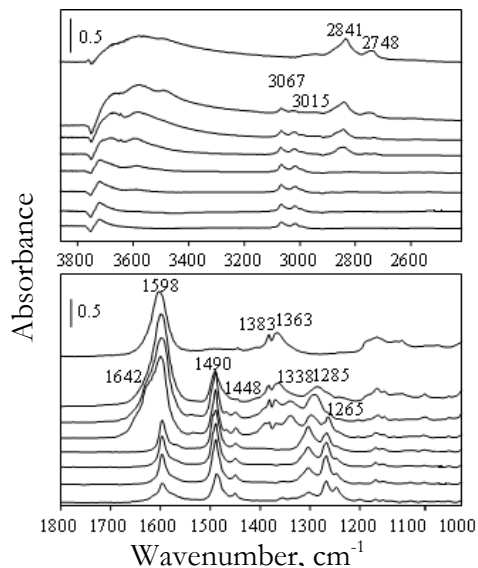


Figure 12. FT-IR spectra recorded after adsorption at room temperature on MgO of formaldehyde and then of phenol and evacuation, and after heating under vacuum at increasing temperatures. From top to bottom at room temperature, formaldehyde and then phenol, room temperature, 100°C, 200°C, 300°C, 350°C, 400°C, 450°C.

Figure 11 plots the spectra recorded after pre-adsorption of phenol at room temperature and subsequent adsorption of formaldehyde, and by heating the sample up to 450°C. Figure 12 plots the spectra recorded by inverting the order of reactants adsorption on MgO. In the former case formaldehyde peaks are not evident; this is due to the stronger adsorption of phenol over surface sites. On the contrary, when phenol is adsorbed after formaldehyde, the aromatic adsorbs on MgO, but there is no substantial variation in the concentration of adsorbed formaldehyde. These data can be interpreted on the basis of the literature information available on the adsorption of these molecules over MgO (see also the Discussion Section). In fact, phenol interacts strongly with Mg-O pairs [12,13]. On the contrary, with formaldehyde a weaker interaction between the aldehydic O atom and Mg develops. Therefore, the adsorption of formaldehyde leaves several Mg-O pairs on the surface available for the adsorption of phenol; however, the

latter does not displace formaldehyde because a prerequisite for phenol adsorption is the accessibility of free Mg-O pairs. On the other hand, the pre-adsorption of phenol leads to a saturation of the surface; since the interaction of formaldehyde with the catalyst is not strong enough to compete efficiently with the aromatic, the amount of formaldehyde adsorbed is very low.

When the temperature is increased, new bands appear. In the first case (Figure 11) bands at 1448 and 1250 cm^{-1} are due to *o*-cresol formation, being attributed respectively to $-\text{CH}_3$ bending and C-O stretching. This means that the low amount of formaldehyde adsorbed rapidly reacts with the phenolate species. In the second case bands attributed to formaldehyde disappear for temperatures higher than 300°C. One relevant feature is the concomitant development of a shoulder at 1642 cm^{-1} (ν C=O) and a peak at 1468 (δ CH) cm^{-1} , both corresponding to the most intense bands of adsorbed salicylaldehyde (Figure 9). These features disappear at 300°C, while bands attributed to *o*-cresol develop. These results are in agreement with catalytic tests, and confirm that in the 200-to-300°C temperature range it is possible to isolate salicylaldehyde, the intermediate in the formation of *o*-cresol. On the contrary, at higher temperatures the aldehyde is not isolated, probably because of its rapid transformation into *o*-cresol.

3.4. Discussion

3.4.1. Formaldehyde as the alkylating agent: a comparison with methanol

In literature, the direct alkylation of aromatics with aldehydes and ketones has been less studied than the corresponding alkylation with alcohols, alkyl halides or alkenes, because of the tendency to give oligomeric by-products [14-18].

Lercher et al. [19,20] reported that in the basic-catalysed methylation of toluene to styrene with methanol, the conditions to obtain side-chain alkylation are the dehydrogenation of methanol to formaldehyde, and the development of a strong interaction between the methyl group of toluene and the basic oxygen atoms, to form a partial negative charge on the C atom. An aldol-type condensation

occurs, with C-C bond formation. The formation of formaldehyde and of an intermediate formate species in the side-chain alkylation of alkylaromatics with methanol was also proposed by other authors [21-23].

As regards the alkylation of activated aromatics with methanol, to our knowledge the hypothesis that formaldehyde might play a direct role was first cited in a patent [24], which claimed alkaline earth oxides as catalysts for the gas-phase reaction between methanol and phenol. In the open literature, some authors suggest a possible role of aldehydes in the alkylation with alcohols, but no experimental proof has ever been provided [25-32]. For instance, Gopinath et al [25] identified formaldehyde, dioxymethylene and formate by means of IR study when feeding methanol over Cu/Co/Fe/O catalysts. However the authors argued that methanol dehydrogenation did not occur in the presence of phenol, due to the competition of the two reactants for adsorption on the same sites. Radhe Shyam et al [29] suggested that in the vapor-phase alkylation of pyridine with methanol over a Zn/Mn/Fe/O ferrosinell system, formaldehyde attacks intermediate dihydropyridine to yield 3-picoline, but no experimental evidence was provided by the authors of the effective need for formaldehyde as the true alkylating agent. In the methylation of 1-naphthol catalysed by alumina, Klemm et al. [30] proposed that the main methylating agents were either the adsorbed methanol, coordinated to the acidic site, or the methyl carbonium ion, but also did not exclude the possibility that either formaldehyde, formed by dehydrogenation of methanol, or the hydroxymethyl carbonium ion, $^+\text{CH}_2\text{OH}$, might be the true electrophilic agent [31].

Our results indicate that analogies exist between the gas-phase methylation of phenol with methanol [5] and with formaldehyde. With basic catalysts, the performance in phenol methylation is similar when either of the two reactants is fed. On the other hand, the catalyst type, either basic or acidic, has little influence on the nature of the products when formaldehyde is used as the methylating agent, while quite different is the nature of products obtained over the two catalysts when methanol is the reagent [5]. This indicates that the active species in phenol

methylation with methanol is not the same when either basic or acid catalysts are used, whereas it is the same when the reaction is carried out with formaldehyde. Furthermore, this implies that the major role in the basic-catalysed methylation of phenol is not played by methanol itself, but by one of the products of methanol transformation, i.e., either formaldehyde or methylformate. These hypotheses are discussed more in detail below.

The results obtained in phenol methylation with formaldehyde over MgO and Mg/Fe/O can be explained by considering formaldehyde as the true alkylating agent in the reaction of phenol methylation with methanol, and with formaldehyde, too. According to this hypothesis, the dehydrogenation of methanol to formaldehyde is the necessary requisite for the methylation with basic catalysts. A large proportion of formaldehyde is then decomposed to light compounds, but a part of it reacts with phenol to yield *o*-cresol. Therefore, the true molar ratio between formaldehyde and phenol is much lower than the feed ratio (3.7/1), and much lower than the methanol/phenol feed ratio used in tests with methanol (10/1) [5]. Indeed, the extent of methanol decomposition observed in methanol/phenol reactivity tests was by far less than that of formaldehyde. In fact, the yield of light compounds from methanol never exceeded 15% [5], while with formaldehyde the extent of formaldehyde transformation is almost total. This difference is due to the higher reactivity of the aldehyde as compared to methanol, and to the presence of a large amount of water, that favors the disproportionation of formaldehyde. Despite this, the conversion degree of phenol with formaldehyde was similar to that obtained with methanol. This means that formaldehyde is much more reactive than methanol to the aromatic ring, due to electrophilic properties of the C atom in the carbonyl moiety.

The nature of the phenolic products and their relative quantities were also quite similar when either of two reactants was used with basic catalysts. One minor difference concerns the formation of anisole that in the reaction between phenol and methanol over MgO was obtained with selectivity lower than 10%, while it did not form at all in the reaction with formaldehyde. Another difference concerns the

formation of salicylaldehyde as the reaction intermediate; this was detected with selectivity close to 30% at low temperature in the phenol/formaldehyde reaction with the Mg/Fe/O catalyst and with the H-mordenite, while it was not observed at all with these catalysts in the phenol/methanol reaction. This is likely due to the fact that with methanol the rate-determining step of the reaction is the dehydrogenation of methanol to formaldehyde [5], which then rapidly attacks the aromatic ring; this implies that the concentration of the adsorbed phenolic intermediates is very low under these conditions. When instead formaldehyde is directly fed, the concentration of the phenolic intermediates is relevant and the latter may in part desorb into the gas phase.

An alternative hypothesis is that methanol is the true alkylating agent in the reaction of phenol methylation with methanol, and also with formaldehyde. In fact, a fraction of formaldehyde is transformed into methanol and formic acid by means of the Cannizzaro reaction. However, it is worth noting that in the reaction between phenol and formaldehyde the concentration of methanol in the reaction environment is low, in the best case equimolar to the amount of CO₂ formed. Therefore, in formaldehyde/phenol tests the effective molar ratio between methanol and phenol is around 1, which is much lower than in tests carried out by directly feeding the methanol/phenol mixture [5]. If methanol were the true alkylating agent even in formaldehyde/phenol tests, a much lower conversion of phenol than that obtained in methanol/phenol tests should be expected, since the conversion of phenol is greatly affected by the methanol/phenol feed ratio [5]. On the contrary, the conversion of phenol was greater, for the same temperature and contact time, with formaldehyde than with methanol. Finally, it is worth noting that the large extent of formaldehyde transformation to methanol (Figures 1-2) was due to the excess of water fed; in fact, water is one co-reactant of the Cannizzaro reaction. In tests carried out with methanol, instead, no water was fed, and the amount of water generated in the reaction was comparatively very low [5].

Therefore, all the data obtained support the hypothesis that in the gas-phase phenol alkylation with methanol, catalyzed by basic catalysts, the true

alkylating agent is not methanol, but formaldehyde. This hypothesis is now discussed more in detail.

3.4.2. Formaldehyde as the alkylating agent in the basic-catalyzed reaction between phenol and methanol

Our catalytic tests of phenol methylation with formaldehyde have evidenced that the nature of the methylating species determines the type of phenolic products. On the other hand, the catalyst affects the type of methylating agent when methanol is the reactant, while it has little effect on it with formaldehyde. This also supports the hypothesis that in the presence of a basic catalyst, the true active species in phenol methylation with methanol is not the alcohol. This would explain why, at low temperature, the main product of the reaction between phenol and methanol with the H-mordenite catalyst is anisole [5], which, conversely, is formed in low yield starting from formaldehyde. In fact, under these conditions methanol is protonated by the acidic catalyst and reacts either with another molecule of methanol to yield dimethylether or with phenol to yield anisole. When formaldehyde is the reactant, the electrophilic carbonyl bond rapidly attacks the aromatic ring.

Therefore, the results support the hypothesis that the catalyst, either acidic or basic, plays its main role in the generation of the methylating species, whereas it has little influence on the reaction pathway between the adsorbed phenol and the methylating species and on the type of phenolic products finally obtained. If this hypothesis is correct, the use of a basic catalyst and of a methylating agent that does not dehydrogenate should yield the same phenolic products obtained with the acidic catalyst and methanol, i.e., anisole at low temperature and cresols/polyalkylphenols at high temperature. In fact, with a basic catalyst, methyl iodide - the activation of which may only occur by generation of a $\text{CH}_3^{\delta+}$ species - gave the same distribution of products (Figure 8) that is obtained with methanol/phenol and the H-mordenite [5].

IR spectra recorded after co-adsorption of phenol and formaldehyde evidenced the following:

Phenol develops a much stronger interaction with the MgO surface than formaldehyde;

The reaction between phenol and formaldehyde requires the pre-adsorption and activation of phenol and the development of the phenolate species, but likely formaldehyde does not require to be at the adsorbed state in order to give the electrophilic attack on the activated aromatic ring.

When the reaction is between adsorbed phenol and adsorbed formaldehyde, salicylaldehyde can be isolated as the reaction intermediate if moderate reaction temperatures, i.e., lower than 300°C, are used.

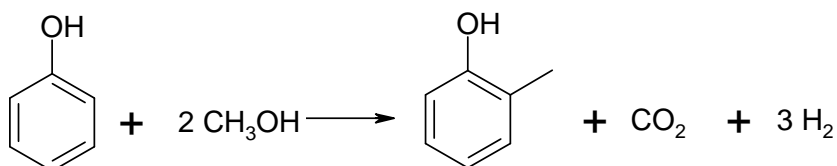
Salicylaldehyde is the intermediate in *o*-cresol formation.

Reactivity tests made with variation of the residence time (Figure 4) confirmed that salicylaldehyde is one primary product in the reaction between phenol and formaldehyde, and that salicylaldehyde is consecutively transformed to *o*-cresol. However, the presence of other reactions leading to *o*-cresol cannot be excluded.

Salicylaldehyde may form by rapid dehydrogenation of salicylalcohol that, by analogy with the hydroxymethylation reaction, can be assumed to be the first product of the reaction between phenol and formaldehyde. If salicylalcohol is consecutively transformed before it may desorb into the gas phase, it cannot be identified as one primary reaction product. Other reactions that may occur on salicylalcohol are (i) the condensation with another phenol molecule to yield (PhOH)-CH₂-(PhOH), one possible precursor of cresol [33], or (ii) the reduction of the hydroxymethyl to methyl group by formaldehyde or by hydrogen (the latter formed by dehydrogenation of formaldehyde). In this case, a parallel primary formation of *o*-cresol should also contribute to phenol conversion; indeed, data of Figure 4 do not allow exclude this possibility. The transformation of salicylaldehyde to *o*-cresol may also occur by reaction of the former with either methanol or

formaldehyde; this leads to the reduction of the carbonyl to the methyl group and to the oxidation of the reductant to CO_2 .

Therefore, the reaction between phenol and methanol in basic catalysis likely includes a reductive step by either methanol or formaldehyde, for an overall stoichiometry:



3.4.3. Methylformate as the alkylating agent: a comparison with methanol

Methylformate is a weak alkylating agent, and is employed in the Zerbe and Jage process [34] for the synthesis of anisole from alkali metal phenolate, through the classical base-catalysed Williamson ether synthesis. Methylformate is generated in-situ by reaction between methanol and CO at 180°C , and high pressure. The reaction between phenol and methylacetate catalysed by Mg-zeolites also yields anisole as the main reaction product at $T < 350^\circ\text{C}$, while at higher temperatures, *o*-cresol and xylenols form [35].

Results obtained in phenol methylation with methanol over basic catalysts [5] demonstrated that with these catalysts methylformate is one product of methanol transformation, and that indeed it may represent the true alkylating species. Moreover, it was found that the yield of the main products obtained by the high-temperature decomposition of methylformate, i.e., CH_4 and CO_2 , was considerably affected by the presence of phenol. In fact, while in the absence of phenol the two compounds formed in almost equimolar amount, the presence of the aromatic led to a substantial decrease in methane formation as compared to carbon dioxide. This might be interpreted as being due to the insertion of the methyl group on the aromatic ring from intermediately formed methylformate, the remaining part of the molecule being released in the form of carbon dioxide and hydrogen.

Results obtained in the present work, for the reaction between phenol and methylformate, indicate that with the catalyst characterised by the stronger dehydrogenation activity (Mg/Fe/O), a very low amount of anisole is formed, while the latter is a predominant product of the reaction with MgO. This suggests that methylformate may directly act as the methylating agent, with the introduction of the methyl group to yield anisole and the concomitant release of CO₂. In fact, the amount of CH₄ generated from methylformate decomposition was practically nil. The C atom of the methyl group in the ester is not sufficiently electrophilic to attack the aromatic ring, while it reacts with the O atom in the phenolate. Conversely, when methylformate is decomposed to CH₃OH + CO to a great extent, and methanol is dehydrogenated to formaldehyde, i.e., with Mg/Fe/O, the prevailing product is that of C-methylation, *o*-cresol.

Therefore, our results demonstrate that with basic catalysts and under mild reaction conditions, at which methylformate is not greatly decomposed, the ester may act as a methylating agent on phenol to yield anisole. However, when methanol is the reactant [5], methylformate forms only under those conditions at which the alcohol is dehydrogenated to formaldehyde. The latter then either forms methylformate (which, however, is rapidly decomposed due to the high reaction temperature), or reacts with phenol to yield C-alkylated compounds. In tests made by feeding the formalin solution, methylformate formed only in minor amount, because the Cannizzaro reaction was the preferred path for formaldehyde transformation.

The distribution of products obtained with the H-mordenite and methylformate was quite similar to that obtained with methanol [5], and different from that obtained with formaldehyde. Therefore, at low temperature either the methylformate, activated by protonation of the carbonylic O atom, or the methanol obtained by decomposition of methylformate, reacted with phenol to produce anisole. At high temperature (i.e., T > 350°C), methanol gave ring-substitution to cresols and polyalkylated phenols.

3.5. Conclusions

Figure 13 summarizes the results obtained in this study and in our previous work on phenol methylation with methanol over basic catalysts [5].

In the gas-phase methylation of phenol with methanol, the catalyst type, either basic or acidic, plays its main role in the generation of the methylating agent. With the acidic catalyst, the activation of methanol generates an electrophilic species that reacts with phenol to produce anisole at low temperature, whereas at high temperature the preferred products of the reaction are *C*-alkylated compounds.

Conversely, with basic catalysts the dehydrogenation of methanol is the necessary step for the formation of a more electrophilic species; formaldehyde then either reacts rapidly with phenol to yield *o*-cresol, or gives rise to the parallel formation of methylformate. At low temperature, methylformate may yield anisole by reaction with phenol, but at high temperature it decomposes to lighter compounds. Salicylaldehyde is the intermediate product in the reaction between phenol and formaldehyde, and is the precursor for the formation of *o*-cresol.

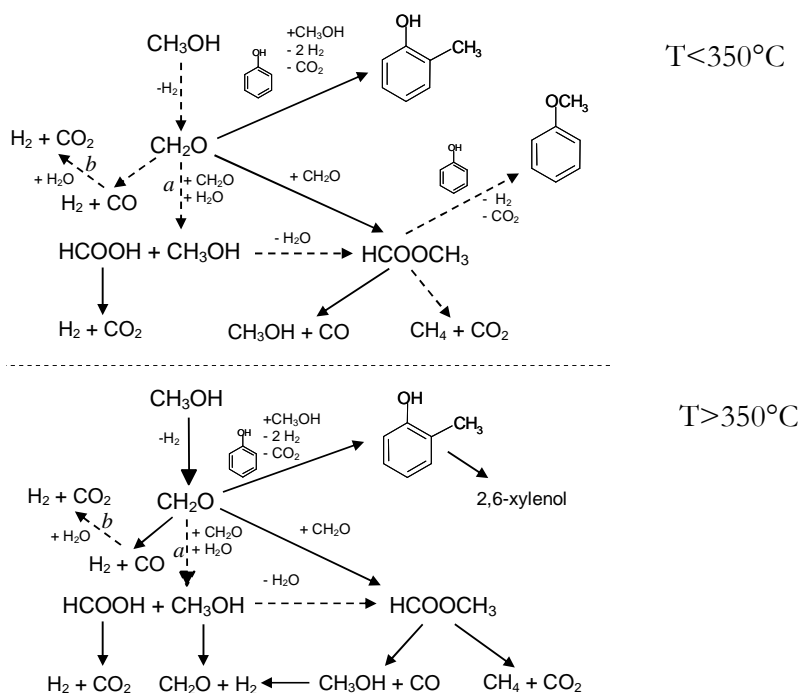


Figure 13. Schematic representation of the main reactions occurring in the gas-phase methylation of phenol with methanol in basic catalysis. Dotted arrows represent reactions kinetically less favored. *a*: favoured in the presence of water (tests with formalin solution). *b*: favoured in the presence of water and of Fe.

Therefore, the nature of the products obtained by reaction between phenol and methanol is governed by the transformations occurring on methanol, which are a function of the catalyst type. This is also demonstrated by the results of (a) the reaction between phenol and formaldehyde over the acid catalyst, with the formation of the same products that are typically obtained in the basic-catalysed methylation of phenol, and (b) the reaction between phenol and methyl iodide over the basic catalyst, with the formation of the same products that are obtained in the acid-catalysed methylation of phenol.

3.6. References

- [1] K. Tanabe, T. Nishizaki, *Proceed. 6th ICC*, G.C. Bond et al. (Eds), The Chemical Society, London (1977), p. 863.
- [2] K. Tanabe, *Stud. Surf. Sci. Catal.*, 20 (1985) 1.
- [3] K. Sreekumar, S. Sugunan, *J. Mol. Catal. A* 185 (2002) 259
- [4] T. Tsai, F. Wang, *Catal. Lett.* 73 (2001) 167.
- [5] N. Ballarini, F. Cavani, L. Maselli A. Montaletti, S. Passeri, D. Scagliarini, C. Flego, C. Perego, *J. Catal.* 251 (2007) 423.
- [6] US Patent 4,933,509 (1989), assigned to General Electric.
- [7] H. Grabowska, W. Kaczmarczyk, J. Wrzyszczyk, *Appl. Catal.*, 47 (1989) 351.
- [8] H. Grabowska, W. Mista, J. Trawczynski, J. Wrzyszczyk, M. Zawadzki, *Appl. Catal. A*, 220 (2001) 207.
- [9] F. Cavani, L. Maselli, D. Scagliarini, C. Flego, C. Perego, *Stud. Surf. Sci. Catal.*, 155 (2005) 167.
- [10] S. Velu, C.S. Swamy, *Appl. Catal. A*, 162 (1997) 81.
- [11] US Patent 6,897,175 (2005), assigned to General Electric.
- [12] R.N. Spitz, J.E. Barton, M.A. Barteau, R.H. Staley, A.W. Sleight, *J. Phys. Chem. B* 90 (1986) 4067.
- [13] D.R. Taylor, K.H. Ludlum, *J. Phys. Chem.* 76 (1972) 2882.
- [14] Z. Hou, T. Okuhara, *Chem. Comm.* (2001) 1686.
- [15] A. Corma, H. Garcia, J. Miralles, *Microp. Mesop. Mater.* 43 (2001) 161.

- [16] J. Tateiwa, E. Hayama, T. Nishimura, S. Uemura, *Chem. Lett.*, (1996) 59.
- [17] J. Tateiwa, E. Hayama, T. Nishimura, S. Uemura, *J. Chem. Soc. Perkin Trans. 1*, (1997) 1923.
- [18] T. Nishimura, S. Ohtaka, A. Kimura, E. Hayama, Y. Haseba, H. Takeuchi, S. Uemura, *Appl. Catal. A*, 194 (2000) 415.
- [19] A.E. Palomares, G. Eder-Mirth, J.A. Lercher, *J. Catal.*, 168 (1997) 442.
- [20] A.E. Palomares, G. Eder-Mirth, M. Rep, J.A. Lercher, *J. Catal.*, 180 (1998) 56.
- [21] S.T. King, J.M. Garces, *J. Catal.*, 104 (1987) 59.
- [22] H. Itoh, A. Miyamoto, Y. Murakami, *J. Catal.*, 64 (1980) 284.
- [23] G. Madhavi, S.J. Kulkarni, K.V.V.S.B.S.R. Murthy, V. Viswanathan, K.V. Raghavan, *Appl. Catal. A* 246 (2003) 265.
- [24] S.B. Hamilton, US Patent 3,446,856 (1969), assigned to Schenectady.
- [25] T. Mathew, M. Vijayaraj, S. Pai, B.B. Tope, S.G. Hegde, B.S. Rao, C.S. Gopinath, *J. Catal.*, 227 (2004) 175.
- [26] S. Sato, K. Koizumi, F. Nozaki, *J. Catal.*, 178 (1998) 264.
- [27] S. Sato, R. Takahashi, T. Sodesawa, K. Matsumoto, Y. Kamimura, *J. Catal.*, 184 (1999) 180.
- [28] A.H. Padmasri, A. Venugopal, V. Durgakumari, K.S. Rama Rao, P. Kanta Rao, *J. Molec. Catal. A*, 188 (2002) 255.
- [29] A. Radhe Shyam, R. Dwivedi, V.S. Reddy, K.V.R. Chary, R. Prasad, *Green Chem.*, 4 (2002) 558.

- [30] L.H. Klemm, J. Shabtai, D.R. Taylor, *J. Org. Chem.*, 33 (1968) 1480.
- [31] E.I. Heiba, P.S. Landis, *J. Catal.*, 3 (1964) 471.
- [32] A.R. Gandhe, J.B. Fernandes, *J. Mol. Catal. A* 226 (2005) 171.
- [33] I. B. Borodina, , E. B. Pomakhina, , Ts. M. Ramishvili, , O. A. Ponomareva, A. I. Rebrov, I. I. Ivanova, *Russ. J. Phys. Chem.* 80 (2006) 892.
- [34] C. Zerbe, F. Jage, *Brennstoff-Chemie* No 5, 16 (1935) 88.
- [35] K. Shanmugapriya, S. Saravanamurugan, M. Palanichamy, B. Arabindoo, V. Murugesan, *J. Molec. Catal. A*, 223 (2004) 177.

Chapter 4

The interaction between the reactants and the surface

4.1. Introduction

The major problem of the industrial process of phenol methylation is the decomposition of methanol and, consequently, a large excess of methanol is usually fed, in order to reach an acceptable per-pass conversion of phenol [1]. In this context it is surprising that the potential role of methanol surface chemistry and eventual decomposition during the alkylation of phenols is hardly addressed [2,3,4]. It should be noted here that usually the alkylation of aromatic rings is catalyzed by acids [5,6] and that bases catalyze the side chain alkylation of toluene with methanol. For the latter reaction, the dehydrogenation of methanol to formaldehyde was shown to be a prerequisite [7-9].

In the present chapter, we explore the catalysis with MgO as typical (albeit not most active) catalyst with the aim of establishing the mechanism of catalysis alkylation of aromatic compounds with nucleophilic functionalisation. Phenol is used as substrate for conversion, as its simplicity offers a better route for probing the surface chemical species by a combination of *in situ* vibrational spectroscopy and theoretical calculations. The measurements and calculations allow us to postulate and test the kinetic sequence of elementary steps and to lead to clear

design parameters for the selective alkylation of functionalised aromatic compounds.

4.2. Experimental

The catalysts employed were a commercial MgO, supplied by Acros Organics, and a synthesized MgO, having specific surface areas of 12 and 68 m²/g, respectively [10].

Catalytic tests were carried out by vaporization of a methanol/phenol liquid mixture (methanol/phenol molar ratio 10/1; liquid flow 0.0061 ml/min; phenol supplied by Sigma Aldrich, 99+% purity; methanol supplied by Carlo Erba Reagenti) in a N₂ stream (gas flow 20 Nml/min). The composition of the feed gas was the following (molar fractions): methanol 0.108, phenol 0.011, and nitrogen 0.881. The residence time was 2.7 s (in experiments varying the temperature), or was varied in order to obtain very low phenol conversions. In the latter case, the reaction temperature was 250°C. Total pressure was atmospheric. The gas/vapors stream was fed to a tubular glass reactor (length 30 cm, internal diameter $\frac{3}{4}$ "), containing either 1 cm³ of catalyst (catalyst weight 0.85 g, experiments with varying temperature) or variable amounts of catalyst (experiments with varying residence time) shaped in 30-60 mesh particles.

For the FT-IR, MgO samples were pressed into thin self-supported wafer and activated in situ in the IR cell at 450°C under vacuum for 2 h. Before measuring the IR spectra, the activated sample was contacted with 2-4 mbar of the sorptive either at 250°C, or at increasing temperatures from ambient to 550°C. For recording spectra, 25 scans were co-added. The IR spectra reported are displayed as difference absorbance spectra of the sample with and without the absorbed molecule.

4.3. Results

4.3.1. Catalytic phenol methylation

Figure 1 compiles the results of the catalytic gas-phase methylation of phenol with methanol over the low-surface-area MgO as function of the reaction temperature, displaying the conversion of phenol and the selectivity to the reaction products.

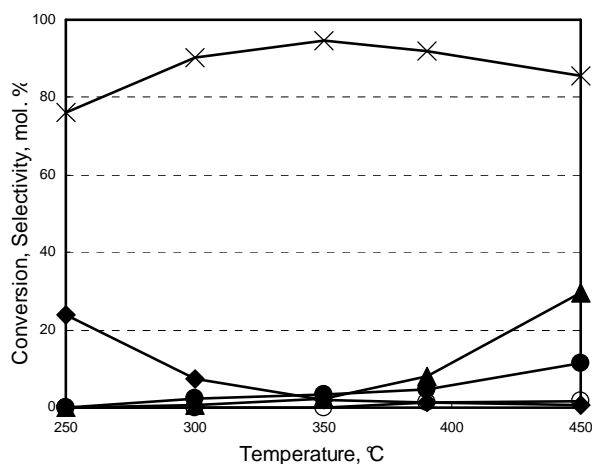


Figure 1. Conversion of phenol (▲), and selectivity to anisole (◆), *o*-cresol (×), *p*-cresol (○) and 2,6-xyleneol (●), over MgO as function of the reaction temperature.

The conversion of phenol was low, despite the high methanol/phenol feed ratio [10,11]. The main product of reaction was *o*-cresol. At low temperatures, also anisole formed (selectivity less than 10%), but its selectivity decreased disappearing above 350°C. The selectivity to *o*-cresol declined slightly with increasing reaction temperature due to the formation of 2,6-xyleneol. *p*-Cresol formed in negligible amounts (selectivity lower than 1%). The product distribution was very similar to those obtained with other MgO catalysts reported [10,11].

The variation in selectivity at 250°C as a function of the conversion of phenol is shown in Figure 2. The primary products were salicylic aldehyde and anisole; however, also a direct contribution for *o*-cresol cannot be excluded, indicating that three parallel reaction pathways exist.

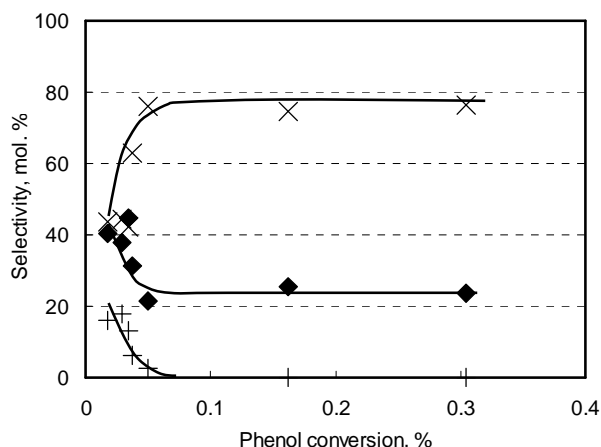


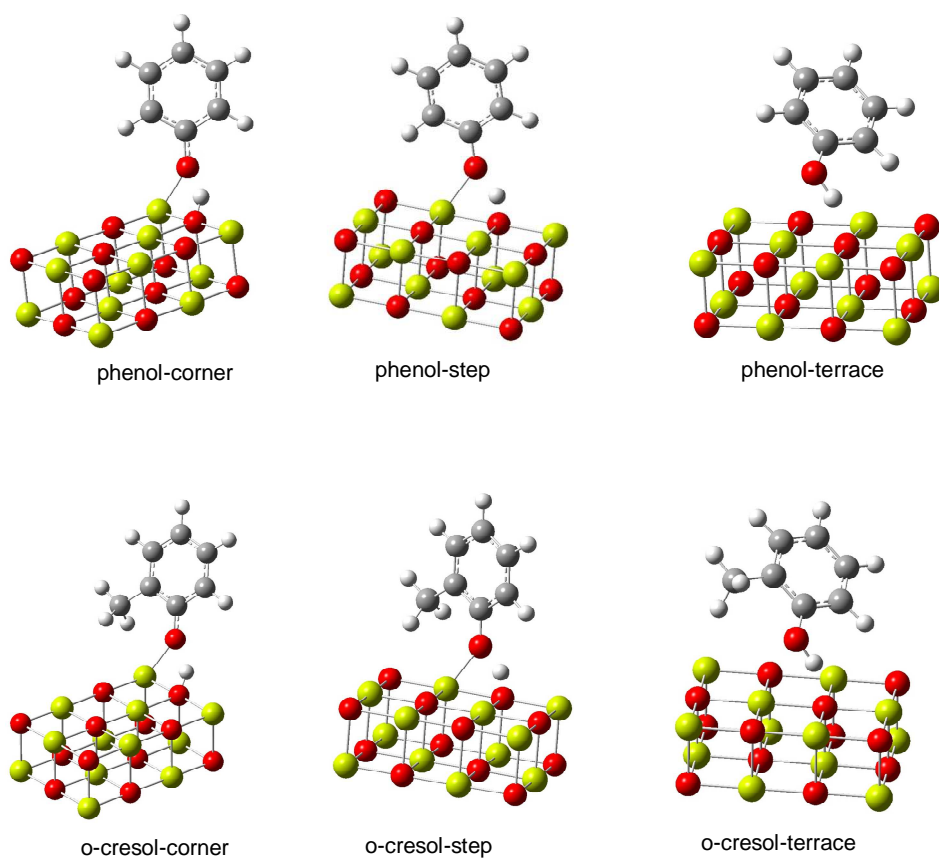
Figure 2. Selectivity to products as function of phenol conversion over MgO at 300°C Symbols: anisole (◆), salicylic aldehyde (⊕) and *o*-cresol (×)

With increasing conversion, (residence time) salicylic aldehyde was reduced to *o*-cresol. Thus, *o*-cresol is produced *via* a direct and an indirect pathway *via* formation of salicylic aldehyde. At phenol conversion above 0.05%, anisole and *o*-cresol were the only reaction products. The two products do not interconvert.

Salicylic aldehyde is likely formed by reaction between phenol and formaldehyde, the latter having formed by methanol dehydrogenation, [10,11]. Salicylic aldehyde is a very reactive intermediate that can be recovered only under very unusual reaction conditions, i.e., low temperatures as well as extremely low contact times and phenol conversions (Figure 2). At low temperatures, however, the dehydrogenation of methanol to formaldehyde is less favored [11]. Therefore, the question arises whether salicylic aldehyde is the reaction intermediate in the formation of *o*-cresol under reaction conditions leading to high phenol and methanol conversion. It should be noted that the reaction between phenol and formaldehyde should lead to the formation of salicylic alcohol as a first intermediate, not to salicylic aldehyde. In order to explore the proposed reaction pathway theoretical calculations and IR spectroscopic measurements were combined to understand surface structures and potential intermediates.

4.3.2. Sorption of phenol, *o*-cresol, salicylic alcohol, and salicylic aldehyde on MgO

Figure 3 compiles the optimized models for the adsorption of phenol, *o*-cresol, salicylic alcohol and salicylic aldehyde on three different sites of a $(\text{MgO})_{12}$ cluster representing MgO surface sites. In order to account for differences in the coordination of Mg and O, the sites for adsorption considered are those corresponding to the corner, step (edge), and terrace positions.



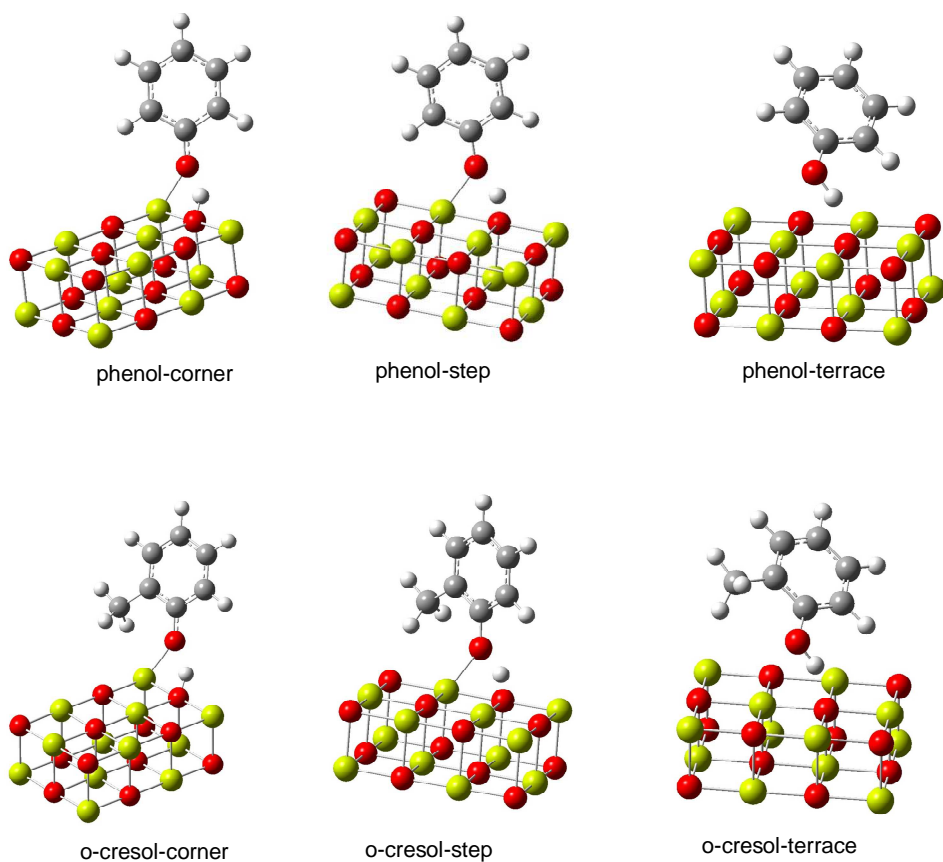


Figure 1. Optimized structured

Tables 1 - 4 compile the main molecular properties in the adsorbed state, i.e., adsorption energy, interatomic distances, and the COH angle at equilibrium. For comparison, the reference values for the corresponding isolated molecules are also given.

Table 1. Main molecular properties of phenol adsorbed on MgO surface: adsorption energy (E_{ads}), interatomic distances (d) and angle (\hat{A}) at equilibrium. In parenthesis are given the BSSE corrected adsorption energies.

	phenol-isolated	phenol-corner	phenol-step	phenol-terrace
$E_{\text{ads}}/\text{kcal mol}^{-1}$		-43	-27 (-20)	-17 (-10)
$d(\text{Mg}_{\text{cry}}\text{-O}_{\text{mol}})/\text{\AA}$		1.909	2.021	2.691
$d(\text{O}_{\text{cry}}\text{-H}_{\text{mol}})/\text{\AA}$		1.001	1.055	1.647
$d(\text{O-H})/\text{\AA}$	0.966	1.709	1.421	1.010
$d(\text{C-O})/\text{\AA}$	1.389	1.342	1.346	1.363
$A(\text{C}\hat{\text{O}}\text{H})/^\circ$	108.83	128.77	128.71	111.29

Table 2. Main molecular properties of *o*-cresol adsorbed on MgO surface: adsorption energy (E_{ads}), interatomic distances (d) and angle (\hat{A}) at equilibrium. In parenthesis are given the BSSE corrected adsorption energies.

	<i>o</i> -cresol-isolated	<i>o</i> -cresol-corner	<i>o</i> -cresol-step	<i>o</i> -cresol-terrace
$E_{\text{ads}}/\text{kcal mol}^{-1}$		-40	-24 (-17)	-14 (-8)
$d(\text{Mg}_{\text{cry}}\text{-O}_{\text{mol}})/\text{\AA}$		1.912	2.037	2.661
$d(\text{O}_{\text{cry}}\text{-H}_{\text{mol}})/\text{\AA}$		1.000	1.070	1.646
$d(\text{O-H})/\text{\AA}$	0.965	1.704	1.393	1.010
$d(\text{C-O})/\text{\AA}$	1.370	1.340	1.349	1.366
$A(\text{C}\hat{\text{O}}\text{H})/^\circ$	109.41	141.00	122.65	111.08

Table 3. Main molecular properties of salicylic alcohol adsorbed on MgO surface: adsorption energy (E_{ads}), interatomic distances (d) and angle (\hat{A}) at equilibrium. In parenthesis are given the BSSE corrected adsorption energies.

	salicylic alcohol isolated	salicylic alcohol corner	salicylic alcohol step	salicylic alcohol terrace
$E_{\text{ads}}/\text{kcal mol}^{-1}$		-54	-35 (-22)	-30 (-16)
$d(\text{Mg}_{\text{cry}}\text{-O}_{\text{mol}})/\text{\AA}$		1.997	2.057	2.492
$d(\text{O}_{\text{cry}}\text{-H}_{\text{mol}})/\text{\AA}$		0.972	1.037	1.053
$d(\text{O-H})/\text{\AA}$	0.977	2.426	1.519	1.449
$d(\text{C-O})/\text{\AA}$	1.361	1.315	1.346	1.316
$A(\text{C}\hat{\text{O}}\text{H})^\circ$	106.94	52.245	107.82	104.65
$d(\text{Mg}_{\text{cry}}\text{-O}_{\text{Alc}})/\text{\AA}$		2.384	2.258	2.317
$d(\text{O}_{\text{cry}}\text{-H}_{\text{Alc}})/\text{\AA}$		1.749	1.415	1.948
$d(\text{O-H}_{\text{Alc}})/\text{\AA}$	0.966	0.996	1.051	0.981
$d(\text{CH}_2\text{-O}_{\text{Alc}})/\text{\AA}$	1.444	1.439	1.431	1.441

Table 4. Main molecular properties of salicylic aldehyde adsorbed on MgO surface: adsorption energy (E_{ads}), interatomic distances (d) and angle (\hat{A}) at equilibrium. In parenthesis are given the BSSE corrected adsorption energies.

	salicylic aldehyde isolated	salicylic aldehyde corner	salicylic aldehyde step	salicylic aldehyde terrace
$E_{\text{ads}}/\text{kcal mol}^{-1}$		-61	-25 (-17)	-4 (6)
$d(\text{Mg}_{\text{cry}}\text{-O}_{\text{mol}})/\text{\AA}$		2.049	2.152	2.244
$d(\text{O}_{\text{cry}}\text{-H}_{\text{mol}})/\text{\AA}$		0.974	1.007	1.031
$d(\text{O-H})/\text{\AA}$	0.989	1.758	1.586	1.496
$d(\text{C-O})/\text{\AA}$	1.339	1.295	1.306	1.308
$A(\text{C}\hat{\text{O}}\text{H})^\circ$	107.03	115.98	128.91	142.70
$d(\text{Mg}_{\text{cry}}\text{-O}_{\text{Ald}})/\text{\AA}$		2.101	2.198	2.273
$d(\text{C=O}_{\text{Ald}})/\text{\AA}$	1.235	1.253	1.241	1.225

The adsorption energies on the terrace site are in general weak. The adsorption energies are higher for step sites and the highest on corner sites, i.e., the values increase with decreasing coordination of the atom. With increasing strength of interaction the phenolic O-H bond length in the molecule increases causing a more pronounced distortion in the molecular geometry. For adsorption on terrace sites, the O-H group interacts associatively. Upon adsorption on coordinatively unsaturated sites the OH group dissociates. It should be noted that adsorption of phenol on MgO is reported to lead to phenolate species and surface OH groups [12]. The energetically most favored adsorption configuration is that one in which the adsorbed molecule adopts an orthogonal orientation with respect to the MgO surface. In agreement with literature [13,14], we would like to conclude that this orientation is caused by the repulsion of the aromatic ring by the electron rich surface oxygen.

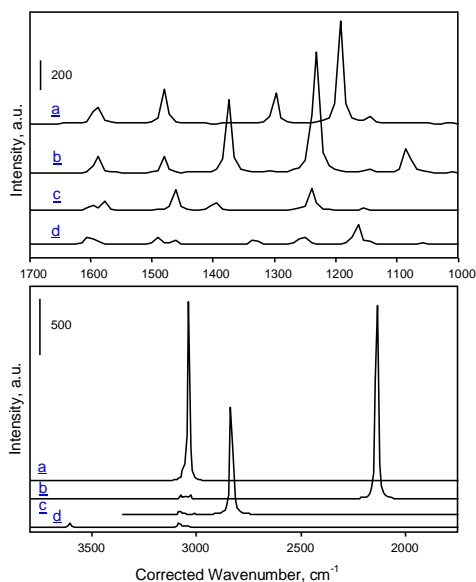


Figure 4. Calculated IR spectra of phenol adsorbed on MgO, corner site (a), step site (b), terrace site (c) and free molecule (d).

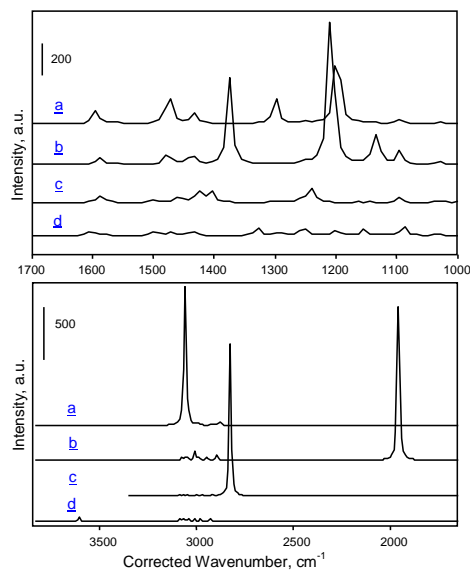


Figure 5. Calculated IR spectra of *o*-cresol adsorbed on MgO, corner site (a), step site (b), terrace site (c) and free molecule (d).

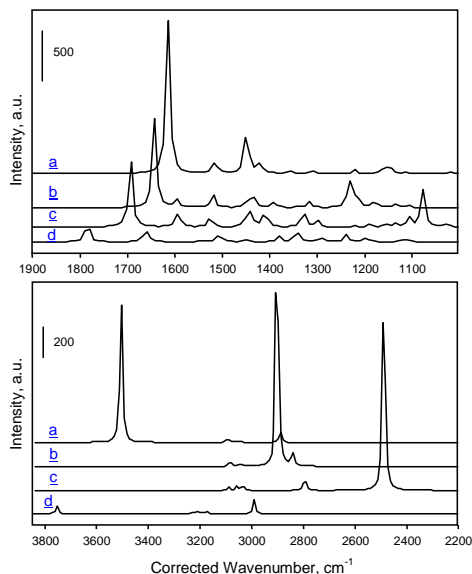


Figure 6. Calculated IR spectra of salicylic aldehyde adsorbed on MgO, corner site (a), step site (b), terrace site (c) and free molecule (d).

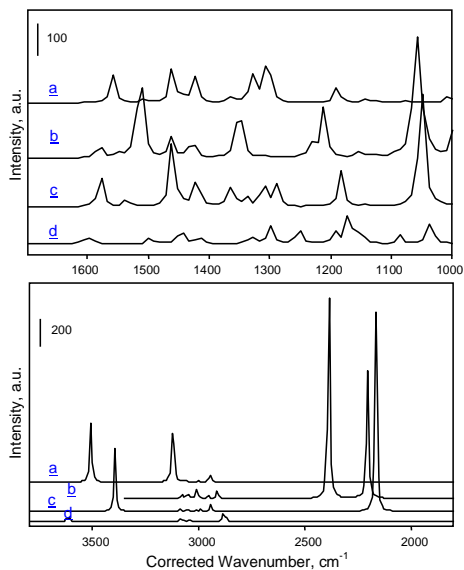


Figure 7. Calculated IR spectra of salicylic alcohol adsorbed on MgO, corner site (a), step site (b), terrace site (c) and free molecule (d).

Figures 4-7 compare the IR spectra calculated for sorptive molecules adsorbed over the different defective sites of MgO with the calculated spectrum of the gas-phase molecule. In the case of phenol (Figure 4), the spectra of the adsorbed molecules are similar, the only relevant difference being the frequency of C-O stretching band at 1300 cm^{-1} when phenol is adsorbed in the corner position, but at considerably lower values for the step (1237 cm^{-1}) and the terrace (1241 cm^{-1}) positions differences in the C-O bond strength. The same is observed for *o*-cresol (Figure 5). In the case of salicylic aldehyde (Figure 6), the main difference between spectra is the frequency of the C=O stretching, that shifts from 1616 cm^{-1} for the molecule adsorbed in the corner position, to 1693 cm^{-1} for the gas-phase molecule. Finally, also in the case of salicylic alcohol the main difference between the spectra concern the frequencies assigned to C-O and O-H vibrations, i.e., the alcohol dissociates on corner and edge sites and adsorbs associatively at the terrace sites.

In all spectra of adsorbed molecules, a very intense band above 2000 cm^{-1} is assigned to an O-H stretching vibration. Specifically, in the case of phenol and *o*-cresol adsorption on the corner and the edge site, the phenolic OH group

dissociates, and the intense band observed in the calculated spectrum is related to the MgO-H vibration. On the contrary, for adsorption of these molecules on the terrace site, the phenolic OH is undissociated, and the band in the calculated spectrum refers to this latter bond. The case for salicylic alcohol and salicylic aldehyde are different. In this latter case, the model predicts the dissociation of the phenolic OH on all types of sites. When the interaction of phenol with the adsorption site leads to a weakening of the phenolic O-H bond, the calculated wavenumber becomes lower than that one of OH in free phenol (for the latter, the experimental value was 3648 cm^{-1} , the calculated one, 3663 cm^{-1}), in which $d\text{ O-H} = 0.966\text{ \AA}$. When the latter bond dissociates on the corner or step site, the $\text{O}_{\text{cry}}\text{-H}$ bond formed ($d\text{ }1.001\text{ \AA}$ for phenol on the corner site and 1.055 \AA on the step site) shows the vibration at 3038 cm^{-1} for the corner site and at 2137 cm^{-1} for the step site.

At this point we would like to note that the calculation of the stretching vibration of hydroxy groups on magnesia is greatly affected by the type of program and the basis set used for the computation. This has been recently addressed by Chizallet et al. [15]. Therefore, relevant differences are observed between the experimental vibration of the phenolic OH in the free and adsorbed molecule (which are observed above 3600 cm^{-1} , in both cases) and the corresponding calculated frequencies. Nevertheless, the method used by us for computation is internally consistent, with respect to the relationship between the bond length of the -OH group and the calculated frequency. In fact, if we consider the length of the shorter O-H bond in the Ph-O---H---O-Mg complex (that in the case of the corner and step, is the Mg-OH, because the phenol is dissociated into phenolate, whereas in the case of the terrace is the Ph-OH), taken from Tables 1-4, for the four molecules investigated, and plot it versus the corresponding vibrational frequency a perfect linear correlation is obtained

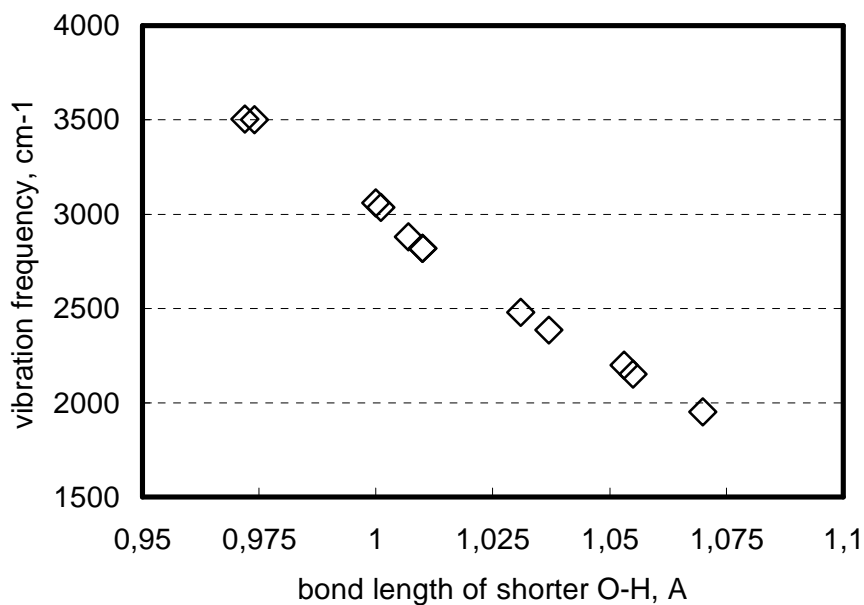


Figure 8. Calculated vibration frequency of the shortest O-H bond in the Ph-O---H---O-Mg complex for adsorbed phenol, *o*-cresol, salicylic aldehyde and salicylic alcohol in function of the calculated O-H bond length.

Experimental IR spectra were recorded after adsorption of the molecules on commercial low-surface-area MgO and on synthetic high-surface-area MgO.

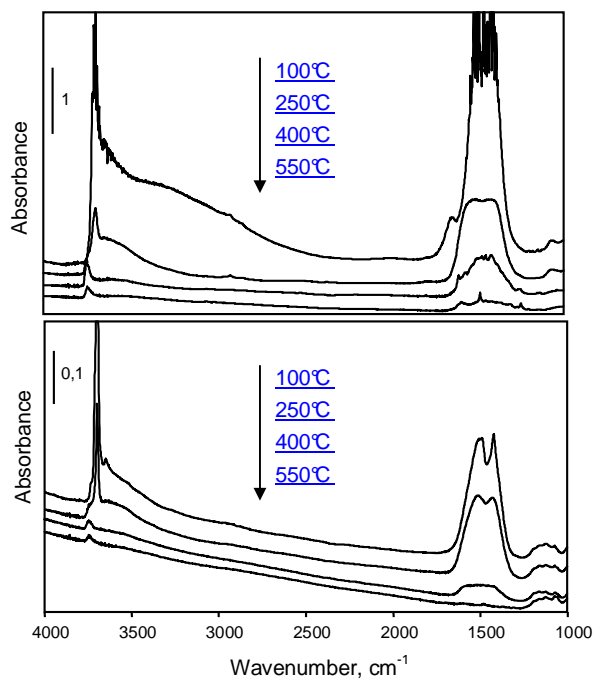


Figure 8. IR spectra of high (a) and low surface area (b) MgO activated in dynamic vacuum (10^{-5} mbar) at different activation temperatures

The IR spectra of the two materials after evacuation at increasing temperatures are depicted in Figure 8. The spectra for the two materials are similar, but the bands attributed to the carbonate and to the OH groups are more intense for the high-surface-area MgO.

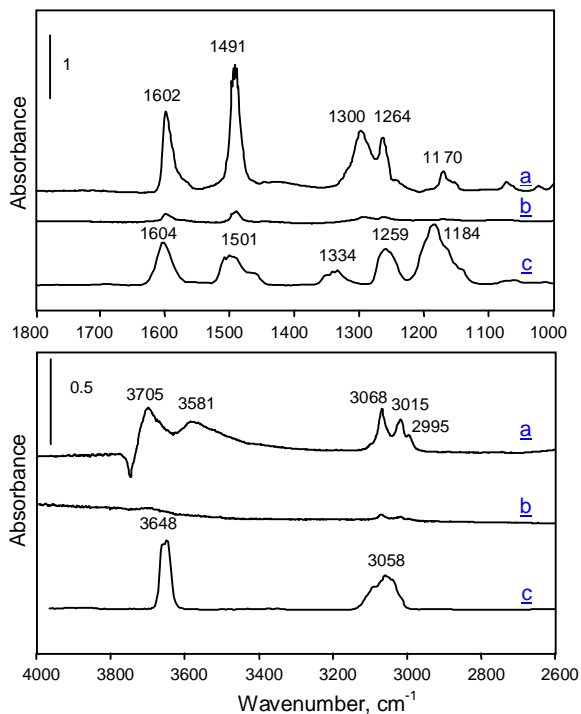


Figure 9. Difference IR spectra of phenol adsorbed over high-surface-area (a) and low-surface-area (b) MgO, and gas-phase phenol (NIST library) (c).

Figure 9 compiles the difference IR spectrum of phenol after adsorption on activated commercial and synthetic MgO at 250°C, and the reference gas-phase spectrum. Table 5 summarizes the experimental and calculated frequencies, and the corresponding vibration modes. Calculated wavenumbers correspond to adsorption at the corner site, which according to the computational study is the energetically preferred one.

Table 5. Vibrational frequencies and assignments of chemisorbed phenol

$\nu_{\text{theor.}} (\text{cm}^{-1})$	$\nu_{\text{exp.}} (\text{cm}^{-1})$	Assignments
1056	1074	δ (CH)
1134	1152	δ (CH)
1144	1170	δ (CH)
1192		δ ($\text{O}_{\text{cry}}\text{H}$)
1262	1264	δ (CH), ν (CC), δ ($\text{O}_{\text{cry}}\text{H}$)
1298	1300	ν (CO), δ (CH)
1304		δ (CH), ν (CC)
1434		δ (CH)
1478	1491	ν (CO), δ (CH)
1561		ν (CC), δ (CH)
1590	1602	ν (CC), δ (CH)
3038		ν ($\text{O}_{\text{cry}}\text{H}$), ν (CH)
3043	2995	ν (CH)
3047	3015	ν (CH)
3060		ν (CH)
3064	3068	ν (CH)
3079		ν (CH)

A small negative band at 3740 cm^{-1} indicates that some phenol molecules interact with residual OH groups on the MgO surface. Two small bands of perturbed OH groups at 3705 and 3581 cm^{-1} are also observed. Between 3010 and 3070 cm^{-1} bands of stretching vibrations of C-H in the aromatic ring are observed, at 1602 cm^{-1} and at 1491 cm^{-1} the C-C ring vibrations, and at 1170 and at 1074 cm^{-1} the band of C-H bending. The band at 1300 and 1264 cm^{-1} are attributed to C-O

stretching mode. The correspondence between the experimental and the calculated spectrum for the phenol adsorbed on the corner site is very good when considering the empirical correction discussed above.

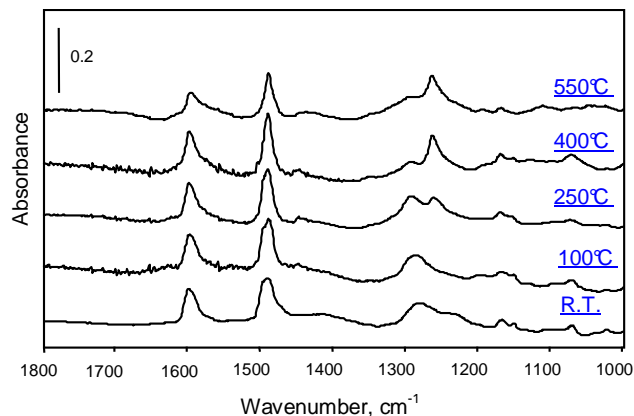


Figure 10. Difference IR spectra of phenol after adsorption at room temperature over low-surface-area MgO, and after heating at increasing temperatures.

Figure 10 compiles the difference IR spectrum of phenol adsorbed over commercial MgO recorded at increasing temperatures, after adsorption at room temperature. When the temperature is increased, the most relevant differences appear in the range between 1250 and 1300 cm⁻¹, with a progressive increase of the intensity of the band at 1264 cm⁻¹ (attributed to the C-O vibration in undissociated phenol) and the corresponding decrease of that at 1296 cm⁻¹ (attributed to the C-O of phenolate). These variations indicate the progressive weakening of the interaction between phenol and MgO.

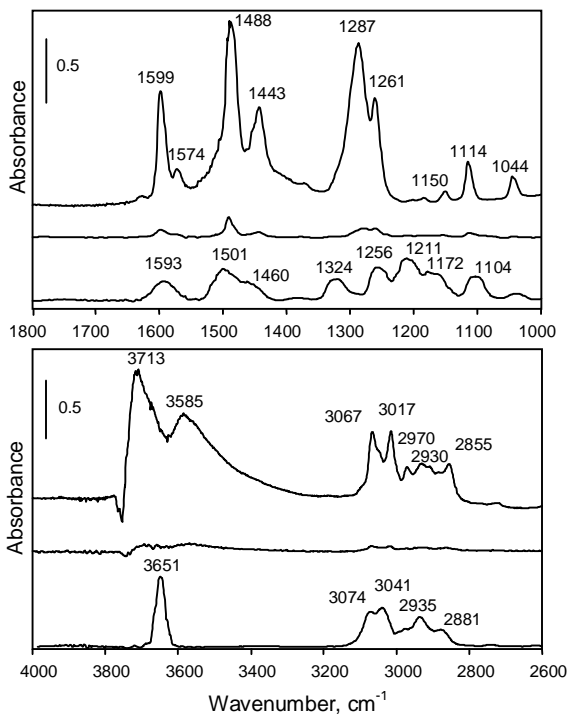


Figure 11. Difference IR spectra of *o*-cresol adsorbed over high-surface-area (a) and low-surface-area (b) MgO, and gas-phase *o*-cresol (NIST library) (c).

Figure 11 shows the difference spectra of *o*-cresol adsorbed on MgO and the gas-phase spectrum; Table 6 summarizes the calculated and experimental frequencies, and the corresponding vibration modes.

Table 6. Vibrational frequencies and assignments of chemisorbed *o*-cresol

$\nu_{\text{theor.}} (\text{cm}^{-1})$	$\nu_{\text{exp.}} (\text{cm}^{-1})$	Assignments
1027		$\delta (\text{CH})_{\phi}$
1095	1114	$\delta (\text{CH})$
1133		$\delta (\text{CH})_{\phi}$
1163		$\delta (\text{CH}), \nu (\text{ph-C})$
1249	1261	$\delta (\text{CH})$
1294		$\delta (\text{CH}), \nu (\text{CC})$

1299	1278	δ (CH), ν (CO)
1361		δ (CH) _{CH3}
1431	1444	δ (CH) _{CH3} , δ (CH), ν (CC)
1441		δ (CH) _{CH3}
1462		δ (CH) _{CH3}
1474	1491	δ (CH), ν (CC), ν (CO)
1560	1573	ν (CC), δ (CH)
1593	1599	ν (CC), δ (CH)
2877	2866	ν (CC) _{CH3}
2918	2926	ν (CC) _{CH3}
2993	2974	ν (CC) _{CH3}
3040	3025	ν (CC) _{ϕ}
3043		ν (CC) _{ϕ}
3059		ν (O _{cryst} H) _{ϕ} , ν (CC) _{ϕ}
3077	3068	ν (CC) _{ϕ}

As with phenol, a small negative band is observed at 3740 cm⁻¹, together with two bands of perturbed OH groups at 3713 and 3585 cm⁻¹. As for phenol, the adsorption at 250°C leads to an alteration of vibration modes of phenolic OH in the 1200 cm⁻¹ region, due to the dissociation of the hydroxyl group. The stretching vibrations of C-H in methyl, although of low intensity, are present at 2970, 2930 and 2855 cm⁻¹ for the adsorbed molecule; this means that the adsorption occurs in such a way to allow the interaction of the methyl group with the surface. Also in this case, there is a good correspondence between the experimental spectrum and the calculated one for adsorption on the corner site.

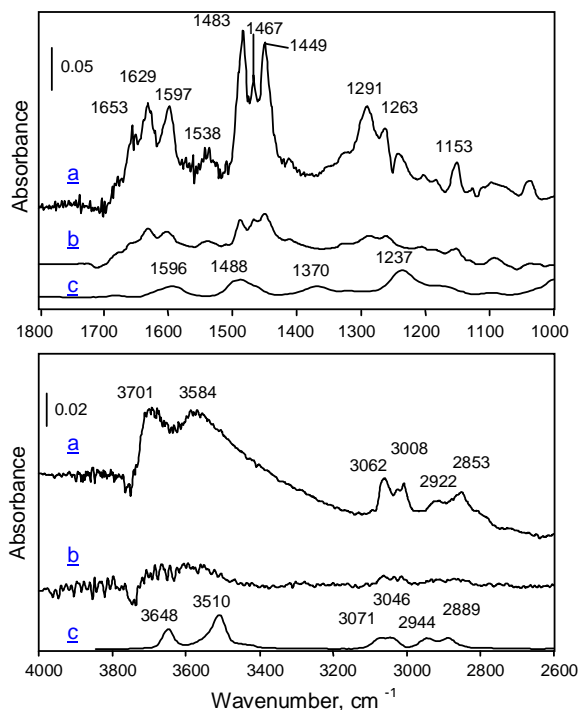


Figure 12. Difference IR spectra of salicylic alcohol adsorbed over high-surface-area (a) and low-surface-area (b) MgO, and gas-phase salicylic alcohol (NIST library) (c).

Figure 12 shows the difference IR spectrum of adsorbed salicylic alcohol and the gas-phase spectrum. Table 7 summarizes the calculated and experimental frequencies, and the corresponding vibration modes.

Table 7. Vibrational frequencies and assignments of salicylic alcohol

$\nu_{\text{theor.}} (\text{cm}^{-1})$	$\nu_{\text{exp.}} (\text{cm}^{-1})$	Assignments
1007		$\delta (\text{CH})_{\phi}$
1076	1094	$\delta (\text{CH})$
1127	1132	$\delta (\text{CH})_{\phi}$
1141	1153	$\delta (\text{CH}), \nu (\text{ph-CH}_2\text{O})$
1189		$\delta (\text{CH})_{\Delta\text{lc}}, \delta (\text{CH})_{\phi}$
1233	1263	$\delta (\text{CH})_{\phi}, \delta (\text{CH})_{\Delta\text{lc}}$

1298	1291	δ (CH) $_{\phi}$, ν (ph-O)
1308		δ (CH), ν (ph-O)
1329		δ (CH) $_{Alc}$, δ (OH) $_{Alc}$
1362		δ (CH) $_{Alc}$, δ (OH) $_{Alc}$
1423		δ (CH) $_{Alc}$
1442	1449	δ (CH) $_{Alc}$
1459	1467	δ (CH) $_{Alc}$, δ (CH) $_{\phi}$, ν (ph-O) $_{Alc}$
	1483	
1505	1538	ν (CC) $_{\phi}$, δ (CH)
1557	1601	ν (CC) $_{\phi}$, δ (CH)
	1629	
2944	2875	ν (CH) $_{Alc}$
2995	2922	ν (CH) $_{Alc}$
3043	3008	ν (CH) $_{\phi}$
3057		ν (CH) $_{\phi}$
3066	3062	ν (CH) $_{\phi}$
3078	3111	ν (CH) $_{\phi}$
3119		ν (OH) $_{Alc}$
3506		ν (O $_{cry}$ -H)

The difference spectrum indicates adsorption on OH groups (negative band at 3740 cm⁻¹) and shows perturbed OH groups at 3701 and 3584 cm⁻¹. The bands between 2800 and 2950 cm⁻¹ are attributed to C-H stretching of the hydroxymethyl group, while bands between 3000 and 3100 cm⁻¹ are attributed to the C-H stretching vibrations of the aromatic ring. Band at 1449 cm⁻¹ is attributed to the bending of the C-H in the hydroxymethyl group. At 1597 and 1538 cm⁻¹ the

aromatic C-C stretching vibrations and at 1281 cm^{-1} the stretching of the bond between the O atom and the aromatic ring are observed. The band at 1153 cm^{-1} is assigned to the C-CH₂OH stretching vibration. The band at 1629 cm^{-1} in the spectrum of the adsorbed alcohol is tentatively attributed to a minor fraction of salicylic aldehyde formed upon adsorption (see below). The main difference between the experimental and the gas-phase spectrum concerns the C-O stretching vibration shifting from 1237 cm^{-1} (in the gas-phase spectrum) to 1291 cm^{-1} (in the experimental one). Differences with the calculated spectrum are also non-negligible, and might be attributed to the fact that the alcohol indeed rapidly reacts after adsorption at 250°C .

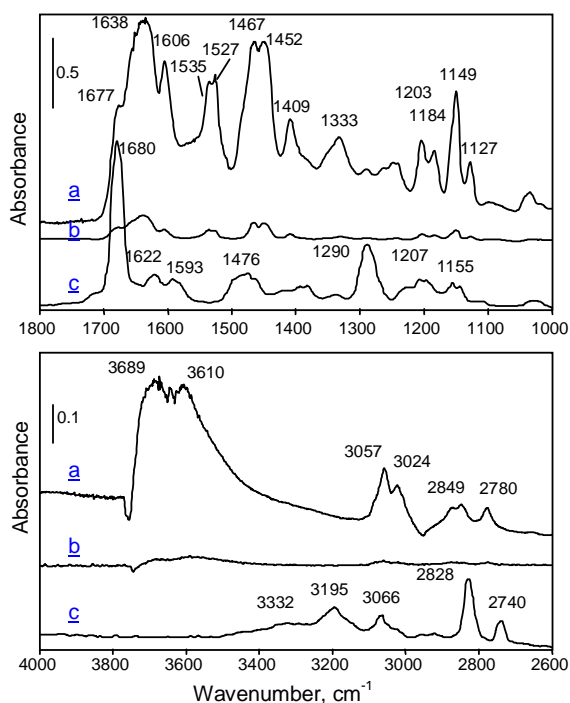


Figure 13. Difference IR spectra of salicylic aldehyde adsorbed over high-surface-area (a) and low-surface-area (b) MgO, and gas-phase salicylic aldehyde (NIST library) (c).

Figure 13 shows the difference IR spectra of adsorbed salicylic aldehyde and its gas-phase spectrum. Table 8 summarizes the calculated and experimental frequencies, and the corresponding vibration modes.

$\nu_{\text{theor.}} (\text{cm}^{-1})$	$\nu_{\text{exp.}} (\text{cm}^{-1})$	Assignments
1115	1126	δ (CH)
1145	1149	δ (CH)
1157	1183	ν (ph-CHO), δ (CH), ν (CC),
1221		δ (CH)
1310		ν (CC), δ (CH)
1358	1331	δ (CH), ν (CC) $_{\phi}$
1420	1409	δ (CH) $_{\text{Ald}}$
1438	1449	δ (CH), ν (CC)
1450	1466	δ (CH), ν (ph-O)
1515	1535	ν (CC), δ (CH)
1605	1606	ν (CC), δ (CH), ν (CO) $_{\text{Ald}}$
1614	1639	ν (CO) $_{\text{Ald}}$, δ (CH) $_{\text{Ald}}$, ν (ph-O)
	2779	Fermi resonance
2886	2876	ν (CH) $_{\text{Ald}}$
3050		ν (CH) $_{\phi}$
3061		ν (CH) $_{\phi}$
3080	3025	ν (CH) $_{\phi}$
3093	3062	ν (CH) $_{\phi}$
3501		ν (O $_{\text{cry}}$ H)

The good agreement between the experimental and the calculated spectrum allows exclude secondary reactions of the aromatic aldehyde such as the dismutation via the Tishchenko reaction [16].

For adsorbed salicylic aldehyde, bands between 3000 and 3090 cm^{-1} (attributed to the C-H stretching bands of the aromatic ring) as well as bands at 2876 and 2779 cm^{-1} (attributed the stretching of the C-H band of the aldehyde group) are observed; the latter one, not present in the calculated spectrum, derives from the Fermi resonance [17]. The characteristic band of the aldehyde C=O stretching vibration appears at 1638 cm^{-1} . The strong shift to lower wavenumbers compared to the gas-phase spectrum is due to the interaction of the carbonyl group with Mg^{2+} cations acting as Lewis acid sites. The bands at 1606 and 1535 cm^{-1} are attributed to the aromatic ring stretching vibrations, while the bands between 1409 and 1467 cm^{-1} to C-H bending vibrations. The band at 1333 cm^{-1} is attributed to C-O, being remarkably shifted with respect to the corresponding bands in *o*-cresol and salicylic alcohol spectra. The band at 1149 cm^{-1} corresponds to the vibration of C-CHO. According to the computational model, the salicylic aldehyde is deprotonated leading to an enhanced resonance effect and the consequent alteration of the vibrations of the carbonyl group. The stabilization of the aldehyde group by the basic O^{2-} and by the Mg^{2+} cation is in agreement with the shift experimentally found for the carbonyl bond stretching.

It is important to note that the aldehyde interacts with MgO at 250°C but does not undergo any transformation. This implies that salicylic aldehyde can be isolated as an intermediate in the reaction between phenol and methanol.

4.3.3. IR Spectra of methanol under reaction conditions

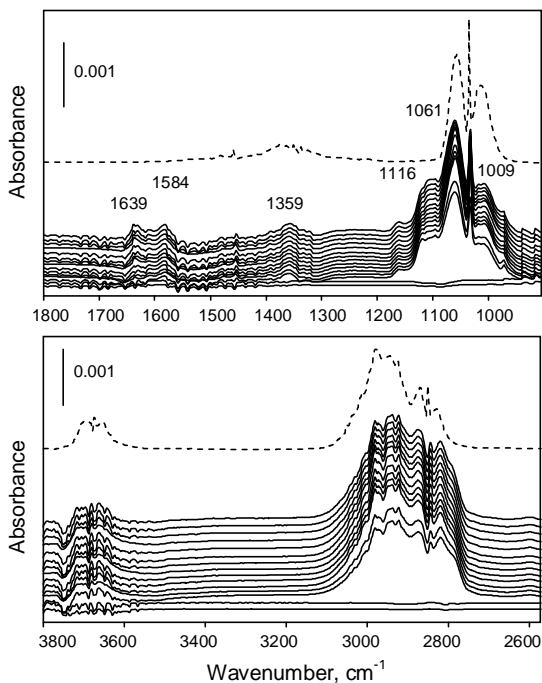


Figure 14. Details of spectral regions from the spectra recorded by flowing methanol at 250°C (dotted spectrum: gas-phase methanol) over the high-surface-area MgO.

Figure 14 compares the difference spectra registered in the presence of flowing methanol at 250°C over the high-surface-area MgO, with the gas-phase spectrum of methanol. The shape and intensity of the bands indicates that some contribution of gas-phase methanol is present in the difference spectra. On the other side, the difference between the spectrum of methanol in the gas phase and that of flowing methanol over MgO also shows that bands due to surface structures can be discriminated from the overlaying gas-phase spectra.

An increase of the feed time led to an increase of the intensity for bands at 971, 1009 (sh) and 1031 cm^{-1} ; the same occurred for the most intense peak at 1061 cm^{-1} . Bands at 1108 cm^{-1} and 1160 cm^{-1} are assigned to adsorbed methanol. The latter band is attributed to the rocking vibration of methyl group [5]. In this region, the bands due to vibrations of gas-phase methanol are easily recognized. At above 1300 cm^{-1} , bands at 1359, 1394, 1455 and 1584 cm^{-1} are observed. In the

wavenumber region of C-H stretching bands characteristic of gas-phase methanol overlapped with bands attributed to adsorbed methanol. Broad, ill resolved bands with maxima at 2790, 2821, 2842, 2873, 2921, 2942, 2981 and 3006 cm^{-1} were found. A broad band was observed between 3550 and 3730 cm^{-1} , together with a negative peak at 3747 cm^{-1} attributed to hydrogen bonding on MgOH groups.

One relevant aspect of this experiment is the asynchronous variation of the intensities during the reaction of methanol, especially in the region between 1200 and 1800 cm^{-1} . The relative intensities of bands at 1322, 1332, 1359, 1392, 1455, 1477 and 1584 cm^{-1} remained approximately constant. The bands with maxima at 1610 and 1639 cm^{-1} appeared only after some minutes after methanol was admitted and finally became more intense than the band centered at 1584 cm^{-1} . These bands are attributable to stretching vibrations of carbonates having different coordination [18]: $\nu_s \text{COO}^-$ at 1320, 1360 and 1390 cm^{-1} , and $\nu_{as} \text{COO}^-$ at 1637, 1610 and 1583 cm^{-1} , while the νCH_3 falls at 1332 cm^{-1} . The shoulder at 2790 cm^{-1} is likely due to the combined mode $\nu_s(\text{COO}^-) + \nu(\text{CH})$. The band with maxima at 1610 and 1637 cm^{-1} (and the corresponding symmetric stretching vibrations) can be attributed to the formation of bidentate carbonates, while that one at 1584 cm^{-1} is related to the development of formate species (1584 ν_{as} , 1390 ν_s , 2790 $\nu\text{C-H}$) [19]. Therefore, data indicate the initial formation of formates, followed by the slower formation of carbonates.

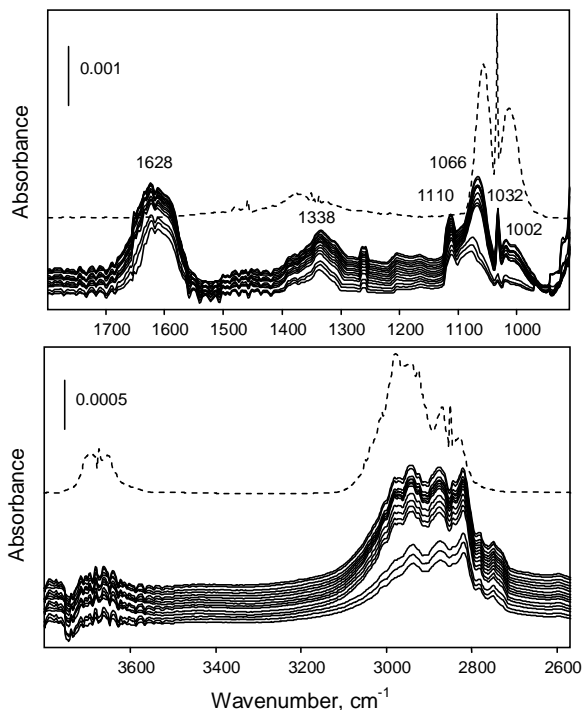


Figure 15. Details of spectral regions from the spectra recorded by flowing methanol at 450°C (dotted spectrum: gas-phase methanol) over the high-surface-area MgO.

Figure 15 displays the spectra recorded at 450°C. Under these conditions, the contribution of gas-phase methanol was lower than at 250°C. The band in the region between 1500 and 1700 cm^{-1} has maxima at 1612 and 1623 cm^{-1} , with shoulders at 1590 and 1560 cm^{-1} . The band is similar to that one obtained by dosing CO_2 over MgO [20]. In contrast with what observed at 250°C, there was no asynchronous variation of bands; this is likely due to the fact that the reaction having the higher activation energy was kinetically favored at the higher temperature. An evident phenomenon is the development of negative peaks in the hydroxyl zone at 3747 cm^{-1} , and at 1540 cm^{-1} (νCOO^-) in the carbonates zone; it is evident the presence of a methanol decomposition phenomenon. At 2780 and 2750 cm^{-1} are the bands due to the stretching vibration of the aldehydic C-H bond.

4.3.4. IR Spectra during reaction of methanol and phenol

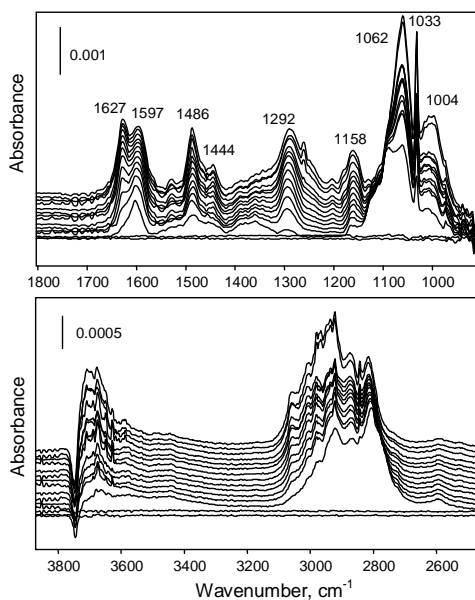


Figure 16. In-situ spectra recorded at 250°C while feeding methanol and phenol over high-surface-area MgO.

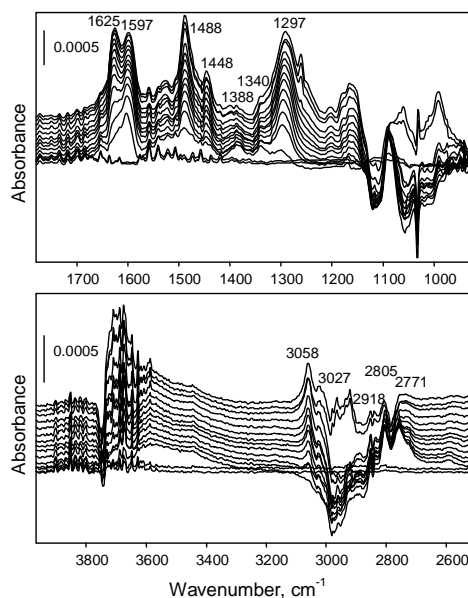


Figure 17. Difference IR spectra of surface species while passing methanol and phenol over high-surface-area MgO (Fig.16) and the IR spectra in the presence of methanol (Fig. 14)

Spectra recorded while feeding methanol and phenol at 250°C over the high-surface-area MgO, after subtraction of the MgO spectrum, are shown in Figure 16. Figure 17 reports the same spectra, but with the subtraction of the corresponding spectra obtained when only methanol was fed at the same time on stream (Figure 14). This allows minimize the interference of methanol (in the gas phase and adsorbed state) and of its products of transformation. Clearly, this is valid only provided the reaction network of methanol transformation is the same both in the absence and in the presence of phenol. Indeed, the spectra obtained have negative bands, likely due to the fact that the corresponding products formed from methanol either did not form in the presence of phenol or readily reacted with the latter.

It is evident that the spectrum recorded after reaction not only includes the bands relative to adsorbed reactants, but also additional bands due to the reaction products. One important feature was the band at 1597 cm^{-1} , that was present both

in the spectrum recorded after reaction and in the spectra of reaction intermediates as well. Also the band at 1486 cm^{-1} was present in all spectra, but not in that of adsorbed salicylic alcohol. The band at 1080 cm^{-1} is likely to be attributed to methanol. An intense peak at 1627 cm^{-1} was also present in the spectrum of adsorbed salicylic aldehyde (but it cannot be excluded it to be due to a formate species). In the spectral region between 3200 and 2600 cm^{-1} , the band at 2811 cm^{-1} can be attributed to methanol or to a product of its transformation, while bands between 3061 and 3010 cm^{-1} are due to aromatic C-H vibrations.

The main time dependent features of the spectra shown in Figure 16 include (i) the progressive increase of the band at 1444 cm^{-1} with time being attributed to the CH_3 bending vibration in *o*-cresol, (ii) the concomitant decrease of the intensity of the aldehydic C-H stretching band between 2700 and 2800 cm^{-1} and (iii) the increase of band at 1627 cm^{-1} .

The difference spectra (Figure 17) show the progressive increase of intensity for bands at 1297 , 1340 , 1388 , 1448 , 1488 , 1625 , 3027 and 3058 cm^{-1} , and the decrease of intensity for bands at 2918 , 2805 and 2771 cm^{-1} . This indicates that at short times on stream the relative concentration of the adsorbed species changes remarkably. At first, bands at 1597 , 1486 are in line with the rapid formation and adsorption of *o*-cresol. With time on stream, an aromatic compound with a C=O group (bands at 2771 , 2805 cm^{-1} , 1625 cm^{-1}), i.e., salicylic aldehyde, increases in concentration. Both products seem to be stable under the reaction conditions probed and evidences for the interconversion are not observable in the *in situ* IR spectra.

4.4. Discussion

4.4.1. The interaction of reactants and products with MgO

The interaction of methanol with MgO (as model oxide for basic oxides) has been studied by several authors [21-26] and it is well established that MgO catalyzes the dehydrogenation of methanol [27]. Chemisorption is claimed to occur

via heterolytic dissociation [23] involving the formation of hydroxyl groups and CH_3O^- anions [28]. Further abstraction of H^- by an accessible Mg^{2+} cation or a carbonaceous residue completes the step. Formation of surface formate species may occur through nucleophilic interaction of an adjacent oxygen atom with the carbon of the methylene group. Alternatively two sorbed formaldehyde molecules may disproportionate (via a nucleophilic attack) to formate and a methoxy species [25,29]. Formate may decompose to CO and H_2 . Alternatively, adsorbed methoxy and formate species may yield methylformate (Tishchenko reaction), which is able to decompose at high temperatures to methane and CO_2 .

The present data show that already at 250°C the interaction of methanol with the clean catalytic surface generates formate and carbonates species, clear evidences of the dehydrogenation of methanol and of the strong interaction with the basic surface. At high temperature the extent of methanol decomposition was relevant indicating that the formaldehyde generated is very reactive and is rapidly transformed to light compounds, i.e., CO , CH_4 and CO_2 , as also found in catalytic measurements over MgO .

In line with earlier reports [12,30,31] the present data show that the adsorption of phenol and phenol analogs (*o*-cresol, salicylic alcohol and salicylic aldehyde) on highly coordinatively unsaturated sites (corner sites) is energetically favorable. In this case, the interaction between MgO and the adsorbate is very strong, and leads to the dissociation of the sorbate at room temperature. The close agreement of the calculated and observed IR spectra for the phenol adsorbed on the corner sites support the interpretation.

4.4.2. The reaction between adsorbed reactants

In literature, the mechanism of reaction between phenol and methanol catalyzed by basic oxides is believed to occur by a direct electrophilic substitution on the aromatic ring with only few papers considering a possible role of formaldehyde. Palomares et al. [8,9] demonstrated that in the base - catalyzed side-chain methylation of toluene to styrene, it is important that (i) methanol needs to

be dehydrogenated to formaldehyde forming a strongly positively polarized C atom (through the interaction between the carbonyl and the metal cation), and (ii) the methyl group of toluene needs to interact with the basic oxygen atoms, to form a partial negative charge on the C atom. In consequence, an aldol-type C-C bond formation may occur followed by dehydration and the formation of the C=C moiety. The limiting factor in this chemistry is the low stability of the intermediately formed formaldehyde, which would lead to partial decomposition at the reaction temperatures required for side chain alkylation.

The question arises if intermediately formed formaldehyde would also play an important role in the C-alkylation of phenol over basic catalysts. Due to the higher intrinsic reactivity of the aromatic ring methylation may occur under milder reaction conditions and with catalysts having lower basic strength than for the side-chain alkylation of toluene.

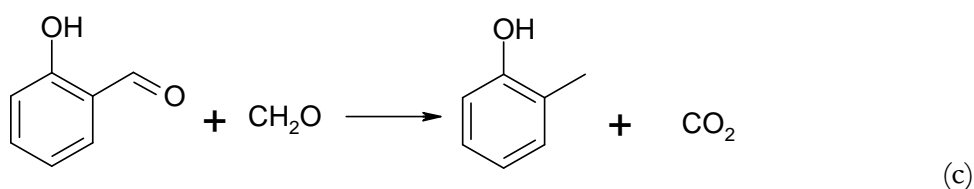
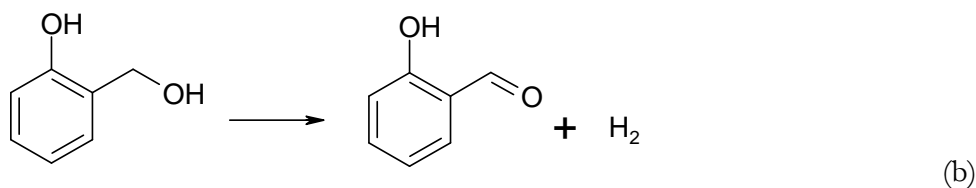
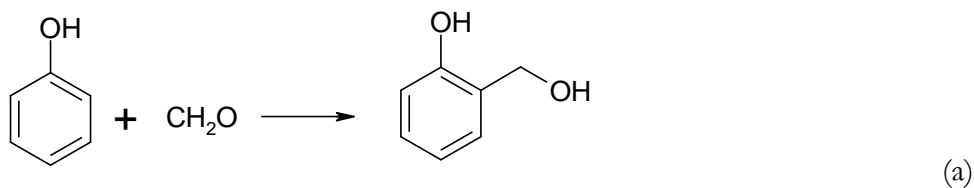
Indirect evidence for such chemistry has been reported in the literature. Using IR spectroscopy Gopinath et al [32] studied the development of formaldehyde, dioxymethylene and formate species from methanol on Cu/Co/Fe/O catalysts (decomposition of the products above 300°C), but also reported that due to the competition of phenol for adsorption on the sites responsible for methanol oxidation, decomposition did not occur in the presence of both compounds. Padmasri et al. [33] also speculated that in the reaction between phenol and isobutanol on MgO and on calcined hydrotalcites, the alkoxy species might dehydrogenate forming an adsorbed, isobutyraldehyde-like intermediate. The latter then was reported to react with phenol to yield either *o*-butenylphenol, after dehydration of the intermediate alcohol, or 2-butenylphenol.

In recent contributions [10,11] it was shown by us that under conditions favoring methanol dehydrogenation, formaldehyde is the true reacting species with the phenolate yielding *o*-cresol and 2,6-xyleneol. The products obtained at low temperature and conventional contact time are anisole and *o*-cresol, the latter dominating between 300 and 450°C (Figure 1). It is important to note that the

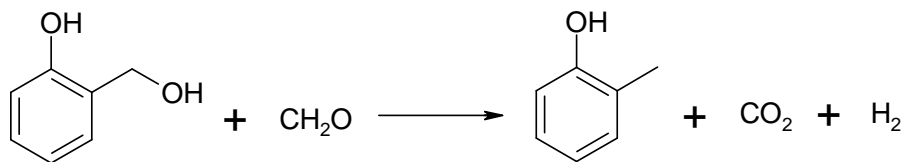
lower the temperature is, i.e., the lower the degree of dehydrogenation of methanol, the more significant the formation of anisole becomes.

The catalytic tests demonstrate that at moderate temperature (i.e., 250°C) salicylic aldehyde is a primary reaction product (next to *o*-cresol and anisole), which can be isolated only at very low phenol conversions (low contact time). As it is seen as product accumulating also with higher time on stream (see Figs. 16 and 17) we conclude that when more products and reactants are sorbed at the surface, salicylic aldehyde reacts preferentially with surface species to *o*-cresol. Under conditions of low surface coverage, salicylic aldehyde is not further converted to consecutive products, because the low concentration of adsorbed methanol and formaldehyde make the secondary reaction less likely. When the concentration of molecules at the adsorbed state increases, salicylic aldehyde is rapidly transformed to *o*-cresol. We speculate at present that the salicylic aldehyde transformation occurs in bimolecular disproportionation-like reaction (intermolecular H-transfer) from adsorbed methanol, formaldehyde or from another functionalized aromatic compound. It is interesting to note that also a fraction of anisole is consumed as the conversion and time on stream increases presumably via hydrolysis of the methyl-phenyl ether bond.

The reaction between an activated aromatic molecule and formaldehyde is also known as hydroxymethylation, and leads to the formation of salicylic alcohol in the case of phenol. This reaction occurs in the liquid phase at moderate temperatures, and is catalyzed by acidic and basic catalysts [34,35]. The IR spectra of adsorbed salicylic alcohol (see characteristic bands at 1653 and 1629 cm^{-1} in Figure 12) indicate that at least a significant fraction is rapidly transformed to salicylic aldehyde. We suggest that a significant fraction of salicylic alcohol or aldehyde will be reduced at the alcohol/aldehyde group by formaldehyde leading to *o*-cresol. The reaction route between chemisorbed phenol and adsorbed formaldehyde would include hydroxymethylation (a), dehydrogenation (b) and reduction of salicylic aldehyde (c) as shown below.



Note that a direct reduction of salicylic alcohol to *o*-cresol by formaldehyde is also possible. It should be emphasized that salicylic alcohol is too reactive to be observed under reaction conditions.



The third primary product, anisole, is only observed at low temperatures. It is formed by direct reaction between activated methanol and phenol with water as the leaving group. Because at high temperature, i.e., under conditions at which methanol dehydrogenation occurs with feasible rates, the only reaction products are *o*-cresol and 2,6-xyleneol, we conclude that the reaction occurs in a concerted mechanism using the polarization of the phenol OH and methanol C-O bond. Alternatively it could be speculated that anisole is formed by a reaction between phenolate and methylformate (formed by dimerization of HCHO). At higher temperature, methylformate readily decomposes to e.g., CH₄, CO₂.

4.5. Conclusions

The combination of catalytic tests, IR spectroscopy of adsorbed reactants, products and possible intermediates together with a computational study as well as *in situ* IR spectra during reaction allows giving a full description of the reaction network in the methylation of phenol (see Figure 18).

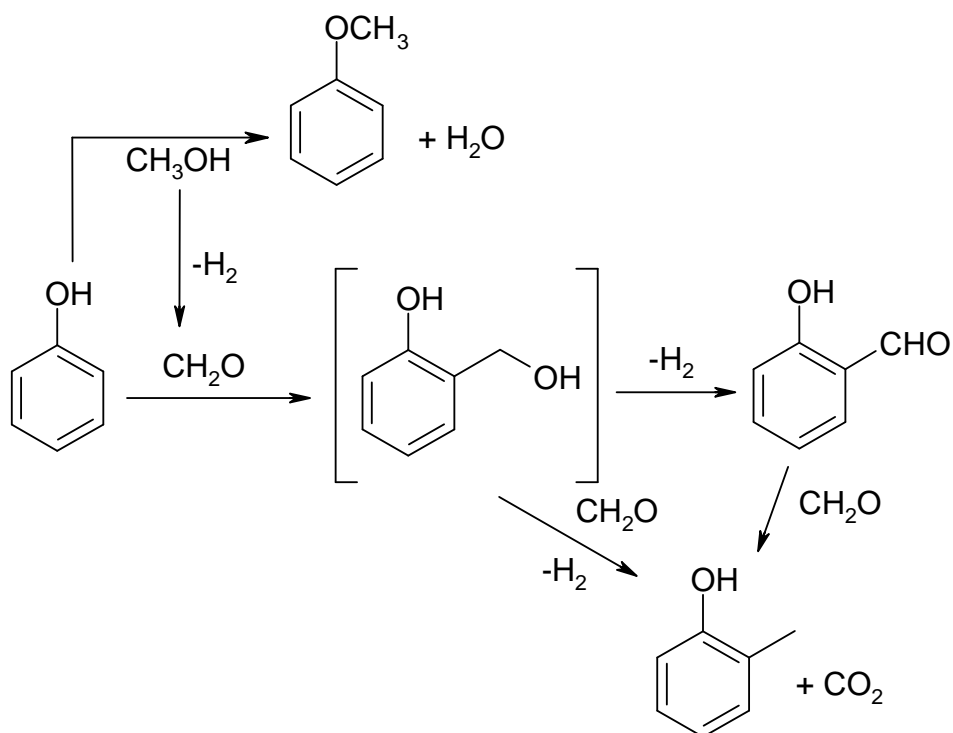


Figure 18. Overall reaction scheme of phenol methylation with methanol catalyzed by MgO

The nature of the products generated by methanol interacting with the catalyst is a function of the reaction conditions, and it affects the primary products obtained in phenol methylation. Under conditions at which the extent of methanol dehydrogenation is low, i.e., low temperature, the main primary products of reaction are anisole and *o*-cresol. Under conditions more favorable for methanol dehydrogenation, anisole is no longer formed, and *o*-cresol becomes the only reaction product. 2,6-xylolol forms in significant concentrations above 350°C and for high phenol conversion. The adsorption of phenol on MgO generates a phenolate species, and the energetically preferred mode of adsorption is on the

corner site of MgO, with an almost orthogonal orientation of the aromatic ring with respect to the catalyst surface. The adsorption of *o*-cresol and of the reaction intermediates, salicylic alcohol and salicylic aldehyde, at the corner site of MgO is also energetically favoured. In all cases, the adsorbed molecules dissociate forming a phenolate-like species and a hydroxyl group.

The reaction between adsorbed phenolate and formaldehyde likely generates salicylic alcohol via hydroxymethylation, which is rapidly dehydrogenated to salicylic aldehyde. At 250°C and for very low conversions and short residence time, salicylic aldehyde is one of the primary reaction products. However, the aldehyde is very rapidly transformed into *o*-cresol, and is not detectable for phenol conversion higher than 0.05%. Below 250 °C anisole and *o*-cresol are formed, the latter being speculated to form via direct reduction of salicylic alcohol by formaldehyde.

In-situ spectroscopy shows salicylic aldehyde to be the reaction intermediate in *o*-cresol formation. The latter is observed during the initial accumulation of adsorbed species on the catalyst surface, i.e., while a low surface coverage prevails. It is not observed under steady conditions, i.e., when the catalyst surface is fully covered, in line with the fact that salicylic aldehyde is only observed at extremely low conversions.

Overall the results demonstrate that subtle tailoring of the base properties allow to use methanol in a dual role as alkylating agent and as reducing agent of the alcohol/aldehyde group created. While this is important for the selective alkylation of phenols, the insight into the reaction may even be more important for the defunctionalization of substituted phenols potentially available at large scale from deconstructed lignin.

4.6. Acknowledgments

I wish to acknowledge prof. J.A. Lercher from Technische Universität München.

4.7. References

- [1] US Patent 4,933,509 (1989), assigned to General Electric.
- [2] V. Durgakumari, S. Narayanan, J. Molec. Catal., 65 (1991) 385.
- [3] S. Sato, K. Koizumi, F. Nozaki, J. Catal. 178 (1998) 264.
- [4] P.D. Chantal, S. Kaliaguine, J.L. Grandmaison, Appl. Catal. 18 (1985) 133.
- [5] M. Bregolato, V. Bolis, C. Busco, P. Ugliengo, S. Bordiga, F. Cavani, N. Ballarini, L. Maselli, S. Passeri, I. Rossetti, L. Forni, J. Catal. 245 (2007) 283.
- [6] R. Pierantozzi, A.F. Nordquist, Appl. Catal. 21 (1986) 263.
- [7] S.T. King, J.M. Garces, J. Catal. 104 (1987) 59.
- [8] A.E. Palomares, G. Eder-Mirth, J.A. Lercher, J. Catal. 168 (1997) 442.
- [9] A.E. Palomares, G. Eder-Mirth, M. Rep, J.A. Lercher, J. Catal. 180 (1998) 56.
- [10] N. Ballarini, F. Cavani, L. Maselli, S. Passeri, S. Rovinetti, J. Catal. 256 (2008) 215.
- [11] N. Ballarini, F. Cavani, L. Maselli, A. Montaletti, S. Passeri, D. Scagliarini, C. Flego, C. Perego, J. Catal. 251 (2007) 423.
- [12] R.N. Spitz, J.E. Barton, M.A. Barteau, R.H. Staley, A.W. Sleight, J. Phys. Chem. B 90 (1986) 4067.
- [13] K. Tanabe, T. Nishizaki, Proceed. 6th ICC, G.C. Bond et al. (Eds), The Chemical Society, London (1977), p. 863.
- [14] K. Tanabe, H. Hattori, T. Sumiyoshi, K. Tamaru, T. Kondo, J. Catal. 53 (1978) 1.

Chapter 4

- [15] C. Chizallet, G. Costentin, M. Che, F. Delbecq, P. Sautet, *J. Am. Chem. Soc.*, 129 (2007) 6442
- [16] K. Tanabe, K. Saito, *J. Catal.* 35 (1974) 247.
- [17] D. F. Eggers, Jr., W. E. Lingren, *Anal. Chem.* 28 (1956) 1328.
- [18] Y. Fukuda, K. Tanabe, *Bull. Chem. Soc. Japan* 46 (1973) 1616.
- [19] G. Busca, J. Lamette, J.-C. Lavalley, V. Lorenzelli, *J. Am. Chem. Soc.* 109 (1987) 5197.
- [20] J.V. Evans, T.L. Whateley, *Trans. Faraday Soc.* 63 (1967) 2769.
- [21] G. Busca, *Catal. Today* 27 (1996) 457.
- [22] J.C. Lavalley, *Catal. Today* 27 (1996) 377.
- [23] J. Günster, G. Liu, J. Stultz, S. Krischok, D.W. Goodman, *J. Phys. Chem.* 104 (2000) 5738.
- [24] C. Di Valentin, A. Del Vitto, G. Pacchioni, S. Abbet, A.S. Wörz, U. Heiz, *J. Phys. Chem. B* 106 (2002) 11961.
- [25] X.D. Peng, M.A. Barteau, *Langmuir* 5 (1989) 1051.
- [26] L.J. Burcham, L.E. Briand, I.E. Wachs, *Langmuir* 17 (2001) 6164.
- [27] P. Mars, J.J. Scholten, P. Zwietering, *Adv. Catal.* 14 (1963) 35.
- [28] M. Ziolek, J. Kujawa, O. Saur, J.C. Lavalley, *J. Phys. Chem.* 97 (1992) 9761.
- [29] N.D. Lazo, D.K. Murray, M.L. Kieke, J.H. Haw, *J. Am. Chem. Soc.* 114 (1992) 8552.
- [30] D.R. Taylor, K.H. Ludlum, *J. Phys. Chem.* 76(20) (1972) 2882.

- [31] H. Hattori, K. Shimazu, N. Yoshii, K. Tanabe, *Bull. Chem. Soc. Japan* 49 (1976) 969.
- [32] T. Mathew, M. Vijayaraj, S. Pai, B.B. Tope, S.G. Hegde, B.S. Rao, C.S. Gopinath, *J. Catal.* 227 (2004) 175.
- [33] A.H. Padmasri, A. Venugopal, V. Durgakumari, K.S. Rama Rao, P. Kanta Rao, *J. Molec. Catal. A* 188 (2002) 255.
- [34] J. Lecomte, A. Finiels, P. Geneste, C. Moreau, *Appl. Catal. A* 168 (1998) 235.
- [35] M. Ardizzi, F. Cavani, L. Dal Pozzo, L. Maselli, R. Mezzogori, *Stud. Surf. Sci. Catal.* 158 (2005) 1953.

Chapter 5

The reaction pathway of the phenol methylation

5.1. Introduction

In the previous chapters we have demonstrated that the methylation of phenol with basic dehydrogenating catalytic systems is very selective to ortho-C-methylated compounds. We also demonstrated that the reaction occurs not by the direct methylation with methanol but with formaldehyde. In fact tests done indicate that the reaction is more active when the methylating agent is formaldehyde. Moreover, with particular reaction conditions several intermediates were observable in the catalytic environment, like for instance salicylic aldehyde.

In the present chapter we focus our attention on the mechanism to explain the reasons because the methylation of phenol is so highly selective to the ortho-ring-methylation. The study was carried out by using a reactivity approach and a computational approach

5.2. Experimental

The reactivity tests were performed using a magnesium-iron mixed oxide (Mg/Fe) having a Mg/Fe molar ratio 0,25 (see Chapter 2.1).

Catalytic tests were carried out by vaporization of the reactants on a tubular glass reactor containing either 1 cm³ of catalyst (catalyst weight 0.85 g, experiments with varying temperature) shaped in 30-60 mesh particles.

Phenol/methanol reactivity tests. A methanol/phenol liquid mixture (methanol/phenol molar ratio 10/1; liquid flow 0.0061 ml/min; phenol supplied by Sigma Aldrich, 99+% purity; methanol supplied by Carlo Erba Reagenti) in a N₂ stream (gas flow 20 Nml/min) was fed. The composition of the feed gas was the following (molar fractions): methanol 0.108, phenol 0.011, and nitrogen 0.881. The residence time was 2.7 s. In the low-residence time catalytic tests the residence time was varied by varying the amount of the catalytic bed.

Phenol/formaldehyde catalytic tests. An aqueous phenol/formaldehyde solution, containing 20.6 wt % formaldehyde, 0.4 wt % methanol and 6,25 wt % phenol (supplied by Sigma Aldrich, 99+% purity), remainder water, in a N₂ stream (N₂ gas flow 20 Nml/min) was fed. The aqueous formalin solution was prepared containing the minimal amount of methanol; the latter is usually added in commercial formalin solutions to limit formaldehyde polymerization. The reactor feed composition was the following (molar fractions): nitrogen 0.71%, formaldehyde 0,058% (considering all the formaldehyde oligomers as being in the monomeric form), methanol 0.001, phenol 0.0058% and water 0.22.

Reactivity tests with intermediates. Tests with salicylic alcohol were performed feeding an aqueous solution of salicylic alcohol with (or without) methanol, in which the salicylic alcohol/methanol molar ratio was 1/10 and water was 60 wt%, water was added in order to prevent the polymerization of the solution in the feeding line. The organic and N₂ streams were changed in order to varying the residence time.

In the tests with salicylic aldehyde the molar ratio between aldehyde and methanol was 1/10.

Finally 2-metoxymethylphenol was fed alone.

Computational calculation details are reported in section 2.5.

5.3. Results and discussions

5.3.1. Catalytic tests

Figure 1 and 2 show the results of the catalytic tests done feeding the phenol/methanol solution over the Mg/Fe mixed oxide catalyst.

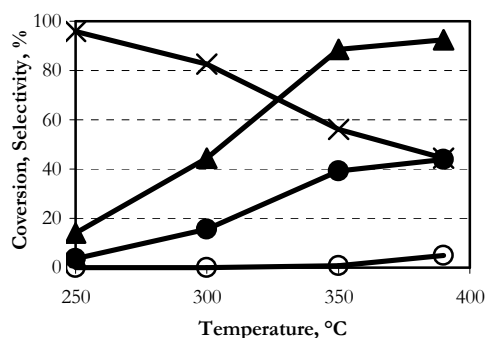


Figure 1. Conversion of phenol (▲), molar selectivity to *o*-cresol (×), 2,6- xylene (●) as a function of temperature

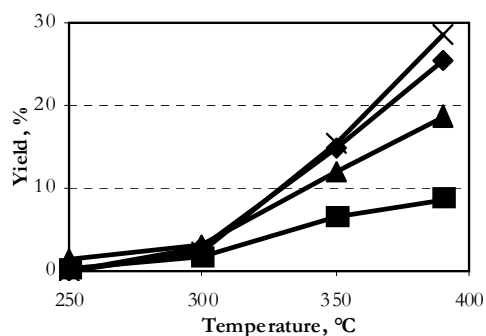


Figure 2 Molar yield CO (■), CO₂ (▲), CH₄ (×) and H₂ (◆) as a function of temperature.

As reported in the literature [1], the prevailing products of the reaction with dehydrogenating catalytic systems (see Figure 1) are ortho-C-alkylated compounds, in particular 2,6-xylene and *o*-cresol. There was only negligible presence of anisole and *p*-cresol. The catalytic tests confirm the elevated regio- and chemoselectivity of the reaction.

Figure 2 shows the yields of methanol decomposition products. Incondensable gas analysis reveals a large amount of CO₂, CO, CH₄ and H₂, that increase with the temperature. As previously described, and here confirmed, the phenol conversion and the distribution of the products of the phenol methylation are strictly correlated to the methanol decomposition grade. In particular, as we describe in a previous chapter, the methylation of phenol occurs with high regio- and chemoselectivity.

Results showed in Figure 3 demonstrated that the methylation of phenol to methylated products is more active when the alkylating species is the formaldehyde.

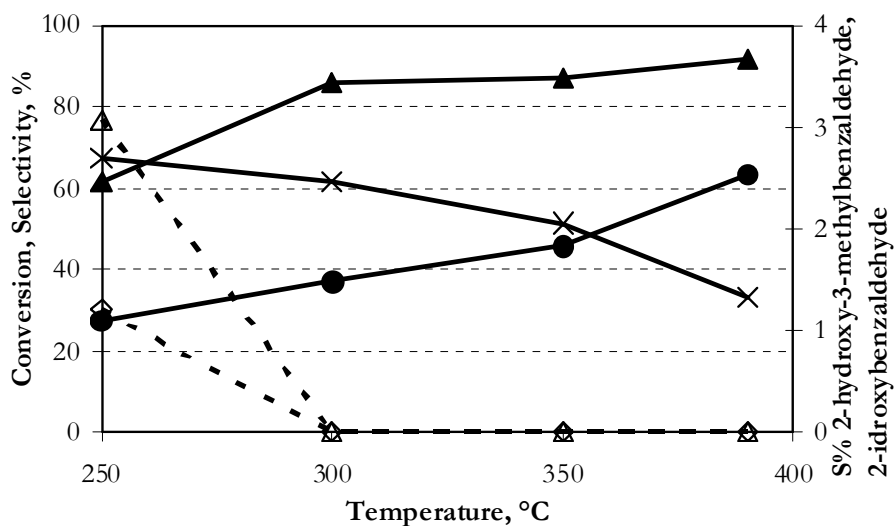


Figure 3. Conversion of phenol (▲), molar selectivity to *o*-cresol (×), 2,6-xyleneol (●), 2-hydroxy-3-methylbenzaldehyde (Δ) and 2-hydroxybenzaldehyde (◊) as a function of temperature.

The figure shows that with formaldehyde the conversion of phenol is very high also at low temperatures. It is also worth noting that products obtained with formaldehyde are the same as those obtained with methanol but with a higher selectivity to 2,6-xyleneol, that is, a secondary product. At lower conversion, salicylic aldehyde and 2-hydroxy-3-methylsalicylaldehyde are also formed. These results confirm what was formerly obtained with Mg/Fe mixed oxides and with other basic catalysts, like MgO, that formaldehyde is a better methylating agent than methanol. Moreover, the presence of aldehydic by-products suggests that the formation of *o*-cresol occurs via a multistep mechanism, as already hypothesised.

5.3.2. Theoretical approach

In order to investigate the reasons why the methylation of phenol proceeds through the reaction between phenol and formaldehyde and not directly by electrophilic aromatic substitution (EAS) with methanol, as widely reported in the literature, we used a theoretical approach.

The computational study has been performed with a cluster simulating MgO. The system was chosen because the catalytic behaviour of MgO is

comparable with that of other oxides, that are able to dehydrogenate methanol to formaldehyde and to give ortho-C-methylated products. Moreover MgO cluster is easier to study because of its cubic geometry.

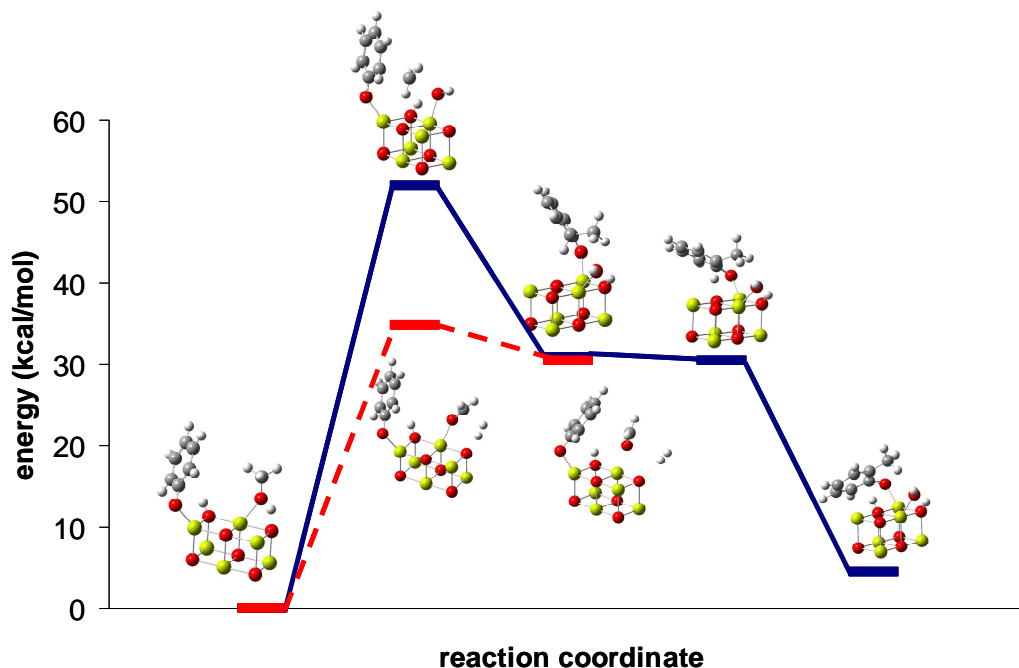


Figure 4. Reaction pathways for EAS and methanol dehydrogenation (dotted line)

Figure 4 compares the reaction pathway for the methylation of phenol with methanol via an EAS-type mechanism and the reaction pathway for the dehydrogenation reaction of methanol to formaldehyde. As show in the figure the methylation reaction evolves passing through a Wheland intermediate. In this case the rate determining step is the formation of the Wheland intermediate, that has an activation energy of 51 kcal/mol. On the contrary, the dehydrogenation reaction proceeds with one step only and with a lower value of activation energy. The results confirm that the most favoured reaction of the methanol with basic catalysts is not the methylation of phenol via EAS, but its dehydrogenation to formaldehyde.

These results can explain why the methanol cannot be the true alkylating agent, but do not explain why the reaction between phenol and methanol with

basic catalyst is so regio-selective. To understand the role of the catalysts during the methylation reaction, a theoretical calculation of the reaction pathway for ortho- and para-methylation by reaction between phenol and formaldehyde (hydroxymethylation reaction) was performed.

Figure 5 shows several systems where phenol and formaldehyde (the reactants) and salicylic alcohol (the product) are chemisorbed on different MgO sites. For all of them, the energy for the formation of corresponding possible intermediates and/or transition state were calculated.

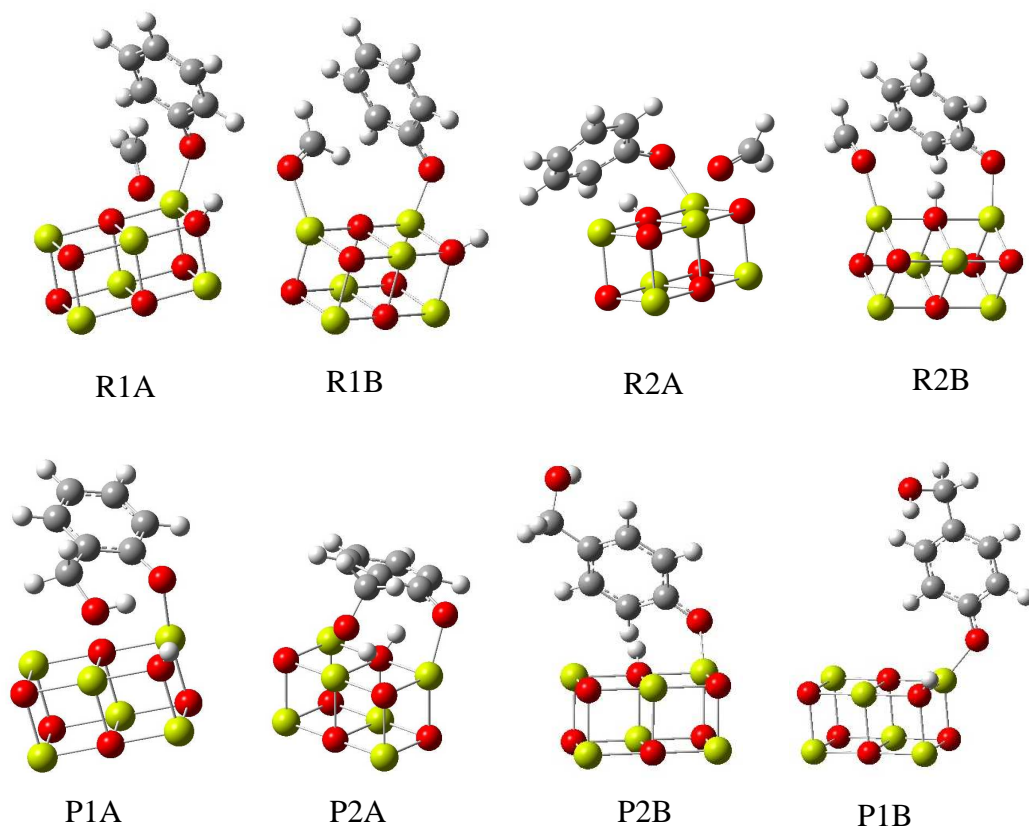


Figure 6 shows the most favourable reaction pathway for the formation of para-hydroxymethylated phenol.

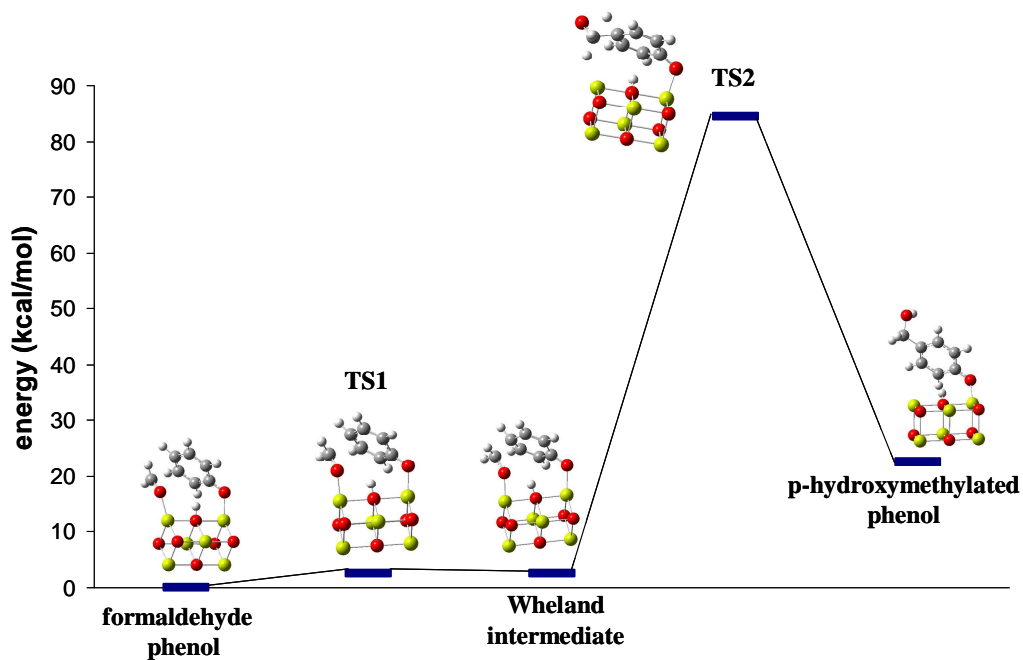


Figure 6. Reaction pathway for para-methylation

The reaction proceeds with two steps; the first one has a very low activation energy 3 kcal/mol, considerably lower than the second one (83 kcal/mol). Moreover, the latter is also greater than the higher one observed for the EAS (Figure 4).

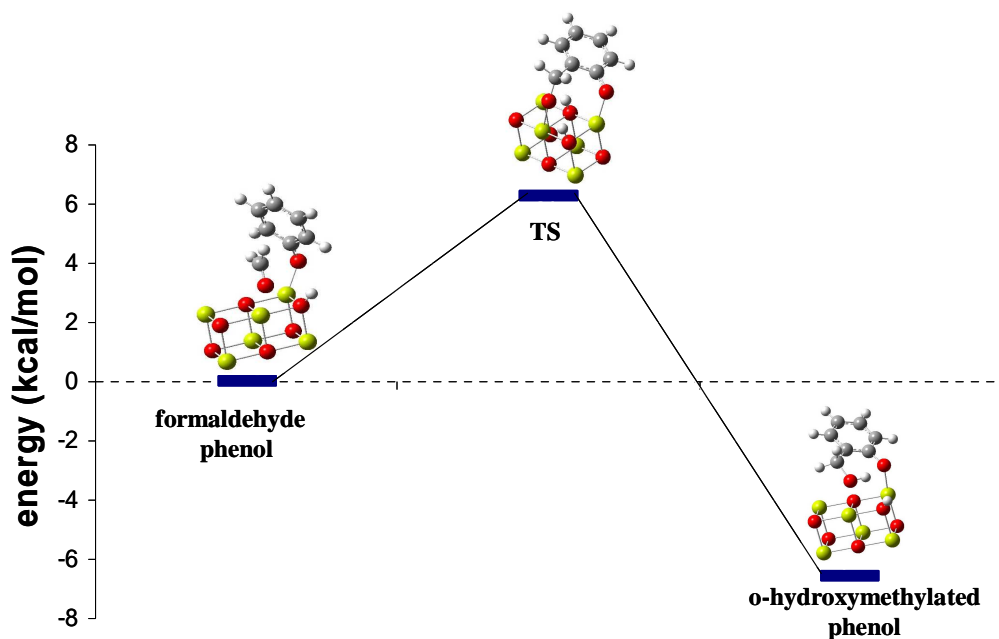


Figure 7. Reaction pathway for ortho-methylation

Figure 7 shows the reaction pathway for the formation of the ortho-methylated product. It is worth noting that in this case there was no stable intermediates, and only one transition state, and that the activation energy value was much lower than that obtained in all the previous reactions, 7 kcal/mol.

By comparing the activation energy values for the ortho- and para-hydroxymethylation reactions, it is possible to affirm that the high selectivity of the methylation reaction with basic catalyst is strictly correlated with the adsorption geometry of phenol on the surface. It is demonstrated that over basic catalysts, the phenolate species adsorbs adopting an orthogonally-oriented geometry with respect to the catalyst surface. In the case of the ortho-hydroxymethylation, the abstraction of the hydrogen bonded to the phenol ring, being the ortho position very close to the surface, is favoured by the interaction with the surface oxygen. This effect is probably more pronounced with very defective crystals in which oxygen can be unsaturated.

5.3.3. The evolution of the reaction

The theoretical approach has explained the reasons why the true alkylating agent in the methylation of phenol cannot be methanol, and why with basic catalysts the formation of *p*-cresol is unfavoured. Another important key point in the mechanism of the reaction is the evolution of the hydroxymethylated compound to *o*-cresol. In the previous chapter we reported that salicylic aldehyde and salicylic alcohol were formed at low phenol conversion when the reaction was carried out with MgO. To confirm that the previously described products were not formed only with MgO, low residence time catalytic tests were performed with Mg/Fe mixed oxide (the same catalyst used for the reactivity tests reported in the previous paragraph). Figure 8 reports the selectivity to the products observed during the low-residence-time catalytic tests, by feeding the phenol/methanol solution over the Mg/Fe mixed oxide catalyst.

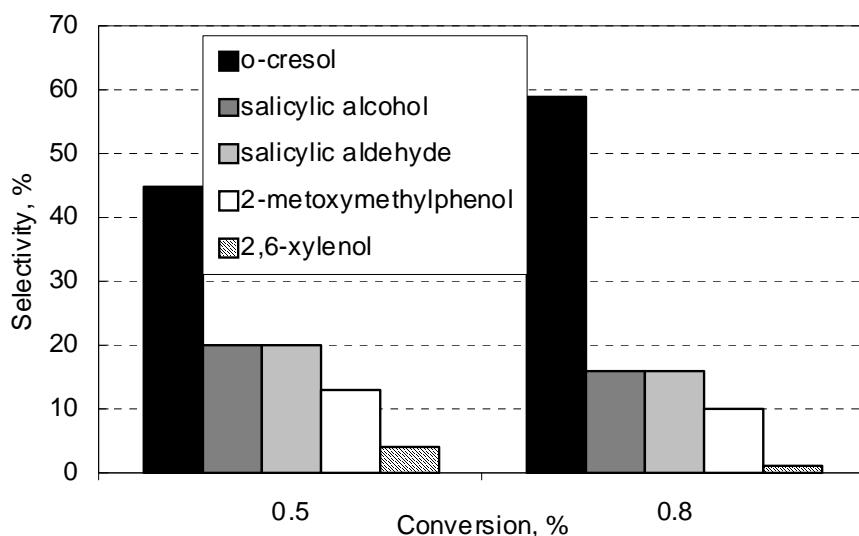


Figure 8. Selectivity of *o*-cresol, salicylic alcohol, salicylic aldehyde, 2-methoxymethylphenol and 2,6-xyleneol as a function of the phenol conversion.

The products observed were salicylic aldehyde, salicylic alcohol, 2-methoxymethylphenol, *o*-cresol and 2,6-xyleneol. These results are in agreement with those obtained with MgO, confirming that the salicylic alcohol is the primary

products. It is well known that the main products in the reaction of phenol with formaldehyde is salicylic alcohol, that is also a precursor in the phenol formaldehyde resins polymerization. The other products, salicylic aldehyde and 2-methoxymethylphenol, can be formed by consecutive reactions occurring upon the alcohol: (i) via dehydrogenation for the formation of the aldehyde, and (ii) via reaction with methanol for the ether.

In order to confirm that the isolated compounds could be effective intermediates in the formation of *o*-cresol, we carried out reactivity tests by directly feeding salicylic alcohol and methanol, over the Mg/Fe mixed oxide catalyst. Results are reported in Figure 9.

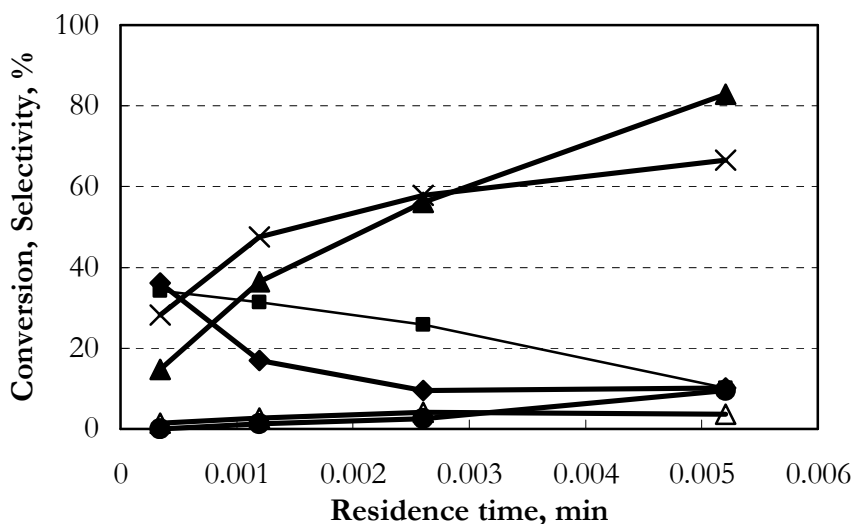


Figure 9. Conversion of salicylic alcohol (▲), molar selectivity to *o*-cresol (×), 2,6-xyleneol (●), phenol (Δ) salicylic aldehyde (◆) and 2-methoxymethylphenol (■) as a function of residence time.

Due to the high reactivity of salicylic alcohol, the reaction was carried out at low temperature and varying the residence time, in order to isolate the reaction intermediates. The products distribution and the evolution of the selectivity of the reaction products confirm that salicylic alcohol is transformed into *o*-cresol. In fact, increasing the residence time the final products were phenol, *o*-cresol and 2,6-xyleneol, the two latter being the same obtained when phenol and methanol are the

reactants. It is also worth noting that if the products selectivity is extrapolated to nil conversion, the main products are salicylic aldehyde and 2-metoxymethyl phenol.

To better understand the influence of methanol on the transformation of salicylic alcohol, we carried out a test by feeding a solution of salicylic alcohol in water, without methanol. The results (reported in Figure 10) show that salicylic alcohol can be converted into salicylic aldehyde and o-cresol even without methanol. For comparison a solution containing salicylic alcohol, water and methanol was also fed.

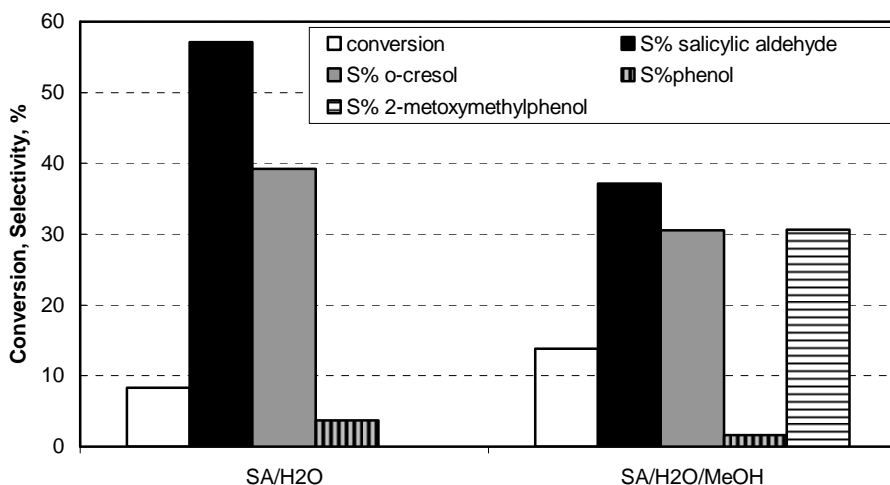
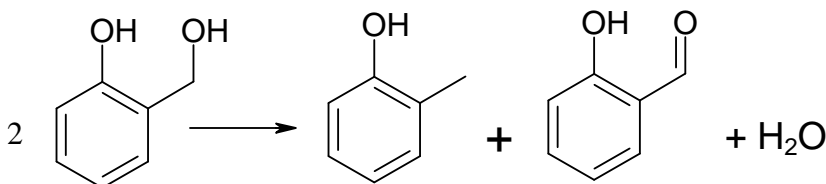


Figure 10. Conversion of salicylic alcohol, molar selectivity of o-cresol, salicylic aldehyde, salicylic alcohol and 2-metoxymethylphenol

These results suggest that the formation of o-cresol can occur by a direct disproportionation reaction between two molecules of salicylic alcohol.



In fact, the formation of the two compounds is almost equimolar. A slightly higher formation of salicylic aldehyde can be attributed to the dehydrogenation of the alcohol.

It is also worth noting that when methanol is not present, 2-metoxymethylphenol is not formed, that confirms that the latter derives only by reaction between methanol and salicylic alcohol.

Figures 9 and 10 show that salicylic aldehyde is formed by transformation of the alcohol, and that moreover it is relatively stable in the reaction environment, especially when methanol is not present. This suggests that salicylic aldehyde indeed needs methanol (or formaldehyde) to be converted further. Therefore, we carried out tests by feeding salicylic aldehyde and methanol (Figure 11). The conversion of salicylic aldehyde is correlated to the reaction temperature.

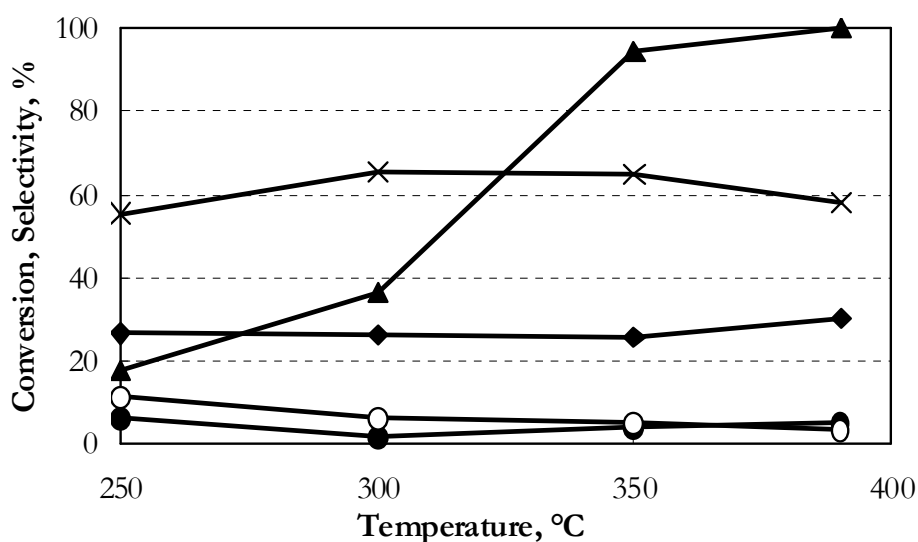
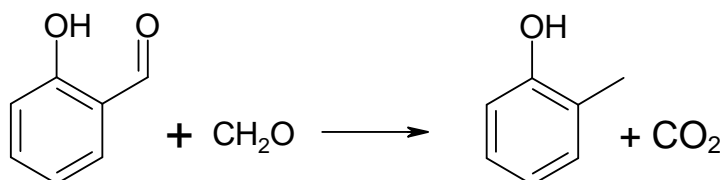
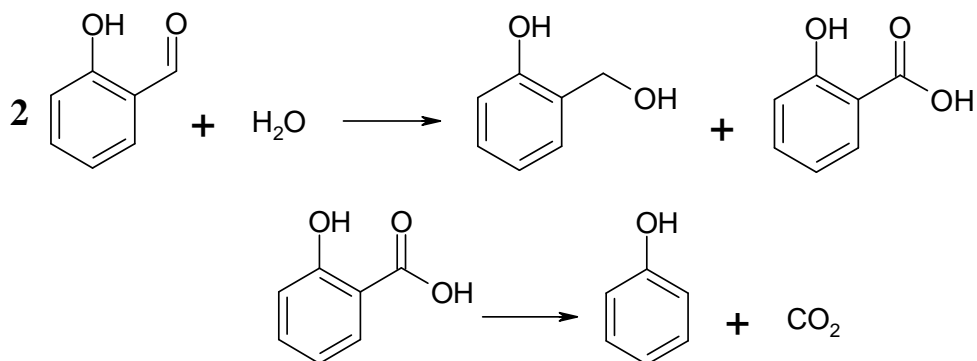


Figure 11. Conversion of salicylic aldehyde (▲), molar selectivity to *o*-cresol (×), 2,6-xyleneol (●), phenol (◆) and polymethylated (○) as a function of temperature.

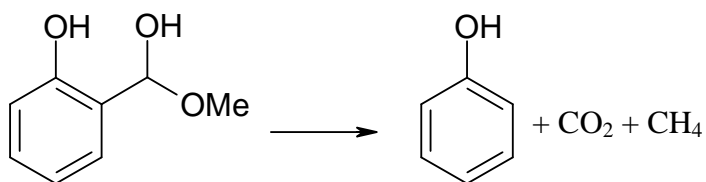
For temperatures lower than 400°C, the main products obtained were phenol and *o*-cresol. The *o*-cresol and phenol selectivities, that are almost constant until 400°C, seem to demonstrate that their formation occurs by reaction with formaldehyde (or methanol).



The formation of phenol might occur by decarboxylation of salicylic acid, the latter having been formed together with salicylic alcohol in the Cannizzaro-like disproportionation of salicylic aldehyde:



However, tests made by feeding pure salicylic aldehyde, without methanol, evidenced that there was no formation of the products. Therefore, the formation of phenol does not occur neither by loss of CO on salicylic aldehyde, nor by bimolecular reaction of the aldehyde with itself. It is likely that either the reaction between salicylic aldehyde and formaldehyde leads to the formation of the ester (a sort of Tishchenko-like dimerization involving two different aldehydes), or the reaction between salicylic alcohol and methanol leads to the formation of an emiacetale. In both cases, the compounds obtained might finally decompose, in the same way as the decomposition of methylformate occurs.



Finally, we tested the reactivity of 2-metoxymethylphenol without methanol (Figure 12).

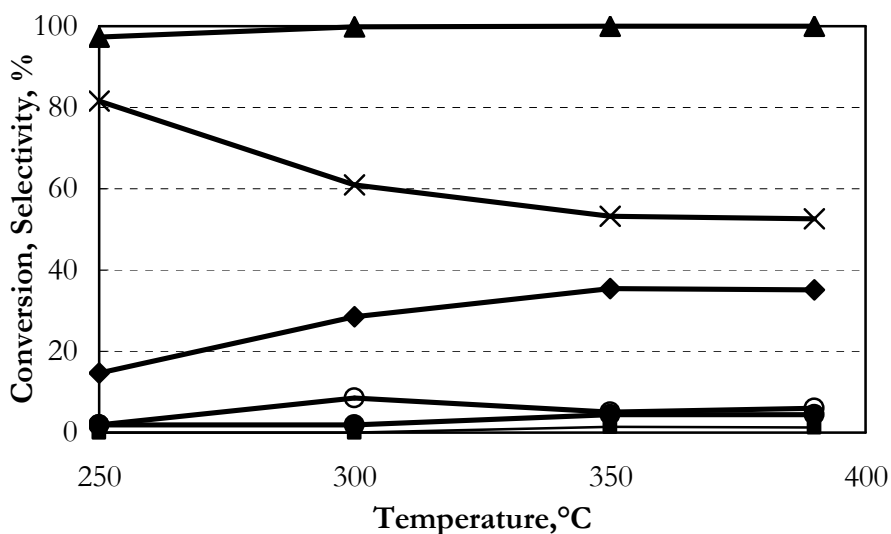
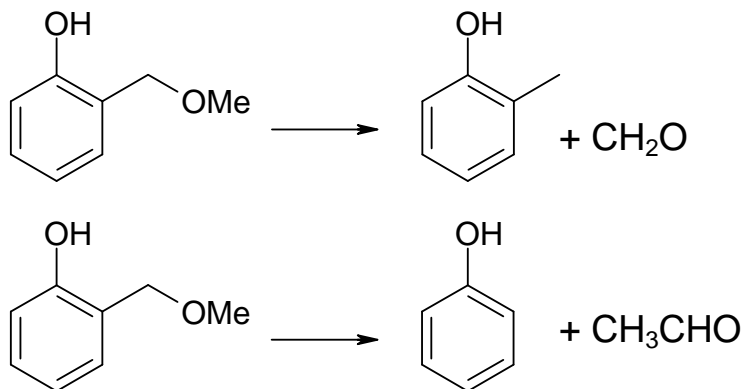


Figure 12. Conversion of 2-metoxymethylphenol (▲), molar selectivity to *o*-cresol (×), 2,6-xyleneol (●), phenol (◆), polymethylated (○) and p-cresol (■) as a function of temperature.

In this case the conversion of the reactant was close to 100% even for low temperature and the main products were *o*-cresol and phenol. The test indicates that the 2-metoxymethylphenol, yielded by reaction between salicylic alcohol and methanol, is very reactive and that it converts into phenol and *o*-cresol by decomposition.



5.4. Conclusions

As previously reported for other catalysts active in the ortho-C-methylation of the phenol like for example MgO, with Mg/Fe/O the true alkylating agent in

the phenol methylation reaction is formaldehyde. As demonstrated feeding formaldehyde, instead of methanol, with phenol upon the catalysts the reaction is more active and selective to dimethylated phenol compounds.

By means of computational study was possible to explain the reasons because methanol cannot be the true methylating agent, this is due to the fact that the activation energy for the methanol dehydrogenation is lower than that one for the direct methylation via electrophilic aromatic substitution. Moreover the computational approach allows to explain also the high selectivity of the reaction, in particular the results suggest that the ortho-methylation is favoured by geometrical effect.

Low-contact-time reactivity tests allow to observe several reaction intermediates such as salicylic alcohol, salicylic formaldehyde and 2-metoxymethylphenol. The latter is a typical product in the reaction between methanol and salicylic alcohol.

Figure 13 summarize the reaction mechanism in which all the observed intermediates are reported.

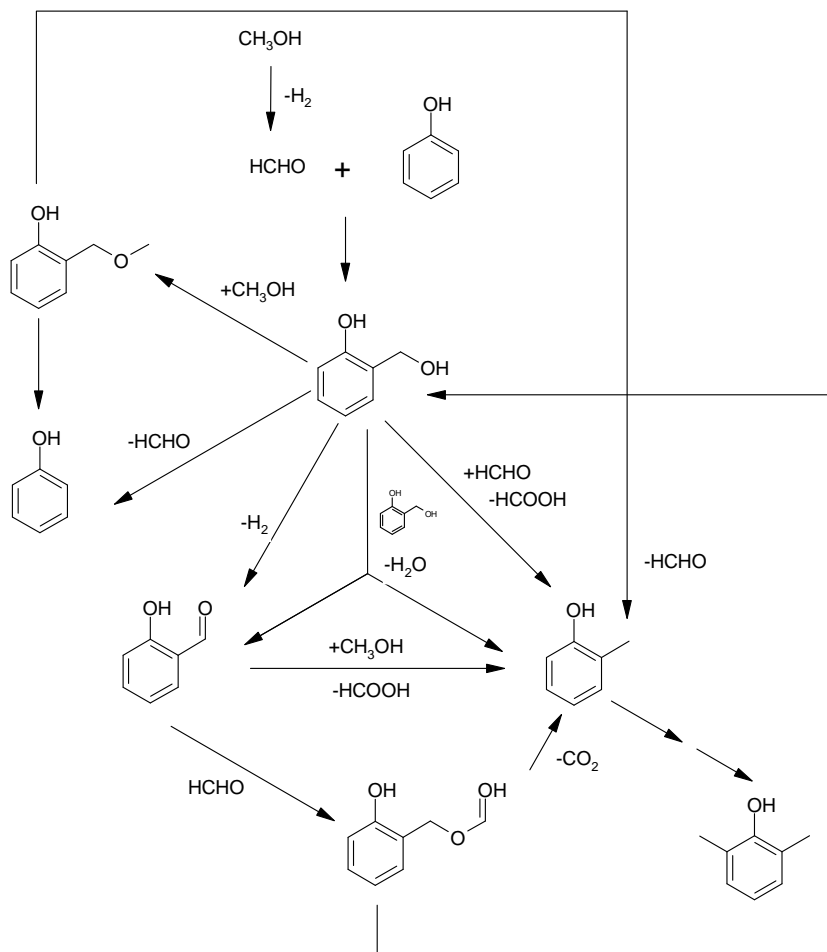


Figure 13. Proposed reaction mechanism for the base-catalysed phenol methylation

5.5. References

- [1] N. Ballarini, F. Cavani, L. Maselli, A. Montaletti, S. Passeri, D. Scagliarini, C. Flego, C. Perego, *J. Catal.* 251 (2007) 423.

Chapter 6

Nanoparticulate CoFe_2O_4 spinel catalysts: the effect of morphology on catalytic performances

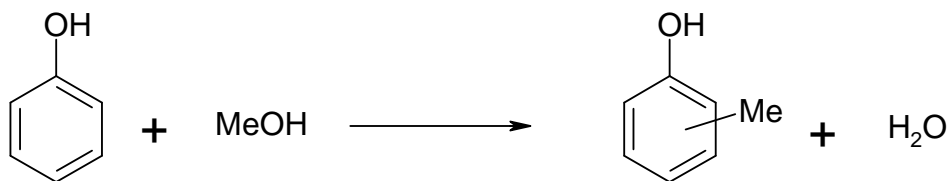
Part 1

6.1. Introduction

Inorganic materials with spinel structures are very versatile compounds offering flexible composition, structural stability and possibility for bifunctional redox or acid/base properties. The general formula for spinel compounds is AB_2O_4 , in which A^{2+} atoms of metal fill the tetrahedral sites while the B^{3+} atoms fill the octahedral sites. Inverse spinel compounds are formed when B^{3+} cations occupy the tetrahedral sites, with the octahedral sites comprised of a 1:1 ratio of A^{2+} and B^{3+} cations [1,2]. Common spinels compounds are the “ferrites” family [3], including the magnetite, Fe_3O_4 whose catalytic activity, depends strongly on the distribution of the cation in the octahedral and tetrahedral sites and the redox properties of the $\text{Fe}^{3+/2+}$ sites [4].

Cobalt ferrite (CoFe_2O_4) is an interesting material with an inverse spinel structure that can be readily prepared by coprecipitation [5]. The formation of

cobaltite nanoparticles has been investigated using membranes as templates, mechanical methods [6] and micelles [3,7]. By varying the synthesis conditions it is possible to control the shape and the cation distribution in the crystalline structure and in turn correlate these changes with the catalytic properties of the resulting materials. In this context, spinel-type cobaltites can be considered bifunctional systems, since they combine both basic and redox catalytic behavior. For instance, Fe-based or Co-based spinels are used both for redox-type catalysis [8,9], and for the basic-catalyzed gas-phase methylation of phenol [10,11]. In general, spinel-type systems offer interesting activity and regio-selectivity in the alkylation of activated aromatics, because of the possibility of modulation of the O nucleophilicity in mixed oxides as compared to the corresponding single metal oxides. Indeed, in recent papers it was demonstrated that the true mechanism of the gas-phase phenol alkylation with methanol includes two steps, (i) the (oxi)dehydrogenation of methanol to formaldehyde, that also is the rate-determining step of the process, and (ii) the electrophilic hydroxymethylation of formaldehyde onto the aromatic ring [12,13]. On the other hand, in the absence of any acid-type activation of the formaldehyde generated, the reaction rate also is a function of the concentration of activated phenol, i.e., of the adsorbed phenolate species. The generation of the latter species occurs by proton abstraction by the O²⁻ species, the basicity of which is a function of the nature of the metal cations in the oxide. Therefore, this reaction is a useful model for finding relationships between chemical physical features and reactivity of bifunctional catalysts.



Here we report on the synthesis of nanostructured inverse spinel CoFe₂O₄ and correlate their particle size and physicochemical characteristics with their catalytic behaviour in the vapour-phase methylation of the phenol.

6.2. Experimental

6.2.1. Catalyst characterization

Catalysts were obtained as described in Section 2.1. Co-precipitated samples were calcined respectively at 450°C (CF-2A), 550°C (CF-2B) and 750°C (CF-2C).

Elemental analysis was undertaken on a Hitache Z-5300 Polarised Zeeman Atomic Absorption Spectrophotometer with a 240.7 nm cobalt lamp and 248.3 nm iron lamp. All the spinels were dissolved in HNO₃ and deionised water in glass volumetric flasks. Standards of 1, 2.5 and 5 ppm for iron and 1, 2 and 3.3 ppm for cobalt in deionised water were made for calibration purposes.

TPR analysis employed a gas composition of 20 mL min⁻¹ H₂ with a temperature ramp of 20°Cmin⁻¹ up to 1000°C. Differential Thermal Analysis (DTA) data and mass loss (from TGA/TPR) data was collected.

A Tecnai 12 BioTWIN by FEI transmission electron microscope was used for obtaining detailed images of the CoFe₂O₄, operating at 120 kV. Approximately 2 mg of each sample were suspended in ~ 5 ml of ethanol. 10 µl of the resulting solution was pipetted onto a gold grid and the solvent allowed evaporating for 15 minutes before being analysed.

XPS measurements were performed using a Kratos AXIS HSi instrument equipped with a charge neutralizer and Mg K_α X-ray source. Spectra were recorded at normal emission using an analyzer pass energy of 20 eV and X-ray power of 225 W. Spectra were Shirley background-subtracted across the energy region and fitted using CasaXPS version 2.1.9.

6.2.2. Methylation of Phenol

The methylation of phenol was performed in a continuous down-flow tubular steel AISI 316L reactor at temperatures ranging from 250 and 450°C, using a methanol (Carlo Erba Reagenti) and phenol (supplied by Sigma Aldrich,

99+% purity) molar feed ratio of 10:1 which was fed into the reactor via a syringe pump.

For the reaction, the powder was pelleted and sieved to an average particle size of 30-60 mesh then loaded into the reactor tube to form a 0.5 cm³ catalyst bed (0.7 g). The reactor was purged with flowing N₂ (10 cm³ min⁻¹) then heated to the reaction temperature after which the liquid organic feed was introduced (0.00305 cm³ min⁻¹). The composition of the feed gas was the following (molar fractions): methanol 0.108, phenol 0.011, and nitrogen 0.881. Overall gas residence time was 2.7 s. Total pressure was atmospheric.

6.3. Results

6.4. Bulk and surface characterization of calcined samples

The successful synthesis of CoFe₂O₄ was first probed by elemental analysis which reveals a bulk Co:Fe ratio of 1:2 for all materials (Table 1).

Table 1: Bulk characteristics of calcined samples

Sample	Calcination Temperature / °C	Bulk Co / wt%	Bulk Fe / wt%	Bulk Co:Fe	Surface area / m ² g ⁻¹	Crystalite size / nm
CF-2A	450	23.2	44.9	CoFe _{2.05}	84	17
CF-2B	550	23.8	46.2	CoFe _{2.05}	46	22
CF-2C	750	24.6	47.6	CoFe _{2.05}	7	50

The spinel phase and variation in particle size was further probed by powder XRD (Figure 1) that reveals a series of reflections consistent with the CoFe₂O₄ spinel structure.

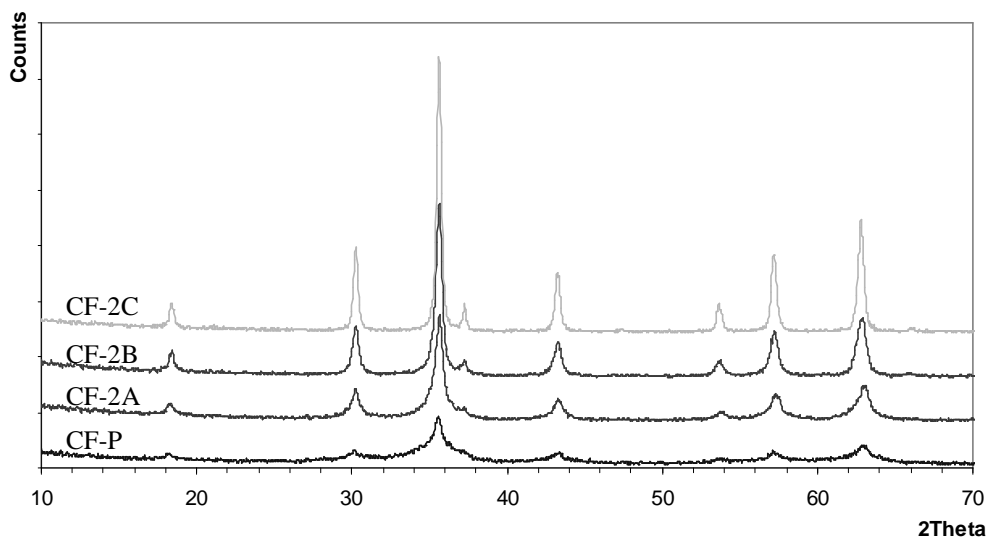


Figure 1. X-Ray diffraction spectra of calcined samples. CF-P is the pattern of the freshly precipitated and dried sample.

These reflections were present already in the pattern of the freshly precipitated sample, CF-P. Calcination above 450°C results in progressive sharpening of these peaks indicative of particle growth. Scherrer line broadening analysis on the (220), (311), (511) and (400) peaks reveal that the volume averaged particle size increases from 17 to 50 nm respectively (Table 1). Particle sintering and growth is accompanied by a significant decrease in surface area from 84 to 7 m²g⁻¹.

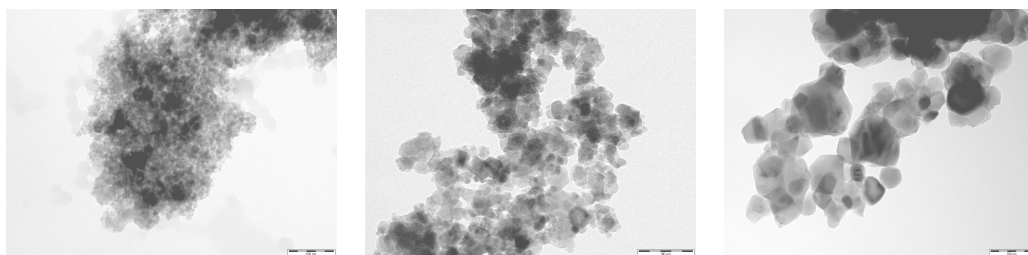


Figure 2. TEM images of calcined samples

The observed particle sizes are in good agreement with TEM (Figure 2) which reveals the material calcined at 450°C is comprised of small agglomerates of

spherical \sim 8-16 nm particles. Following calcination at 750°C significant particle growth is observed with more cubic like particles formed of size 36-80 nm.

Table 2: Surface composition of calcined samples

Sample	Surface Co / at %	Surface Fe / at %	Surface O / at %	Surface C / at %	Surface $\text{Co}_x\text{Fe}_y\text{O}_z$
CF-2A	8.2	17.8	53.9	20.2	$\text{CoFe}_{2.2}\text{O}_{6.6}$
CF-2B	9.7	18.4	54.0	17.9	$\text{CoFe}_{1.9}\text{O}_{5.6}$
CF-2C	12.2	18.5	58.4	10.8	$\text{CoFe}_{1.5}\text{O}_{4.8}$

XPS analysis on these CoFe_2O_4 nanoparticles (Table 2) also reveals a striking dependence of surface composition on particle size. All particles appear to be oxygen rich, which would be consistent with oxygen termination of the spinel clusters. However as the particle size increases, the Co:Fe ratio is also observed to vary from 1:2 to 1:1.5; a trend which can be rationalised by considering the surface termination of different crystal planes of the CoFe_2O_4 spinel structure. CoFe_2O_4 has a cubic inverse spinel crystal structure in which the Co^{2+} cation occupies one half of the octahedral coordination sites while the Fe^{3+} cations occupies the other half of the octahedral coordination sites as well as all of the tetrahedral coordination sites. The surface termination of spinel structures varies considerably for the different crystal planes [14,15], as shown for spinel structures such as ZnAl_2O_4 , where Zn^{2+} sites are not exposed at the surface.

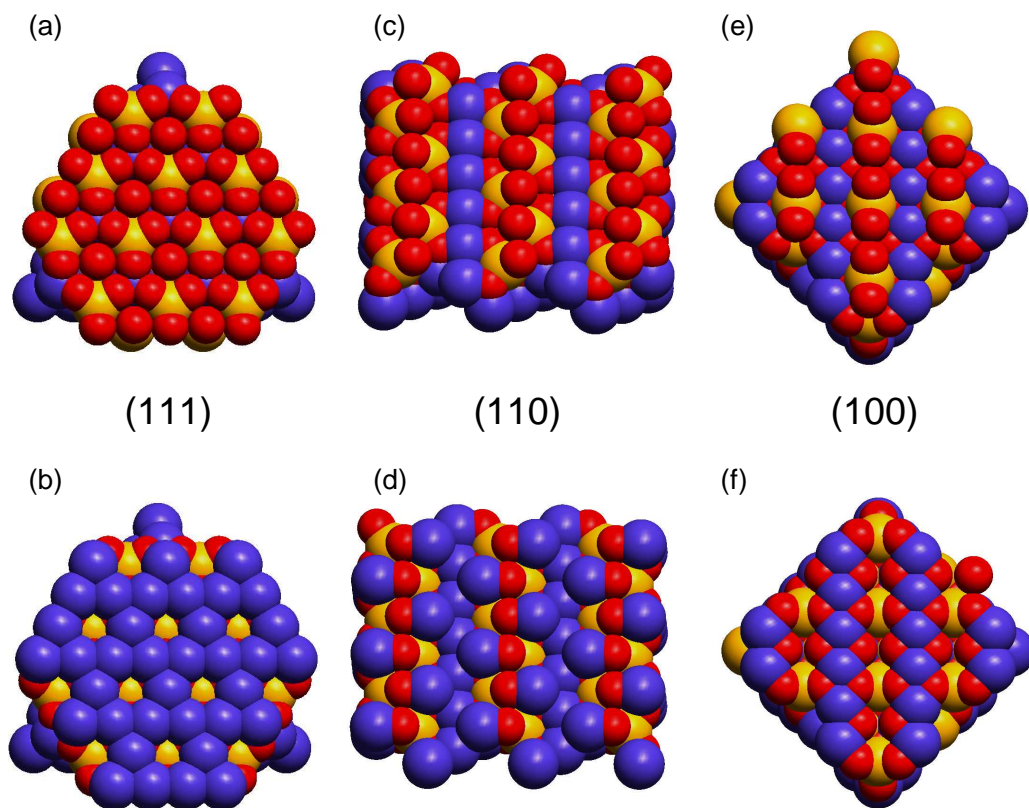


Figure 3. (111) and (100) faces of CoFe_2O_4 (Red = O^{2-} , Blue = Octahedral ($\text{Fe}^{3+}/\text{Co}^{2+}$ site, Orange = tetrahedral Fe^{3+} site). In addition all surfaces may be oxygen/-OH terminated.

Figure 3 shows the ideal structures of possible low index (111), (110) and (100) crystal faces of the CoFe_2O_4 inverse spinel structure. The (111) plane can be cut so that it exposes exclusively (a) tetrahedral Fe^{3+} or (b) octahedral $\text{Co}^{2+}/\text{Fe}^{3+}$ sites. Likewise the (110) face can also be cut so that it exposes (c) a mixture of octahedral and tetrahedral sites only or (d) only octahedral sites. Finally the (100) face can expose (e) a mixture of octahedral $\text{Co}^{2+}/\text{Fe}^{3+}$ and tetrahedral Fe^{3+} sites or (f) just octahedral $\text{Co}^{2+}/\text{Fe}^{3+}$ sites. Examination of the surface composition of all these faces show that their Co:Fe:O ratio differ between the faces and from that of the bulk. The (111) surface (a) of CoFe_2O_4 exposes higher oxygen and Fe content than any of the low index faces which is also consistent with the observed variation in surface composition by XPS. However, the equilibrium structure of large spinel clusters is predicted to be based on a (100) terminated structure, whereas smaller

clusters expose more (111) and (110) faces [16]. Indeed calculations on spinel structures of Co_3O_4 suggest that the tetrahedrally terminated (111) and octahedrally terminated (110) are the most stable crystal faces [17]. It thus seems reasonable to suggest that the small CoFe_2O_4 particles, in CF-2A sample, are comprised of more (111) tetrahedral Fe^{3+} terminated clusters, while the larger particles formed with increased calcination temperature expose more (100) face giving rise to an increased Co:Fe ratio and decreased surface oxygen content.

High-resolution XPS spectra of Fe and Co for the CF-2C and CF-2A samples are shown in Figures 4a and 4b. Both regions exhibit complex shake-up satellite structures arising from multiplet interactions between the core hole generated on photoemission and the unpaired 3d valence electrons which are characteristic of the presence of high spin Fe^{3+} and Co^{2+} centres [18].

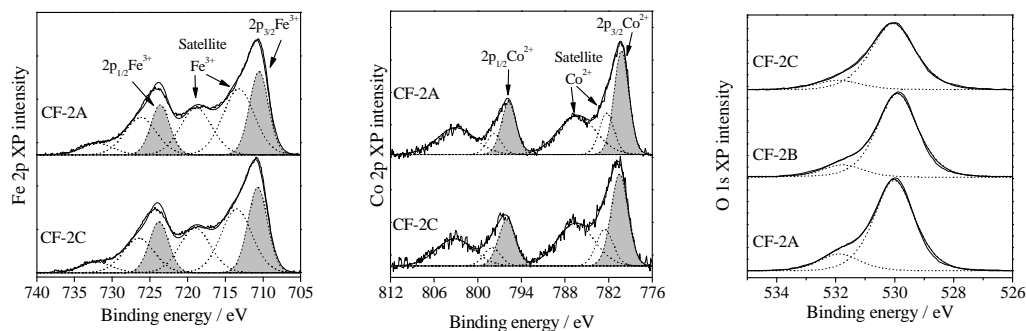


Figure 4. XPS spectra of Co-Fe nanoparticles (calcined samples). (a) Fe_{2p} ; (b) Co_{2p} ; (c) O_{1s} .

In contrast Fe^{2+} and Co^{3+} have spin paired valence electrons and do not exhibit such intense multiplet splitting [19]. Figure 4a shows the Fe_{2p} region in which the peaks at 710.8 and 723.9 eV are attributable to the $2p_{3/2}$ and $2p_{1/2}$ spin orbit split components. Additional doublets at 713.5, 726.5 and 719.2, 732.5 eV are assigned to the Fe^{3+} satellite transitions are in good agreement with the literature [20,21]. Likewise the Co spectra (Figure 4b) are consistent with Co^{2+} with peaks arising at 777.3 and 792.7 eV from the principal $2p_{3/2}$ and $2p_{1/2}$ transitions, along with corresponding pairs of satellites at 779.3, 794.8 and 783.5, 800 eV [22]. The ratio of the satellite peaks to the main Fe_{2p} or Co_{2p} transitions are independent of

particle size, suggesting there is no increase in Fe²⁺ or Co³⁺ following high temperature calcination.

Figure 4c shows the corresponding O_{1s} spectra which reveal that the 7 nm CoFe₂O₄ clusters exhibit two peaks at 530 and 532 eV in a ~ 4:1 ratio which are attributed to O²⁻ and surface CO₃²⁻/OH⁻ sites [23]. Following higher temperature calcination the intensity of the 532 eV state decreases suggesting surface dehydroxylation occurs as the particles sinter to form larger clusters.

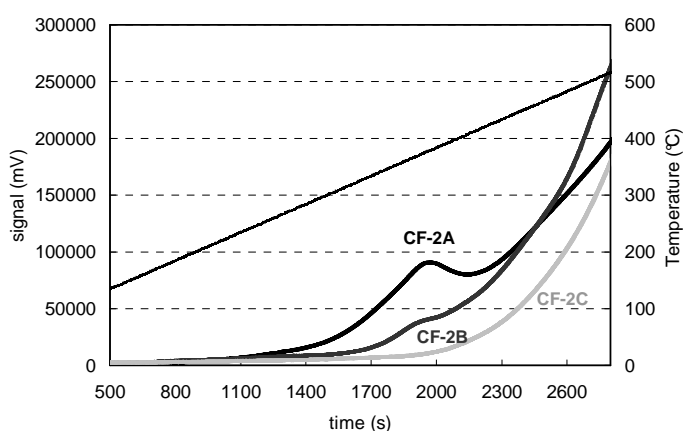


Figure 5. TPR (with measurement of hydrogen consumption) of Co-Fe nanoparticles (calcined samples).

Figure 5a shows the results of TPR/TGA analysis. All samples show an initial weight loss attributed to water desorption at ~100 °C, then at >350 °C there is a second weight loss which is evident in the case of sample CF-2A, is shifted towards higher temperature in sample CF-2B and is absent in the case of sample CF-2C. Similar results were obtained by means of TPR tests when the amount of hydrogen consumed was measured (Figure 5b); the reduction peak with maximum at around 350°C is a shoulder of the main peak, the latter attributable to the reduction of the bulk spinel. This shoulder however is relatively intense in the case of sample CF-2A, less intense in the case of sample CF-2B and apparently absent (or very weak) for sample CF-2C. The reduction peak at low temperature is clearly

attributable to a species having high reducibility, and hence either to surface defects, or may reflect the different surface termination of the nanoparticles and be attributed to the reduction of surface Fe^{3+} tetrahedral sites [24]. It is worth noting that when the TPR measurements were repeated on samples that had first been pre-reduced, and then reoxidized in air flow, the profile of the CF-2A and CF-2B became similar to that one of fresh sample CF-2C. This is a clear indication of the fact that the differences present in calcined samples had disappeared as a consequence of the reductive and reoxidation treatment (see also the section relative to the characterization of used catalysts).

Raman spectra of samples recorded at room temperature are shown in Figure 6. The measurements further confirm that all samples were CoFe_2O_4 with a cubic inverse-spinel structure [25,26].

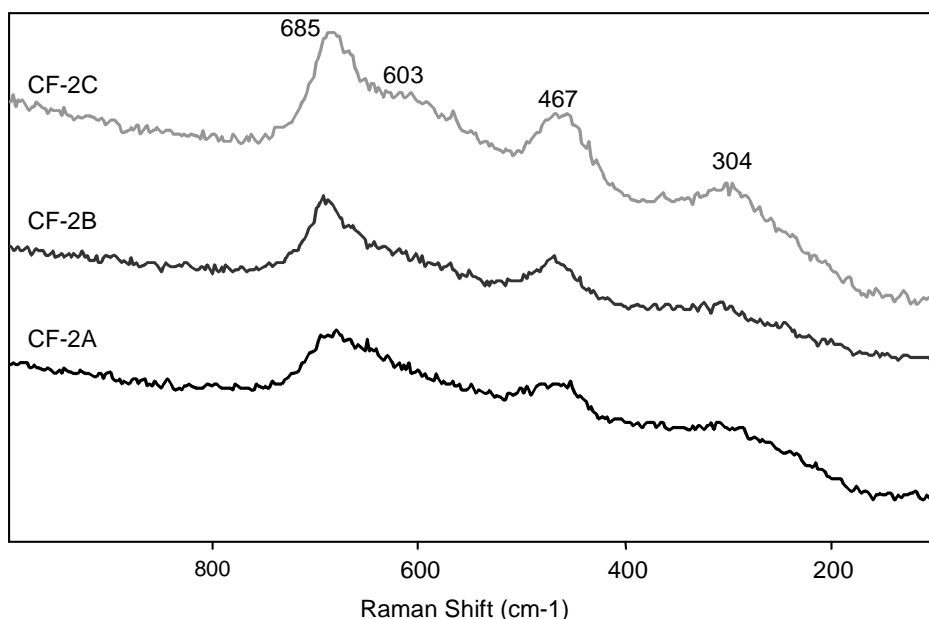


Figure 6. Raman spectra of Co-Fe nanoparticles (calcined samples).

The factor group analysis in spinels predicts five Raman active modes. The modes at $\sim 600 \text{ cm}^{-1}$ and $\sim 685 \text{ cm}^{-1}$ are related to the T-site mode that reflects the local lattice effect in the tetrahedral sublattice. Other peaks at $\sim 200 \text{ cm}^{-1}$, $\sim 305 \text{ cm}^{-1}$ and $\sim 465 \text{ cm}^{-1}$ correspond to the O-site mode that reflects the local lattice

effect in the octahedral sublattice [25]. In sample CF-2C, the most crystalline one, all these features were evident, whereas in less crystalline samples the bands were very broad, and only the three most intense bands were attributed. These spectra confirm that the main morphological differences between samples, evidenced by means of bulk techniques, were also maintained at the surface and subsurface level.

6.4.1. The reactivity in the gas-phase methylation of phenol

Figure 7 summarizes the catalytic performance of sample CF-2A as a function of the reaction temperature; specifically, reactivity tests of Figure 7(a) were carried out on the fresh calcined sample, whereas results reported in Figure 7(b) refer to the reactivity of the sample after the high-temperature tests shown in Figure 7(a).

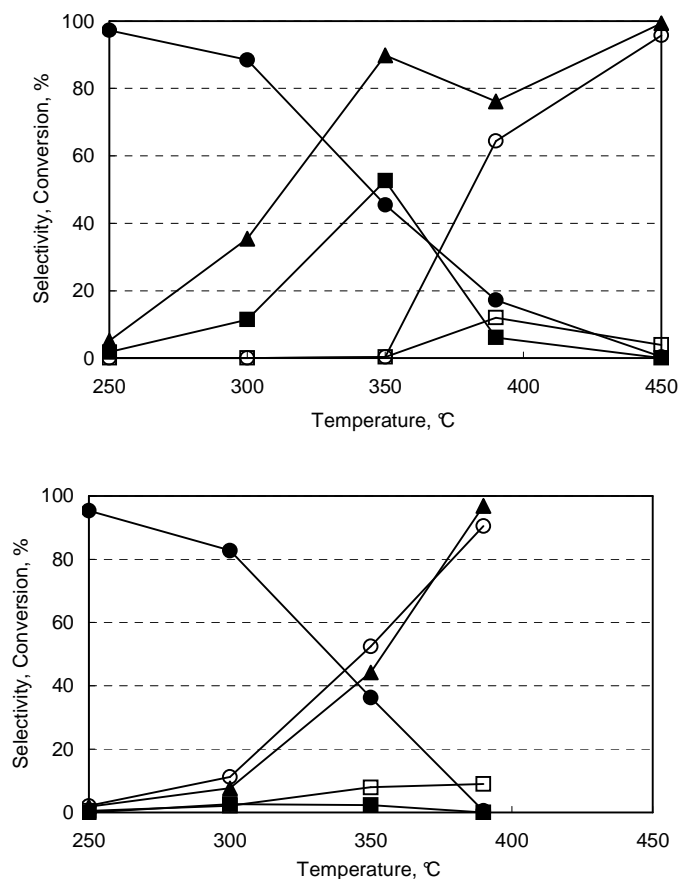


Figure 7. Catalytic performance in phenol methylation of the fresh calcined sample CF-2A (top) and of the same sample after reactivity tests of Figure 7a (bottom), as a function of temperature. Symbols: phenol conversion (▲), selectivity to *o*-cresol (●), to 2,6-xylenol (■), to benzene (○) and to toluene (□).

Various effects are worth of mention. First, the anomalous behavior of phenol conversion; in fact, after an initial increase of conversion observed for an increase of temperature in the 250-to-350°C range, the conversion first declined (T 390°C) and then increased again (T 450°C). When a fresh sample was loaded again and catalytic tests of Figure 7(a) were repeated, the behavior was fully replicated. However, when the activity of the catalyst was checked again after the first set of experiments (Figure 7(b)), the behavior was completely different from that one of the freshly calcined catalyst shown in Figure 7(a). Evidently, the used catalyst was less active than the fresh one in the temperature range between 250 and 350°C;

remarkably, the behavior shown in Figure 7(b) did not further change when catalytic measurements were repeated.

A second important aspect concerns the very high regio- and chemo-selectivity of the reaction. In fact, with the fresh catalyst the only product formed at low temperature was *o*-cresol, the selectivity of which decreased in favour of 2,6-xyleneol when the temperature was raised from 250 to 350°C. The low selectivity to anisole and *p*-cresol is a feature typically observed with basic catalysts, including redox-type single oxides and mixed oxides [12,13]. The cobalt ferrite, however, shows an outstanding 100% selectivity to ortho-C-methylated compounds (*o*-cresol and 2,6-xyleneol), which is rarely observed in the gas-phase methylation of phenol with methanol. At above 350°C the behavior changed; the selectivity to these two compounds rapidly declined, and at 450°C the only reaction products were those of phenol and *o*-cresol dehydroxylation, i.e., benzene and toluene, respectively. The used catalyst, however, gave again *o*-cresol as the main reaction product when used at temperatures below 350°C.

These data indicate that the characteristics of the freshly calcined catalyst are profoundly modified during reaction when temperatures higher than 300-350°C are used. Moreover, data suggest that the spinel becomes reduced in the reaction environment (see also the characterization of the used catalyst), giving rise *in-situ* to a catalyst that is very active in the dehydroxylation of phenol and *o*-cresol at temperature higher than 350°C, but still catalyzes the ortho-C-methylation of phenol at moderate temperature.

The question now is which is the reducing agent for the spinel during phenol methylation. Figure 8 shows the yields to the products of methanol decomposition, formed during tests of phenol methylation. It is shown that the extent of methanol decomposition was relevant.

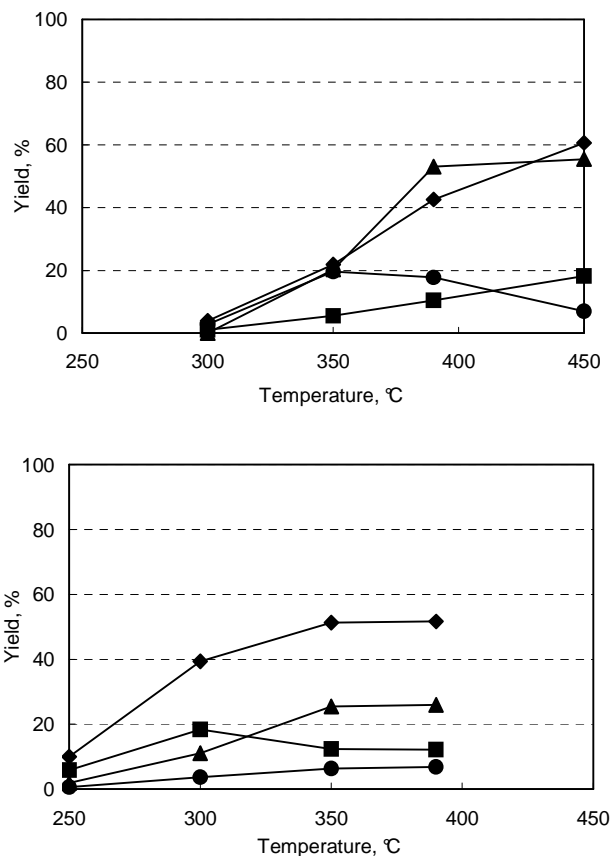


Figure 8. Decomposition of methanol during phenol methylation of the fresh calcined sample CF-2A (top) and of the same sample after reactivity tests of Figure 8a (bottom), as a function of temperature. Symbols: yield to CO₂ (▲), to CO (■), to CH₄ (●), and to H₂ (◆).

The extensive formation of H₂ is a clear evidence of the dehydrogenation of methanol to formaldehyde and of the latter to CO. With the calcined sample, the main product of methanol decomposition was CO₂; the latter formed either by combustion of methanol, or by decomposition of methylformate to CO₂+CH₄, the ester being formed either by reaction between formic acid and methanol or by the dimerisation of formaldehyde. However, since the yield to CO₂ was remarkably higher than that of methane, a possible contribution of both reactions is likely. It is worth noting that the yield of CO and that of hydrogen had similar trends in function of temperature; the yield to methane, instead, showed a maximum at 350°C.

The used sample (Figure 8(b)) was more active in H₂ and CO formation at low temperature, and less active in CO₂ formation at 390°C than the fresh calcined sample (Figure 8(a)). These differences are due to the lower oxidizing property of the used catalyst; moreover, the hydrogen formed by methanol and formaldehyde dehydrogenation was not transformed to water.

The data presented indicate that the progressive reduction of the ferrite is due to the consumption of bulk oxygen by methanol; the latter dehydrogenated to formaldehyde, and the hydrogen produced is oxidized to water, so causing the reduction of metal cations and the removal of the O ions from the lattice of the oxidized catalyst. As a consequence of this, the progressive reduction of the oxide considerably modified its catalytic properties, in regards to both phenol methylation and methanol decomposition.

6.4.2. The characterization of used catalysts

Reactivity tests had led us to formulate the hypothesis that catalysts underwent profound modifications during reaction. Figure 9 reports the XRD patterns of catalysts downloaded after reaction tests; it is worth noting that the three catalysts had been used for similar reaction times and at comparable reaction conditions.

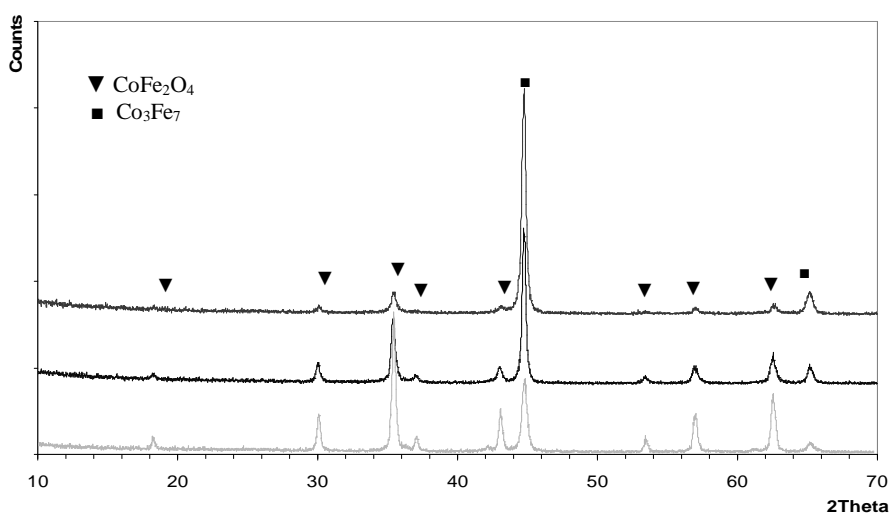


Figure 9. X-Ray diffraction spectra of used samples.

All used samples showed the reflections corresponding to a metallic Co/Fe alloy, besides those of the original spinel. However, the intensity ratio of the two sets of reflections was different; in fact the less crystalline sample CF-2A was almost completely reduced to the metallic state, whereas the most crystalline one, CF-2C, still showed a considerable amount of the oxidic compound. This was a consequence of two factors, that contributed in accelerating the reduction of the CF-2A sample: (a) the presence of the more reducible sites, (b) the higher surface area. Also, it is worth noting that a reoxidation treatment in air of sample CF-2A, after the reduction with methanol at 300°C, led to a spinel compound having chemical physical properties which were different from those observed in the freshly calcined CF-2A sample, and very similar to those of the fresh CF-2C catalyst: surface area (18 m²/g, compared to 84 m²/g for the fresh CF-2A sample), XPS Co/Fe atomic ratio (1/1.95, compared to 1/2.51) and morphology (Figure 10, comparing the TEM pictures of fresh and used + reoxidized CF-2A, with the same picture magnification).

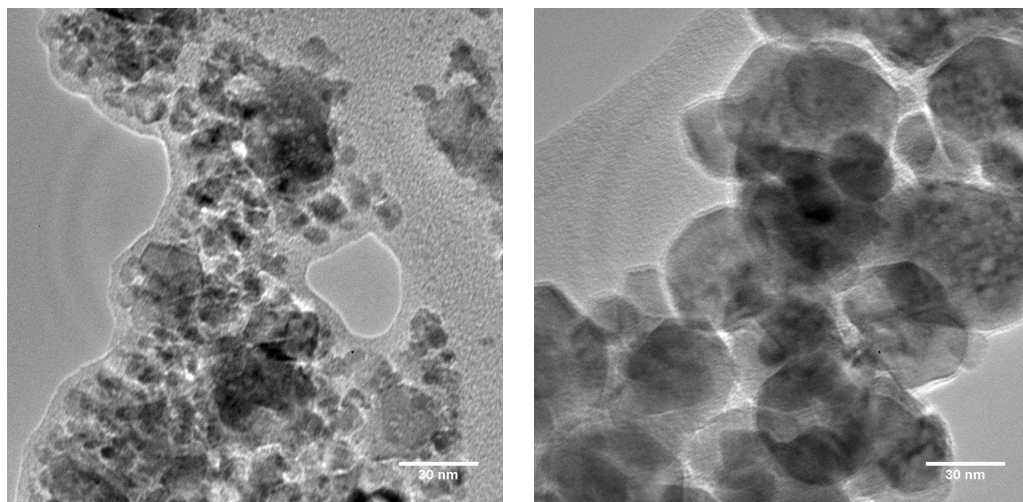


Figure 10. TEM images of fresh (left) and used (right) CF-2A samples.

The redox process (partial reduction in methanol stream and reoxidation in air) had evidently caused a sintering of the less crystalline sample CF-2A.

6.4.3. The catalytic behaviour in function of chemical-physical features

Table 3 compares the TOF of samples, measured at 300°C at the very beginning of the reaction time; results were taken almost immediately after the start-up of the reaction.

Table 3: Comparison of initial catalytic activity in phenol methylation at 300°C.

Catalyst	Initial phenol / methanol conv., %	Initial aeral TOF $\text{mol}_{\text{phenol}} \text{min}^{-1} \text{m}^{-2} (10^{-8}) /$	Initial aeral TOF $\text{mol}_{\text{methanol to lights}} \text{min}^{-1} \text{m}^{-2}$ $(10^{-8}) / \text{mol}_{\text{methanol to alkylated}}$ $\text{Ph} \text{min}^{-1} \text{m}^{-2} (10^{-8})$
CF-2A	43 / 9	5.2	6.0 / 5.3
CF-2B	47 / 12	10.4	15.5 / 10.4
CF-2C	7 / 6	10.2	72.9 / 10.0

At these conditions, it can be assumed that the characteristics of the samples were still those of the fully oxidized spinels; therefore catalytic properties can be associated to the chemical-physical properties of the corresponding freshly calcined catalysts.

At 300°C the CF-2A sample showed the lower activity, despite the presence in this sample of the more reducible sites (Figure 5). This can be attributed to the lower overall surface concentration of metal ions (Fe+Co) in the less crystalline sample (see XPS characterization of calcined catalysts, Table 2). Moreover, it is worth noting that indeed on the fully oxidized catalyst, the reduction of the oxide did not occur because of the dehydrogenation of methanol to formaldehyde (the rate-determining step of the reaction), but instead because of the oxidation of the hydrogen formed to water (the same reaction occurring in H_2 -TPR tests). Therefore, the presence of more reducible sites in sample CF-2A may have no direct implication on the acceleration of the reaction of the rate-determining step. At these conditions (i.e., 300°C), the extent of methanol dehydrogenation was low (overall methanol conversion 6-12 %), and the TOF was controlled by the surface

concentration of activated methanol species, being the generation of the phenolate favoured on the fully oxidized compound. The dehydrogenation of methanol, instead, involves Me-O pairs, and therefore the reaction rate is affected by the concentration of both Me and O sites.

Even greater was the difference between the samples in regard to the TOF for the methanol decomposition to light compounds; this is reported in Table 2, where the aeral TOF is splitted into the two values for the transformation of the alcohol to light compounds and for the incorporation of the methyl group on the aromatic ring. In the case of sample CF-2A, the two numbers were similar, whereas in the case of sample CF-2C the former one was by far greater than the latter one. In other words, sample CF-2C was more active than CF-2A in methanol dehydrogenation, because of the greater surface concentration of metal ions, but due to the lower concentration of ionic oxygen species and hence to the relatively lower amount of adsorbed phenolate species, this did not lead to a correspondingly higher conversion of phenol. With this catalyst, most of the formaldehyde formed did not attack the phenolate ring but instead decomposed to yield light compounds.

A progressive modification of catalyst features during reaction also did correspond to a non-stable catalytic performance in function of time-on-stream. This is shown in Figure 11, compiling the phenol conversion, the selectivity to *o*-cresol, and the selectivity to benzene of fresh samples CF-2A and CF-2C at 300 (Figure 11(a)) and at 390°C (Figure 11(b)), in functions of the reaction time.

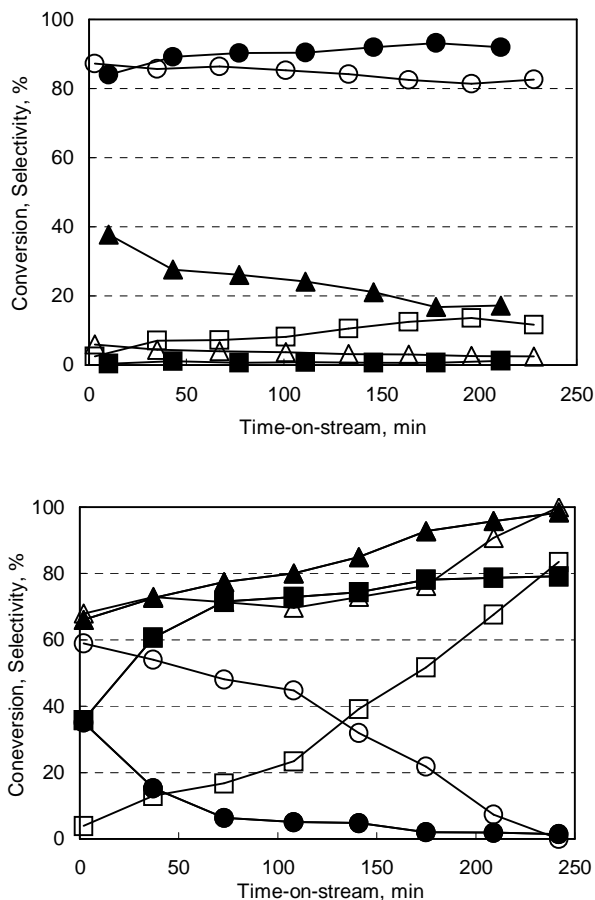


Figure 11. Catalytic performance in phenol methylation of the fresh calcined sample CF-2A (full symbols) and of the fresh CF-2C (open symbols) samples in function of time-on-stream at 300°C (11a) and at 390°C (11b). Symbols: phenol conversion (▲,△), selectivity to *o*-cresol (●,○), and to benzene (■,□).

Both samples showed a variation of catalytic performance during reactivity measurements. For what concerns the conversion of phenol, at 300°C both samples exhibited a progressive decline of activity, that however was much more evident for the CF-2A sample. In this latter case, after approximately 200 minutes time-on-stream the conversion was approximately half the initial one. However, the distribution of products was not much varied, *o*-cresol remained the prevailing compound. With the CF-2A sample, a slight increase of the selectivity to *o*-cresol did occur with the concomitant decrease of the selectivity to 2,6-xylene, whereas the formation of dehydroxilated compounds was very low (less than 5% selectivity

to benzene). With the CF-2C catalyst, showing a lower phenol conversion, the slight decline of selectivity to *o*-cresol did correspond to the increase of benzene formation. Therefore, at 300°C the reduction of the samples by the hydrogen generated led to an activity decline, probably because of the progressive decrease of the number of active sites, and specifically of the O sites responsible for the proton abstraction from phenol. In this case, therefore, the presence of more reducible sites in sample CF-2A and hence a more rapid removal of the O sites responsible for phenol activation (those present in large amount on the fully oxidized samples), was the reason for the decline of activity, more evident in the case of sample CF-2A.

The results obtained at 390°C provided further indications. In this case, in fact, sample CF-2A showed a slow but progressive increase of catalyst activity, and at the same time quite a relevant increase of the selectivity to benzene and a decline of that to *o*-cresol. This indicates that at high temperature the progressive reduction of the catalyst led to a decline of the rate of *o*-cresol formation, but at the same time caused the generation of new sites that at high temperature were very active in phenol dehydroxilation. The same did occur with the CF-2C sample, but all the phenomena occurred more slowly than with the less crystalline samples. Indeed, the conversion apparently did not change during the first 150 minutes reaction time; this likely derived from the fact that the removal of the O ions (the phenomenon responsible for the decline of activity in *o*-cresol formation) and the concomitant generation of reduced metal sites, very active in phenol dehydroxilation occurred more slowly than with the CF-2A sample. This also corresponded to the smaller variations in the selectivity to *o*-cresol and to benzene experimentally observed.

The yields to light compounds formed by methanol decomposition at 390°C in function of the reaction are shown in Figures 12(a) and 12(b), for catalysts CF-2A and CF-2C, respectively.

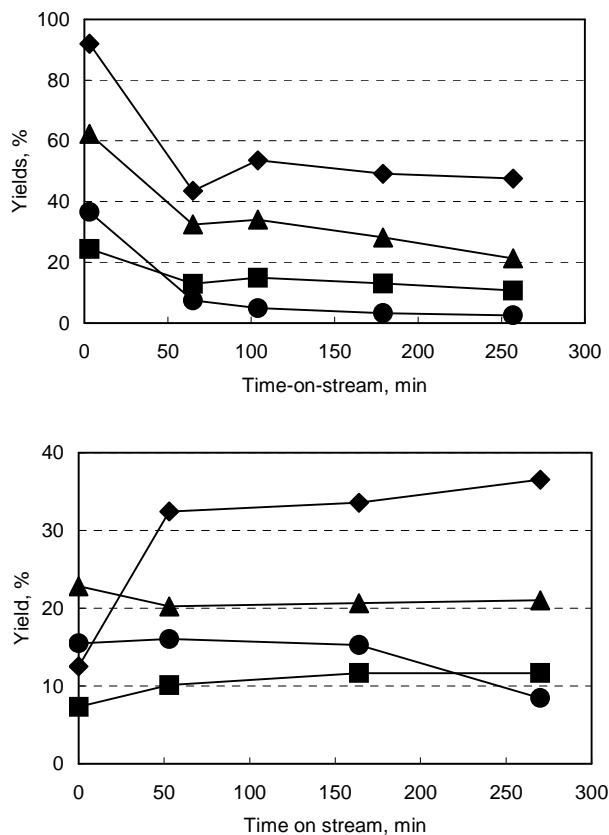


Figure 12. Methanol decomposition during phenol methylation of the fresh calcined sample CF-2A (12a) and CF-2C (12b) samples. Symbols: yield to CO_2 (▲), to CO (■), to CH_4 (●), and to H_2 (◆).

In the case of the CF-2C sample, no major variations in the formation of the C-containing compounds were shown; however, the formation of H_2 was initially low, and then showed a marked increase, due to the fact that the hydrogen formed was in part transformed to water on the oxidized catalyst, whereas it remained substantially unconverted with the reduced compound.

Considerably different was the behavior of sample CF-2A; in fact, in this case the yields to the C-containing compounds showed a decline in function of the reaction time, a behavior similar to that observed for phenol. The same occurred for the hydrogen yield, that at the very beginning was very high. The very quick reduction by the hydrogen generated, with removal of bulk oxygen and formation of water, led to a progressive decline of the activity also in methanol

dehydrogenation, because of the rapid decrease of the surface concentration of Me-O pairs.

6.5. Conclusions

Co-precipitation and thermal sintering were successfully used to synthesise CoFe_2O_4 spinels with different dimensions over the range 7-50 nm, shape and surface area. XPS revealed that the surface composition of the spinel clusters is dependent on calcination temperature. As the calcination temperature was increased the surface Fe content decreased, suggesting a transition from crystals terminated in (111) faces to those exposing more (110) or (100) facets as the crystallite size increases. In less crystalline systems, the presence of highly reducible surface sites was evidenced by means of TPR measurements.

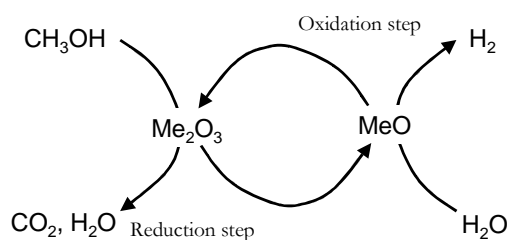
Catalytic properties in the gas-phase methylation of phenol with methanol were greatly affected by the morphology of catalysts. In less crystalline systems, a higher areal TOF for methanol conversion was related to the higher surface concentration of Me-O pair sites; the latter are hypothesized to be responsible for the dehydrogenation of methanol to formaldehyde. The reduction of the spinel by the hydrogen generated caused the progressive reduction of the spinel to a Co/Fe alloy, and a corresponding shift from the catalytic behaviour of a “basic” catalyst, active in the regio- and chemo-selective methylation of phenol to *o*-cresol, to a reduced compound, more active at high temperature in the dehydroxylation of phenol to benzene and *o*-cresol to toluene. The quicker reduction of the less crystalline system, due to the presence of more reducible sites, caused a faster transition from the oxidized spinel to the reduced compound.

Part 2

6.6. Introduction

As demonstrated in the previous part, CoFe_2O_4 is a very active catalyst for phenol methylation reaction and the morphological properties play an important role on the activity and on the deactivation, that is due to the reduction of the catalyst.

The strong reducibility, that is a problem for the catalytic point of view when the oxide is used in the methylation reaction, can be utilized for the hydrogen production processes. In fact the reduced nanosized metal is able to react with water yielding hydrogen, via the multistep reaction reported below [27,28].



In this part we are going to study the influence of the crystal sizes of the prepared CoFe_2O_4 with respect the carbon deposition during the reduction step and the yield of hydrogen produced in the oxidation step.

6.7. Experimental

Employed catalysts were obtained by co-precipitation, as described in Section 2.1. Co-precipitated samples were calcined respectively at 450°C (CF-450) and 750°C (CF-750).

Sample were characterized by means of powder X-ray diffraction (XRD) and by Thermal Programmed Reduction (TPR).

Reactivity tests were carried out by first contacting the fresh calcined oxide with a 16mol% methanol in N₂ stream, and then by feeding water vapours (29mol% in N₂) as the oxidant for the reduced spinel. Both steps were carried out at 420°C.

Coke quantitative analysis was performed by means of Thermal Programmed Oxidation (TPO) together with a mass spectroscopy analysis.

6.8. Results and discussions

6.8.1. Samples characterization

Powdered XRD analysis, shown in Figure 13, confirms that the synthesised CoFe₂O₄ samples were successfully prepared, in fact only the reflects assigned to the spinel phase CoFe₂O₄ can be observed.

Scherrer line broadening analysis on the (220), (311), (511) and (400) peaks reveal that the volume averaged particle sizes for sample CF-450 and CF-750 were respectively 13 to 32 nm. BET analysis reveals that the particle specific surface areas were respectively 55 and 10 m²g⁻¹. (Table 4).

Table 4. crystal size and specific surface area of the samples

Catalyst	Crystal size, nm	Surface area, m²/g
CF-450	13±2	55±5
CF-750	32±4	10±3

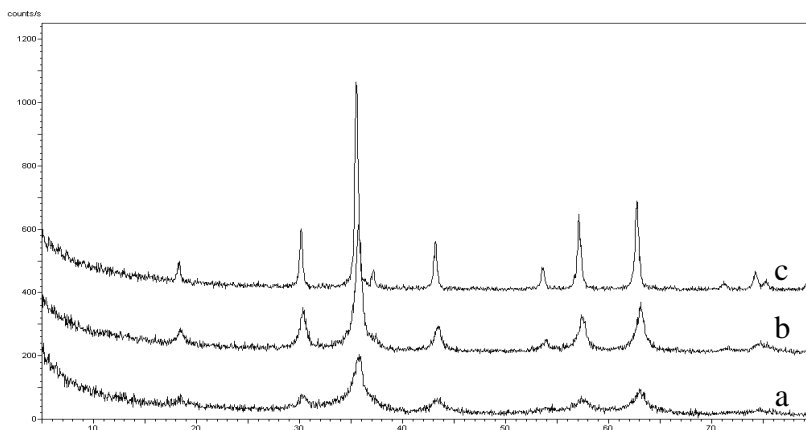


Figure 13. X-Ray diffraction spectra of: a) freshly precipitated and dried sample CF-P, b) CF-450, c) CF-750

Thermal programmed reduction profiles, here not reported, were in accordance with those obtained with samples discussed in Chapter 6 Part 1. Also in this case the more defective sample, that obtained by calcination at 450°C , was the more reducible. The different tendency to reduction disappears after the first red/ox cycle.

6.8.2. Reduction step

To evaluate the behaviour of the two samples during reaction conditions, reactivity tests feeding methanol stream were performed.

Figure 14 shows the yields of CO , CO_2 , H_2 and CH_4 , that are the products of the methanol decomposition, as a function of time-on-stream for both the samples at 420°C .

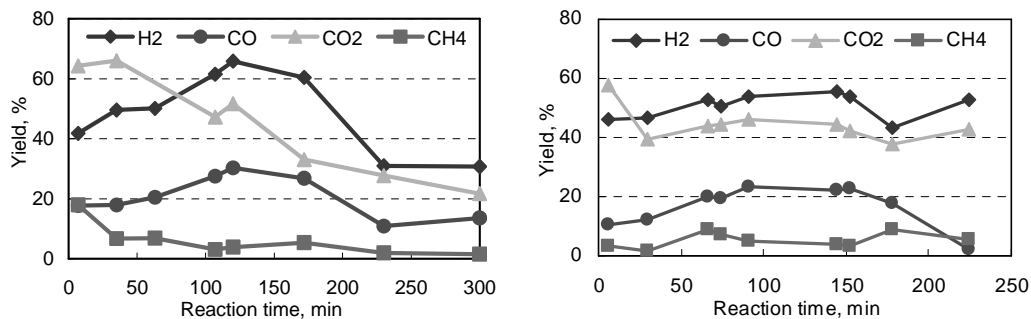


Figure 14. Decomposition of methanol with sample CF-2A (left) and with CF-750. Symbols: yield to CO₂ (▲), to CO (●), to CH₄ (■), and to H₂ (◆).

The anaerobic oxidation of methanol by the spinels produced CO₂, CO, CH₄ and H₂. With both oxides, total conversion of methanol was achieved at 420°C during the first 5 hours reaction time. CO₂ was the main product; however, with CF-450, the yield to CO₂ showed a progressive decrease, from the initial value of 60% (for the fully oxidized sample), down to 20% after 5 hours reaction time. Also the yield to CH₄ decreased from 20% to 5%. The yield to H₂ on the fresh catalyst was 40%, water being the main co-product of methanol oxidation; yield then increased (with a corresponding decrease of water formation), and reached a maximum value (65%) after 2 hours reaction time. The yield to CO had the same trend as that of H₂; this is a clear indication that H₂ was produced by dehydrogenation of methanol to formaldehyde and to CO.

In the case of CF-750, the initial yield to CO₂ was the same as for CF-450; however, the decline of yield was much lower than that experimentally observed with the less crystalline sample. Moreover, also the yields to CO and H₂ showed smaller variations than those shown by CF-450.

As demonstrated in the previous Part, with the increasing of the time-on-stream, upon a reductive atmosphere, two effects happen over the catalytic surface: the reduction of the catalysts and the coke deposition. The latter

proceeds preferentially over the metal reduced surface and therefore is a consequence of the reduction.

To evaluate a correlation between the reduction rate and the time-on-stream, powder XRD analyses of samples, used for variable times were performed. Diffraction pattern, reported in Figure 15, reveal several important aspects.

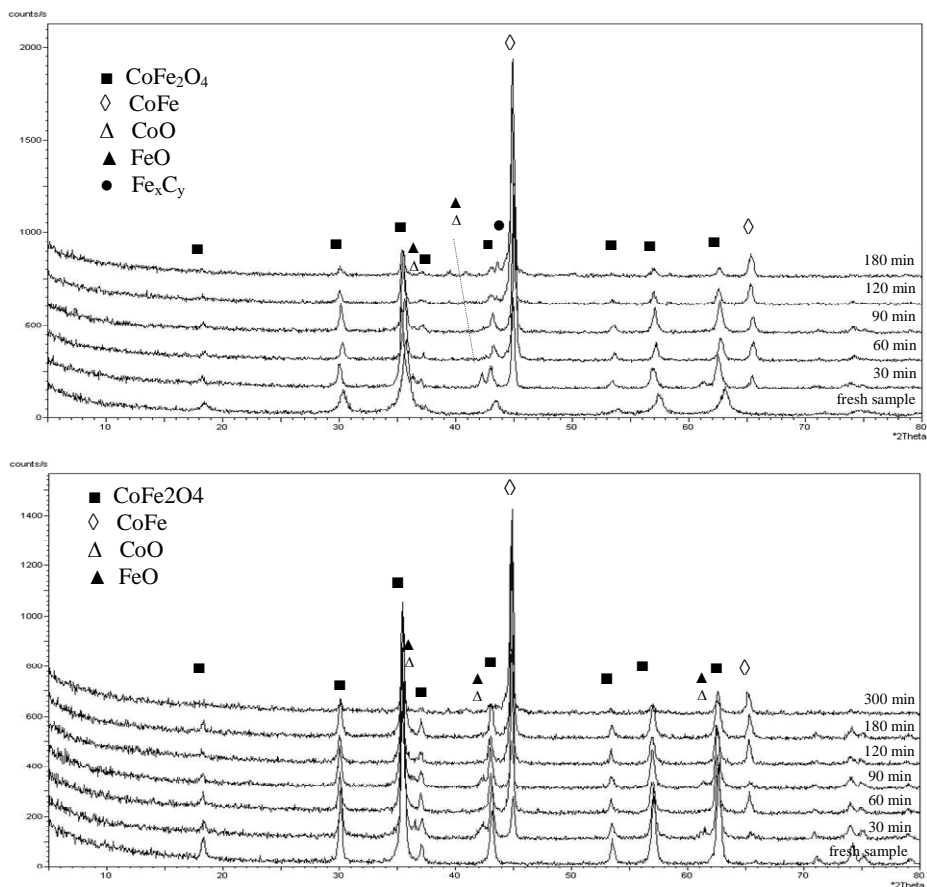


Figure 15. X-Ray diffraction spectra of: CF-450 (top) and CF-750 (bottom) kept in contact with methanol stream at 420°C for variable time-on-stream.

For both the samples, reflects attributable to the spinel phase decrease after few minutes and new reflects, attributable to metallic Co/Fe alloy, CoO and FeO appear.

In the case of sample CF-450, the reduction was faster and the reflects attributed to the spinel phase, that were more broaden, disappear after a shorter time. Moreover, the pattern indicates also the presence of iron carbide.

With the more crystalline sample CF-750 the progressive reduction was slower, moreover no formation of metal carbide was observed in this case.

The differences between the two samples experimentally observed cannot be simply ascribed to the different surface area of the two samples. Since with both samples the reaction was carried out under conditions leading to total methanol conversion, the greater variation of performance shown by CF-450 as function of the reaction time is attributable to a different ratio between the rate of C and H₂ migration towards the core of crystallites and that of ionic oxygen towards the surface

The amount of deposited coke was evaluated by using TPO analysis with mass spectrometer. For the tests the catalysts was kept in contact with a diluted oxygen stream and then heated, the amount of CO₂, that was quantified by integration of the mass signal, was correlated to the amount of deposited coke. Results are shown in Figure 16.

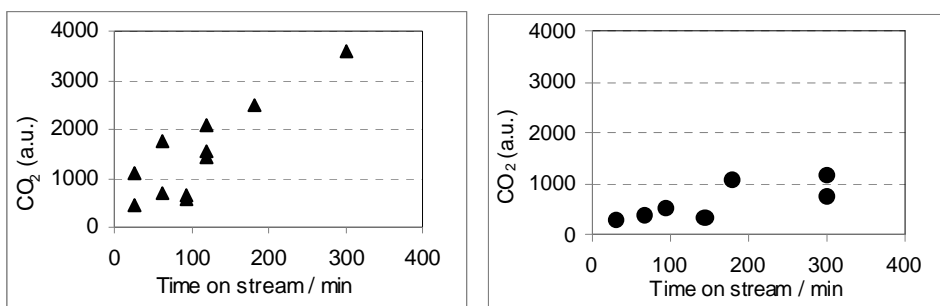


Figure 16. amount of CO₂ revealed with TPO analysis with sample kept in contact with methanol for different time-on-stream. Top: CF-450, bottom CF-750.

It is worth mentioning that with sample CF-450 the amount of carbon dioxide obtained was bigger than that obtained with the other sample. The bigger amount of CO₂, and therefore of the deposited coke, observed for the sample CF-450 can be correlated to the bigger specific surface area. Moreover,

because the coke deposition is a consequence of the catalyst reduction, the different rate of coke formation can be associated to the different tendency to the reduction, in fact the previously shown results indicate that for sample CF-450 the reduction is faster.

6.8.3. Oxidation step

The reoxidation step with water led to the formation of the CoFe₂O₄ spinel with both samples and at the same time of hydrogen.

Figure 17 shows the yield of H₂ obtained with samples CF-450 and CF-750 after the reduction step with methanol for 180 min.

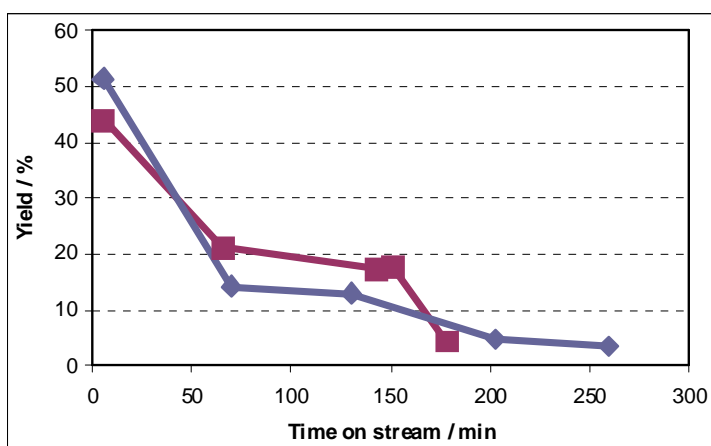


Figure 17. Yield to H₂ with CF-450 (◆) and CF-750 (■)

It is worth mentioning that the obtained yield in hydrogen was similar for the two tested samples.

In the reactors outcoming products stream there was also a little concentration of CO₂ yield by coke oxidation but no CO was revealed. The values of H₂ and CO₂ concentration present in the products stream is shown in the Table below.

Table 5. composition of the products stream

	%H ₂	%CO ₂
CF-450	22,58	5,18
CF-750	16,42	3,03

XRD characterization after contact with water samples were almost completely reoxidated, as demonstrated in Figure 18.

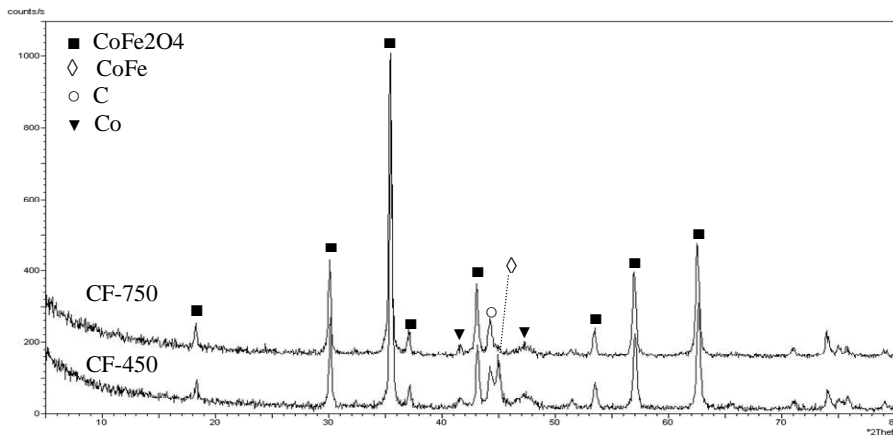


Figure 18. X-Ray diffraction spectra of CF-450 and CF-750 after reoxidation with water at 420°C

It is worth noting that with both the samples reflects attributable to a graphitic phase and metallic Co are observable. Moreover, in the case of sample CF-450, there is also a little concentration of CoFe alloy phase.

For both the samples the reflects are more sharp on respect the respectively fresh samples, that indicates a sintering of the particles. The Following Table report the average crystalline size obtained by using the Sherrer equation.

Table 6. comparison of specific surface area and crystal size between fresh and reoxidated samples

	Fresh samples		Reoxidated samples	
	SSA (m ² /g)	Crystal size (nm)	SSA (m ² /g)	Crystal size (nm)
CF-450	55	13	9	54
CF-750	10	32	6	55

6.9. Conclusions

Two samples of CoFe₂O₄ with different particle size were studied by means of catalytic tests by characterization before and after reactivity tests. Both the samples were able to totally decompose methanol at 420°C and the decomposition products distribution for the two samples were similar. The main differences between the samples were regarding the tendency to the reduction. In fact the more defective sample, CF-450, was demonstrated easily to reduce in the reactivity conditions.

Both reduced samples can reduce water yielding H₂. After the first redox cycle, the morphological properties of the samples were very similar.

6.10. Acknowledgments

I wish to acknowledge prof. K. Wilson and A. F. Lee from University of York.

6.11. References

- [1] C.N.R. Rao, A. Muller, A.K. Cheetham "The Chemistry of Nanomaterials: Synthesis, Properties and Applications", 2004 Wiley-VCH Verlag GmbH & Co. KGaA.
- [2] H.H. Kung, M.C. Kung, Catal. Today, 97 (2004) 219.

- [3] D.S. Mathew, R. S. Juang, *Chem. Eng. J.*, 129 (2007) 51.
- [4] K.Sreekumar, S. Sugunan, *Appl. Catal. A*, 230 (2002) 245.
- [5] K.Sreekumar, S. Sugunan, *J. Mol. Catal. A*, 185 (2002) 259.
- [6] E. Manova, T. Tsoncheva, D. Paneva, I. Mitov, K. Tenchev, L. Petrov, *Appl. Catal. A*, 277 (2004) 119.
- [7] V. Pillai, D.O. Shah, *J. Magnet. Magn. Mater.*, 163 (1996) 243.
- [8] E. Manova, T. Tsoncheva, Cl. Estournes, D. Paneva, K. tenchev, I. Mitov, L. Petrov, *Appl. Catal. A* 300 (2006) 170.
- [9] T. Mathew, S. Malwadkar, S. Pai, N. Sharanappa, C.P. Sebastian, C.V.V. Satyanarayana, V.V. Bokade, *Catal. Lett.* 91 (2003) 217.
- [10] K. Sreekumar, S. Sugunan, *J. Mol. Catal. A* 185 (2002) 259.
- [11] T. Mathew, M. Vijayaraj, S. Pai, B.T. Pope, S.G. Hedge, B.S. Rao, C.S. Gopinath, *J. Catal.* 227 (2004) 175.
- [12] N. Ballarini, F. Cavani, L. Maselli, A. Montaletti, S. Passeri, D. Scagliarini, C. Flego, C. Perego, *J. Catal.*, 251 (2007) 423.
- [13] N. Ballarini, F. Cavani, L. Maselli, S. Passeri, S. Rovinetti, *J. Catal.* 256 (2008) 215.
- [14] J.P. Jacobs, A. Maltha, J.G.H. Reintjes, J. Drimal, V. Ponec, H.H. Brongersma, *J. Catal.* 147 (1994) 294.
- [15] M.A. Valenzuela, J.P. Jacobs, P. Bosch, S. Reijne, B. Zapata, H.H. Brongersma, *Appl. Catal. A* 148 (1997) 315.
- [16] M.J. Davies, S.C. Parker, G.W. Watson, *J. Mater. Chem.*, 4 (1994) 813.

- [17] J. Ziółkowski, Y. Barbaux, J. Molec. Catal. 67 (1991) 199.
- [18] D. Briggs, M.P. Seah, "Practical Surface Analysis: Auger and X-Ray Photoelectron Spectroscopy" 2nd Ed., Wiley 1996.
- [19] A.P. Grosvenor, B.A. Kobe, M.C. Biesinger, N.S. McIntyre, Surf. Interf. Anal. 36 (2004) 1564.
- [20] G. Bhargava, I. Gouzman, C.M. Chun, T.A. Ramanarayanan, S.L. Bernasek, Appl. Surf. Sci. 253 (2007) 4322.
- [21] T. Droubay, S.A. Chambers, Phys. Rev. B 64 (2001) 205414
- [22] K. Takubo, T. Mizokawa, S. Hirata, J.-Y. Son, A. Fujimori, D. Topwal, D.D. Sarma, S. Rayaprol, E.-V. Sampathkumaran, Phys. Rev. 71 (2005) 073406.
- [23] J.-G. Kim, D.L. Pugmire, D. Battaglia, M.A. Langell, Appl. Surf. Sci., 165 (2000) 70.
- [24] A. Khan, P.G. Smirniotis, J. Molec. Catal. A 280 (2008) 43.
- [25] Y. Qu, H. Yang, N. Yang, Y. Fan, H. Zhu, G. Zou, Mater. Lett., 60 (2006) 3548.
- [26] W.H. Wang, X. Ren, J. Cryst. Growth, 289 (2006) 605.
- [27] H. Kaneko, N. Gokon, N. Hasegawa, Y. Tamaura, Energy 30 (2005) 2171
- [28] P. Chiesa, G. Lozza, A. Malandrino, M. Romano, V. Piccolo, Int J Hydrogen Energy 33 (2008) 2233

Chapter 7

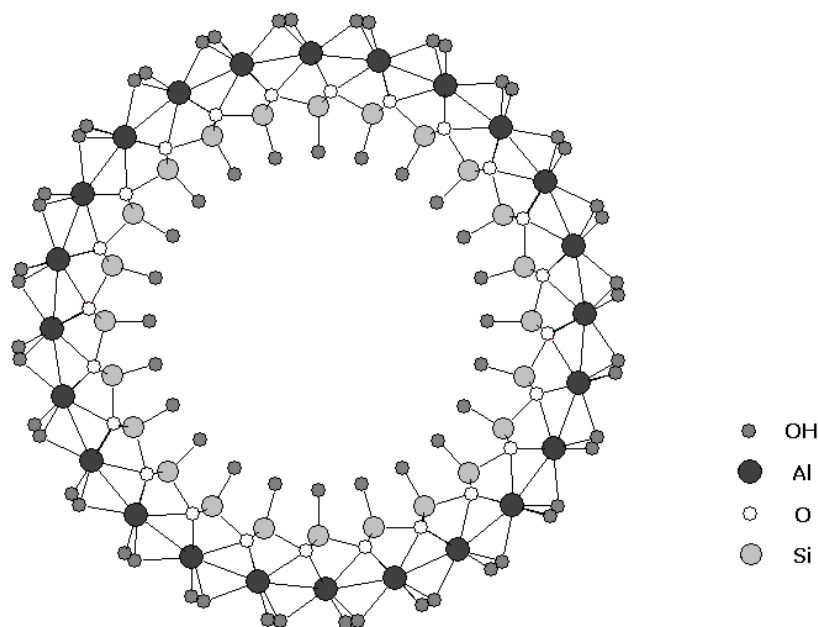
Imogolite, a nanostructured acid catalyst

7.1. Introduction

Proper Imogolite (from the Japanese “Imogo”, clay soil) is a material of volcanic origin [1], with chemical composition $(\text{OH})_3\text{Al}_2\text{O}_3\text{SiOH}$ and a fascinating nanotubes structure [2], illustrated in Scheme 1. Formation of imogolite can be described considering a single $\text{Al}(\text{OH})_3$ gibbsite sheet and substituting, on one side only, three OH groups with an orthosilicate unit O_3SiOH . Being Si-O bonds shorter than Al-O bonds, the gibbsite-like sheet curls up, eventually forming nanotubes. When the process is not successful, an amorphous phase forms, proto-imogolite.

Imogolite may also be obtained via sol-gel synthesis, the most common methods being those due to Farmer *et al.*, and Wada *et al.* [3-5], respectively. Natural imogolite nanotubes are several μm long, with an outer and inner diameter of 1.0 and 2.0 nm, respectively [2], whereas the outer diameter of synthetic imogolite increases to *ca.* 2.7 nm. Electron diffraction measurements [2] and computer models [6] showed that the most likely structures for natural and synthetic imogolite are nanotubes with 10 and 12 gibbsite units in the cross-section, respectively. These structural findings are in agreement with later molecular dynamics simulations, showing that the strain energy has a minimum for nanotubes with 24 Al atoms in the cross-section (corresponding to 12 gibbsite units) [7].

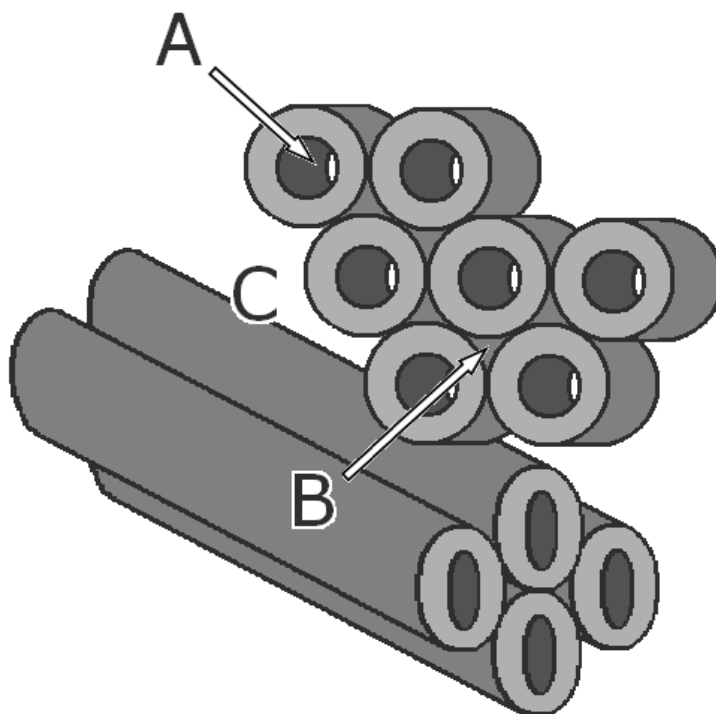
The structure represented in Scheme 1 for natural imogolite allows a few considerations over internal silanols. The distance between two adjacent silanols in the same circumference results to be 0.26 nm and that between two silanols of two adjacent circumferences is 0.40 nm. Silanols density can therefore be calculated by considering through simple geometric considerations: it results to be 9.1 OH nm^{-2} , *i.e.* much higher than the average silanols density at the surface of hydrated amorphous silicas (ca. 5 OH nm^{-2}). Taking into account the rigidity of the pseudo-crystalline structure and the distances among them, internal silanols are expected not to show sizable interactions between them.



Scheme 1

Once formed, nanotubes organize into a porous network of interwoven bundles, with three kinds of pores, shown in Scheme 2: A) intra-tube pores (about 1 nm wide); B) inter-tubes pores, the spacings between three aligned tubes in a regular packing (0.3 – 0.4 nm wide); C) slit mesopores among bundles [8,9]. It is

probable that inter-tubes pores are too small to allow any adsorption phenomenon [8,9].



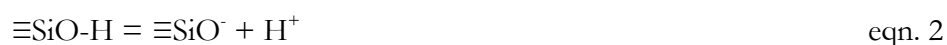
Scheme 2

Though much less famous than Carbon NanoTubes, imogolite nanotubes exhibit interesting features, and offer potential applications in gas adsorption, separation and storage [6,8,9], anions/cations retention from water [10-14] and catalysis [15,16]. The study of the surface properties, *e.g.* the type and abundance of acidic Lewis and/or Brønsted species, and the exploitation of such systems has not been developed yet: the present paper constitutes a pioneering attempt in the field.

From a catalytic point of view, most interesting features are: i) the nanoporous structure; ii) the outer surface covered by Al(OH)Al groups; iii) the inner surface lined by $\equiv\text{SiOH}$ groups. Being the outer Al atoms octahedrally coordinated, no relevant acidity is expected for such sites [17]. Catalytic activity

should be related to inner silanols, so that the nanopore structure should be effective in promoting shape-selective diffusion of reactants, by favouring the preferential formation of small products with respect to “bulky” side-products.

Besides gas-solid reactions, imogolite is also considered for aqueous phase reactions, since, depending on pH, the outer surface may have a positive net charge [18] and, correspondingly, the inner surface a negative net charge, due to the equilibria:



This feature probably accounts for the formation of closely packed bundles of several hundred tubes, since bound counterions may hold nanotubes together [18].

Being a hydrated alumino-silicate, its hydration/dehydration behaviour is of paramount importance in dictating the optimal operating conditions for any application requiring a surface interaction. On heating, imogolite loses physically adsorbed water below 200°C, whereas loss of water because of hydroxyl condensation only occurs at about 400°C [19], *i.e.* at a temperature higher than with protoimogolite. Dehydroxylation at 500°C is accompanied by breakdown of the tubes [18] and formation of a lamellar alumino-silicate, with new surface functionalities. NMR studies shown that in imogolite nanotubes only tetrahedral Si atoms and octahedral Al atoms are present, whereas after structural dehydroxylation new environments create for both Si and Al [19], the latter being present also as tetrahedral and five-coordinated aluminium.

To investigate the surface functionalities of proper imogolite (IM), of the amorphous protoimogolite phase (PR-IM) and of the lamellar material deriving from its structural dehydroxylation (L-IM), a joint FT-IR and catalytic study has been carried out. The interaction with several probe molecules, namely carbon monoxide, ammonia, phenol and methanol, showing quite different acid-base properties, was studied, aiming at the understanding of active sites accessibility and reactivity, also in relation to the potentiality of these materials in catalyzing acid-

base reactions. In this regard, the reaction between phenol and methanol was chosen as a probe test in electrophilic aromatic substitution, in particular the accessibility under flow conditions of acidic sites in IM. Reactivity towards the same reaction was also measured for PR-IM and L-IM. For comparison, catalytic measurements were also carried out with alumina and silica, assumed to represent the reactivity of the outer and inner surfaces of IM, respectively.

7.2. Experimental

7.2.1. Methods

FESEM pictures were collected with a High Resolution FESEM instrument (LEO 1525) equipped with a Gemini Field Emission Column.

BET surface area and pore sizes of powders outgassed at 150°C were measured by means of N₂ adsorption/desorption at -196°C on a Quantacrome Autosorb 1C instrument. The Non Local-DFT method was used to evaluate pores size distribution (PSD), by applying a N₂ – silica kernel.

FT-IR spectra of both KBr pellets and self-supporting wafers were collected on a Equinox 55 Spectrophotometer, equipped with MCT cryodetector. Self-supporting wafers (optical density of about 10 mg cm⁻²) were treated under high vacuum (residual pressure < 10⁻³ mbar) at 150, 300 and 500°C, prior to the adsorption of probe molecules. The latter were: a) carbon monoxide. Being the interaction very weak, FT-IR measurements were carried out at the nominal temperature of nitrogen normal boiling point (NBP); b) ammonia, phenol and methanol, adsorbed at room temperature.

Samples are identified by the acronym of the solid followed by the temperature (in Celsius) of the pre-treatment, *e.g.* IM-150 stands for imogolite heated at 150°C. Note that IM-500 coincides with L-IM.

7.2.2. Catalytic tests

Catalytic tests with PR-IM, IM-300 and L-IM were carried out by vaporization of a methanol/phenol liquid mixture (methanol/phenol molar ratio 7/1; phenol supplied by Sigma Aldrich, 99+% purity; methanol supplied by Carlo Erba Reagenti) in a N₂ stream. The composition of the feed gas was (molar fractions): methanol 0.094, phenol 0.013, nitrogen 0.893. Overall gas residence time was 0.78 s. Total pressure was atmospheric. For catalytic tests carried out with γ -Al₂O₃ and SiO₂, the composition of the feed gas was (molar fractions): methanol 0.108, phenol 0.011, nitrogen 0.881. The gas/vapors stream was fed to a glass reactor containing 1 cm³ of catalyst, shaped in 30–60 mesh particles. Catalysts weights were: PR-IM, IM-300 and IM-500 0.92 g, γ -Al₂O₃ 0.78 g and SiO₂ 0.34 g.

7.3. Results and discussion

7.3.1. Textural characterization

Figure 1 reports low angle XRD patterns of fresh imogolite IM, IM-300 and L-IM, along with that of PR-IM (inset).

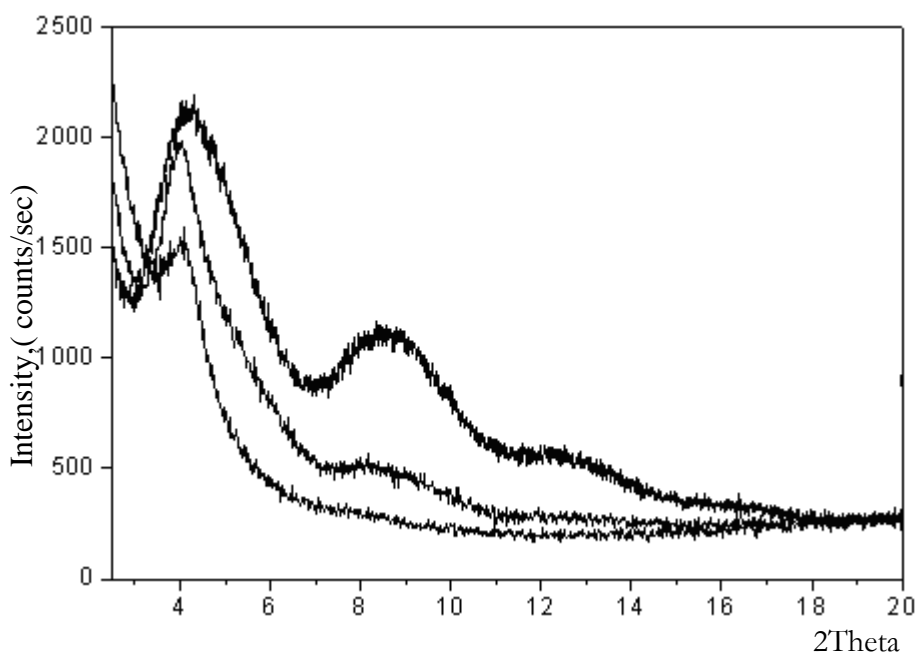


Figure 1: Low angle ($2\theta = 2.5^\circ - 20^\circ$) powder XRD patterns, from top to bottom of fresh imogolite (IM-r.t.), IM-300 and L-IM.

Results are quite in agreement with what expected. PR-IM is amorphous [18], whereas IM diffraction patterns show the peaks of the hexagonal structure into which bundles of nanotubes are organized.

From the (100) reflection at $2\theta = 4.18^\circ$, a centre-to-centre distance between two adjacent nanotubes is calculated to be 2.54 nm, in agreement with the literature [2]. The nanotubular structure is preserved at 300°C (IM-300), notwithstanding a limited loss of long range order, whereas after treatment at 500°C only one peak is seen at $2\theta = 4.04^\circ$, due to the formation of a lamellar phase [19].

Figure 2a reports N_2 isotherms at -196°C: with PR-IM, IM-150 and IM-300, Type I isotherms are observed, typical of microporous materials according to IUPAC classification, with small hysteresis loops due to limited external mesoporosity, most probably deriving from slit mesopores among bundles (Scheme 2).

Pore size distribution, specific surface area and tubular diameters are reported in Table 1.

Table 1. Samples properties

Sample	BET SSA ($m^2 g^{-1}$)	Total Pore Vol. ($cm^3 g^{-1}$)	Micropores Vol. ($cm^3 g^{-1}$) ¹	Inner diameter (nm) ²	Outer diameter (nm) ³
IM-150	213	0.20	0.01	-	-
IM-300	362	0.26	0.04	0.98	2.44
IM-500	197	0.16	0.02	-	-
PROTO-IM	178	0.09	0.03	-	-

Larger pores are due to heterogeneous inter-bundles voids in the fibrous network shown by the FESEM picture in Figure 2. PR-IM appears instead as hollow spheres, as reported in the inset at a lower magnification.

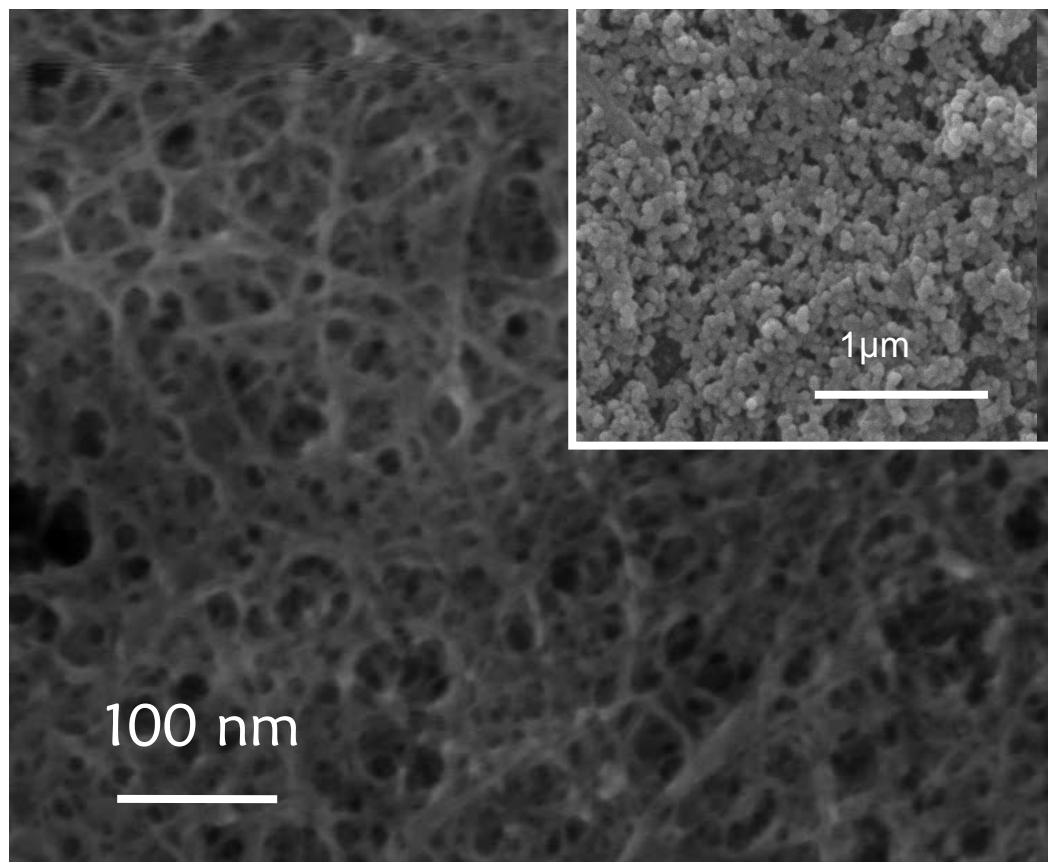


Figure 2: FESEM (Field Emission Scanning Electron Microscopy) picture of fresh IM. Inset to Figure: SEM picture, taken at lower magnification, of PR-IM.

7.3.2. FT-IR spectroscopic characterization of bare samples.

Figure 3 reports FT-IR spectra of an IM self-supporting wafer, outgassed at r.t.; 150; 350, and of L-IM. In the hydroxyls stretch region ($3800 - 3000 \text{ cm}^{-1}$), spectra are dominated by intense absorption due to H-bond.

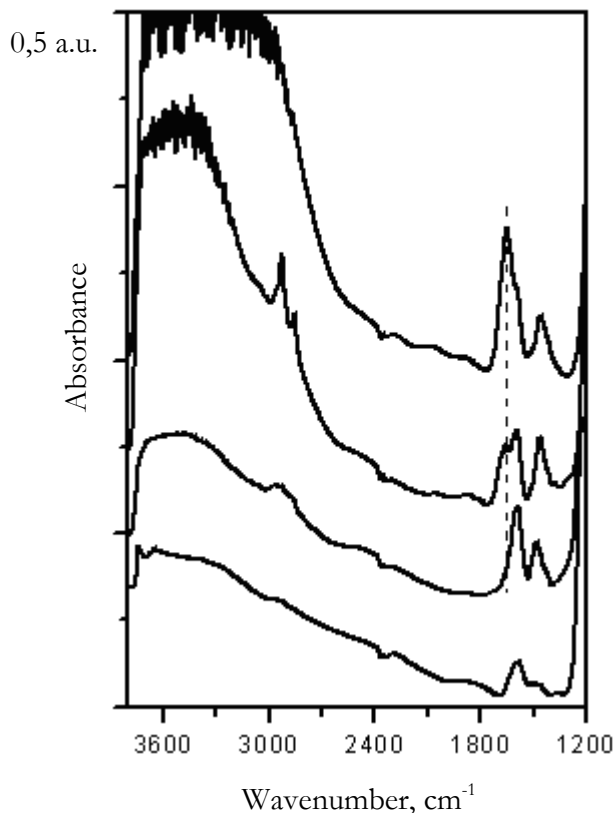


Figure 3: FT-IR spectra of imogolite outgassed for 1 hour, from bottom to top: at r.t. (IM-r.t.); 150°C (IM-150); 300°C (IM-300) and 500°C (L-IM).

Besides adsorbed molecular water, imogolite nanotubes present surface hydroxyls, both external and internal: the former may interact, besides with water molecules, also with neighbouring nanotubes. At lower wavenumbers, bands at 1595 and 1465 cm^{-1} are seen, assigned to carbonate-like species on the outer surface, like those formed on aluminum hydroxide [17]. The dotted vertical line at 1650 cm^{-1} indicates the band due to the bending mode of water, removed at 300°C. At this temperature, nanotubes are still stable (Figure 1) and inner pores with 0.98 nm diameter become accessible.

It may be concluded that water, present both at the external and internal surface, is removed at 300°C, rendering inner $\equiv\text{SiOH}$ groups accessible to probes.

With L-IM, the hydroxyl spectrum dramatically changes: several components are seen at 3743, 3734, 3646 cm^{-1} , with a broad signal at lower frequencies due to H-bonded hydroxyls. XRD showed the loss of tubular structure at 500°C, with formation of a new lamellar alumino-silicate with high Al content (Al/Si = 2).

7.3.3. FT-IR spectroscopic characterization of acidic species: adsorption of CO and NH₃.

To study both accessibility and acidity of inner silanols, CO has been dosed on IM-150 and IM-300 at the nominal temperature of -196°C, the NBP of N₂: in the presence of free silanols, a band at 2156 cm^{-1} is expected, characteristic of the stretching mode of CO interacting with $\equiv\text{SiOH}$ [20]. Figure 5 compares the relevant spectra in the 2250 – 2050 cm^{-1} range, after subtraction of bare samples spectra in Figure 4.

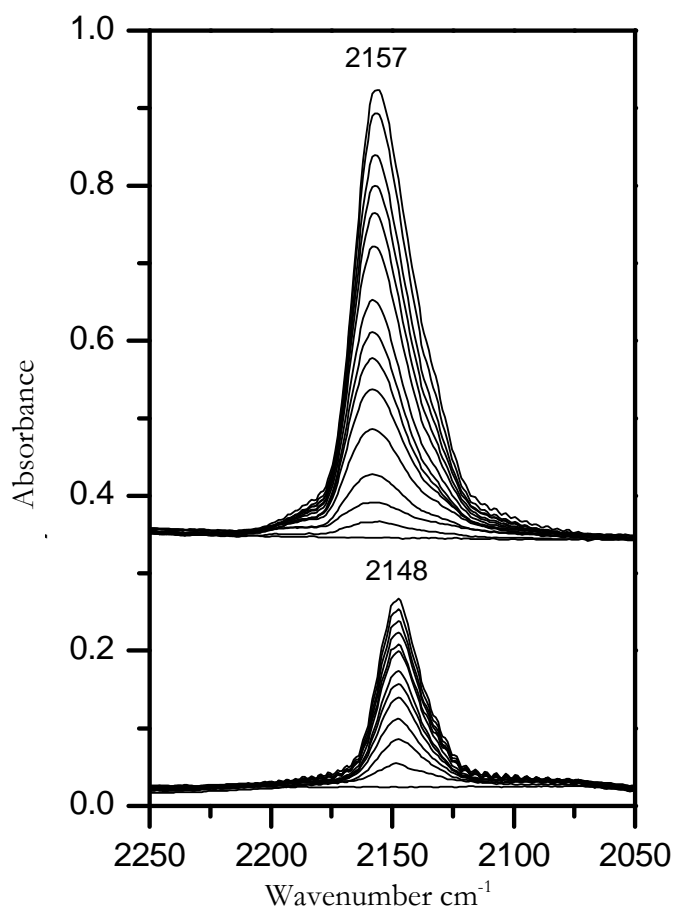


Figure 4: CO stretch range (2250 – 2050 cm^{-1}) of difference FT-IR spectra, obtained after dosing CO (equilibrium pressures: 0.5 – 15 mbar) on IM-150 (lower part of the Figure) and IM-300 (upper part of the Figure).

With IM-150 (lower part of Figure 4), only one band is observed at 2148 cm^{-1} : the limited shift with respect to the free molecule in gas phase (2143 cm^{-1}) indicates a weak interaction of electrostatic nature. The observed wavenumber (2148 cm^{-1}) is close to that reported in the literature for CO/ H_2O dimeric complexes (2144 – 2149 cm^{-1}), formed after CO adsorption on ice: this suggests a weak interaction of CO with water molecules, probably at the outer surface [21].

With IM-300 (upper part of Figure 4), the expected band at 2157 cm^{-1} is observed, due to CO on inner silanols [20], together with a minor band at ca. 2190

cm^{-1} probably due to CO adsorbed on weak Al^{3+} Lewis sites at the outer surface [22]. Finally, the shoulder at 2134 cm^{-1} , showing up at higher equilibrium pressures, is ascribed to physisorbed CO (liquid-like phase), as observed in zeolites microcavities [23].

Figure 5 reports difference spectra recorded under comparable CO pressures on L-IM: as a whole, bands are less intense, indicating that fewer sites are accessible to this probe.

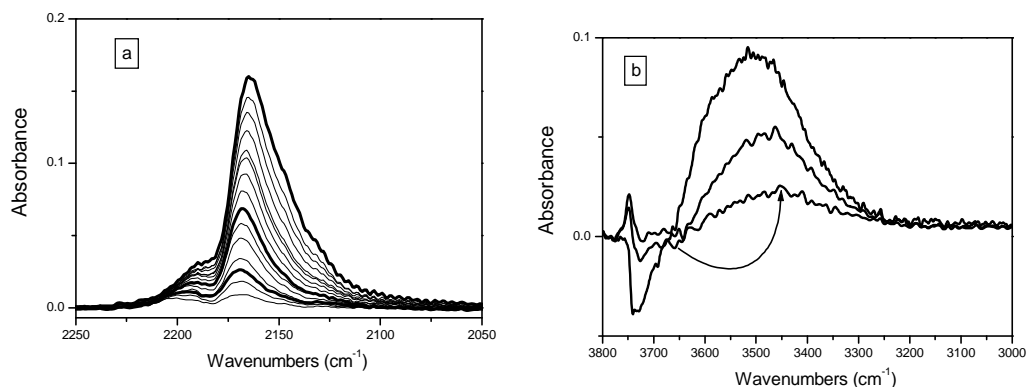


Figure 5: a) CO stretch range ($2250 - 2050 \text{ cm}^{-1}$) of difference FT-IR spectra, obtained after dosing CO on L-IM (equilibrium pressures: $0.5 - 15 \text{ mbar}$). b) OH stretch region ($3800 - 3000 \text{ cm}^{-1}$) of bold curves in Figure.

In the CO stretching range (Figure 5a), a minor band is seen at 2203 cm^{-1} , shifting with coverage to 2188 cm^{-1} , together with a main band at 2170 cm^{-1} , shifting to 2166 cm^{-1} . Both bands are reversible upon evacuation at low temperature: the former is assigned to CO adsorbed onto coordinatively unsaturated Al^{3+} , as at the surface of transition aluminas [17]; the latter to CO interacting with hydroxyls more acidic than silanols, as discussed below.

Figure 5b reports the OH stretching region ($3800 - 3000 \text{ cm}^{-1}$) of the spectra represented as bold curves in Figure 5a: the negative band of hydroxyls H-bonded to CO is rather broad, with at least three components at 3743 , 3725 and 3660 cm^{-1} . Upon CO adsorption, the bands at 3743 and 3725 cm^{-1} both shift by about -240 cm^{-1} , and that at 3660 cm^{-1} undergoes a bathochromic shift of about 210 cm^{-1} .

These shifts are too large to be due to silanols or AlOH species, and are therefore ascribed to Brønsted-like sites. It can be recalled that: i) species absorbing at 3660 cm^{-1} , have been previously observed on similar materials, *i.e.* Al-rich ($\text{Al/Si} = 0.4$) micelle-templated silicates [22], and were ascribed to Si-O-Al(OH)-O-Si species, undergoing with CO a shift of *ca.* 220 cm^{-1} ; ii) on amorphous aluminosilicates with Al/Si in the 1 – 2 range, 3748 cm^{-1} hydroxyls were observed to shift of *ca.* 230 cm^{-1} , the corresponding CO stretch mode being at 2169 cm^{-1} [24].

This means that the high temperature treatment leading to the formation of a new lamellar structure brings about the formation of a family of heterogeneous Brønsted sites of increased acidity. The observed shifts are similar to those due to Brønsted hydroxyls in mildly acidic zeolites (H-Y): this feature may render L-IM very interesting as an acidic catalyst.

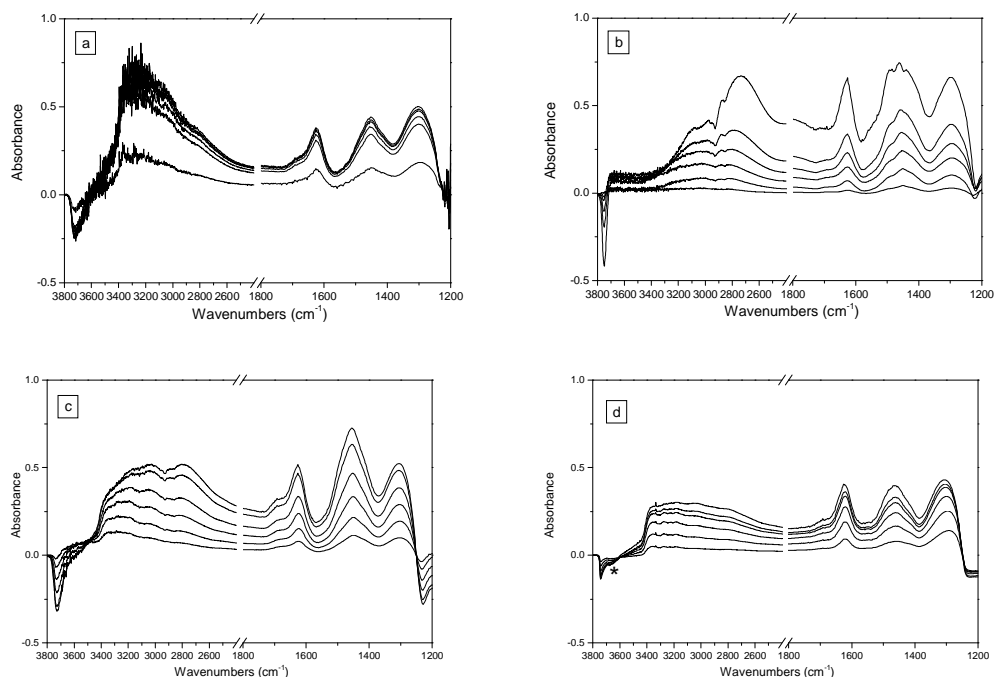


Figure 6: Difference FT-IR spectra, obtained after dosing increasing NH_3 on PR-IM-300 (a); IM-150 (b); IM-300 (c) and L-IM (d) (equilibrium pressures: 0.5 – 35 mbar).

NH_3 was dosed at room temperature on PR-IM, IM-150, IM-300 and L-IM. After ammonia dosage on PR-IM (Figure 6a), bands are seen at 1625, 1450 and 1300 cm^{-1} : the first is due to ammonia sitting on Al^{3+} Lewis sites, whereas both the 1450 and 1300 cm^{-1} bands are due to ammonium species formed on Brønsted acidic sites. Interaction with ammonia is only reversible at 300°C , indicating the presence of medium-strength acidic sites.

Upon NH_3 dosage on IM-150 (Figure 6b), similar bands are seen at 1630, 1450 and 1290 cm^{-1} . The 1630 cm^{-1} band is due to NH_3 molecules coordinated to outer Al^{3+} Lewis sites; the latter two bands, instead, are due to poly-dentate NH_4^+ species. Correspondingly, in the OH stretch region, a band decreases at 3750 cm^{-1} , the typical frequency of isolated silanols, and a broad absorption increases at about 2935 cm^{-1} . This is assigned to NH_3 interaction with few free silanols, actually not accessible to a weak base like CO, but able to coordinate NH_3 . Therefore, 1450 and 1290 cm^{-1} bands are probably due to multiple interaction of NH_3 with more than one silanol, being the inner surface of nanotubes lined by $\equiv\text{SiOH}$.

Interaction with ammonia is only reversible after outgassing at 500°C , *i.e.* at a temperature higher than with proto-imogolite: this is surprising, due to the poor acidity of silanols usually observed on silicas [20] and at the outer surface of zeolites, and it is probably ascribable to difficult diffusion of ammonia inside the nanotubes still filled by water, which also interacts with ammonia.

Similar spectral features are observed after NH_3 dosage on IM-300 (Figure 6c), although the negative band of silanols is broader: after water removal at 300°C , all silanols are actually accessible to NH_3 and heterogeneity may arise between silanols inside the nanotubes and silanols at the opening of nanotubes, for example.

With L-IM (Figure 6d), adsorption of NH_3 reveals the presence of both Lewis and Brønsted sites, and a component at 3660 cm^{-1} (asterisk) is clearly seen, in agreement with CO adsorption.

7.3.4. FT-IR spectroscopic characterization of hydroxyls accessibility to reactants of catalytic tests: adsorption of phenol and methanol at room temperature.

Further FT-IR measurements were performed basically on IM-300, the sample showing accessible silanols and still the nanotubes structure.

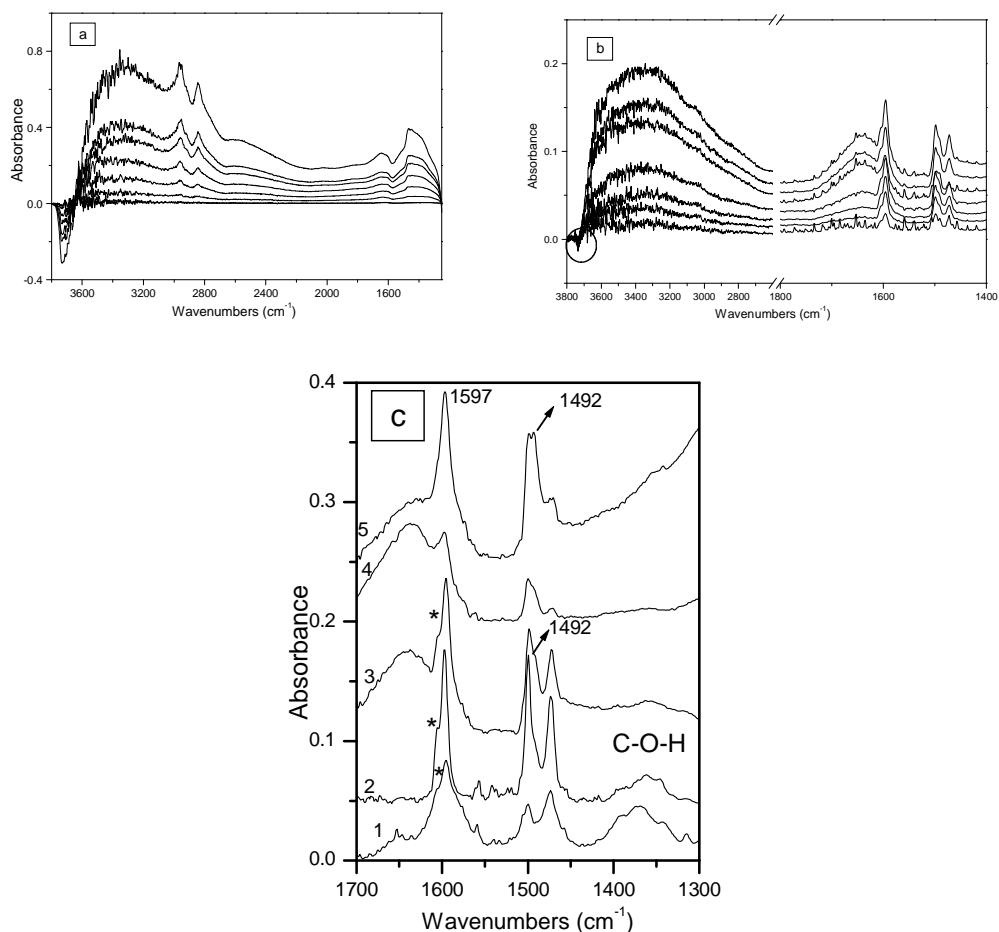


Figure 7: Difference FT-IR spectra, recorded on IM-300 after dosing a) phenol (equilibrium pressures: 0.05 – 2.5 mbar) and b) methanol (equilibrium pressures: 0.05 – 5.0 mbar). (c) C=C aromatic ring stretch range of spectra of phenol in KBr disk (1) and adsorbed on silica (2); IM-300 (3); PR-IM-300 (4) and L-IM (5).

Figure 7a reports difference spectra, obtained by increasing methanol equilibrium pressure (0.05 – 5 mbar) on IM-300: 2963 and 2844 cm⁻¹ bands are due to the $\nu_s(\text{CH}_3)$ and $2\delta_s(\text{CH}_3)$ modes, respectively: in the lower wavenumbers range,

the $\delta(\text{CH}_3)$ bending modes are seen. The negative band in the OH stretch range is due to silanols interacting with the OH group of methanol. As with ammonia, interaction with methanol is reversible above 300°C.

Figure 7b reports difference spectra collected after dosing 0.05 – 2.5 mbar of phenol: in the OH stretch range (3800 – 2800 cm^{-1}), the negative band of hydroxyls interacting with phenol is very weak, indicating that few silanols are accessible to this probe in the adopted experimental conditions, *i.e.* at room temperature in static operation. It must be noted that the minimum Van de Waals diameter of phenol is 0.57 nm, *i.e.* about one half of nanotubes inner diameter. Due to H-bond with phenol, the silanols stretching mode is shifted by ca. - 400 cm^{-1} , as observed when dosing phenol on an amorphous silica used for comparison (spectra not shown).

Interaction with phenol is reversed after outgassing for 1h at 300°C, indicating a strong interaction, most probably with adsorbing sites at the outer surface.

In order to understand the nature of adsorbed phenol, Figure 7c compares the spectra of phenol, in the C=C ring stretch range, adsorbed on a KBr disk (curve 1), on amorphous silica (curve 2), on IM-300 (curve 3), on PR-IM (curve 4) and on L-IM (curve 5).

Phenol adsorbed on silica (curve 1) shows: i) a band at 1598 cm^{-1} with a shoulder at 1605 cm^{-1} , assigned to the modes 7b and 7a of the aromatic ring; ii) two bands at 1499 and 1472 cm^{-1} , due to the modes 19a and 19b; iii) a broad envelop of bands below 1400 cm^{-1} , assigned to the in plane C-O-H bending vibration [25].

Interestingly, after adsorption of phenol on IM-300 (curve 3), a new component is seen at 1492 cm^{-1} and the in plane C-O-H bending vibration bands become less intense. This may indicate that phenol is interacting not only with inner silanols, but also with other species, located at the outer surface of nanotubes.

With L-IM (curve 5), the component at 1605 cm^{-1} and the C-O-H bending vibration are absent, and the band at 1492 cm^{-1} is as intense as that at 1499 cm^{-1} .

These features, previously observed after phenol adsorption on alumina and Na-X zeolite, were ascribed to phenol de-protonation with formation of surface phenolate species [25,26]. This is evidence that L-IM has a basic-type behaviour in regard to phenol, since it abstracts the proton of –OH group, generating phenolate species. Furthermore, the broad band seen with IM-300 and L-IM around 1640 cm^{-1} can be due to the formation of water by reaction of surface hydroxyls with phenolic proton.

As to silanols acidity and accessibility, results reported in this work show that silanols behave as free-silanols, in that the observed shift with ammonia, methanol and phenol is the same as on silica and the CO stretch band is at 2157 cm^{-1} , but their abundance at the inner surface of nanotubes enhances the strength of interaction between the surface and the adsorbed molecules, thus hindering their diffusion inside nanotubes.

Multiple interactions of silanols with molecules like water, ammonia, methanol and phenol could therefore explain unexpected phenomena like i) the high temperature of water removal (300°C) and ii) the formation of irreversible ammonium species by interaction of ammonia with relatively weak Brønsted acids as silanols.

At the same time, in contrast with the high pliability of Si-O-Si bonds in amorphous silicas [27], structural rigidity of imogolite nanotubes does not allow silanols condensation without structural collapse, rendering imogolite more similar to crystalline silica-based materials, like silicalite, for example.

7.3.5. Catalytic results of gas-phase phenol methylation with methanol

This reaction was chosen as a test reaction because of the following reasons:

1. Adsorption tests showed that both molecules, phenol and methanol, may interact with the silanols in imogolite. The acidity of these sites, although very weak, is strong enough to activate these molecules. However, indications were derived that the access of

molecules to these moieties might be hindered. The two reactants possess very different molecular size, and are supposed to have quite different diffusivity properties. Therefore, they can be used to discriminate the access to external Al(OH)Al and internal Si-OH sites in imogolite.

2. The gas-phase alkylation of phenol is a facile reaction, that may occur either on acidic or basic sites, even with sites having weak strength [28,29]. Moreover, the nature of the products formed is affected by the strength of the active sites; in general, weaker sites lead to the preferred formation of O-alkylation products (anisole), whereas stronger sites lead preferentially to C-alkylation, with production of cresols and polyalkylated phenols. Therefore, this reaction can be used as a tool for the characterization of active sites reactivity.
3. Methanol itself may undergo side reactions, with formation of dimethylether first, and then aliphatic and aromatic hydrocarbons, precursors of coke [30]. These latter reactions are catalysed by strong acid sites, and therefore they should not occur with weak acid sites. Therefore, transformations occurring on methanol may also provide information on the active site accessibility under gas-flowing conditions.

7.3.6. The reactivity of PR-IM

Figure 8 shows the effect of the reaction temperature on the catalytic performance of PR-IM. The material showed a relevant catalytic activity, giving 27% phenol conversion at 300°C. At this temperature, the main products were *o*-cresol, polyalkylated phenols and anisole; *p*-cresol and polyalkylated anisoles formed in lower amount.

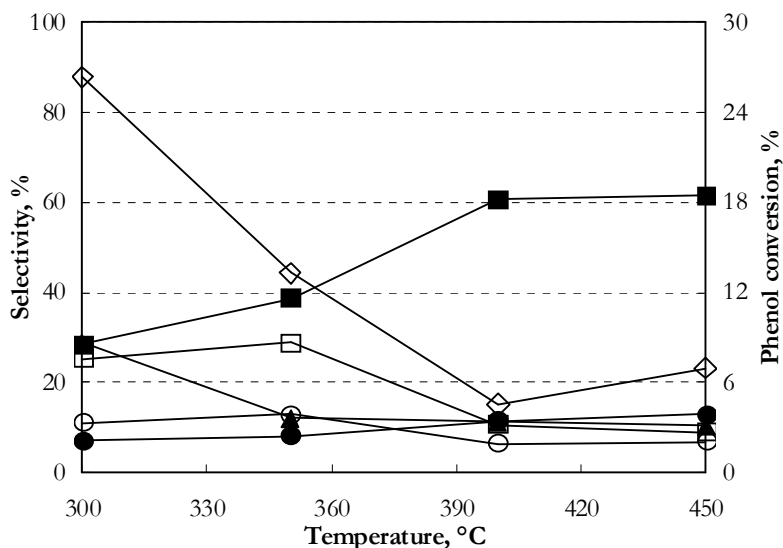


Figure 8: Effect of temperature on catalytic performance of proto-imogolite. Symbols: phenol conversion (Δ), selectivity to *o*-cresol (\blacksquare), selectivity to *p*-cresol (\bullet), selectivity to 2,6-xyleneol (\circ), selectivity to other polyalkylated aromatics (\square).

The distribution of products at 300°C is similar to that one typically observed with H-mordenites and H- β zeolites [31]. However, when the reaction temperature was increased, an evident deactivation was responsible for the remarkable decline of phenol conversion. At the same time, the selectivity to polyalkylated phenols decreased, and that one to *o*- and *p*-cresol increased, due to the decreased contribution of consecutive reactions. The deactivation behaviour also was quite similar to that observed for zeolites, due to the accumulation of coke formed by the hardening of aliphatic and aromatic hydrocarbons originated by methanol transformation [32,33].

The deactivation of PR-IM was confirmed by measurements made on the fresh catalyst, recorded as a function of the reaction time (Figure 9).

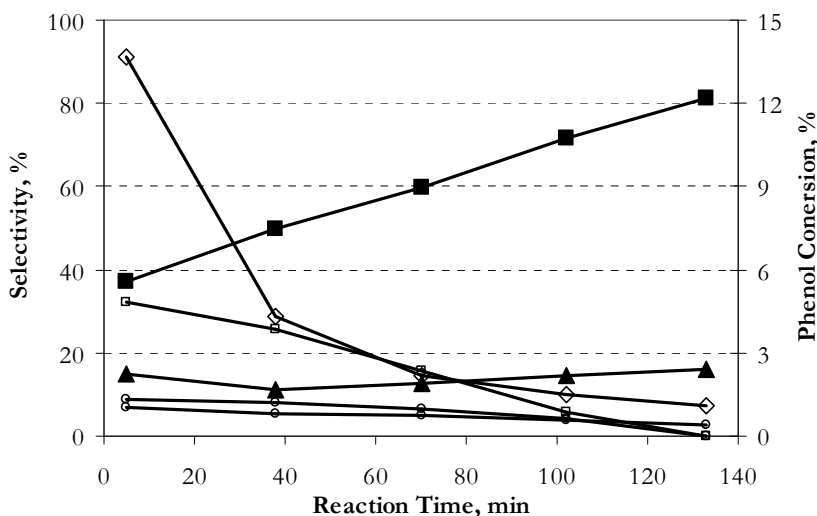


Figure 9: Effect of reaction time on catalytic performance of proto-imogolite. Symbols: phenol conversion (\diamond), selectivity to *o*-cresol (\blacksquare), selectivity to anisole (\blacktriangle), selectivity to *p*-cresol (\bullet), selectivity to 2,6-xylene (\circ), selectivity to other polyalkylated aromatics (\square). Temperature 350°C.

The progressive decrease of phenol conversion led to an increase of selectivity to *o*-cresol and to a decrease of that to polyalkylated phenols. Surprisingly, the selectivity to anisole was not affected by the change of phenol conversion, and that to *p*-cresol decreased and became nil after 2 hour reaction time. This means that the formation of polyalkylated aromatics occurred by transformation of *o*-cresol, whereas the para isomer did not undergo consecutive reactions. The spent catalyst was fully coked, confirming the acidic properties of this material.

These tests demonstrate that the amorphous material, precursor of imogolite formation, has medium-strength acid sites that are fully accessible to both phenol and methanol, in agreement with characterization tests made by adsorption of probe molecules.

7.3.7. The reactivity of IM-300 and L-IM

Reactivity tests were carried out with the imogolite after thermal treatment at 300°C (IM-300) and at 500°C (L-IM, Figure 10).

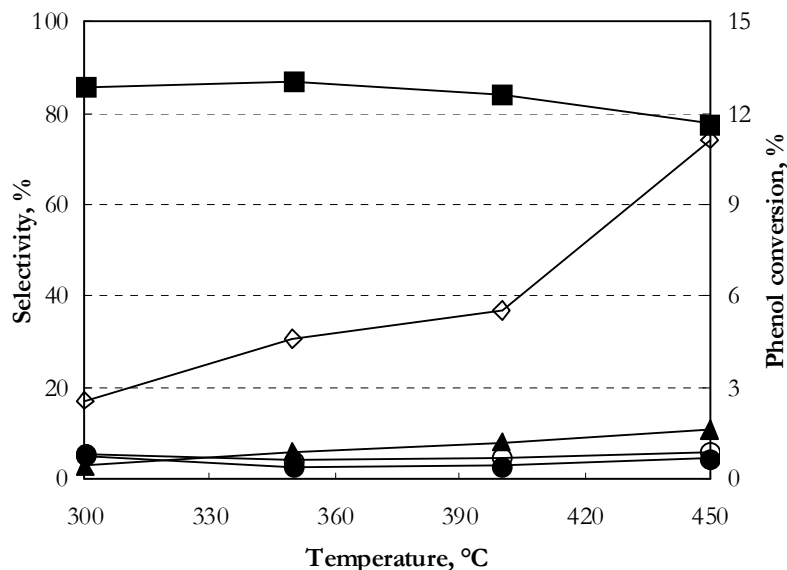


Figure 10: Effect of temperature on catalytic performance of IM-500. Symbols: phenol conversion (\diamond), selectivity to *o*-cresol (\blacksquare), selectivity to anisole (\blacktriangle), selectivity to *p*-cresol (\bullet), selectivity to 2,6-xylenol (\circ).

Sample IM-300 was inactive at 300°C; in fact, the phenol conversion was 0.03%, remarkably lower than that obtained with the PR-IM; the two only compounds detected were *o*-cresol and anisole, each one with a selectivity of approximately 50%. On the other hand, the conversion of methanol was approximately 20%, the products formed being dimethylether (with the co-product water) and 2,2-dimethoxypropane. The latter compound is the ketal formed by the acid-catalyzed reaction between acetone and methanol, the ketone being likely formed by dehydrogenation (via H-transfer) of isopropanol. The latter is the product of the acid-catalyzed hydration of propylene, the olefin being typically obtained by transformation of methanol over strongly acid sites. Therefore, the acidity offered by the IM-300 sample is strong enough to catalyze transformations of methanol. On the other hand, phenol cannot access to the active sites, and does not react with methanol at all. This is confirmed also by FT-IR spectra reported in Figure 7, which showed that phenol interacts with few silanols and is adsorbed at the outer surface as phenolate species.

The spent IM-300 sample contained a minor amount of coke, much less than that one accumulated on the PR-IM sample. Since the formation of coke is unlikely to occur inside the nanotubes of imogolite, this indicates that methanol reacted with both silanols inside the imogolite nanotubes, yielding lighter compounds (*i.e.* dimethylether and 2,2-dimethoxypropane), and also with the external Al(OH)Al sites, giving rise to the formation of heavier compounds and finally of coke.

Figure 10 shows the behaviour of L-IM. This sample was much more active than IM-300; in fact, the conversion at 300°C was low ($\approx 3\%$), but nevertheless two orders of magnitude higher than that of IM-300. Moreover, there are two relevant differences with respect to the performance of PR-IM (Figures 8 and 9): (a) there is no evident deactivation phenomenon, that was instead the case with PR-IM; (b) the distribution of products of the two materials are quite different. In fact, with L-IM the main product was *o*-cresol, showing a selectivity close to 80% regardless of temperature and conversion. At 450°C, the selectivity to anisole was 10% and that to *p*-cresol 4%, the only polyalkylated compound being 2,6-xylenol, formed with selectivity of 3%. With PR-IM, at the same temperature and for a similar value of phenol conversion, the selectivity to 2,6-xylenol was 8%, that to other polyalkylated phenols was 10% and to *p*-cresol 13%. This difference indicates that the type and strength of the active sites in the two materials was different.

7.3.8. The reactivity of reference materials: alumina and silica

In order to understand better the differences experimentally observed, we carried out reactivity tests with alumina (Figure 11.a) and with silica (Figure 11.b).

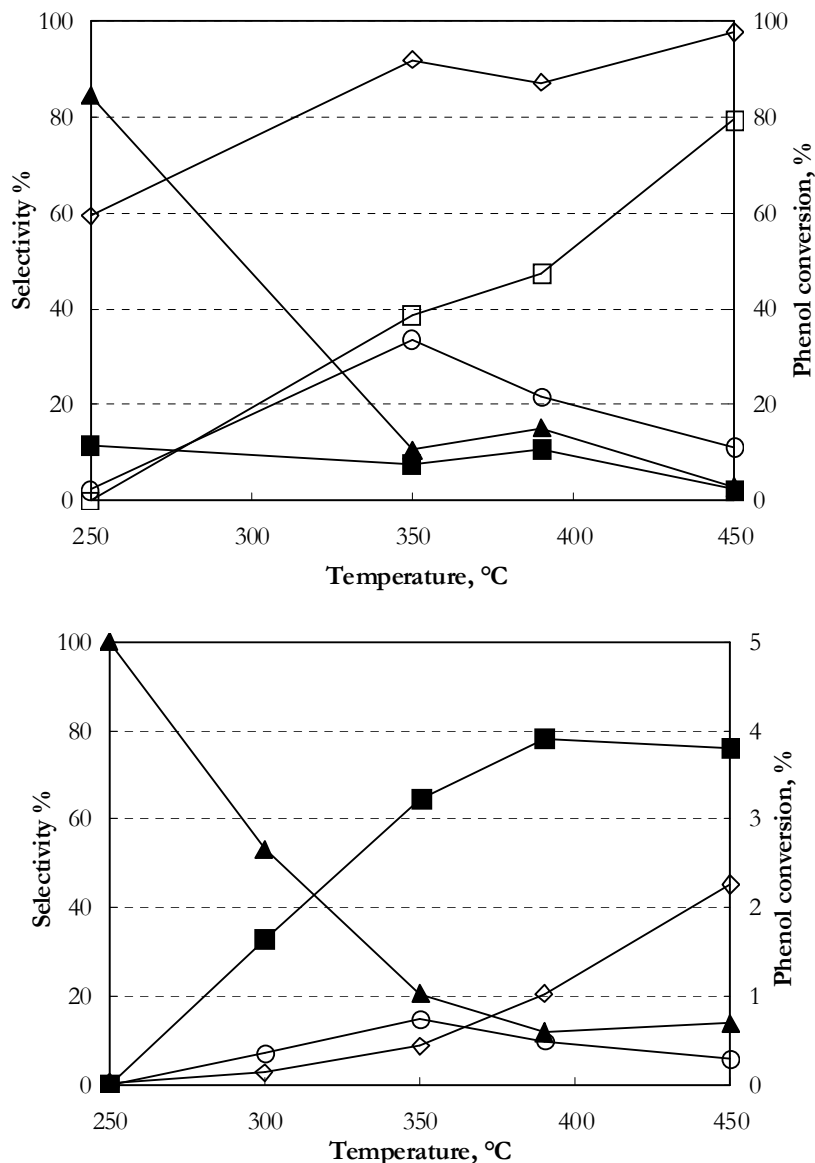


Figure 11: a) Effect of temperature on catalytic performance of Al₂O₃. Symbols: phenol conversion (◇), selectivity to *o*-cresol (■), selectivity to anisole (▲), selectivity to 2,6-xylene (○), selectivity to other polyalkylated aromatics (□). b): Effect of temperature on catalytic performance of SiO₂. Symbols: phenol conversion (◇), selectivity to *o*-cresol (■), selectivity to anisole (▲), selectivity to 2,6-xylene (○), selectivity to other polyalkylated aromatics (□).

Alumina was very active, showing 60% phenol conversion at 250°C; a partial deactivation was responsible for the observed decrease of conversion at 350°C. At low temperature, the prevailing product was anisole, the selectivity of which however decreased rapidly in favour of the formation of polyalkylated

phenols, amongst which the prevailing one was 2,6-xylenol. This behaviour indicates the different activation energy between O-alkylation, leading to anisole, and C-alkylation, the latter being preferred at high temperature [34]. The prevalent mono-alkylated compound was *o*-cresol, *p*-cresol formed only in trace amount. This behaviour also indicates the amphoteric behaviour of alumina in this reaction; the Al(OH)Al surface groups have an acidic behaviour towards methanol, that is activated with formation of an electrophilic species. On the other hand, the surface has a basic behaviour to phenol, that adsorbs and generates a phenolate species, the protons being abstracted by the nucleophilic Al-O-Al oxygen [35-37]. Because of the repulsion between the aromatic ring and the surface, the phenolate adopts an orthogonal orientation; this adsorption mode favours the attack at the ortho position in phenol, and finally leads to the formation of *o*-cresol and 2,6-xylenol.

On silica, the conversion of phenol was very low, because of the low acidity of surface silanols [20]; the low acidity is also the reason for the absence of any deactivation phenomenon. The only product at low temperature was anisole. The increase of temperature led to the preferred formation of *o*-cresol, with negligible formation of *p*-cresol. Despite the very low conversion, the selectivity to 2,6-xylenol was higher than 10%.

Apart from the very different activity, the behaviour of the two reference materials was not much different; both yielded in prevalence anisole at low temperature, regardless of the conversion achieved, and both gave C-alkylation products at high temperature. The latter was either *o*-cresol, when the conversion achieved was low (*i.e.*, on silica), or 2,6-xylenol and other polyalkylated aromatics, when the conversion was high (*i.e.*, on alumina).

7.3.9. The comparison of catalytic materials

The distribution of products obtained in the gas-phase methylation of phenol over PR-IM is similar to that observed with alumina and with silica. The relevant deactivation phenomena confirm the existence of surface acidic sites having medium-strength, as also evidenced by FT-IR characterization. One

difference with respect to alumina and silica concerns the selectivity to *p*-cresol; the latter was 10-15% with PR-IM, whereas it was negligible with both reference compounds. The regio-selectivity in the ring-alkylation of phenol with methanol is regulated by the charge density of the O atom in the oxidic catalyst, the latter being the lower with silico-aluminates and the greater with ionic oxides typically showing a basic behaviour [38-42]. In general, highly nucleophilic O atoms not only generate the phenolate species, but also force the latter to adopt an orthogonal orientation with respect to the surface, finally leading to high regio-selective C-alkylation and to the preferred formation of *o*-cresol. Therefore, the PR-IM catalytic behaviour is more similar to a zeolite [28] than to alumina.

The behaviour of L-IM (Figure 10) is different from both those of silica and alumina, and that of PR-IM. In fact, with L-IM the main product of reaction was *o*-cresol, at both low and high temperature. Anisole formed with low selectivity at 300°C; selectivity then increased when the reaction temperature was increased (10% at 450°C), a behaviour opposite to what usually found with Brønsted acid-type materials.

In some aspects, the behaviour of L-IM is similar to what observed with basic materials [29], showing high chemo- (C-alkylation largely preferred over O-methylation) and regio- (ortho-C-alkylation largely preferred over para-C-alkylation) selectivity in the gas-phase phenol alkylation with methanol. This behaviour agrees with the experimental finding that L-IM gives the strongest interaction with phenol and generates phenolate species (Figure 8). Due to the high nucleophilicity of the O atom, the phenolate adopts the orthogonal orientation typically observed with basic oxides, that explains the regio-selectivity experimentally observed. On the other hand, the presence of medium-strength acid sites is responsible for the small, but non negligible formation of anisole. Therefore, L-IM appears to have amphoteric behaviour, resulting from the combined reactivity of the acid and basic sites present on its surface. Strongly nucleophilic O²⁻ ions are generated by the high-temperature dehydration of imogolite, leading to strained Al-O-Al(Si) bonds which easily open by abstraction

of the acid phenolic proton and coordination of the phenolate to the Al^{3+} cation. The same occurs in strongly dehydrated alumina, where the nucleophilicity of the O^{2-} is responsible for the “basic” behaviour of the solid towards phenol [35-37].

Another peculiarity of the L-IM material is the absence of relevant deactivation phenomena, as confirmed by the relatively low amount of coke accumulated on the catalyst. This behaviour is also typically observed with basic catalysts [28,29]; a contribution, however, deriving from the lamellar-type morphology of the sample, which may favour the counter-diffusion of products limiting the generation of the hydrocarbon-pool precursor of coke formation, cannot be excluded.

7.4. Conclusions

PR-IM has a markedly acidic character, leading to a catalytic behaviour very similar to that of zeolitic-type materials, both in regards to the distribution of the reaction products and the presence of deactivation phenomena. Besides the overall lower surface area, the hollow spheres morphology of proto-imogolite allows methanol and phenol molecules to access active sites, both at the inner or outer surface of particles.

With IM, several factors must be accounted for: first of all, below $300^{\circ}C$, nanotubes are partially filled by water, and therefore, besides few inner silanols interacting with NH_3 , only $Al(OH)Al$ groups and few Al^{3+} Lewis sites at the outer surface may be accessed by probes.

At $300^{\circ}C$, water is definitely removed and the inner surface, covered by silanols, becomes actually accessible to bases with different strength, CO and NH_3 , and to bigger molecules, *i.e.* methanol and phenol. Due to its bulky structure, however, phenol access to silanols is limited by geometric/diffusional constraints, leading to a non-negligible conversion of methanol, but to a quite negligible degree of phenol conversion. As to surface hydroxyls acidity, interaction with NH_3 is strong, probably due to multiple interaction of ammonia with more than one silanol, since the inner surface is lined by $SiOH$ groups, and to difficult diffusion

across μm -long nanotubes. However, the hypothesis that the unusual acidic behaviour of silanols may derive from a peculiar structural feature of the solid cannot be completely ruled out and deserves further studies.

Finally, L-IM develops both medium-strength acidic and basic surface features, which result into an “amphoteric” catalytic behaviour. FT-IR spectroscopy showed, on the one hand, the presence of acidic Brønsted –like sites, similar to hydroxyls in high Al-content alumina-silicates and mildly acidic zeolites: on the other hand, the presence of basic sites is shown by the formation of phenolate species upon phenol adsorption. Basic properties, indeed, lead to phenol de-protonation and to the preferred formation of o-cresol, with negligible formation of p-cresol, as usually observed with basic-type solids.

7.5. Acknowledgments

For this part I wish to acknowledge B. Bonelli, I. Bottero and prof. E. Garrone from Politecnico di Torino.

7.6. References

- [1] N. Yoshinaga, A. Aomine, *Soil Sci. Pl. Nutr.* 8(3) (1962) 22.
- [2] P.D.G. Cradwick, V.C. Farmer, J.D. Russell, C.R. Masson, K. Wada, N. Yoshinaga, *Nature Phys. Sci.* 240 (1972) 187.
- [3] V.C. Farmer, M.J. Adams, A.R. Fraser, F. Palmieri, *Clay Miner.* 18 (1983) 459.
- [4] V.C. Farmer, A.R. Fraser, *Proceedings of the International Clay Conference* (M.M.Mortland and V.C. Farmer Ed.) Elsevier, Amsterdam (1978) 547.
- [5] S.I. Wada, A. Eto, K. Wada, *Proceedings of the International Clay Conference* (M.M.Mortland and V.C. Farmer Ed.) Elsevier, Amsterdam (1978) 348.

- [6] P.I. Pohl, J.-L. Faulon, D.M. Smith, *Langmuir* 12 (1996) 4463.
- [7] S. Konduri, S. Mukherjee, S. Nair, *Phys. Rev. B* 74 (2006) 033401.
- [8] W.C. Ackerman, D.M. Smith, J.C. Huling, Y.-W. Kim, J.K. Bailey, C.J. Brinker, *Langmuir* 9 (1993) 1051.
- [9] M.A. Wilson, G.s.H. Lee, R.C. Taylor, *Clays and Clay Miner.* 50(3) (2002) 348.
- [10] L. Denaix, I. Lamy, J.Y. Bottero, *Colloids Surf. A* 158 (1999) 315.
- [11] C.J. Clark, M.B. McBride, *Clays and Clay Miner.* 32(4) (1984) 291.
- [12] R.L. Parfitt, A.D. Thomas, R.J. Atkinson, R. St. C. Smart, *Clays and Clay Miner.* 22 (1974) 455.
- [13] Y. Arai, M. McBeath, J.R. Bargar, J. Joye, J.A. Davis, *Geochim. Cosmochim. Acta* 70 (2006) 2492.
- [14] J.B. Harsh, S.J. Traina, J. Boyle, Y. Tang, *Clays and Clay Miner.* 40(6) (1992) 700.
- [15] S. Imamura, Y. Hayashi, K. Kajiwara, H. Hoshino, C. Kaito, *Ind. Eng. Chem. Res.* 32 (1993) 600.
- [16] S. Imamura, T. Kokubu, T. Yamashita, Y. Okamoto, K. Kajiwara, H. Kanai, *J. Catal.* 160 (1996) 137.
- [17] C. Morterra, G. Magnacca, *Catal. Today* 27 (1996) 497 and references therein.
- [18] J.P. Gustafsson, *Clays and Clay Miner.* 49(1) (2001) 73.

- [19] K.J. MacKenzie, M.E. Bowden, J.W.M. Brown, R.H. Meinhold, *Clays and Clay Miner.* 37(4) (1989) 317 and references therein.
- [20] G. Ghiotti, E. Garrone, C. Morterra, F. Boccuzzi, *J. Phys. Chem.* 83 (1979) 2863.
- [21] A. Givan, a. Loewenschuss, C.J. Nielsen, *Vibrat. Spectrosc.* 12 (1996) 1.
- [22] B. Bonelli, B. Onida, J.D. Chen, A. Galarneau, F. Di Renzo, F. Fajula, E. Garrone, *Microporous Mesoporous Mater.* 67 (2004) 95.
- [23] S. Bordiga, C. Lamberti, F. Geobaldo, A. Zecchina, G. Turnes Palomino, C. Otero Areán, *Langmuir* 11 (1995) 527.
- [24] W. Daniell, U. Schubert, R. Glöckler, A. Meyer, K. Noweck, H. Knözinger, *Appl. Catal. A*, 196 (2000) 247.
- [25] T. Beutel, *J. Chem. Soc. Faraday Trans.* 94 (1998) 985.
- [26] T. Mathew, M. Vijayaraj, S. Pai, B.B. Tope, S.G. Hegde, B.S. Rao, C.S. Gopinath, *J. Catal.* 227 (2004) 175.
- [27] R.K. Iller: *The Chemistry of Silica: Solubility, Polymerization, Colloid and Surface Properties, and Biochemistry of Silica* (John Wiley and Sons, New York, 1979).
- [28] N. Ballarini, F. Cavani, L. Maselli, A. Montaletti, S. Passeri, D. Scagliarini, C. Flego, C. Perego, *J. Catal.* 251 (2007) 423.
- [29] N. Ballarini, F. Cavani, L. Maselli, S. Passeri, S. Rovinetti, *J. Catal.* 256 (2008) 215.
- [30] I.M. Dahl, S. Kolboe, *J. Catal.*, 149 (1994) 458.

- [31] M. Bregolato, V. Bolis, C. Busco, P. Ugliengo, S. Bordiga, F. Cavani, N. Ballarini, L. Maselli, S. Passeri, I. Rossetti, L. Forni, *J. Catal.* 245 (2007) 283.
- [32] J.F. Haw, W. Song, D.M. Marcus, J.B. Nicholas, *Acc. Chem. Res.*, 26 (2003) 317.
- [33] Ø. Mikkelsen, S. Kolboe, *Microp. Mesop. Mater.*, 29 (1999) 173.
- [34] R.F. Parton, J.M. Jacobs, H. van Ooteghem, P.A. Jacobs, *Stud. Surf. Sci. Catal.*, 46 (1989) 211.
- [35] L.H. Klemm, J. Shabtai, D.R. Taylor, *J. Org. Chem.*, 33 (1968) 1480.
- [36] Y. Fu, T. Baba, Y. Ono, *Appl. Catal. A*, 178 (1998) 219.
- [37] S. Porchet, L. Kiwi-Minsker, R. Doepper, A. Renken, *Chem. Eng. Sci.*, 51(11) (1996) 2933.
- [38] R.J. Davis, *J. Catal.*, 216 (2003) 396.
- [39] Y. Ono, *J. Catal.*, 216 (2003) 406.
- [40] G. Busca, *Phys. Chem. Chem. Phys.*, 1 (1999) 723.
- [41] A. Cimino, F.S. Stone, *Adv. Catal.*, 47 (2002) 141.
- [42] M. Barteau, *Chem. Rev.*, 96 (1996) 1413.

Chapter 8

Methylation of phenol over high-silica beta zeolites

8.1. Introduction

The main limit of zeolites is the low selectivity achieved to one specific compound, since several products are obtained (*O*-alkylated, mono- and poly-*C*-alkylated), the selectivity of which is a function of phenol conversion, reaction conditions and zeolites characteristics. This is not the case for the heterogeneous basic-catalyzed methylation, which is a much more specific reaction. In fact, it almost exclusively yields the products of ortho-*C*-alkylation [1-5].

Furthermore, alkylation reactions over solid acid catalysts, especially with reactants in gaseous phase, usually are accompanied by several unwanted side reactions, triggered by the same surface acidity of the catalyst, leading to a more or less rapid deactivation of the catalyst, due to fouling by carbonaceous deposits, usually referred to as “coke” [6]. However, it is worth noting that, to the best of our knowledge, the scientific literature on the alkylation with alcohols of phenol and of phenol derivatives, especially from the reaction kinetics point of view, does not take into consideration explicitly any catalyst deactivation effect.

The literature on gas-phase alkylation of phenol with alcohols over Beta zeolites is scarce [7-12]. Over Beta zeolite a somewhat different acidity can add to that based on Al^{3+} sites. Indeed, in such a zeolite randomly intergrown structures of

two or even three different polymorphs, with a considerable amount of random stacking faults, leads to a substantial increase of lattice defects and structural disorder [13]. This disorder creates additional internal surface hydroxylated species (SiOH nests of variable geometrical arrangement) and Lewis-type (L) electron acceptor sites. As a consequence, both catalyst activity and resistance to coking are simultaneously affected by all these features, namely zeolite crystal structure and pore width, nature and concentration of surface acid sites and zeolite crystal size [14-16].

The aim of the present work was to investigate the effect on catalytic performance for phenol methylation of properly prepared samples of H-Beta zeolite of similar Si/Al ratio, but much different crystal size. In fact, it is expected that in a complex reaction pattern, including parallel and consecutive reactions, the distribution of products can be greatly affected by the intra-particle residence time of products. Besides reaction rate and selectivity to the various products, the present analysis takes into account the activity decay and the change of selectivity with time-on-stream, looking for correlations between catalytic behaviour and the zeolites physical-chemical characteristics.

8.2. Experimental

8.2.1. Catalysts characterization

The BET specific surface area (SSA) was measured by N₂ adsorption-desorption at liquid nitrogen temperature, on a Micromeritics ASAP 2010 instrument. Zeolite crystal size and shape were determined by scanning electron microscopy (SEM), by either a Cambridge Stereoscan 150 or a Leica LEO 1430 instrument. Elemental analysis was performed on a Varian Liberty 200 inductively coupled plasma (ICP) spectrometer.

Catalyst surface acidity was measured by FT-IR spectroscopy, by means of a Perkin-Elmer 1750 Spectrometer. Self-supporting wafers of pure zeolite were first evacuated at 500°C *in vacuo* (residual p = 10⁻⁶ mbar). Then adsorption of

pyridine was done at room temperature, and desorption was carried out by outgassing the sample at 50, 150, 250, 350, 450°C. The FT-IR spectrum was recorded after evacuation at each temperature level.

8.2.2. Catalytic tests

Methylation of phenol was carried out at four different temperatures, ranging from 320 to 450°C, at atmospheric total pressure. An excess of methanol with respect to the stoichiometric requirement for the methylation of phenol was fed (methanol/phenol feed ratio = 7/1).

0.6 g of catalyst were loaded. The flow rate of reactants was 60 cm³/min of gaseous N₂ and 1.75x10⁻³ cm³/min of organic liquid feeding mixture, so to have a value of residence time $\tau = 0.98 \text{ s} \left(\frac{\text{cm}^3_{\text{catalyst bed}}}{\text{cm}^3_{\text{overall gaseous feeding flow}}} \right)$

When needed, the catalyst was regenerated *in situ* in flowing air (20 cm³/min) by increasing temperature by 5°C/min from room temperature up to 300°C, then by 0.83°C/min up to 350°C, 400°C and 450°C. After each temperature step (*i.e.* at 300, 350, 400 and 450°C) temperature was kept constant for 1 h.

8.3. Results and discussion

8.3.1. Catalysts characterisation

8.3.1.1. Crystal phase, surface area, crystal size and Si/Al ratio

Under the synthesis conditions adopted, BEA zeolite was the only crystalline phase obtained. The XRD patterns matched those reported in literature [17-19]. Our BEA samples (Fig.1) were the result of intergrowth of two polymorphs, A and B [19], or even of a third polymorph C [18]. However, our XRD patterns did not allow any reliable quantitative determination of the polymorph distribution.

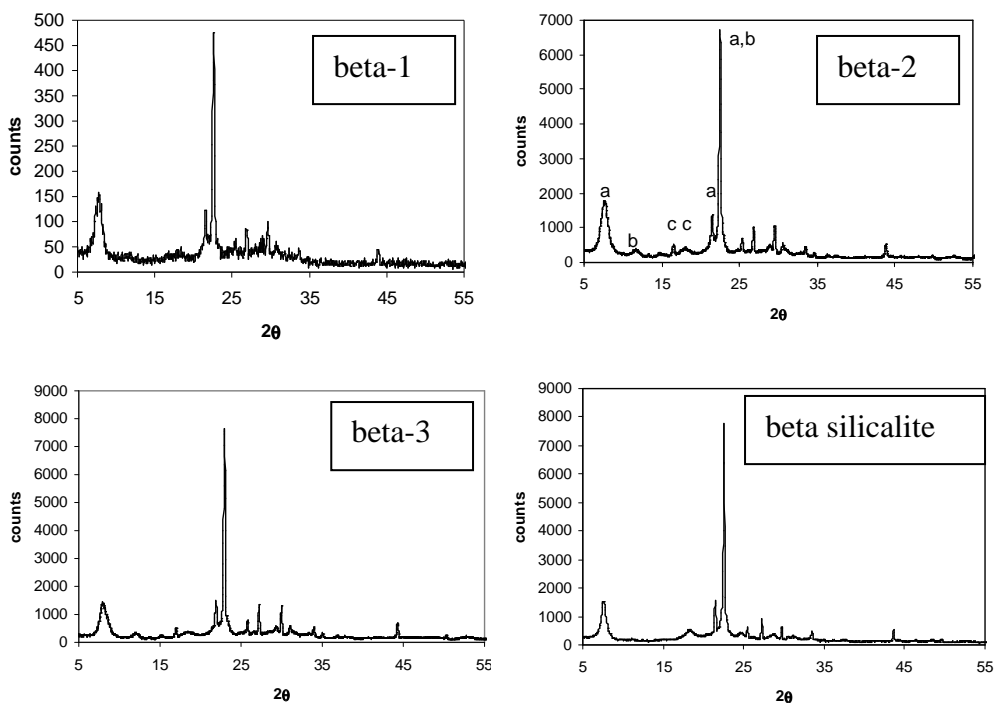
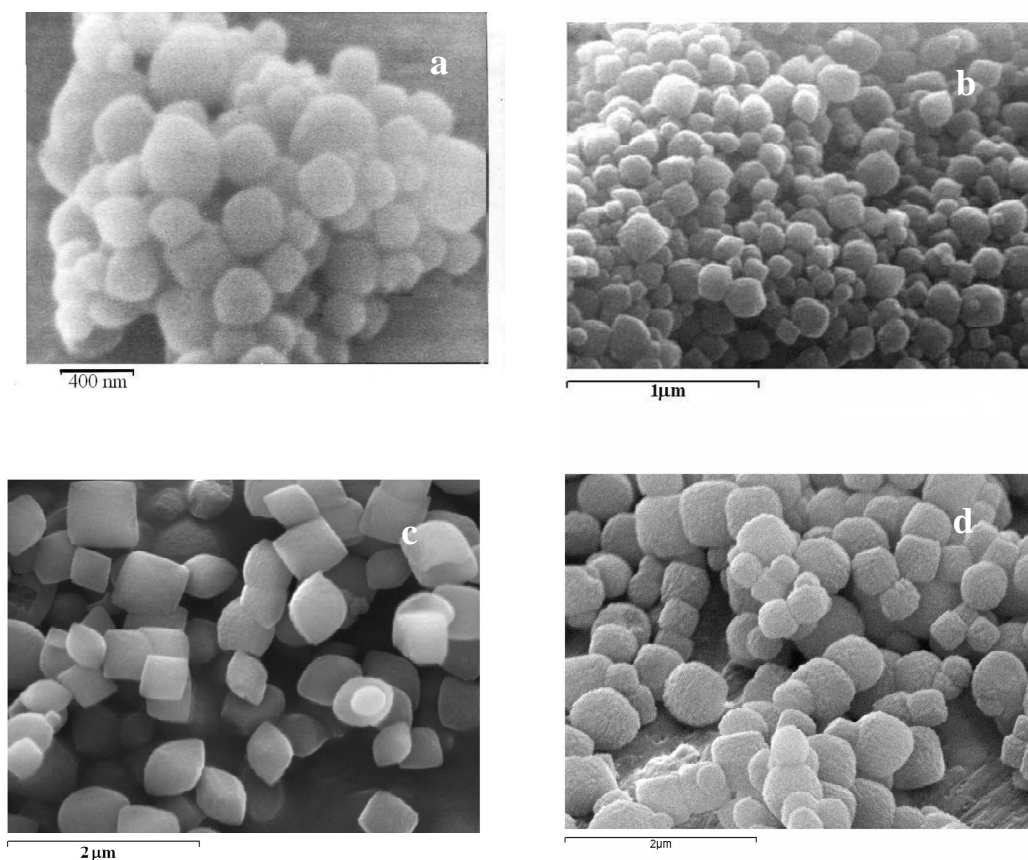


Figure 1. XRD patterns of the catalysts prepared.

SSA ranged from 480 to 570 m²/g (Table 1), typical values for these zeolites. SEM micrographs (Fig.2*a,b,d*) showed that beta-1, beta-2 and beta-silicalite were composed of spheroidal-shaped crystals with a narrow crystal size distribution. The beta-3 crystals appeared slightly cuboidal-shaped (Fig.2*c*). The average size of particles, determined by direct measurement on properly enlarged micrographs for the various zeolites, is given in Table 1. Total pore volume (V_{pTOT}) and micropore volume (V_{pMic}) (Table 1), determined from the total gas volume adsorbed at saturation and t-plot data, may give an idea of the crystallinity of our samples.

Table 1. Main characteristics and energetics of interaction with H₂O and CH₃OH of the investigated catalysts

Catalyst	SiO ₂ /Al ₂ O ₃ mol ratio	Si/Al mol ratio	Al/uc	av. cryst. size (nm)	SSA (m ² /g)	V _{pTOT} (cm ³ /g)	V _{pMicr} (cm ³ /g)	Na ⁺ wt %
beta-1	65	130	≈ 0.5	200	481	0.343	0.239	2.42
beta-2	77	154	≈ 0.4	100	559	0.627	0.266	0.07
beta-3	65	130	≈ 0.5	590	565	0.324	0.299	0.01
beta-silical. silical.	255	510	<0.1	450	529	0.311	0.270	<0.001
beta-10	4.9	9.8	≈ 6	50	360	-	-	-

**Figure 2.** SEM micrographs of: (a) beta-1; (b) beta-2; (c) beta-3; (d) beta-silicalite

ICP analysis showed for all samples a similar $\text{SiO}_2/\text{Al}_2\text{O}_3$ molar ratio (Table 1), except of course for the beta-silicalite. Furthermore, H beta-2 and beta-3 (and mainly beta-silicalite) samples were almost Na-free, whereas the beta-1 sample contained a considerable amount of exchangeable Na^+ ions (Table 1).

8.3.1.2. Acidity characterization by means of pyridine adsorption

Figures 3 a and b show the FT-IR spectra recorded after pyridine adsorption at room temperature, followed by desorption at increasing temperatures, for samples beta-1 and beta-2, respectively.

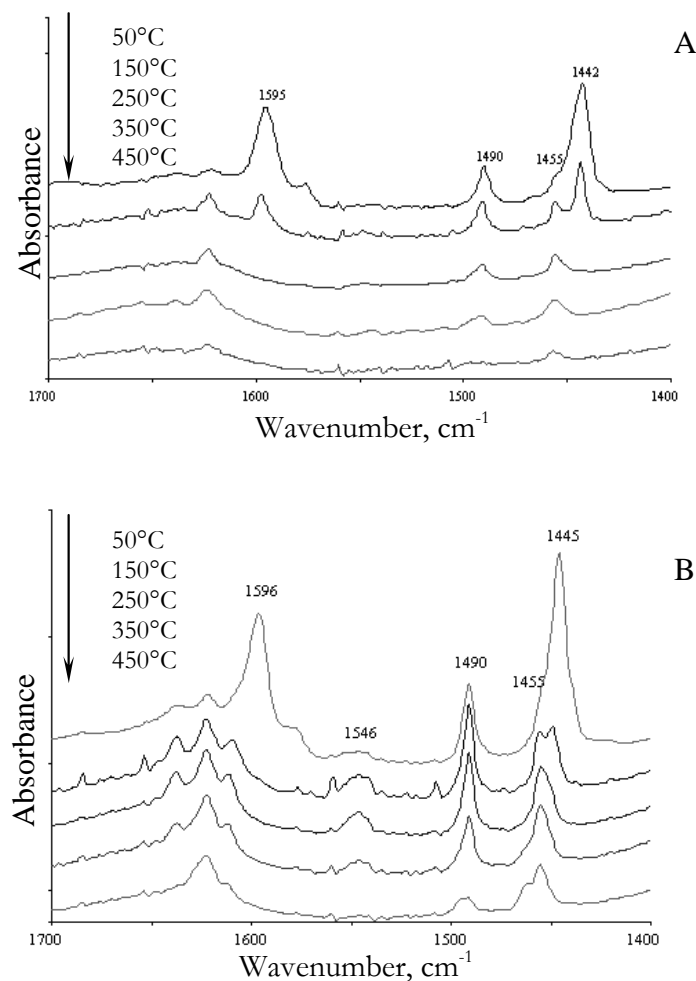


Figure 3. FT-IR spectra of beta-1 (A) and beta-2 (B) catalyst after saturation with pyridine followed by evacuation at progressively increasing temperature.

In the case of beta-1 (Figure 3a) the intensity of the band associated to pyridinium cation (1546 cm^{-1}) is nil, that relative to the interaction with Lewis sites (1455 cm^{-1}) is very weak, and pyridine is totally released already after evacuation at 250°C . Finally, the amount of pyridine interacting with silanols (bands at 1446 and 1596 cm^{-1}) [20] is lower than in beta-2 catalysts (Figure 3b). In beta-1, silanols are clearly the only sites present in non-negligible amount.

In the case of beta-2 (Figure 3b), the strong bands at 1446 and 1596 cm^{-1} , due to pyridine adsorbed on silanols, progressively decrease when increasing temperature and totally disappear after evacuation at 250°C . By contrast, some pyridine adsorbed on Lewis sites (1455 cm^{-1}) remains even after evacuation at 450°C . This indicates the presence of strong Lewis-type acid sites, in line with what found by the other techniques. The band at 1546 cm^{-1} , due to the interaction with Brønsted sites, is very weak, as expected from the low concentration of these sites in high-silica zeolites. When the sample is heated, the intensity first increases, likely due to the evolution of the hydrogen bonding with the $-\text{OH}$ group into pyridinium ions, and then decreases; totally disappearing after evacuation at 450°C . The spectra recorded with beta-3 samples (not reported for brevity) were very similar to those of beta-2.

8.3.2. Catalyst activity and deactivation rate

There is a wide literature dealing with the use of zeolites as catalysts for the liquid-phase and gas-phase methylation of phenol. With MFI zeolites, at temperature higher than 350°C Kaliaguine et al. [21,22] found that the reaction leads to a variety of products, amongst which the most relevant were cresols and xylenols. A mechanism was proposed in which diphenyl ether and anisole (the two products of etherification) are the reaction intermediates and interact with Brønsted sites and carbonium ions to yield C-methylated products. The reaction pattern was confirmed by others [23], who also found that in liquid-phase methylation anisole and cresols are primary products and that anisole undergoes consecutive transformation to cresols.

With H-Y zeolites, at 200°C and phenol conversion lower than 15% O-alkylation was found to be quicker than C-alkylation (the two reactions were substantially parallel), with *o*-/*p*-cresol molar ratio equal to 1.5. Anisole disproportionated into phenol and methyl-anisoles, whereas direct isomerisation of anisole into cresols did not occur. Anisole also acted as an alkylating agent for phenol, to yield cresols and methyl-anisoles. The latter reaction was favoured over the disproportion of anisole in the presence of phenol [24]. An important contribution to C-alkylated compounds also derived from the intra-molecular rearrangement of anisole into *o*-cresol [25]. The exchange of protons with Na or the poisoning with NH₃ led to an increase of the anisole/cresols ratio, indicating that anisole formation required sites with lower acid strength as compared to those needed for cresol formation [26], in agreement with what proposed formerly by Namba et al [27]. Similar results were obtained by other authors [25,28,29].

The reactivity of Al-MCM-41 also is similar to that of H-Y [30], with anisole acting as a reaction intermediate. The mechanism of reaction, involving the direct formation of anisole and cresols and the consecutive transformation of anisole, was recently confirmed by means of *in-situ* measurements by Weitkamp *et al.* [31].

With Beta zeolites, again the formation of anisole and cresols occurred through parallel reactions [7,8]. Anisole then was the intermediate in the formation of cresols. As for the effect of the Si/Al ratio, higher ratios implied a lower phenol conversion and hence a greater selectivity to anisole. No effect of shape-selectivity was found.

As for the electrophilic substitution on phenol, the active species is generated by adsorption of methanol and formation of framework-bound methoxonium (CH₃OH₂⁺) ion and methoxy species, which can coexist at low temperature. However, at higher temperature the equilibrium is shifted towards the methoxy species [32], which acts as the electrophilic alkylating agent on alkylaromatics [33,34].

8.3.2.1. Performance of beta-2 and beta-3 catalysts in phenol methylation

The effect of time-on-stream on conversion of phenol in methylation over the beta-2 catalyst, at four different temperatures, is reported in Figure 4A, whereas Figure 4B shows the corresponding distribution of products, as measured at 450°C.

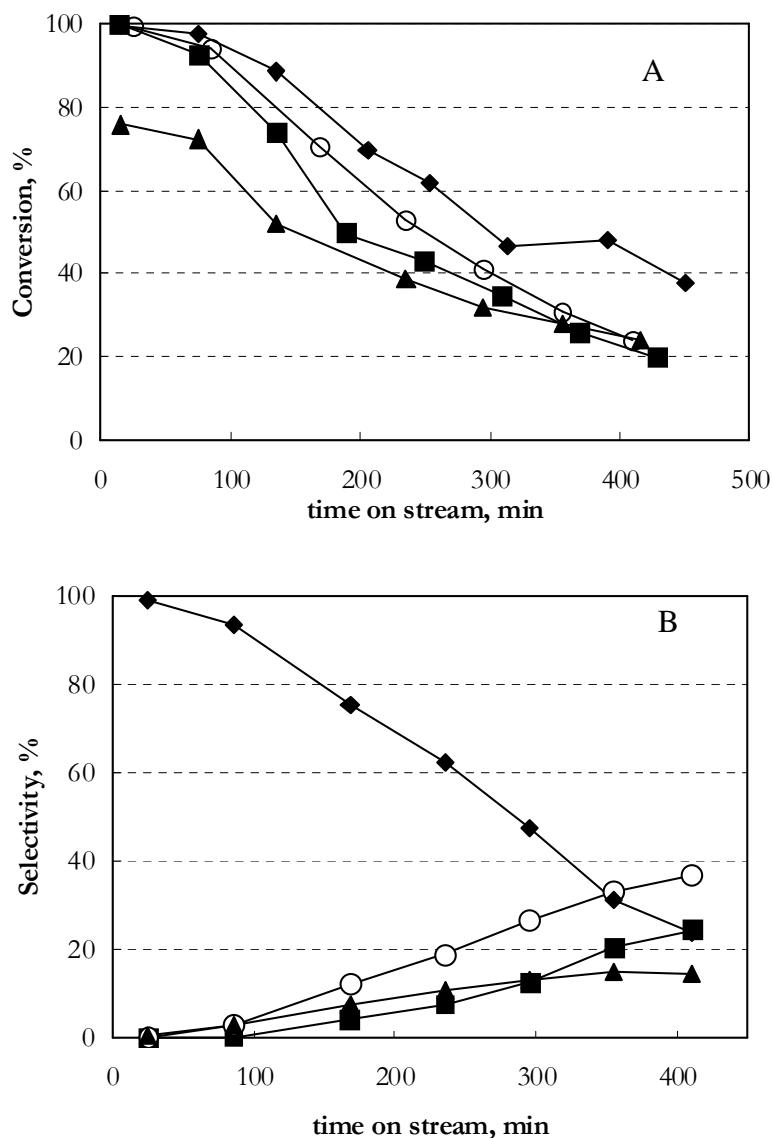


Figure 4. A) Effect of time-on-stream on conversion of phenol in alkylation over beta-2 catalyst at four different temperatures: 320°C (▲), 350°C (■), 390°C (◆) and 450°C (○).

B) Effect of time-on-stream on products distribution in alkylation of phenol over beta-2 catalyst. T = 450°C. Selectivity to poly-alkylated phenol (◆), to o-cresol (○), to p-cresol (▲) and to anisole (■).

The following considerations are of relevance: *i*) There is a considerable deactivation of catalyst with increasing time-on-stream. *ii*) Initial conversion is 100% at temperature higher than 320°C, whereas it approaches 75% at 320°C. *iii*) Deactivation rate appears substantially independent of temperature. *iv*) Deactivation is accompanied by a change in the relative amount of products. Specifically, at total conversion the main products are poly-alkylated compounds (mainly di- and tri-methyl phenols and methyl and di-methyl anisoles), whereas the progressive decrease of conversion leads to a rapid decrease of the latter compounds, with a corresponding increase of primary alkylation products: anisole, *o*-cresol and *p*-cresol. Amongst the latter, the prevailing one is *o*-cresol. *v*) A more detailed investigation of the trend of products formation indicates that the selectivity to cresols decreases monotonously when conversion increases, whereas the selectivity to anisole decreases more rapidly. This is because the cresols undergo consecutive reactions of transformation to diphenols, whereas anisole not only undergoes the analogous consecutive alkylation to methyl-anisole, but also it acts as an alkylating agent by itself. Indeed, it is known that anisole can either rearrange to *o*-cresol (*intra*-molecular rearrangement) or act as an *inter*-molecular alkylating agent, with co-generation of phenol [24,25,30,31]. *vi*) At lower temperatures the distribution of products is similar to that obtained at 450°C. The only difference is the selectivity ratio between anisole and cresols.

It is worth noting that in the alkylation of alkylbenzenes (*e.g.*, of toluene) with methanol it is possible to obtain a high selectivity to the *para*-*C*-alkylated compound. By contrast, in the alkylation of activated arenes, such as phenol, diphenols and aniline, with olefins or with alcohols, the selectivity for the *para*-electrophilic substitution is lower than expected [35]. Indeed, on amorphous acid catalysts, the selectivity to *o*-cresol can even approach 100% [29,36,37]. The low selectivity to *p*-cresol in phenol methylation has been attributed to different reasons [38,39] and specifically: *i*) The alkylation at heteroatom is an intermediate step in *C*-alkylation by the olefin or by the alcohol [40]. *ii*) An interaction exists between the alkylating agent and the oxygen atom of phenol, which favours the alkylation at the

ortho position [24,40]. *iii*) A reaction between adsorbed anisole, which acts as the alkylating agent, and gas-phase phenol can be hypothesised [29], in which the interaction between the two O atoms puts the methyl group of anisole closer to the *ortho* position of phenol. *iv*) Furthermore, even in the homogeneous acid-catalysed electrophilic substitution on phenols, usually *ortho/para* ratios higher than the statistic value 2/1 are found [35,41]. This implies that adsorptive/geometric effects are not the main reason for the regioselectivity observed.

So, the overall mechanism for the acid-catalysed methylation of phenol [29] includes the direct *C*-alkylation at the *ortho* and *para* positions (in confined environments the direct *para-C*-alkylation can be preferred) and the *O*-alkylation to yield anisole, the ratio *C-/O-* alkylation being a function of the catalyst acid strength. The secondary, consecutive *intra*-molecular rearrangement of anisole to *o*-cresol makes the final *ortho/para-C*-alkylation ratio to become very high, especially over less acidic catalysts (*e.g.*, on amorphous materials).

The performance of the beta-3 catalyst is summarized in Figure 5A (effect of time-on-stream on conversion of phenol, at four temperatures) and Figure 5B (effect of time-on-stream on distribution of reaction products, at 450°C).

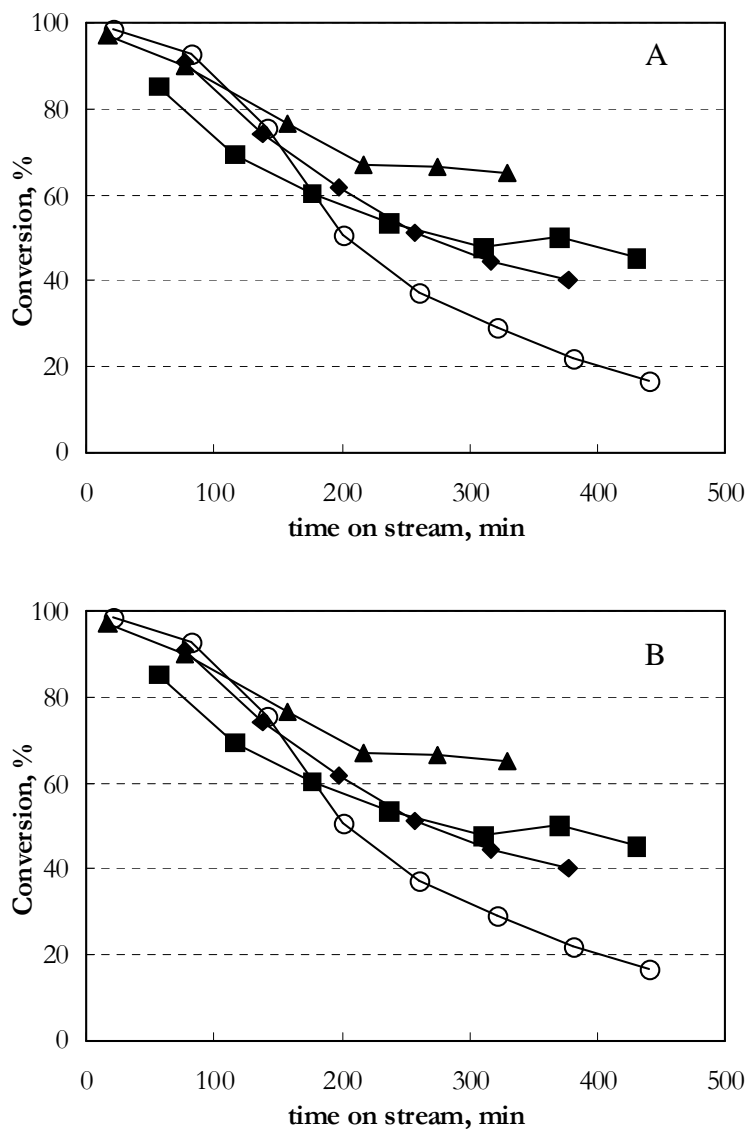


Figure 5 A. Effect of time-on-stream on conversion of phenol in alkylation over beta-3 catalyst at four different temperatures. 320°C (▲), 350°C (■), 390°C (◆) and 450°C (○).

B. Effect of time-on-stream on products distribution in alkylation of phenol over beta-3 catalyst. T = 450°C. Selectivity to poly-alkylated phenol (◆), to o-cresol (○), to p-cresol (▲) and to anisole (■).

The comparison with the data obtained with beta-2 zeolite (Figure 5) highlights that: *1*) The initial activity of the beta-3 zeolite is greater than that of beta-2. This is evident for the runs at 320°C only, since higher temperatures lead to total or almost total conversion for both catalysts. This difference is very likely due

to the higher *intra*-particle residence time of reactants in the larger crystal size zeolite. *ii*) At higher temperatures the deactivation rate seems not much affected by crystal size. Only at 320 and 350°C the beta-2 zeolite exhibits a quicker deactivation rate than beta-3. This is likely due to the shorter mean path within smaller zeolite crystals, whose pores become obstructed more quickly than the longer pores of beta-3. Since the difference is evident at low temperature only, this means that the species responsible for deactivation are not the alkyl-aromatics formed by methanol transformation (the formation of which is favoured at high temperature), but more likely phenol and oxygenated products, the diffusion of which is slower at lower temperature, due to their low volatility and to their stronger interaction with the zeolite acid sites. The characterisation of spent catalysts (*vide infra*) confirm this hypothesis. *iii*) The nature of products and the effect of conversion and of temperature on selectivity do not differ significantly from those observed with beta-2 catalyst.

At last, Figure 6 shows the effect of phenol conversion on the anisole/cresols molar ratio at 320, 390 and 450°C on beta-2 and beta-3 catalysts.

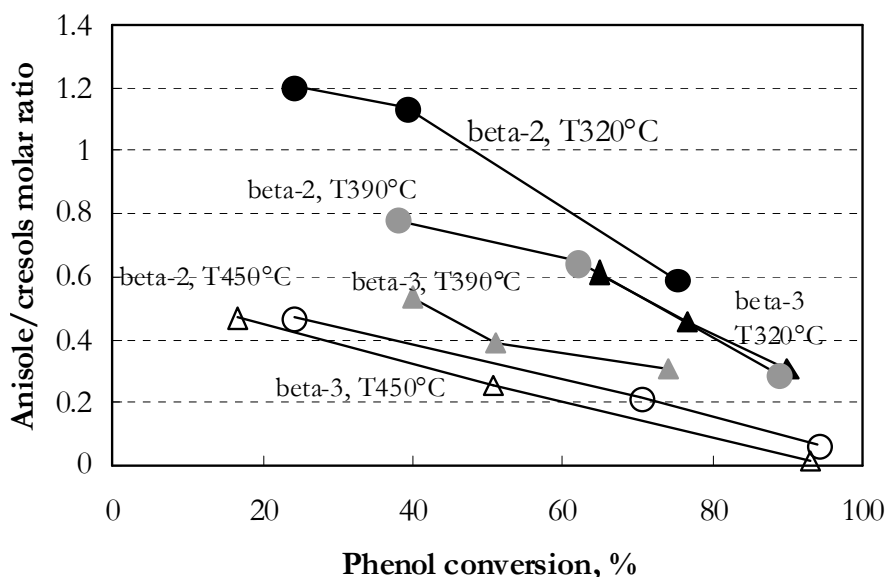


Figure 6. Effect of phenol conversion on the anisole/cresols molar ratio, at 320°C (black symbols), 390°C (grey symbols) and 450°C (white symbols), for the beta-2 (squares) and beta-3 (triangles) catalysts.

One may see that: *i*) The ratio decreases with increasing conversion, due to the secondary, consecutive transformations occurring on anisole, with formation of additional cresols; *ii*) The ratio decreases when increasing temperature at any conversion level, showing that low temperature favours the primary methylation at oxygen (and hence to anisole), with respect to the primary methylation at aromatic carbons.

Even though the comparison between zeolites is arguable when done under conditions that lead to catalyst deactivation and coke accumulation, nevertheless the data of Figure 6 indicate that the anisole/cresols ratio with beta-3 zeolite is systematically lower than for beta-2 at any conversion level and at any temperature. This means that the extent of the consecutive transformation of anisole to cresols is higher in the larger crystal size zeolite, as a consequence of the longer permanence of anisole within the zeolite pores, favouring both the secondary, consecutive *intra*-molecular rearrangement and *inter*-molecular alkylation of anisole.

An effect of crystal size on products distribution was also reported by Moon et al for phenol methylation over MCM-22 [23]. The authors found that *p*-cresol formed preferentially with respect to *o*-cresol, especially in the case of catalysts where the zeolite crystal sizes were greater than 1 μm . It was thus proposed that in the case of MCM-22 the 10MR pores allow easy diffusion of *p*-cresol and that the effect of this phenomenon is enhanced when the crystal size is relatively large. Also in the case of cresols isomerisation, the distribution of isomers (the formation of which occurs both by intramolecular methyl shift and bimolecular disproportionation) was governed by product desorption/diffusion. Shape selectivity favoured monomolecular reactions [42].

8.3.3. Transformation of methanol into poly-alkylated benzenes

During reaction with phenol, methanol also undergoes a parallel transformation to olefins and alkylbenzenes. The relative amount of the two classes of compounds is a function of the reaction temperature, higher temperatures favouring the formation of the latter compounds. Therefore, we also investigated

the formation of alkylbenzenes. The yield to these compounds is shown in Figures 7, for the beta-2 and beta-3 catalysts as a function of time-on-stream at 450°C.

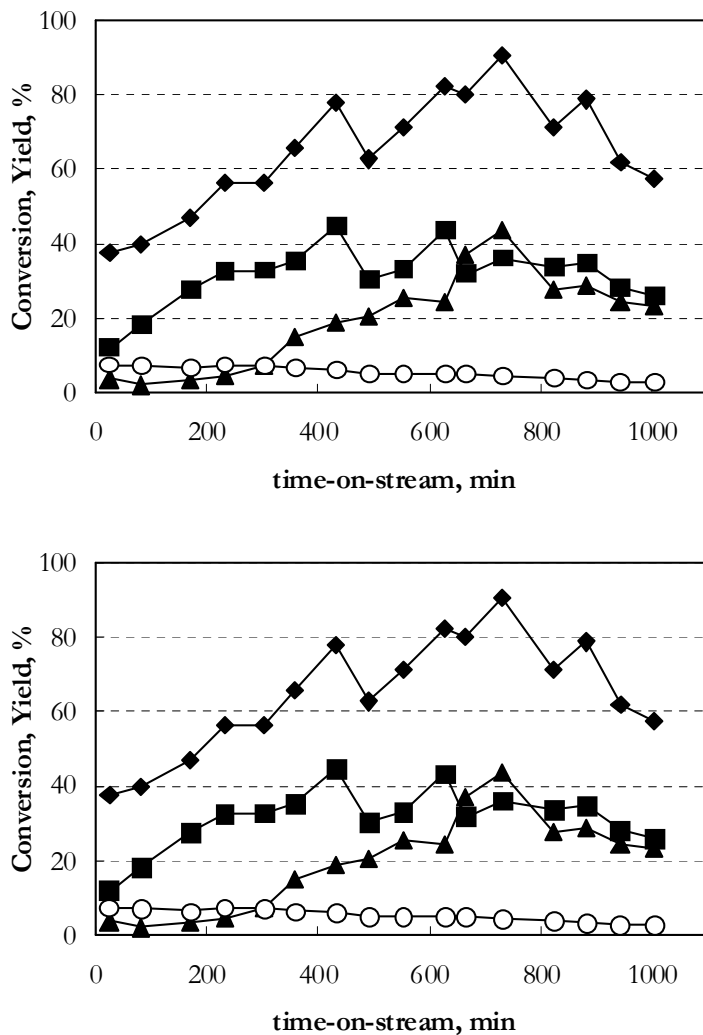


Figure 7 A. Effect of time-on-stream on methanol conversion and on products distribution in poly-alkylbenzenes formation over beta-2 catalyst (yields are calculated with respect to the methanol fed). $T = 450^{\circ}\text{C}$. Symbols: (◆) methanol conversion; (○) selectivity to toluene, (■) to pentamethylbenzene, (▲) to hexamethylbenzene.

B. Effect of time-on-stream on methanol conversion and on products distribution in poly-alkylbenzenes formation over beta-3 catalyst (yields are calculated with respect to the methanol fed). Symbols: (◆) methanol conversion; (○) selectivity to toluene, (■) to pentamethylbenzene, (▲) to hexamethylbenzene.

The same Figures also report the conversion of methanol, which also includes the amount converted for phenol methylation. It is worth noting that no “light” products of methanol decomposition (*i.e.* CO, CO₂, H₂) formed.

The principal products coming from methanol transformation were toluene, pentamethylbenzene and hexamethylbenzene. The yield to these compounds was relevant and the greater fraction of methanol was converted to poly-alkylated benzenes, rather than being involved in phenol methylation. This aspect has never been reported in the literature dealing with the gas-phase methylation of phenol catalysed by zeolites. Furthermore, it is evident that this is one reason for the need of feeding a large excess of methanol with respect to the stoichiometric requirement for the mono-alkylation of phenol. The competitive reaction of methanol transformation to alkylbenzenes makes the amount of methanol available for phenol methylation to become very low.

The conversion of methanol increased during the elapsing reaction time, due to the increased formation of poly-alkylated compounds, whereas, at the opposite, the amount of methanol that reacts with phenol decreased (see Figs. 4 and 5). Therefore, it seems that the active sites for the formation of these compounds are generated during reaction, while the sites responsible for the generation of the active species for the electrophilic substitution at the phenol ring are progressively poisoned. This clearly indicates that the mechanism of the two reactions is different. The conversion of methanol reached a maximum at approximately 800-1000 minutes-on-stream, after which it rapidly fell down, likely because of the considerable amount of coke accumulated in the catalyst, due to the growth of poly-nuclear aromatics.

The behaviour of the two zeolites was not much different, a part from the slightly different value of time-on-stream at which the maximum methanol conversion was attained (700 min for beta-2, against 1000 min for beta-3). This is probably due to the larger crystal size of the latter sample, that made pore filling by coke to take longer time than with the former sample. With both samples the yield to toluene decreased, whereas that to pentamethylbenzene showed a maximum

before the reaction time needed to reach the highest methanol conversion. The yield to the totally alkylated compound (hexamethylbenzene) increased, until the maximum methanol conversion was reached. This indicates that the growth of the molecular weight occurred in a consecutive-steps network fashion.

The formation of alkylated benzenes by self-reaction of methanol over zeolites (the MTG process) includes one first step of dehydration of methanol to dimethylether. Two mechanisms have been proposed, either an indirect pathway, in which the adsorbed methanol reacts with the methoxy species, which then reacts with another methanol molecule to dimethylether [43], or the direct pathway, in which two methanol molecules react over an acid site, with the formation of dimethylether and H₂O in one step [44]. The surface methoxy species SiO(CH₃)Al has been demonstrated to play a role in the formation of dimethylether [45]. The further conversion of the equilibrium mixture of methanol and dimethylether (and water as well) is dominated by a “hydrocarbon pool” route [46,47], in which methanol is directly added onto reactive organic compounds to form aliphatic and aromatic hydrocarbons. The methoxy species also plays a role in the kinetic “induction period”, leading to the reactive hydrocarbon pool.

Alternative “direct” mechanisms have been proposed, in which either a carbenium ion (CH₃⁺) reacts with dimethylether to generate either a carbonium ion (CH₃-CH₃⁺-OCH₃), or an oxonium ylide species. Other mechanisms include a carbene species (:CH₂) as the reaction intermediate (see the review by Haw *et al.* [48] for an analysis of the several mechanisms proposed in literature). The methoxy species acts as an alkylating agent in the presence of aromatic compounds. Furthermore, at T > 170°C, hydrogen atoms are abstracted by basic oxygen atoms of the framework, with formation of surface-stabilized intermediates of ylide or carbene nature [49], which are responsible for the methylation of aliphatic compounds, and for the formation of hydrocarbons, both aliphatic and aromatic (polymethylbenzenes) [50].

In the case of Beta zeolites, the predominant aromatic compounds in methanol transformation at high T are hexamethylbenzenes and

pentamethylbenzenes (in full agreement with our results), while ZSM-5 gave mostly dimethyl and trimethylbenzenes [51]. These compounds can be further converted to naphthalene derivatives, which are finally responsible for the formation of coke precursors and of zeolite deactivation [6].

Our data support the need for an induction period for the formation of these compounds, associated to the generation of a “hydrocarbon pool”. This corresponds to the progressive increase of methanol transformation into poly-alkyl benzenes shown in Figures 7. The progressive transformation of the hydrocarbon pool into heavier and heavier poly-alkylated compounds and to coke eventually leads to the complete deactivation of the catalyst.

8.3.3.1. Coke composition

Thermogravimetric (TG) analysis showed that the weight loss due to burning out of coke components by calcination in air amounted to 3.4%, while for beta-2 it was considerably higher, 12.8%. This obviously relates to the higher acidity of beta-2 as compared to beta-1. The organic matter extracted from beta-2 with CH_2Cl_2 amounted to 12.7%, perfectly in line with the value determined by TG. The GC-QMS analysis of the extracted fraction showed the presence of the following compounds: phenol (8 mol%), *o*- and *p*-cresols (4%), dimethyl-phenols (8%), trimethyl-phenols (15%), tetramethyl-phenols (18%), pentamethyl-benzene (5%), hexamethyl-benzene (5%), 3-ethyl-5-methyl-phenol (1%), 2-hydroxyphenyl-phenylmethanone (15%), 2-methyl-5-(1-methylethyl)-phenol (6%), 1-methoxy-4-methyl-2-(1-methylethyl)-benzene (15%). In the case of beta-1, instead, the following compounds were identified: phenol, cresols, dimethyl-phenols, trimethyl-phenols, tetramethyl-phenols and (dimethyl-ethyl)-phenols. Therefore, with the latter catalyst there was substantially no formation of poly-alkylbenzenes, *i.e.* the species coming from the transformation of methanol. With both catalysts, the insoluble coke recovered after dissolution of the zeolite was almost weightless and presumably composed of high-MW polynuclear species, their very low amount preventing however any reliable quantitative determination.

Therefore, these data indicate that the presence of strong acid sites in beta-2 is responsible for the formation of poly-alkylbenzenes, while silanols (present in both beta-1 and beta-2 samples, though in lower concentration in the former catalyst) are strong enough to catalyse the reaction of phenol methylation. This also indicates that the active methanol species able to attack phenol to yield methylated phenol is different from the species self-reacting to yield poly-alkylbenzenes. Indeed, on one hand the latter species can form only on acid sites much stronger than those required to form the former. On the other hand, the former species, though being not able to generate poly-alkylbenzenes, is electrophilic enough to react with phenol.

Furthermore, beta-1 was less active than beta-2 and beta-3 (data not reported), but did exhibit a deactivation rate comparable to that of the latter catalysts. This indicates that the main reason for catalyst deactivation in phenol methylation is associated to the build-up in catalyst pores of oxygen-containing species (phenol and alkylated phenol compounds). It is worth noting that the analysis of the compounds retained in the pores showed a high concentration of heavier compounds (poly-alkylated phenol), that instead are present in low concentration in the reactors' outgoing products stream. Therefore, heavier phenol derivatives are the species that more accumulate in the porous structure, as expected, due to their more cumbersome structure.

Therefore, two different deactivation mechanisms can be envisaged. One mechanism, responsible for the progressive deactivation of the catalyst in the methylation of phenol, is due to the retention of heavy, oxygenated compounds (*i.e.*, poly-alkylated phenols). This derives from the strong interaction of phenol and phenol derivatives with the active sites, which establishes from the very beginning of the reaction and hinders the generation of the active species responsible for the electrophilic attack to the phenol aromatic ring. Despite this, methanol conversion progressively increases during the first hours-on-stream, due to the fact that methanol is simultaneously converted to alkyl and poly-alkyl benzenes, generated from the building up of the "hydrocarbon pool" inside pores. This is supported

also by the change in the nature of the alkyl benzenes forming along with increasing methanol conversion. However, the progressive hardening of these species generates poly-nuclear aromatics, which in a few hours fills up the pores and eventually deactivates the catalyst.

8.4. Conclusions

High Si/Al ratio BEA-structured zeolite in protonated form is a very active catalyst for the methylation of phenol, leading to cresols and anisole as primary products, which rapidly methylate to poly-alkylated phenols. As deactivation proceeds, the selectivity to cresols and anisole increases substantially, together with a rapid decrease of selectivity to poly-alkylated species.

In this protonated zeolite acidity is prevalently of Brønsted type, independently of zeolite crystal size. However, the main part of the acid sites are of medium-to-low-strength. Indeed, high-strength Lewis-type sites are either almost absent, especially when metal cations partially substitute for protons, or seem to play a role prevalently in catalyst deactivation.

Stacking faults in the zeolite framework, generated by the intergrowth of at least two BEA polymorphs, can increase the concentration of relatively low-strength silanols-based acid sites, which seem however sufficiently active to trigger the phenol methylation primary reaction.

Deactivation is originated essentially by phenol and poly-alkylated phenol-derivatives. Self oligomerisation-cyclisation of methanol to olefins and aromatics, followed by further alkylation to aromatic C atoms, contributes more significantly to catalyst deactivation only for time-on stream values longer than a few hours.

At higher temperature all the zeolites deactivate at a comparable rate, whereas at lower temperature initial catalytic activity is higher for larger crystal size zeolite, due to the longer diffusion time of reactants within zeolite pores, favouring a longer contact with active sites.

At any conversion level and at any temperature the anisole/cresols ratio is systematically lower for the larger crystal size zeolite, since the secondary

transformations of anisole to cresols by both *intra*-molecular rearrangement and *inter*-molecular alkylation of phenol is favoured by the longer residence time of anisole within the zeolite pores.

8.5. Acknowledgments

For this work I would to acknowledge I. Rossetti, L. Forni and M. Bregolato from Univesità di Milano, V. Bolis and C. Busco from Università del Piemonte Orientale, P. Ugliengo and S. Bordiga from Università di Torino

8.6. References

- [1] R. Bal, B.B. Tope, S. Sivasanker, *J. Mol. Catal. A*, 181 (2002) 161
- [2] S. Velu, C.S. Swamy, *Appl. Catal. A*, 145 (1996) 141
- [3] V.V. Rao, V.Durgakumari, S. Narayanan, *Appl. Catal.*, 49 (1989) 165
- [4] S. Velu, C.S. Swamy, *Appl. Catal. A*, 162 (1997) 81
- [5] M. Bolognini, F. Cavani, D. Scagliarini, C. Flego, C. Perego, M. Saba, *Catal. Today*, 75 (2002) 103
- [6] M. Bjørgen, U. Olsbye, S. Kolboe, *J. Catal.*, 215 (2003) 30
- [7] J. Xu, A.-Z. Yan, Q.-H. Xu, *React. Kinet. Catal. Lett.*, 62 (1997) 71
- [8] G. Chen, X. Liu, *Chin. J. Catal.*, 19 (1998) 427
- [9] K. K. Cheralathan, I. S. Kumar, M. Palanichamy, V. Murugesan, *Appl. Catal. A*, 241 (2003) 247
- [10] A. V. Krishnan, K. Ojha, and N. C. Pradhan, *Org. Proc. Res. Dev.*, 6 (2002) 132

- [11] K. Zhang, C. Huang, H. Zhang, S. Xiang, S. Liu, D. Xu, H. Li, *Appl. Catal. A*, 166 (1998) 89
- [12] E. Dumitriu, V. Hulea, *J. Catal.*, 218 (2003) 249
- [13] I.Kiricsi, C.Flego, G.Pazzuconi, W.O.Parker, Jr., R.Millini, C.Perego, G.Bellussi, *J.Phys.Chem.*, 98 (1994) 4627
- [14] G.Bellussi, G.Pazzuconi, C.Perego, G.Girotti, G.Terzoni, *J.Catal.*, 157 (1995) 227
- [15] G.Perego, S.Amarilli, R.Millini, G.Bellussi, G.Girotti, G.Terzoni, *Mesop. Mater.*, 6 (1996) 395
- [16] G.Girotti, *EurpaCat-IV*, Rimini, Sept. 5-10, 1997, Book of Abstracts, KN11
- [17] R.L. Wadlinger, G.T. Kerr, E.J. Rosinski, U.S. Patent 3,308,069 (1967) and reissued U.S. Pat. Re 28,431 (1975) assigned to Mobil Oil Corp
- [18] J.M. Newsam, M.M.J. Treacy, W.T. Koetsier, C. De Gruyter, *Proc. R. Soc. London A*, 420 (1988) 375
- [19] J.B. Higgins, R.B. La Pierre, J.L. Schlenker, A.C. Rohrman, J.D. Wood, G.T. Kerr, W.J. Rohrbaugh, *Zeolites*, 8 (1988) 446
- [20] G. Busca, *Phys. Chem. Chem. Phys.* 1 (1999) 723.
- [21] P.D. Chantal, S. Kaliaguine, J.L. Grandmaison, *Appl. Catal.*, 18 (1985) 133
- [22] M. Renaud, P.D. Chantal, S. Kaliaguine, *Canad. J. Chem. Eng.*, 64 (1986) 787
- [23] G. Moon, W. Böhringer, C.T. O'Connor, *Catal. Today*, 97 (2004) 291
- [24] M. Marczewski, J.-P. Bodibo, G. Perot, M. Guisnet, *J. Molec. Catal.*, 50 (1989) 211

- [25] R.F. Parton, J.M. Jacobs, H. van Ooteghem, P.A. Jacobs, *Stud. Surf. Sci. Catal.*, 46 (1989) 211
- [26] L. Garcia, G. Giannetto, M.R. Goldwasser, M. Guisnet, P. Magnoux, *Catal. Lett.*, 37 (1996) 121
- [27] S. Namba, T. Yashima, Y. Itaba, N. Hara, *Stud. Surf. Sci. Catal.*, 5 (1980) 105
- [28] S. Balsamà, P. Beltrame, P.L. Beltrame, P. Carniti, L. Forni, G. Zuretti, *Appl. Catal.*, 13 (1984) 161
- [29] P. Beltrame, P.L. Beltrame, P. Carniti, A. Castelli, L. Forni, *Appl. Catal.*, 29 (1987) 327
- [30] K. G. Bhattacharyya, A.K. Talukdar, P. Das, S. Sivasanker, *J. Molec. Catal. A*, 197 (2003) 255
- [31] W. Wang, P. L. De Cola, R. Glaeser, I.I. Ivanova, J. Weitkamp, M. Hunger, *Catal. Lett* 94 (2004) 119
- [32] J. Rakoczy, T. Romotowski, *Zeolites*, 13 (1993) 256
- [33] G. Mirth, J. Lercher, *J. Catal.*, 132 (1991) 244
- [34] A. Corma, G. Sastre, P.M. Viruela, *J. Mol. Catal. A*, 100 (1995) 75
- [35] R.F. Parton, J.M. Jacobs, D.R. Huybrechts, P.A. Jacobs, *Stud. Surf. Sci. Catal.*, 46 (1989) 163, and references therein
- [36] J.M. Campelo, A. Garcia, D. Luna, J.M. Marinas, M.S. Moreno, *Stud. Surf. Sci. Catal.*, 41 (1988) 249
- [37] J.M. Campelo, A. Garcia, D. Luna, J.M. Marinas, M.S. Moreno, *Bull. Soc. Chim. France*, 2 (1988) 283

- [38] P. Espeel, R. Parton, H. Toufar, J. Martens, W. Hölderich, P. Jacobs, in “Catalysis and Zeolites. Fundamentals and Applications”, J. Weitkamp and L. Puppe (Eds.), Springer, Berlin, 1999, Ch. 6, p.377
- [39] J.B. Moffat, *Catal. Rev. Sci. Eng.*, 18 (1978) 199
- [40] M. Marczewski, G. Perot, M. Guisnet, *Stud. Surf. Sci. Catal.*, 41 (1988) 273
- [41] Patai “The Chemistry of the Hydroxyl Group”, Interscience Publ. John Wiley & Sons, (1971) 414
- [42] F.E. Imbert, M. Guisnet, F. Gnep, *J. Catal.*, 195 (2000) 279
- [43] T.R. Forester, R.F. Howe, *J. Am. Chem. Soc.*, 109 (1987) 5076
- [44] J. Bandiera, C. Naccache, *Appl. Catal.*, 69 (1991) 139
- [45] W. Wang, M. Seiler, M. Hunger, *J. Phys. Chem. B*, 105 (2001) 12553
- [46] I.M. Dahl, S. Kolboe, *J. Catal.*, 149 (1994) 458
- [47] B. Arstad, S. Kolboe, *J. Am. Chem. Soc.*, 123 (2001) 8137
- [48] J.F. Haw, W. Song, D.M. Marcus, J.B. Nicholas, *Acc. Chem. Res.*, 26 (2003) 317
- [49] P.E. Sinclair, C.R.A. Catlow, *J. Phys. Chem. B*, 101 (1997) 295
- [50] W. Wang, A. Buchholz, M. Seiler, M. Hunger, *J. Am. Chem. Soc.*, 125 (2003) 15260
- [51] Ø. Mikkelsen, S. Kolboe, *Microp. Mesop. Mater.*, 29 (1999) 173

Chapter 9

Coke deposition over zeolites during phenol methylation

9.1. Introduction

The main industrial problem in using zeolites as catalysts for gas-phase methylation of phenol is the deactivation due to the coking over the catalyst's surface. This kind of deactivation is the consequence of the blocking of zeolitic channel and of poisoning of catalytic site [1].

Deactivation by coke formation over active surface of zeolites is a well known phenomena. The main causes of the coke formation is the transformation involving methanol upon the acid site. There methanol is activated and converted to dimethylether. After that, dimethylether, via hydrocarbon pool mechanism is converted to olefin, aromatic compounds and extended conjugated aromatic compounds [2].

The deactivation rate is strictly correlated to the acid strength of the catalysts and their pore structure. The selectivity to aromatic compounds and the type of aromatics formed in the hydrocarbon pool mechanism inside the zeolitic channels are dominated by the shape selectivity of the zeolite. It is known that with large pore zeolites, like for instance H-MOR, examethylbenzene and subsequently fused rings compounds are formed, the latter remain in to the channels and by consequence are the cause of the pores blocking. On the other hand with small pore zeolites, such as H-ZSM-5, only formation of polymethylated benzenes and

naphthalene is permitted, these are able to go out, by consequence H-ZSM-5 zeolites are considered long life catalyst [2].

An other important aspect in the deactivation by coke formation during phenol/methanol process is the role of phenol. That is not often considered in literatures concerning the phenol methylation reaction but it could play an important role in the polymethylated benzene compounds [3].

In the present work we study the influence of acid strength and of zeolites structure on the rate of coke formation. Moreover we study the influence of the phenol in the catalytic environment to understand its role in the coke deposition over zeolites.

9.2. Experimental

H-ZSM-5 samples named CBV2314, CBV5524G and CBV8014 and a H-MOR sample (H-MOR40E) were tested.

In-situ UV/Vis study of coke formation deposited feeding methanol was performed the cell described in section 2.4. The powdered samples were placed into the cell and heated at different temperatures ranging from 300 and 450°C. After few minutes of stabilization, methanol flow was kept in contact with sample flowing a N₂ stream (150 ml/min) in a methanol containing bubbler.

The in-situ UV/Vis tests were performed in a tubular quartz reactor (see section 2.4). During the experiments temperatures were controlled by a thermocouple. In a typical experiments 0.3 g of pelleted catalyst (150-500 μm diameter) were loaded in the reactor between quartz wool. Reagents solution were feed using a syringe pump (0,0061 ml/min). Nitrogen was used as carrier gas (20 ml/min).

9.3. Results and discussions

9.3.1. The influence of the $\text{SiO}_2/\text{Al}_2\text{O}_3$ ratio in the coke formation

To evaluate the influence of the $\text{SiO}_2/\text{Al}_2\text{O}_3$ molar ratio of the different zeolite samples, tests done feeding methanol at various temperature were carried out.

Figure 1 shows the time resolved optical adsorption measurements taken from a $2\ \mu\text{m}$ spot focused on a crystals of the sample during the methanol exposure at 300°C .

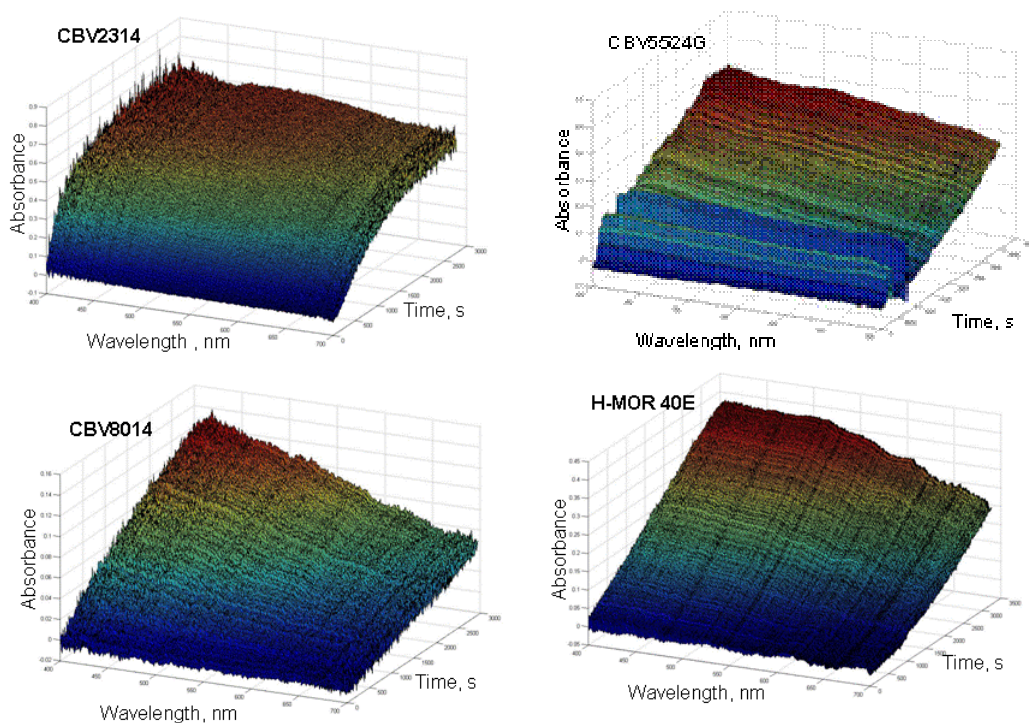


Figure 1. Optical adsorption spectra of the samples recorded feeding the methanol stream at 300°C .

The optical spectra show two broad bands with a maxima at 480 and 660 nm respectively, with intensities increasing with increasing time-on-stream. These bands are present for all the sample but are more intense for the sample CBV2314. The bands around 415 nm is assigned to $\pi-\pi^*$ transition in methyl-substituted benzenium cations [1]. These species play an important role in the hydrocarbon

pool mechanism. The bands around 550 nm are assigned to extended conjugated aromatic species derived from the above mentioned benzenium species. The band around 480 nm is attributable to a trienylcarbenium ion [4].

The temporal evolution of the band at 480 nm as function of time-on-stream at 300°C for the four samples is shown in Figure 2.

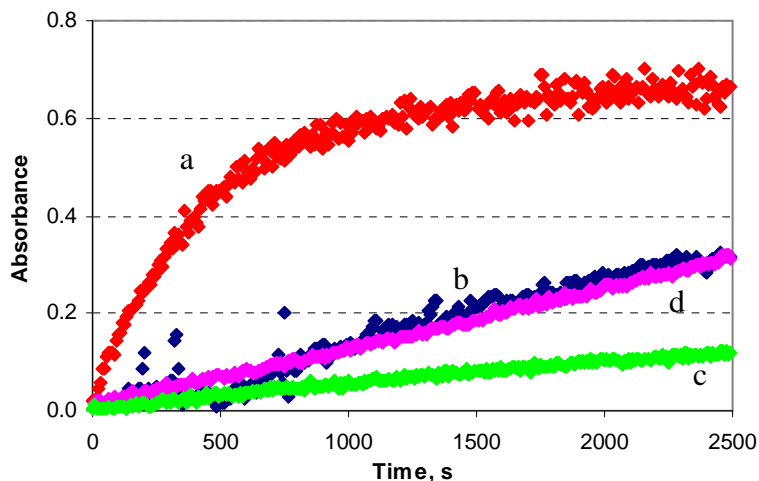


Figure 2. Temporal evolution of the optical absorption at 480 nm as a function of the time-on-stream at 300°C, a) CBV2314, b)CBV5524G, c)CBV8014, d)H-MOR40E

The profiles indicate that with sample CBV2314 the formation of methyl-substituted aromatic compounds is the faster. The profiles obtained from the samples CBV5524G and H-MOR40E are very similar. Finally, the analysis of the profile for the sample CBV8014 indicates that it is characterized by the lower kinetic of formation of aromatic species.

At higher temperature the rate of coke formation increase quickly for all the samples. Figure 3 shows the time resolved optical adsorption taken from the samples at 350°C (not for sample CBV2314). Also in this case the behaviour of sample CBV5524G and H-MOR seem to be similar.

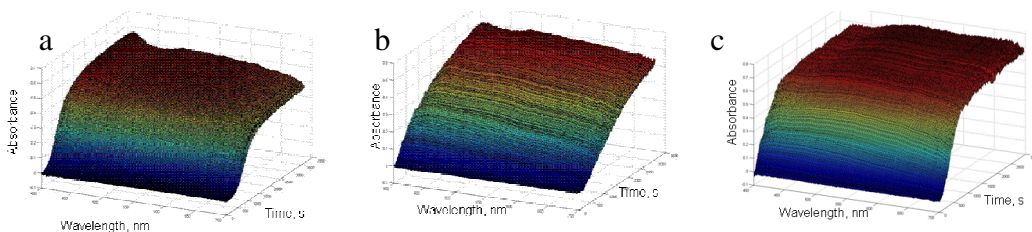


Figure 3. Optical adsorption spectra of the samples recorded feeding the methanol stream at 350°C. a) CBV5524G, b)CBV8014, c) H-MOR40E

The temporal evolution of the absorption band at 480 nm, as function of time-on-stream at 350°C of the samples, is shown in Figure 4.

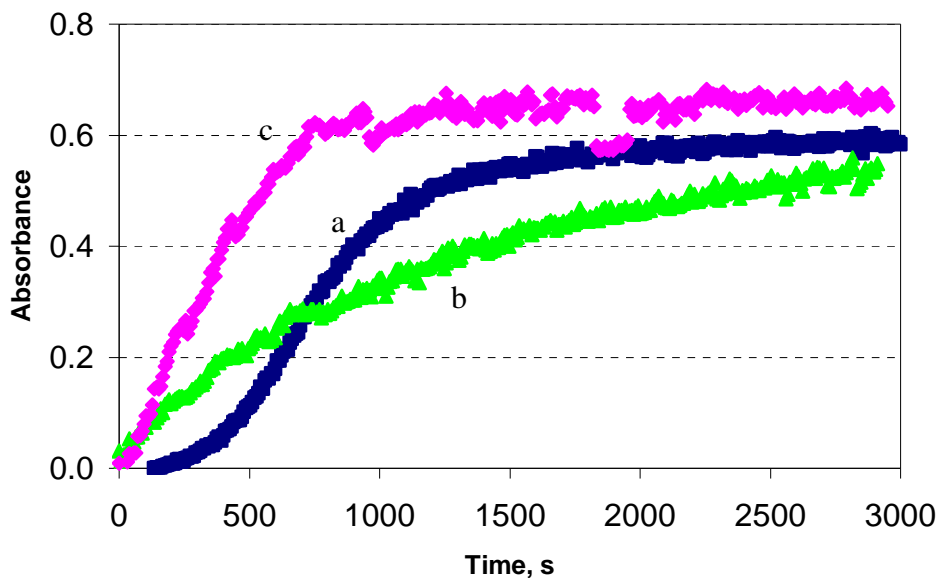


Figure 4. Temporal evolution of the optical absorption at 480 nm as a function of the time-on-stream at 350°C, a)CBV5524G, b)CBV8014, c)H-MOR40E.

Figure 5 compares the time resolved optical adsorption during the methanol exposure at 450°C. In this case the rate of coke formation is very fast. Comparing the temporal evolution of the adsorption band at 480 nm (Figure 6) it is possible to observe a difference rate of coke formation between samples CBV5524G and H-MOR40E.

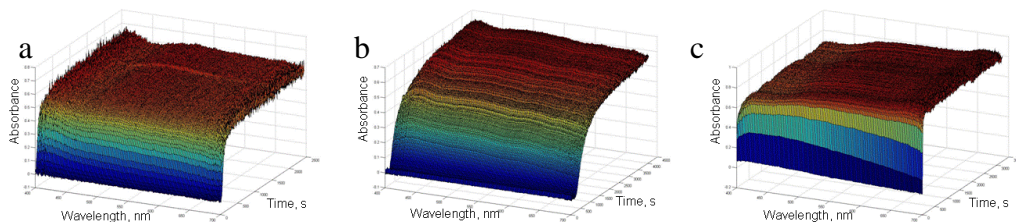


Figure 5. Optical adsorption spectra of the samples recorded feeding the methanol stream at 450°C. a) CBV5524G, b) CBV8014, c) H-MOR40E

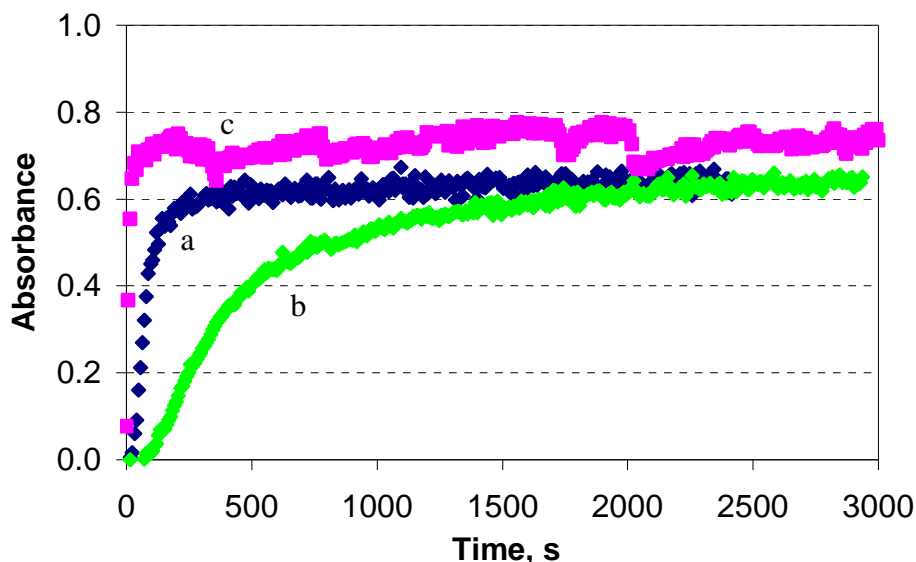


Figure 6. Temporal evolution of the optical absorption at 480 nm as a function of the time-on-stream at 450°C, a) CBV5524G, b) CBV8014, c) H-MOR40E

The above mentioned results demonstrate that a correlation between the coke formation and the $\text{SiO}_2/\text{Al}_2\text{O}_3$ ratio exists. With the reported experimental condition there are only little differences between the samples CBV5524G and H-MOR40E, that are evident only at high temperature.

9.3.2. The role of phenol on coke formation

To evaluate the influence of phenol on coke formation, we carried out tests by feeding a phenol/methanol solution over H-MOR and CBV 5524G. Tests were carried out in a tubular quartz reactor because feeding phenol, that is solid at room temperature, into the FT-IR cell could be problematic.

Figure 7 shows the time resolved optical adsorption measurements taken from a spot focused on a crystals of H-MOR40E, during exposure to the methanol feed at various temperatures, between 275 and 325°C.

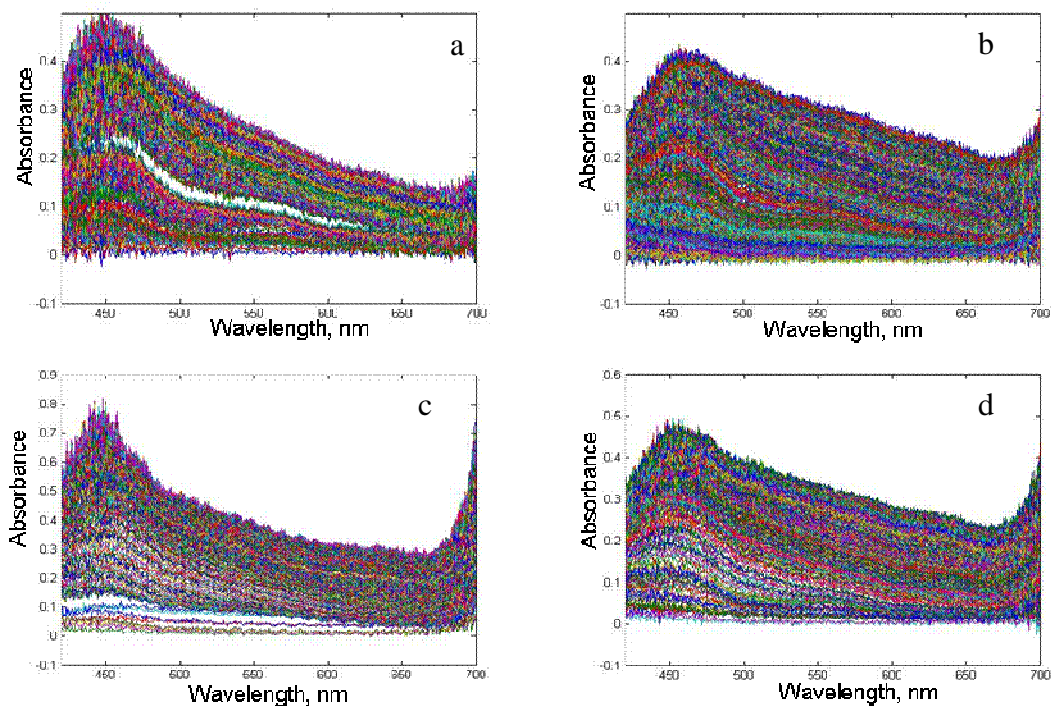


Figure 7. Optical adsorption spectra of the sample H-MOR40E recorded feeding the methanol stream at a) 275°C, b) 300°C, c) 312 °C, d) 325°C

The spectra reveal that coke formation is slower than that observed in the previous tests. This is due to the different experimental conditions. A part from that, the absorbance profiles are similar to those previously described. In all cases, the most intense band is positioned at around 450 nm. This indicates that, with the above mentioned experimental conditions, the formation of extended conjugated aromatic compounds is less favoured.

Figure 8 shows the time-resolved adsorption measurements done at the same conditions previously described, but feeding a phenol/methanol solution.

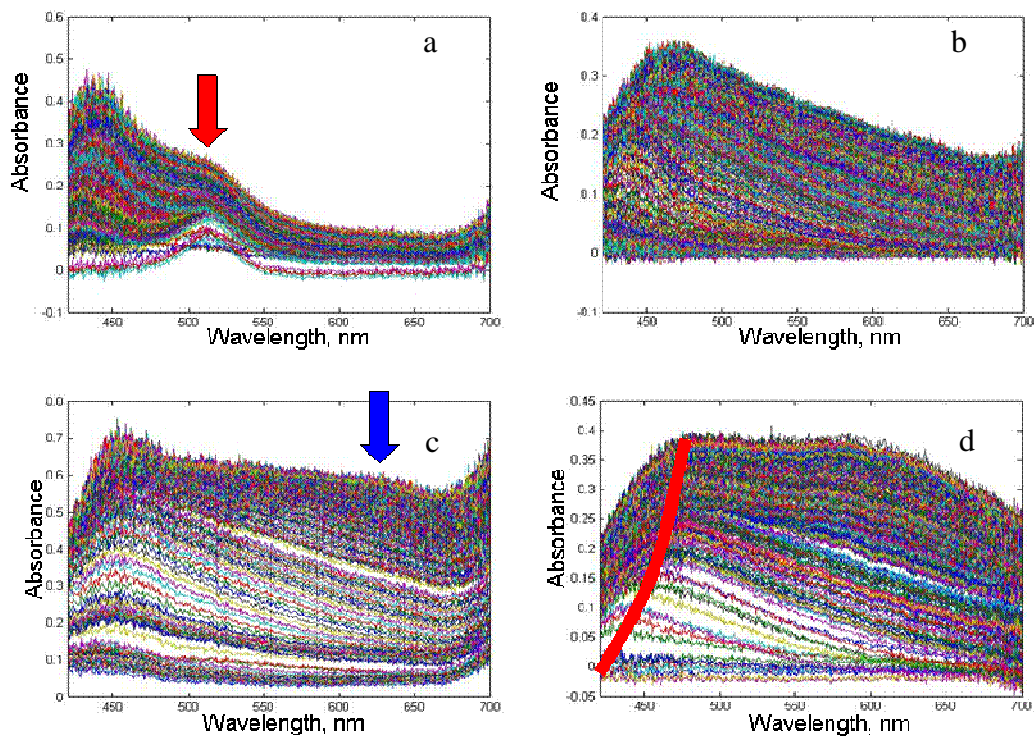


Figure 8. Optical adsorption spectra of the sample H-MOR40E recorded feeding the methanol/phenol stream at a) 275°C, b) 300°C, c) 312 °C, d) 325°C

It is worth noting that in this case there are important differences with respect to the previously recorded spectra. In fact, concerning tests done at the lower temperature, at which the reaction is not very fast, it is possible to observe a band, never observed before, at around 525 nm. This band can be attributed to an aromatic compound formed by reaction between methanol and phenol. Tests done at higher temperature reveal other important differences. For temperatures higher than 300°C, a red shift of the band located at around 400 nm is shown, that is function of time-on-stream. Finally the spectra recorded at 312 and 325°C show an intense band with a maximum at around 600 nm.

The red shift observed in the presence of phenol indicates that increasing the time-on-stream the primary products, polymethylated phenols, grow up yielding conjugated aromatic species. Therefore, after the first aromatic intermediate has formed, the reactants interact with the latter to yield the extended conjugated aromatic species.

Figure 9 shows the time-resolved adsorption measurements done feeding methanol and the phenol/methanol solution over CBV5524G at 300°C.

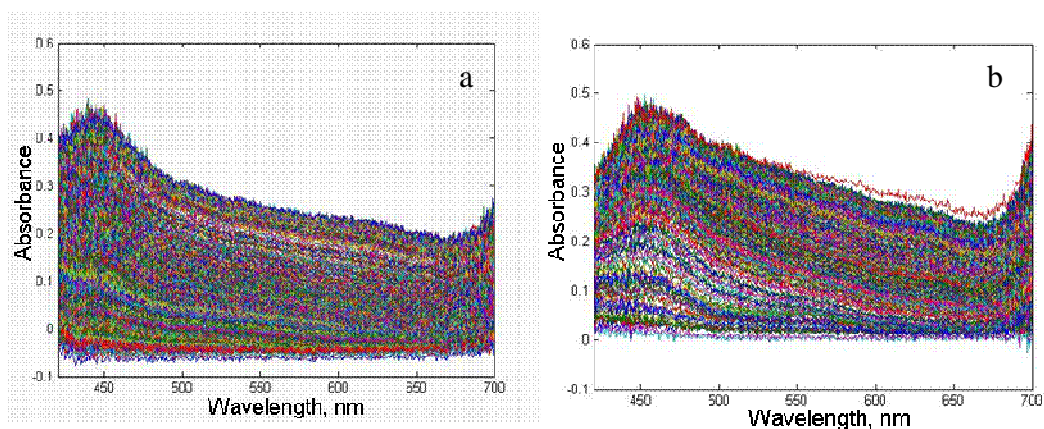


Figure 9. Optical adsorption spectra of the sample CBV5524G recorded feeding a) methanol, b) phenol/methanol

When methanol is fed without phenol, the optical spectrum (Figure 9a) was similar to that obtained with H-MOR, with the most intense band located around 450 nm.

Feeding methanol and phenol solution (Figure 9b), the strong adsorption band is shifted with respect to that observed feeding only methanol. This can be attributed to the methylated phenolic cation, and suggests that phenol plays an important role in coke formation. Comparing these results with those obtained with H-MOR at the same temperature, it is possible to observe an important difference. In particular, with H-MOR the most intense band shifts from 400 nm to 470 nm during increasing time-on-stream; on the contrary, with CBV5524G the most intense band does not shift, and its wavelength is at 450 nm. This difference is attributable to the different pore size distribution. In fact, in the case of CBV2455G the pore size is smaller; phenol can be methylated forming di- and trimethylphenols, but when bigger intermediates are formed pores become occluded. Inside the larger channels of H-MOR, phenol initially yields polymethylated phenols, that later yield policonjugated aromatic species.

9.4. Conclusions

In-situ UV/vis experiments reveal that coke deposition over the tested sample is strongly influenced by the acidity of the zeolites. Experiments show that the greater is the concentration of Brønsted acid sites, the faster is coke formation. Coke formation deriving from the reaction of methanol, via dimethylether, is affected by the pore size at lower temperatures.

The pore size influences coke formation when phenol is fed together with methanol. In this case with the CBV5534G sample, the methylation of phenol and consequently its condensation is limited by the shape control. On the contrary, with H-MOR40E, that has larger pores, polymethylated compounds grow up without limitation forming extended conjugated aromatic compounds.

9.5. Acknowledgments

For this work I wish to acknowledge Prof. B. M. Weckhuysen for hosting me in his laboratory and his co-workers Inge Burrmans, Davide Mores and Eli Stavitski for their technical support during my visiting at the Utrecht University.

9.6. References

- [1] D. Mores, E. Stavitski, M.H.F. Kox, J.Kornatowski, U. Olsbye, B.M. Weckhuysen, *Chem. Eur. J.* 14 (2008) 11320
- [2] J.W. Park, G. Seo, *Appl. Catal. A* 356 (2009) 180
- [3] N. Ballarini, F. Cavani, L. Maselli A. Montaletti, S. Passeri, D. Scagliarini, C. Flego, C. Perego, *J. Catal.* 251 (2007) 423.
- [4] M. Hunger, *Microporous Mesoporous Mater.* 82 (2005)

Ringraziamenti

Ed eccomi qua all'ultima pagina della mia tesi o se vogliamo all'ultima pagina di questa bellissima esperienza iniziata più di tre anni fa! Quando ho iniziato non sapevo bene cosa aspettarmi, se ne sarebbe valsa la pena o se invece sarebbe stata una fregatura ma ora che mi trovo a scrivere queste parole e che i miei pensieri sfogliano le pagine di questo intenso capitolo della mia vita devo dire che se potessi tornare indietro non esiterei a rifare quello che ho fatto.

In questi ultimi tre anni credo di essere cresciuto molto e ciò lo devo, più che ai congressi o alle lezioni frontali..., a tutte le persone che ho incontrato lungo la strada che mi ha portato fin qui. Per questo voglio ringraziare il prof. Cavani per l'opportunità che mi ha dato, per la fiducia che ha riposto in me fin dall'inizio, per tutte le cose che mi ha insegnato e per i consigli che da amico mi sa dare. Voglio, e devo, ringraziare Silvia con la quale ho iniziato questa avventura tre anni fa e con la quale ho condiviso oltre che la scrivania anche i momenti più critici, caotici e delicati della vita di laboratorio. Un grazie veramente di cuore va a Stefania la terza del "tre S group", gruppo denominato anche in un altro modo, nonché la mia prima laureanda, se ripenso al giorno che ha discusso la tesi ancora mi emoziono. Ringrazio poi Dario e Antonio che, come Silvia, hanno condiviso con me i vari momenti del dottorato. Rose e Carlo, miei colleghi e momentaneamente coinquilini. Ringrazio Lucilla e Stefano per il loro prezioso contributo. Non posso poi non ricordarmi di quell'anzianotto di Simonazzi. Un ringraziamento particolare va a Luca che mi ha lasciato veramente un buon lavoro da proseguire. Ringrazio Nazario, Katerina, il dot Castelli, Giuseppe, Patricia, Irene, Elisa e tutti gli altri che hanno finito prima di me. Voglio poi ringraziare il prof. Vaccari, Luca e Stefania e Nicola per il suo aiuto nel corso della mia attività.

Un ringraziamento particolare va anche ai Prof. Sambogna e Ruggeri sempre pronti ad aiutarmi per i problemi metallurgici.

Ringrazio Aurora per la pazienza che ha avuto in questi ultimi mesi, prima quando ero in Olanda e in quest'ultimo periodo quando alla sera ero impegnato a questa tesi.

Infine voglio ringraziare veramente di cuore la mia famiglia, mio fratello Lorenzo, sempre pronto ad aiutarmi in ogni momento e i miei genitori per il sostegno morale, oltre che economico, che mi hanno dato in tutti questi anni.